Large-scale Finite Element Simulation of Seismic Soil-Pile foundation-Structure Interaction

Zhao Ben

National University of Singapore

2013

Large-scale Finite Element Simulation of Seismic Soil-Pile foundation-Structure Interaction

Zhao Ben

A thesis submitted for the degree of doctor of philosophy

Department of Civil & Environmental Engineering

National University of Singapore

2013

Acknowledgements

With great pleasure, I express my sincere and profound gratitude to my supervisors, Prof Lee Fook Hou and Dr. Goh Siang Huat for their erudite and invaluable guidance throughout the study. Their gratitude, analytical and methodical way of working has inspired me and under their guidance I have learned a lot.

In addition, I would like to thank Dr. Hong Sze Han, Dr. Subhadeep Banerjee, Mr. Adrian Tan Seck Wei and other fellow colleagues of NUS Geotechnical Division.

I would like to thank NUS for providing all necessary financial and academic support without which this study would have been a distinct dream.

Finally, grateful acknowledgement is expressed to my family and my fiancée Tian Wei.

Declaration

I hereby declare that this thesis is my original work and it has been written by me in its entirety.

I have duly acknowledged all the sources of information which have been used in the thesis.

This thesis has also not been submitted for any degree in any university previously.

Zhao Ben

03/06/2013

.

Abstract

The pile group effect is an important factor affecting the performance of pile foundations and superstructure under earthquake loading. While this topic has been widely studied over the past fifty years, most of the research was carried out using single piles or small pile groups. However, the pile foundations for tall structures and buildings typically consist of a much larger number of piles spaced quite closely together. Under such conditions, pile-soil-pile interaction effects during seismic excitation are likely to be significant. To date, such interaction effects have not been systematically studied for large pile groups.

In this study, the development of a parallel dynamic finite element program for nonlinear geotechnical analysis is first presented. The program is then used to perform large-scale finite element analyses involving large piled foundation systems constructed in predominantly soft clay ground conditions subjected to earthquake excitation.

The research comprises four major components: (1) the setting up of a network PC cluster and the development of a parallel finite element code for large-scale dynamic simulations; (2) the implementation of the key features for seismic finite element modelling, such as the hysteretic soft soil model with cyclic degradation and the use of solid elements with stress integration for calculating the pile bending moments; (3) parametric studies of the large-scale soil-pile-structure system leading to semi-analytical solutions for the maximum bending moments in the pile group under earthquake loading; (4) extended studies to examine the

influence of the superstructure, uneven soil stratigraphy and earthquake motion characteristics on the large-scale pile group effects.

To perform the large-scale simulations, a PC cluster is set up using a high-speed local network to connect multiple multi-core personal computers. Details of the network configuration and hardware specifications are presented. The development of the parallel dynamic finite element program is described, with emphasis on the choice of iterative solver, method of domain decomposition, and the use of message passing techniques for distributed memory computing. The developed code was successfully tested on several large-scale models of varying sizes, yielding speed-up factors that attest to the computational efficiency and the high performance potential of this numerical tool.

The finite element program is validated using measured data from centrifuge shaking table tests involving small 2x2 pile groups. Also, the computed results are shown to compare favourably with those obtained from ABAQUS 3-D simulations of the same problem. Following this, larger finite element models of 3x3 pile groups up to 9x9 pile groups are set up and analysed to study the effect of pile spacing and pile group size. The computed results show that pile-to-pile interaction effects are significant up to a spacing of about nine diameters, while the effects of pile group size is less obvious although the larger pile group generally induces a larger response. Finally, analyses are also carried out on a large-scale soil-pile-structure model with a 9x21 pile foundation that is representative of typical high-rise building flats and their foundations in Singapore. The computed

accelerations, displacements and pile bending moments are discussed. Furthermore, comparisons of the computed raft accelerations and pile bending moments are also made with the results obtained using an equivalent linear elastic soil model and a simplified pseudo-static approach.

Additional finite element analyses of the large-scale soil-pile-superstructure model are extended to study the influence of different pile size, soft soil layer thickness, soft soil stiffness, superstructure mass and peak ground acceleration. The influence of each factor on the pile foundation response is discussed. By processing the results using dimensional analysis and data fitting, three semi-empirical dimensionless expressions for estimating the maximum bending moments and the critical pile length are obtained. Using these estimated moments and the critical pile length, together with the general trends of the computed bending moment profiles obtained from all the analyses, a simplified bending moment envelope is proposed for seismic pile foundation design.

Additional issues related to the influence of the superstructure, presence of uneven soil geometries and different earthquake motions are considered, and their effects on seismic soil-pile foundation-structure response are examined.

Key words: parallel finite element simulation, seismic interaction, pile foundation, amplification, bending moment

Table of Contents

List of Tables

List of Figures

List of Symbols

σ_{ij}	Total stress vector
σ'_{ij}	Effective stress vector
p	Pore water pressure
p'	Mean effective stress
u_i	Displacement vector of solid
$\dot{u}_i$	Velocity vector of solid
$\ddot{u}_i$	Acceleration vector of solid
K_w	Bulk modulus of pore water
$[M]$	Global mass matrix
$[C]$	Global viscosity matrix
$[K]$	Global stiffness matrix

$S(n)$	Speedup factor of parallel calculation
t_s	Execution time on a single processor
t_p	Execution time on a multiprocessor
EI	Flexural rigidity
ε_p	Bending strain
m_{str}	Sum of equivalent structure mass and raft mass
l_c	Critical pile length
M_1	Maximum pile bending moment at pile head
M_2	Maximum pile bending moment at clay-hard soil layer interface

Chapter 1 Introduction

1.1 Background

Piles and pile groups are commonly used to support tall buildings founded on soft grounds and reclaimed land. Under normal conditions, they may be subjected to lateral loads and moments due to wind loadings or structural eccentricity. During an earthquake, additional bending moments are developed in the piles due to inertial loads applied by the superstructure to the pile head, as well as due to the response and deformation of the surrounding soil. Both inertial loads and soil deformation are directly related to the ground acceleration developed during the seismic event.

It is very difficult, if not impossible, to inspect the existing pile foundations that support many of the buildings and infrastructure in Singapore to assess if they have been adversely affected by the recent tremors arising from the far-field earthquakes in Sumatra. The problem is further compounded by the interaction and reflection of stress waves between the soil and the piles, which creates a complex stress field that cannot be studied using simplified analytical approaches. In cities such as Bangkok and Jakarta, the problem is likely to be even more pertinent since the seismic hazard is greater.

1.2 Pile Foundation Failures during Earthquakes

Cases of damage and failure of piles during earthquake events have been noted. For instance, Mizuno (1987) studied 28 cases of serious pile foundation damage

during earthquake in Japan from the 1923 Kanto earthquake to the 1983 Nihonkai-Chubu earthquake and classify the pile damage cases into five categories as due to soil lateral displacement, embankment movement, soil liquefaction, soil ground vibration and inertial forces from the superstructure. Meymand (1998) summarized pile performance in the past ten strong earthquakes, from 1906 San Francisco Earthquake to 1995 Hyogoken-Nanbu Earthquake, and divided the possible reasons causing pile foundation damage into six classes, as shown in Figure 1-1.

In this study, based on the pile damage characteristics and position, the pile foundation failure cases are classified into five models and reviewed as following:

(1) Bending or Shearing failure of pile head

For loose, cohesionless saturated soils, the seismic vibration may induce liquefaction in the soil around the pile. In the case of cohesive soil, softening or stiffness degradation may occur, especially near the pile head. The loss of lateral soil support and large structural inertial loads could result in excessive bending moment and shear force at the pile head. During the 1962 Niigata Earthquake, pile bending damage under the NHK building were incurred due to liquefaction, as shown in Figure 1-2 (Yoshida and Hamada, 1991). In addition, pile shearing damage were also incurred under the Nigata Family Courthouse, as shown in Figure 1-3 (Hamada, 1991). In the 1978 Off-Miyagi Prefecture Earthquake, Sugimura (1981) noted that the most heavily damaged piles were those located around the structure's perimeters. This suggests that rocking due to inertial loads

from the structure might have overstressed the piles. However, this may also be due to large pile group interaction effects which results in the perimeter piles being subjected to larger moments than the inner piles.

(2) Bending failure at the soil layer interface

Bending damage in piles has also been attributed to large fixed-end or soil support moment at and around the interface between hard soil and soft soil layers. After the 1964 Niigata Earthquake, Fukouka (1966) excavated piles under Yachiyo Bridge and found that precast reinforced concrete piles developed horizontal cracks along the length of the piles, as shown in Figure 1-4.

(3) Pile cap failure

Pile foundation damage has also been attributed to inadequate structural provisions at the pile-to-cap connection, which may render the pile-cap structure incapable of sustaining the additional axial forces, shear forces and bending moments from the pile during earthquake. This may in turn lead to the pile punching through or detaching from the cap. During the 1964 Alaskan Earthquake, the Kenai River Bridge collapsed with piles punched through concrete deck, as shown in Figure 1-5 (Ross *et al.*, 1973). During the 1989 Loma Prieta Earthquake, the pile-supported Highway 1 bridge across the Struve Slough collapsed, as several of the piles punched through the roadway (Seed *et al.*, 1990). During the 1995 Kobe Earthquake, a ramp structure at the Higashi-Kobe mainland ferry pier supported on pile foundations collapsed due to poor or nonexistent connection details between steel piles and cap (Sitar *et al.*, 1995).

(4) Excessive horizontal displacement

Local horizontal ground movement during seismic vibration may drive the pile foundation to experience excessive horizontal displacement and loss of functionality, especially for bridge piles located beside the rivers. During the 1906 San Francisco Earthquake, lateral spreading caused a timber-pile supported railroad bridge to collapse, as shown in Figure 1-7 (Wood, 1908). Similarly, after the 1964 Niigata Earthquake, the pile extracted from the Showa Bridge foundation was found to have undergone about 1m permanent deformation, as shown in Figure 1-8 (Iwasaki, 1972a). Finally, during the 1964 Alaskan Earthquake, abutments laterally spreading toward the channel resulted in compression of the span driving the stringers through the bulkheads and arching the deck over the piers, at several railroad bridges between Portage and Seward, as shown in Figure 1-9 (Mccullouch and Bonilla, 1967).

(5) Excessive pile settlement or tensile pull-out

If the soils along the length of the pile soften due to liquefaction or strain softening, the shaft friction may reduce significantly and could result in excessive settlement or tensile pull-out failure. For instance, during the 1964 Niigata Earthquake, the pile-supported Sakae-bridge settled 330cm due to liquefaction, as shown in Figure 1-10 (Kawakami and Asada, 1966a). In another case, according to Girault (1986), 25 buildings on mat foundations supported by friction piles experienced large settlements (up to 130cm) and tilting, during the 1985 Mexico City Earthquake. The mechanism for these settlements was relaxation of the negative skin friction

on the pile due to partial loss of shear strength during cyclic loading of the sensitive clays.

1.3 Current design method and analysis state of pile foundation under earthquake loading

1.3.1 Requirements and approaches in construction codes

Based on the previous survey reports, most current building codes emphasize the need to design pile foundations for earthquake loading. However, in many cases, no specific design or analytical methods are given.

Eurocode 8 (British Standards Institution., 2006) requires that the piles be designed to resist the inertia forces from the superstructure and kinematic forces arising from the deformation of the surrounding soil. It recommends that, in principle, the piles should be designed to remain elastic, but could be allowed to develop a plastic hinge at the pile head when the elastic design criterion could not be fulfilled. Clause 5.4.2(3) reads "*Analyses to determine the internal forces along the pile, as well as the deflection and rotation at the pile head, shall be based on discrete or continuum models that can realistically (even if approximately) reproduce: the flexural stiffness of the pile; the soil reactions along the pile, with due consideration to the effects of cyclic loading and the magnitude of strains in the soil; the pile-to-pile dynamic interaction effects (also called dynamic "pile-group" effects); the degree of freedom of the rotation at/of the pile cap, or of the connection between the pile and the structure*." Hence, Eurocode 8 acknowledges that the effects of soil-pile interaction on piles should be assessed for conditions

involving (a) sharply different soil stiffness, (b) the support of important structures, and (c) the presence of moderate to high seismicity.

The 2009 International Building Code (IBC, 2009) does require the engineer or designer to consider soil-structure interaction. Chapter 18, "Soils and Foundations", provides minimal design guidance for foundations in seismic design categories C through F. Specific requirements for additional seismic reinforcement are given. In essence, the IBC partially addresses pile integrity under kinematic and inertial loading, but does not explicitly account for the influence of the pile foundation on the ground motions imparted to the superstructure. In chapter 16, “Structural Design Requirements”, both response spectrum and time history analyses are considered for seismic design; however, no provisions are provided to account for soil-structure interaction.

The Japan Road Association’s Seismic Design Specifications of Highway Bridge (1996) adopts the lessons learnt from the 1995 Kobe earthquake, and addresses the classification of ground conditions and inertia forces applied to substructures. The code provides detailed guidelines for considering the decrease in bearing capacity of weak cohesive soil, besides the assessment of liquefaction potential (Unjoh and Terayama, 1998).

The Chinese Building Design Code (GB2001) does not require consideration of soil-structure interaction in general seismic structural analyses except for high-rise reinforced concrete buildings with box-shaped foundations constructed in Type III or IV soft soils with 8 or 9 seismic fortification intensity. For the pile foundation

design, it requires the checking of horizontal and vertical bearing capacity of a single pile subjected to earthquake load. The characteristic value of the seismic bearing capacity can be increased by 25% for piles in non-liquefied sites and reduced for piles in liquefied sites. Besides, the code requires that piles in liquefiable zones be installed with a minimum embedment into a stable layer, but it neglects the potential damage arising from soil stiffness contrast.

The Indian Seismic Code Recommendations (IS-1893: 2002) do not mention soil-structure interaction in design practice. According to the code, the lateral resistance of the soil shall be ignored for laterally loaded piles installed in liquefiable soils. The effect of soft soils is not considered in the code (Banerjee, 2009).

1.3.2 Current state-of-practice for seismic soil-pile interaction design

Due to the unavailability of standardized and validated analysis techniques, practicing engineers usually ignore or greatly simplify the effects of soil-pile-structure interaction in their analyses. The approach commonly adopted for dealing with this complex problem spans two disciplines, geotechnical and structural engineering. Depending on the background and training of the engineer, some simplification or idealization is typically made either for the structure or the soil. For example, a geotechnical engineer might simply model a complex superstructure as an oscillator, while the structural engineer would often idealize the nonlinear soil-pile system as a set of springs. In doing so, the nonlinear interaction effects of the soil-pile-structure system are neglected.

Hadjian *et al.* (1992) conducted a national survey of design practices in the United States related to the seismic response of pile foundations. The reports revealed that geotechnical engineers usually provided load-deflection diagrams to structural engineers for structural analyses. Group effects were treated with empirical or elastic/static interaction solutions, and did not consider the dynamic nature of the problem.

Several methods for the analyses of piles subjected to seismic loadings were presented at the ASCE technical workshop on the lateral response of pile foundations conducted in San Francisco in 1994. Two methods were outlined to analyze pile response due to earthquake loading: (i) imposing the maximum displacement from the free-field ground response on the pile and calculating the bending moment and shear force along the pile; (ii) using a nonlinear dynamic finite element method to model both piles and soil. Meymand (1998) commented that the first approach was conservative in that it does not account for soil-pile interaction.

Kramer (1993) conducted an investigation on the seismic response of the I-90 bridge foundations crossing the Mercer Slough in Bellevue, Washington. A series of field tests were conducted in which the pile head was subjected to static and dynamic loading, and the impedance of the pile group was estimated. Following that, three-dimensional finite element analyses were performed to estimate the pile bending moments. G&E Engineering System (1994) conducted a seismic study for the east span of the San Francisco-Oakland Bay Bridge. Although the

superstructure was analyzed with a high degree of nonlinearity, the foundation was simply simulated using elastic springs. Abghari and Chai (1995) attempted to couple the substructure and superstructure components of the soil-pile-interaction problem by modeling a single pile extracted from a pile group that incorporated the superstructure contribution to that pile. A SHAKE91 (Idriss et al., 1990) site response analysis was carried out, and the resultant free-field displacement time history was applied to nodal points of the dynamic soil-pile interaction code PAR.

Recently, Puri and Prakash (2008) summarized the common methods currently in use for design of piles subjected to earthquake loading as the force or limit equilibrium analysis, and the displacement or p-y analyses.

The preceding discussion reveals that the nonlinear seismic interaction among soil, pile foundation and superstructure is not adequately considered in current engineering practice. In contrast, very simple pseudostatic methods are used to determine the design parameters. The inertial interaction between structure and pile foundation, kinematic interaction between piles and soils, seismically induced pore-water pressure and nonlinear response of soil are neglected in the practical designs.

1.3.3 Previous studies of pile foundations under earthquake loading

The seismic soil-pile-structure interaction has been widely studied with different approaches, including laterally loaded pile tests in the field (Brown *et al.*, 2001; Snyder, 2004), 1-g shaking table tests (Meymand, 1998; Shirato *et al.*, 2008) and

centrifuge shaking table tests (Wilson, 1998; Kagawa *et al.*, 2004), analyses using beam-on-dynamic Winkler foundation approach (Lok, 1999; Goh and O'rourke, 2008), pseudostatic approach (Tabesh and Poulos, 2001; Elahi *et al.*, 2010), and finite element analyses (Lu *et al.*, 2005; Lu, 2006).

Brown *et al.* (2001) and Agarwal *et al.* (2010) conducted full-scale field tests on single pile and small pile groups with lateral static loading and dynamic loading, in both soft cohesive and cohesionless soils. Back-analysis of the measured results were performed to determine site-specific p-y curves and damping characteristics. Besides, the phenomenon of soil stiffness reduction due to pile group effect has been observed in the field tests, and is commonly accounted for using the concept of a p-multiplier. More details and literatures about lateral loading field tests are reviewed in section 2.2. However, in almost all the field tests, the pile is loaded at the pile head, which is distinctively different for the mechanism of seismic loading. Hence, the field tests could not impart the kinematic effect of soil movement on the piles.

Meymand (1998) and Ueng (2010) performed soil-pile interaction tests on the shaking table with a laminar box under 1-g condition. The artificial and measured earthquake motion was fed into the model at its base and then allowed to freely transmit upward. This method could imitate the process and mechanism of seismic soil-pile-structure interaction, including the inertia interaction, kinematic interaction, nonlinear properties and radiation damping in the model system. More details and literatures about 1-g shaking table tests are reviewed in section

2.3.1. However, the shaking table tests have a principal drawback that they are conducted in 1-g condition and cannot capture the realistic soil stress field.

In order to overcome the drawback of 1-g shaking table tests, Kagawa *et al.* (2004) and Ilankatharan (2008) conducted high-g shaking table tests using the geotechnical centrifuge, which could replicate the increased gravitational stress field and a more realistic soil strength profile (Banerjee, 2009). The test results revealed significant kinematic interaction between the soil and piles, inducing large bending moments at pile head. More details and literature about centrifuge shaking table tests are reviewed in section 2.3.2. However, due to the space constraints associated with centrifuge testing, only single pile or small-scale pile groups have been studied.

Due to the significant resources and length of time required for physical testing, especially field tests and shaking table tests, such approaches are not widely used. Hence, theoretical and numerical studies are often adopted. Lok (1999) and Varun *et al.* (2012) developed the beam-on-dynamic-Winkler-foundation method to simulate soil-pile interaction under earthquake loading. The nonlinear springs and dashpots are used to model near-field soil and replicate the kinematic interaction between the soil and pile. More details and literature about the beam-on-dynamic-Winkler-foundation method are reviewed in section 2.4.1. However, inertia effects of the near-field soil are usually neglected in this method. Furthermore, this method ignores the pile-soil-pile interaction and pile group effect; hence it only could be used for single piles or large-spacing pile groups.

Based on the beam-on-dynamic-Winkler-foundation method, Tabesh and Poulos (2001) and Elahi *et al.* (2010) proposed a pseudostatic approach to analyze the seismic response of pile foundations by using static calculation. The kinematic forces from the soil movement and inertia forces from the superstructure are uncoupled and applied on the pile foundation separately. The kinematic and inertia effects are explicit and easy to discuss. This method may be extended to pile groups via the use of p-multipliers. More details and literature about the pseudostatic approach are reviewed in section 2.4.2. However, the pseudostatic approach does not consider the dynamic characteristics of the pile foundation and the interaction between the pile foundation and the near-field soil. Besides, the evaluation of the spring stiffness coefficients and p-multiplier is still highly empirical. Hence, this method yields only approximate solutions for the maximum pile force and lateral displacement.

The most rigorous approach to analyze seismic soil-pile-structure interaction is the finite element method. It could perform seismic soil-pile-structure simulation of pile groups in a fully coupled way, without carrying out separate or independent calculations of the superstructure or site response (e.g. Lu *et al.*, 2005; Uzuoka *et al.*, 2007). It is possible to simulate any arbitrary soil profile and to study three-dimensional effects (e.g. Huang *et al.*, 2004; Uzuoka *et al.*, 2007). Both liquefaction of sand and softening of clay can be replicated with suitable soil constitutive models (e.g. Lu, 2006; Banerjee, 2009). The potential gap that may

form between the pile and soil also can be simulated with interface elements (e.g. Lu *et al.*, 2005; Chang, 2007).

All these previous studies are limited to single piles or small pile groups, with the exception of Lu (2006). On the other hand, most high-rise buildings invariably have large pile foundations with dozens or hundreds of piles. Accordingly, the complexity of the problem will increase as the pile group size increases (Lu, 2006; Shirato *et al.*, 2008). Besides, in areas where soil profiles are variable or highly non-uniform over the length of the building, pile lengths will vary along the building and different parts of the same building may be subjected to different amplification and phase effects of the propagating wave, leading to differential motion. Hence, large-scale analyses that can capture the large pile group response are required.

As previously stated, the response of large pile groups cannot be easily studied using either physical tests or the beam-on-dynamic-Winkler-foundation. The finite element method, theoretically, can model large pile foundations; however, large-scale simulation requires huge computational resources. Lu (2006) developed a parallel finite element program to simulate the pile-supported wharf system, which contains 16 piles with 364,800 degree-of-freedom. However, such a problem scale is still not enough to simulate a large pile foundation typically constructed to support a high-rise building.

Furthermore, many issues related to the response of large pile group systems, such as pile group effects associated with pile spacing and the number of piles, are still

not well understood. According to Gohl (1991)'s shaking table tests, the pile-to-pile interaction is significant for pile spacings of up to six pile diameters, while Kagawa (1983a)'s study indicated that the pile-to-pile interaction may be significant up to thirty pile diameters. Brown *et al.* (2001) and Shirato *et al.* (2008) pointed out that the piles in larger pile groups generally experience larger bending moments compared to those in small pile groups. However, the relationship between the pile bending moment and the group size has not been discussed systematically. More details about previous studies of seismic pile foundation will be discussed in Chapter 2.

1.4 Research objectives and thesis organization

In this study, the large-scale problem of soil-pile group-structure interaction in soft clay during seismic events will be studied numerically, using a specially developed parallel finite element program which runs on a PC cluster.

The main objective of the study is to provide an approach for analyzing large-scale pile foundations and their interaction with the surrounding soil and the supported superstructure under earthquake loading. The analysis incorporates nonlinear soil properties, pile-soil-pile interaction in a group, as well as the inertia interaction between the pile foundation and superstructure.

For carrying out the large-scale simulations, the whole calculated domain is required to reduce the lateral boundary influence while the small element size is required to simulate piles and surrounding soil, which will cause a huge finite

element model with large number of degree of freedom. At the meantime, a large number of time step due to the conflict of long-duration and small time steps is required for seismic simulation. Hence, the calculation work is a big challenge to large-scale finite element simulation for seismic soil-pile foundation interaction, which is beyond the capacity of normal personal computers. The parallel computation is necessary. In this study, a parallel nonlinear finite element program for dynamic analysis was developed and a network cluster of personal computers was set up which allows the code to be run on distributed memory. In this way, it is possible to circumvent or reduce the time and memory constraints that have hindered the analyses of large soil-pile-structure systems involving more than a million degrees of freedom, short of doing so on a supercomputer.

In addition, based on the results from the large-scale analyses, the research also seeks to develop a rational framework for designing pile foundations under seismic loading.

This PhD thesis consists of seven chapters. Chapter 2 reviews the previous studies for seismic soil-pile interaction. Through a detailed discussion of current literature, it will be demonstrated that more research is needed on large-scale soil-pile interaction.

Chapter 3 describes the software and hardware development needed to carry out the large-scale numerical analyses. The details of the nonlinear finite element program for the dynamic analysis of geotechnical problems are presented, with special focus on the parallel features and how they are implemented. The

specifications and set-up of the networked PC cluster are also discussed. The performance and efficiency of the parallel finite element code is examined by comparing its results and computational performance with those obtained using the commercial software ABAQUS.

Several issues related to the modeling of seismic soil-pile-structure problems are discussed in Chapter 4. These include the soil constitutive model, the method of simulating the pile, and the lateral boundary conditions for simulating free-field soil response at a distance from the structure. With these implementations, the finite element program is then validated using centrifuge test measurements. Subsequently, pile group effects arising from pile spacing and pile group size are discussed. Finally, a large-scale finite element model of a soil-pile-structure system is set up, analyzed and the results discussed and compared with those obtained using a linear elastic dynamic analysis and a pseudostatic analysis.

A comprehensive suite of parametric studies is performed in Chapter 5 to study the influence of soft clay depth, pile diameter, structural mass, soil stiffness and peak ground acceleration on the pile foundation response. Using the results of the parametric studies, a framework is proposed for estimating the maximum bending moments at both the pile head and the lower interface between the clay and the underlying hard soil. An expression for estimating the depth of the pile inflection point is also proposed.

In Chapter 6, further analyses are carried out to study the influence of the superstructure's natural period, uneven soil stratigraphy, and the earthquake types.

Finally, some important conclusions and findings are presented in Chapter 7, and recommendations are made for further studies in this area.

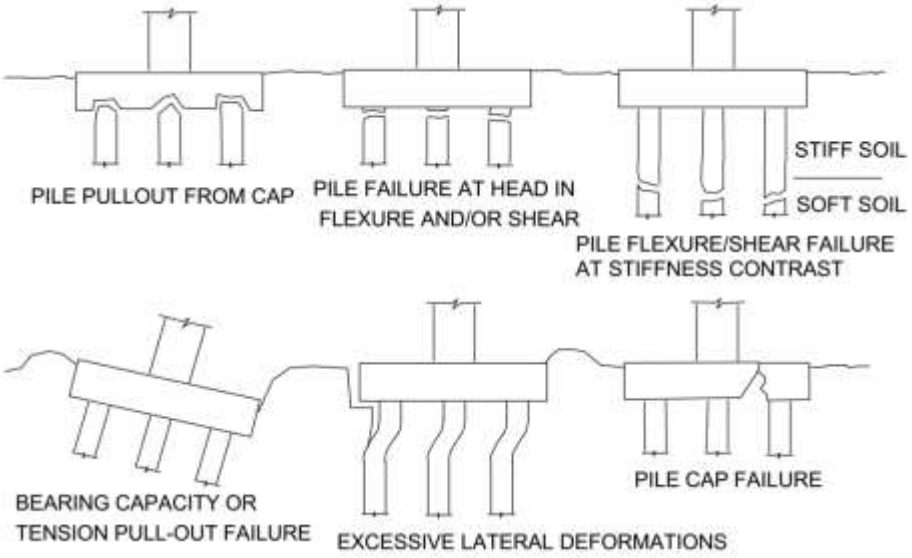

Figure 1-1 Potential failure modes for pile group foundations subjected to seismic shaking (Meymand, 1998)

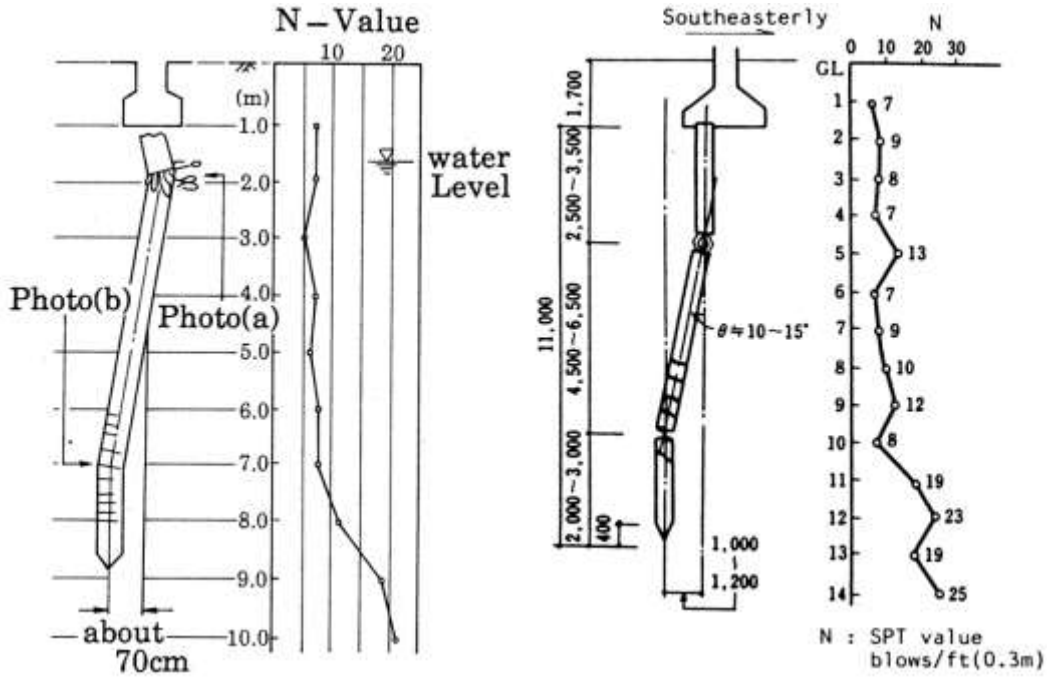

Figure 1-2 Pile damage due to bending, at (a) Niigata Family Court-house and (b) NHK Building during the Niigata Earthquake (Hamada, 1991)

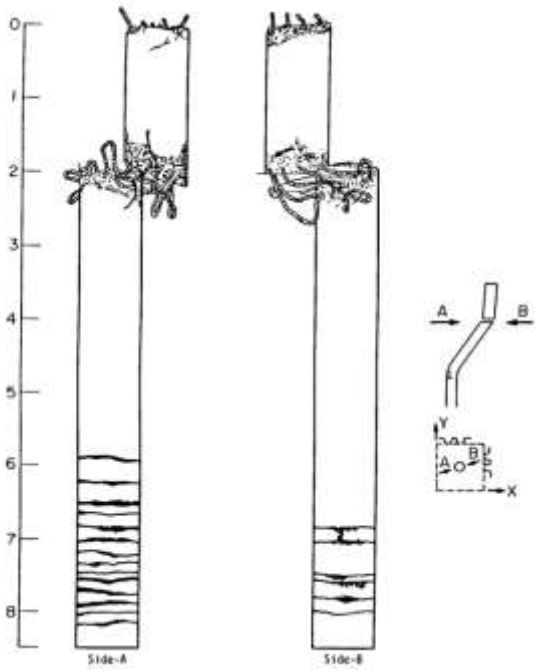

Figure 1-3 Pile damage due to shearing, at Niigata Family Courthouse during the 1964 Niigata Earthquake (Hamada, 1991)

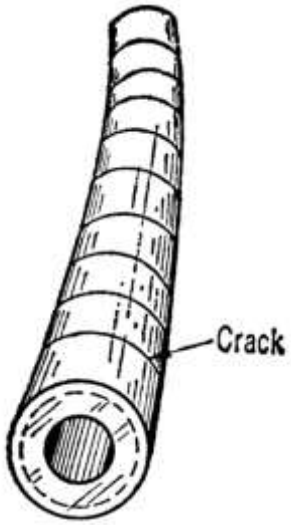

Figure 1-4 Cracked Precast Reinforced Concrete Piles from Yachiyo Bridge during the 1964 Niigata Earthquake (Fukuoka, 1966)

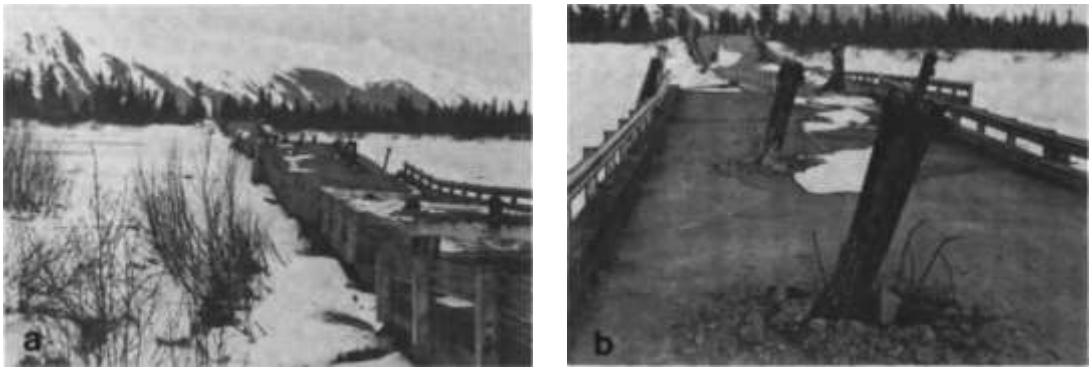

Figure 1-5 Placer River main crossing. (a) Looking north at bridge; stringers and deck have collapsed to stream-bed, (b) Lateral displacement of superstructure; concrete deck penetrated by timber piles (Ross *et al.*, 1973)

Figure 1-6 Pile damaged due to excessive bending moment induced by superstructure inertial forces during the 1995 Kobe Earthquake (Tokimatsu *et al.*, 1996)

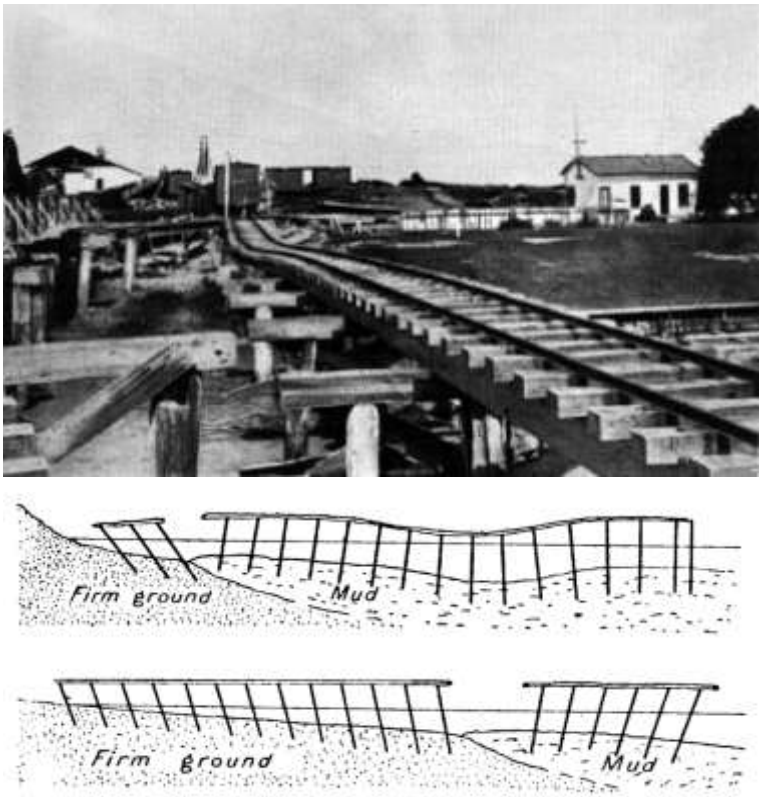

Figure 1-7 Collapse of timber pile supported railroad bridge at Moss Landing due to lateral spreading during the 1906 San Francisco Earthquake (Wood, 1908)

Figure 1-8 Collapse of Showa Bridge due to large lateral deformation during the 1964 Niigata Earthquake (Iwasaki, 1972b)

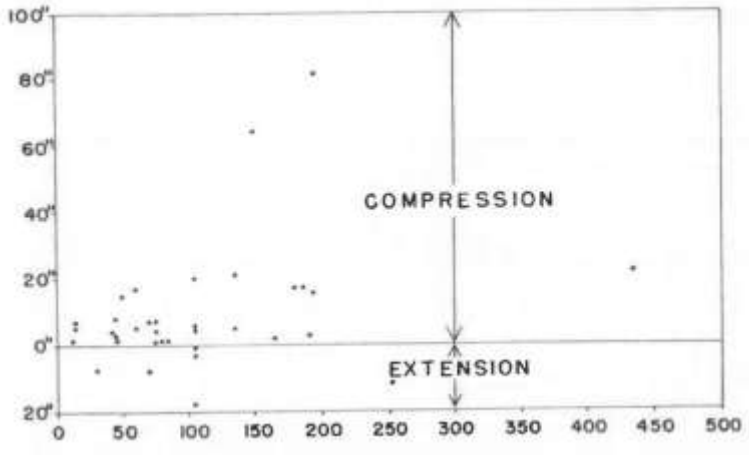

Figure 1-9 Net compression or extension (in inches) versus length of bridges (in feet) (Mccullouch and Bonilla, 1967)

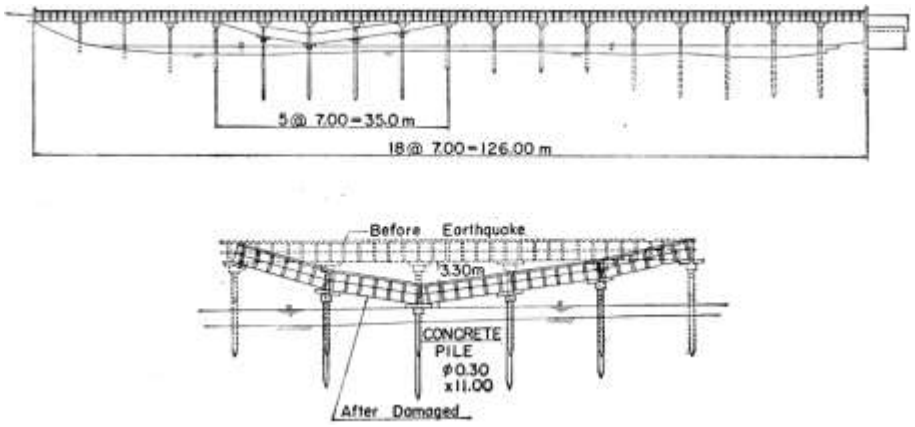

Figure 1-10 Damage of Sakae Bridge due to excessive settlement during the 1964 Niigata Earthquake (Kawakami and Asada, 1966b)

Chapter 2 Previous Studies on Seismic Soil-Pile foundation-Structure Interaction

2.1 Introduction

Besides post-earthquake surveys, other approaches have also been used to study seismic soil-pile-structure interaction, including field tests, laboratory tests and numerical simulation. These approaches will be reviewed in the first part of this chapter. Since this study focuses on the effects of earthquakes on pile groups, previous works on pile groups will be examined in more detail herein. Several issues related to earthquake effects on pile group will then be summarized specifically.

2.2 Full-scale Field Tests

As summarized in Table 2-1, numerous static, cyclic and dynamic field tests on pile groups have been conducted (e.g. Scoot *et al.*, 1982; Brown *et al.*, 1987; Crouse and Cheang, 1987; Blaney and O'neill, 1989; Lam and Cheang, 1995; Rollins *et al.*, 1998; Rollins *et al.*, 2003; Snyder, 2004). Most of the full-scale pile tests were conducted to determine the stiffness and damping characteristics of pile and soil by the application of dynamic loading on the pile head, rather than to assess pile response with earthquake excitation from bedrock. None of the field tests replicated earthquake loadings since the dynamic loads are usually applied at the pile head, the only exception being Rollins *et al.* (2005), who used shallow-buried explosives. Neither of these types of loading represents earthquakes. In earthquake

situation, the seismic waves propagate upwards from the bedrock causing motion in the entire soil layer. As Banerjee (2009) noted, the soil around the piles does not just support the piles, they also exert inertial loading on the piles. Pile head loading cannot replicate this effect.

Secondly, the pile groups tested are generally quite small, typically 3x3 or less. This is not surprising since the amount of energy needed to excite larger pile groups is likely to be prohibitively large. These two limitations underline the two major difficulties of conducting field tests on piles for earthquake response, namely difficulty in simulating bedrock excitation and supplying enough energy to excite large pile groups. Finally, large-scale field tests require significant cost, time and effort. Hence, the number of parameters which can be varied is usually limited.

2.3 Shaking Table Pile Tests

Shaking table test of model piles is a useful approach to understand soil-pile interaction effects under earthquake loading (Meymand, 1998; Boulanger *et al.*, 1999; Kagawa *et al.*, 2004; Yao *et al.*, 2004; Ilankatharan *et al.*, 2006; Chang, 2007; Ilankatharan, 2008; Shirato *et al.*, 2008; Banerjee, 2009), in which pile foundations with structures could be easily constructed and tested. Furthermore, both kinematic and inertial interaction might be studied. However, the 1-g shaking table tests have several principal limitations, including the difficulty to fully satisfy all scale modelling criteria, replicating realistic soil stress fields, and the boundary effects of test containers (Meymand, 1998). In addition, because of the limitation

of space, shaking table tests are often limited to testing single piles or small pile groups.

2.3.1 1-g Shaking Table Pile Tests

Large-scale 1-g shaking table tests have some advantages over field tests. Firstly, they can reasonably replicate the seismic interaction between soil and piles. The specimens are excited from the base which could reproduce the earthquake bedrock excitation. The instrumentation can be installed more readily. As summarized in Table 2-2, numerous 1-g shaking table studies have been conducted on pile groups (e.g. Mizuno *et al.*, 1984; Stanton *et al.*, 1988; Gohl, 1991; Kagawa *et al.*, 1994; Makris *et al.*, 1997; Meymand, 1998; Jakrapiyanun, 2002; Tokimatsu *et al.*, 2005; Shirato *et al.*, 2008; Chau *et al.*, 2009; Ueng, 2010). However, it is also well-recognized that 1-g model tests cannot replicate the stress levels encountered in a large-scale prototype. In particular, for earthquake simulation, inertial effects are likely to be unrepresented in 1-g models. To see why this is so, consider a 1/Nth-scale 1-g model. The volume, and thus the mass of the model, is $1/N^3$ times that of the prototype. On the other hand, overburden effective stress level in the model is only 1/N times that of the prototype. Assuming that modulus varies as the square root of the effective stress, model modulus is $1/\sqrt{N}$ times of the prototype. Hence, the modulus decreases at a slower rate than the mass of the model as the scale factor N is increased, and inertial effects are usually under-represented in a reduced scale 1-g model. For this reason, soil behavior is unlikely to be representative of that in a prototype.

In order to reduce the influence of scale factors, most 1-g shaking table tests used large-sized shaking table and container, so that small-scale factors can be employed. For example, the soil specimen in Shirato *et al.* (2008)'s test was 3.1m in height, and the sand layer in Tao *et al.* (1998)'s test was over 5m in height. However, while large-sized shaking table tests might be suitable for sandy soil, they present some problems when used for studying clay response. Depending on its permeability, the consolidation time for clay in a large container may be very long, taking up to several years in some cases. In some cases, a large pre-load may be applied to speed up the consolidation (e.g. Meymand, 1998). However, once the consolidation load is removed, the clayey soil will swell. When this happens during the pile tests, the soil is in the process of swelling, rather than a state of equilibrium. This gives rise to the difficulty of defining a representative state of the stress during the test, as pointed out by Meymand (1998). It is a well-recognized problem with large-size laboratory testing, and highlights the importance of good quality control of the models (Kagawa *et al.*, 2004).

Even with large-size 1-g shaking tables, the number of piles which can be installed in the group remains small owing to the difficulty of constructing large pile groups, especially in a confined space. Most pile groups in 1-g shaking table tests are 2x2 piles (e.g. Mizuno *et al.*, 1984; Meymand, 1998; Tokimatsu *et al.*, 2005; Chau *et al.*, 2009) and 3x3 piles (e.g. Li *et al.*, 2007; Shirato *et al.*, 2008). It appears that the largest reported pile group used in a 1-g shaking table test was 6x6 piles (Sakajo *et al.* (1995)). However, Sakajo *et al.* (1995)'s tests were conducted in sandy soil

and his focus on pile group resistance to liquefaction. Moreover, group size effects associated with a much larger pile group, e.g. more than 100 piles, was not investigated.

2.3.2 Centrifuge Shaking Table Pile Tests

Compared with field test and large-scale shaking table test, centrifuge testing requires much fewer resources. It's also easy to reproduce a geostatic stress gradient in the soil specimens that is representative of prototype conditions. Furthermore, clay beds in the centrifuge tests can reach a state of geostatic equilibrium under the elevated g-level within a reasonably short time of between 1 to 2 days. This method is widely used for earthquake studies (e.g. Gohl, 1991; Wilson, 1998; Boulanger *et al.*, 1999; Curras *et al.*, 2001; Kagawa *et al.*, 2004; Chang, 2007; Ilankatharan, 2008; Banerjee, 2009), as summarized in Table 2-3. However, most of these tests were conducted on sandy soils. The notable exceptions are Curras *et al.* (2001) who tested pile groups in soft clay bed overlying sand and Banerjee (2009) who tested widely spaced 2x2 pile groups in soft clay beds. However, Banerjee (2009)'s focus was on single piles, and his widely spaced piles connected to a stiff raft were configured essentially to enforce a fix-head condition, which is otherwise very difficult to realize for single piles in model tests.

Owing to the limited space in a centrifuge model, which is usually even smaller than that of a 1-g shaking table model, only small pile groups can be tested. This constraint is particularly acute if the pile groups are to be kept sufficiently far from the sides of the container to minimize boundary effects. For example, the

centrifuge tests reported by Curras *et al.* (2001) were based on small 3x3 pile groups. The centrifuge measurements were compared with those obtained from dynamic beam on nonlinear Winkler foundation analyses. Apart from adopting a p-multiplier of 0.7 to account for pile group effects, following Brown *et al.* (1988), there was no discussion on how the seismic pile responses were affected by the group effects.

2.4 Theoretical and Numerical Studies

The foregoing review of previous experimental work highlighted the difficulties of studying seismic-soil-pile interaction using field and laboratory tests. Field tests are often limited to dynamic pile load tests applied through the pile heads or pile caps. These are not exactly seismic soil-pile interaction tests. The pile groups studied are also relatively small owing to the limited amount of energy which can be supplied. Laboratory 1-g and high-g shaking table tests, on the other hand, do not suffer from energy limitation since the sizes of the models are much smaller than those in field tests. However, they do suffer from limited working space. 1-g model shaking tables are often larger than centrifuge-mounted shaking tables, but 1-g models are also correspondingly larger because of the necessity to increase model size in order to reduce scale distortion. For all these reasons, field and physical model tests on pile groups with more than about 9 piles are very rarely done. As a result, some researchers have resorted to other means of studying seismic soil-pile interaction problems using analytical and numerical approaches.

In this section, a review of the key theoretical and numerical studies related to seismic soil-pile interaction is presented.

2.4.1 Beam-on-Dynamic-Winkler-Foundation Approach

The beam-on-Winkler foundation approach has been used extensively for static and dynamic modelling of soil-pile interaction. A common variant of this is the use of the p-y relations, first proposed by Mcclelland and Focht (1956). They employed triaxial tests to estimate the subgrade reaction modulus of the soil surrounding the pile at various depths. Subsequent studies which used this approach are summarized in Table 2-4.

For seismic soil-pile analysis using the beam-on-Winkler foundation approach, the soil around the pile is divided into the far-field and near-field. The far-field soil behaviour is simulated assuming the earthquake motion at the bedrock is transmitted through the soil as vertically propagating shear waves under free field conditions, that is, the pile is not considered. For a simple elastic medium, such free-field motion could be calculated analytically based on the theory of one-dimensional S-wave propagation. For more complex problems involving nonlinear soil behaviour, computer programs such as SHAKE91 (Idriss and Sun, 1992), SRANG (Kagawa, 1980) and DEEPSOIL (Hashash *et al.*, 2001) can be used. The near-field soil, whose motions are affected by the pile, is modelled using springs or spring-dashpot assemblies. The pile is modelled as a series of beam elements. The motion of pile and simplified superstructure could be calculated using the finite difference method (e.g. Matlock *et al.*, 1978; Kagawa, 1983b) or

finite element method (e.g. Badoni and Makris, 1996). The main difference among these studies lies in the determination of the spring and dashpot properties.

In the early days, only linear elastic springs were used to model the near-field soil (e.g. Meem *et al.*, 1937). While such elastic parameters are relatively simple and easy to determine, such an approach was too simplistic for characterizing the complex nonlinear nature of soil behaviour. Later, an assemblage of nonlinear springs and linear dashpots was used to represent the inelastic soil supports (e.g. Matlock *et al.*, 1978). This was then followed by the use of nonlinear $p - y$ curves derived from lateral pile head loading tests or tri-axial tests to simulate the stiffness of near-field soil. The results from such analyses were compared with measurements from shaking table tests (e.g. Kagawa, 1983b; Nogami *et al.*, 1992; Kavvadas and Gazetas, 1993; Chacko, 1995). More recently, elastic-plastic springs in parallel were used to reproduce soil hysteresis, shear modulus degradation and the gap formation between soil and pile (Lok, 1999).

However, there are still several disadvantages related to the beam-on-dynamic-Winkler-foundation approach. These are as follows:

(1) The spring or spring-dash assembly works individually and cannot reproduce the interaction between the different soil layers.
(2) The existing model captures the kinematic effect of the near-field soil on the pile response, but does not account for the inertial loading on the pile due to soil motion.

(3) The approach was developed based on single pile response, and hence could not account for pile group effects under earthquake loading. Pile group analysis is typically carried out using the equivalent pier concept, in which the pile group is modelled as a single pile whose stiffness is scaled by the number of piles in the group (e.g. Lok, 1999). The reduction of soil resistance due to soil-pile interaction is incorporated into the method using p-y efficiency factors.

2.4.2 Pseudostatic Approach

The pseudostatic approach (e.g. Castelli and Maugeri, 2009; Elahi *et al.*, 2010) is essentially an extension of the beam-on-Winkler-foundation approach, wherein free-field soil displacement is first computed, often using a one-dimensional base excitation code such as SHAKE91 (Idriss and Sun, 1992). The instantaneous maximum displacement profile obtained from SHAKE91 is then applied to the free-field nodes of the soil springs and dashpots, with the nodes at the other end connected to the beam elements representing the pile. The static pile displacements, bending moments and shear forces are then calculated based on the prescribed displacements. Pile group effects are usually accounted for using p-multipliers or efficiency factors. The pseudostatic approach can, to some extent, reveal the mechanisms of seismic interaction among soil-pile-structure, and has been widely studied (e.g. Byrne *et al.*, 1984; Abghari and Chai, 1995; Wilson, 1998; Tabesh and Poulos, 2001; Liyanapathirana and Poulos, 2005; Goh and O'rourke, 2008; Castelli and Maugeri, 2009; Elahi *et al.*, 2010). Several such studies are summarized in Table 2-6.

One of the main issues with this approach is the evaluation of the spring stiffness coefficients. Several methods were proposed to determine these coefficients, such as the static Mindlin's solution (e.g. Tabesh and Poulos, 2001), modified API's (1993) recommended p-y curves (e.g. Wilson, 1998), horizontal subgrade reaction (e.g. Castelli and Maugeri, 2009), theoretical idealization of the elastic-perfectly-plastic model (e.g. Elahi *et al.*, 2010). All these methods are based on the pile response when subjected to lateral loading at the pile head. In some studies, the p-y spring values are back-deduced from shake table tests (e.g. Rovithis *et al.*, 2009). However, as discussed previously, inertial effects from the soil are likely to be under-represented in 1-g shake table tests. Hence, the p-y spring constants from 1-g shake table tests may not be representative of large-scale prototype behaviour. It is well-recognized that experimentally fitted p-y curves are much more representative of real situations than idealized or theoretical p-y curves. In static pile load tests under field conditions, the p-y curves can be readily obtained from lateral loading applied at the pile head. Under earthquake conditions, pile response is affected by loadings from super-structural as well as soil kinematic and inertia effects. As the latter contributions may occur over large segments of the pile length, earthquake loading conditions cannot be adequately simulated by merely head-loading a pile via a shaker at the pile top (Banerjee, 2009). Hence, earthquake p-y curves are not readily deduced from field tests. Instead, they are often obtained from shake table tests. In such cases, scale distortion may, in some cases, limit the usefulness of such p-y curves.

The inertial effects of the soil are also difficult to evaluate. In fact, it is uncertain if they are caused by the far- or near-field soil. Banerjee (2009) showed that ground surface motion of the soil in the vicinity of the pile is different from that of either the pile or the free-field soil. Similarly, p-multipliers are often adopted from static scenarios (e.g. Brown *et al.*, 1987) or else back-deduced from model tests (e.g. Shirato *et al.*, 2008).

2.4.3 Finite Element Method

The finite element method provides a powerful, rigorous, and flexible approach for seismic soil-pile-structure interaction problems. It can account for seismic soil-pile-structure interaction and pile group effects in a fully coupled way, without requiring independent calculations of superstructure or site response (e.g. Lu *et al.*, 2005; Uzuoka *et al.*, 2007). In principle, it is possible to simulate any arbitrary soil profile and to study three-dimensional effects (e.g. Huang *et al.*, 2004; Uzuoka *et al.*, 2007). Both liquefaction of sand and softening of clay could be reproduced with suitable soil constitutive models (e.g. Lu, 2006; Banerjee, 2009). The potential gap between pile and soil also could be simulated with interface elements (e.g. Lu *et al.*, 2005; Chang, 2007). Hence, this method has been widely used in research and practical design (e.g. Ahn and Gould, 1989; Guin and Banerjee, 1998; Lok *et al.*, 1998; Huang *et al.*, 2004; Lu *et al.*, 2005; Lu, 2006; Chang, 2007; Huang *et al.*, 2008; Lu *et al.*, 2008; Banerjee, 2009; Chau *et al.*, 2009; Mahboubi and Panaghi, 2010), and several typical cases are summarized in Table 2-5.

In practice, however, there are still several limitations associated with the use of the finite element method. First, it uses a finite computation domain to simulate the semi-infinite soil media, which will introduce several truncated surfaces at the boundaries of the model. Each truncated boundary surface will reflect or absorb vibrational energy, which may distort the calculations and adversely affect the results. In order to overcome this problem, Estorff and Firuziaan (2000) used boundary elements on the boundaries of the finite element domain, to simulate a semi-infinite medium. This approach was also adopted by Rizos and Wang (2002). Kim *et al.* (2000) formulated a three-dimensional transmitting boundary to reduce the influence of the reflected energy from lateral boundaries on the foundations. A similar absorbing boundary was proposed by Komatitsch and Tromp (2003). Javan *et al.* (2008) extended Kim's work to a new transmitting boundary for the dynamics saturated porous media. In another way, Wang *et al.* (2009) used an artificial boundary with spring and dashpots to analyze saturated porous media. However, all these artificial boundary approaches are frequency-dependant, and cannot absorb or transmit all passing energy in the time domain calculation. To date, there are still no transmitting boundaries which have good broadband energy absorption characteristics.

Another shortcoming of the finite element method is the large amount of computational resources required for large-scale problems involving big soil domains and complex foundations. As this method involves the calculation of the displacement degrees of freedom for all the nodes and strains/stresses for all the

integration points in the model at each time step, it may result in a long computational time when carrying out dynamic analysis involving thousands of time steps or more. Also, a very large memory is needed to store the temporary data generated during the calculations, especially for three-dimensional simulation and solid-fluid coupling simulation. In the early days of such computations, only small models with coarse meshes could be calculated (e.g. Trochanis *et al.*, 1988), as shown in Figure 2-7. Maheshwari *et al.* (2004b) proposed a successive-coupling incremental scheme to reduce the calculation size, as shown in Figure 2-9. In this method, the motions at the pile cap and the forces produced from the column bases are transmitted from one substructure to another when moving to the next time step. In order to simulate larger models, a parallel computational approach was incorporated into the finite element method. In this approach, the whole computation was divided into smaller parts and distributed to multi processors or computers (Lu, 2006). However, the maximum number of degrees-of-freedom in Lu (2006) studies was only about 364,800, because he used a sparse matrix solver which was not readily parallelizable.

The third drawback of the finite element method is that the results may depend significantly on the details of the algorithm such as the shape function, locations of integration points, integration quadrature, time-stepping method, strain and stress-retrieval algorithm as well as error correction algorithm, amongst others. These may not be transparent to the users, especially when using commercial software whose proprietary source codes are not made available. Hence, when using commercial software as a black box, one should not take for granted the

robustness of the computations and correctness of the results. For this reason, finite element computations often require validation before practical use. For example, Lu *et al.* (2005) used shaking table tests and Banerjee (2009) used centrifuge tests to evaluate their finite element calculations.

2.5 Earthquake research at the National University of Singapore

To address the limitation associated with the above design approach, and to better understand the fundamental mechanisms underlying seismic soil-pile-raft interaction, a research program was initiated at the National University of Singapore (NUS) in the late 1990s to study the seismic response of soft soil deposits and their interaction with foundation systems. Initial studies were carried out using sand and clay beds without any piles or structures present (Niu, 1997; Zhao, 1999)

Banerjee (2009) extended this work by carrying out experimental and numerical studies on the seismic response of pile-raft foundations constructed in soft soils. His work began with the laboratory characterization of the dynamic properties of the Malaysian Kaolin clay used in the experiments, focusing on the strain-dependent modulus reduction behavior, the strain-dependent damping ratio and the degradation effects under repeated cycling. A strain-dependent hyperbolic-hysteretic soil model was then proposed which incorporates the observed features of strain-softening and cyclic degradation.

Centrifuge experiments were then carried out by Banerjee to evaluate the seismic response of single piles installed in Kaolin clay beds. In his experiments, the piles were arranged in a 2×2 layout and a connected to a raft with prototype dimensions of 12.5m × 7.5m × 0.5m. To minimize interaction effects between the piles, the pile spacings were set at 11 and 6 diameters in the directions parallel and perpendicular to the strongbox shaking respectively. The results thus obtained may be considered representative of a single pile case. The loadings from superstructure were also considered by adding plates on top of the raft.

Banerjee (2009) also carried out 3-D finite element analyses that incorporate the hyperbolic hysteretic soil model to model the centrifuge experiments of the pure clay beds, as well as those containing the pile-raft systems. The results showed that the measured raft response and the bending moments in the pile could be reasonably captured by the 3-D analyses. The validated 3-D model was then used to carry out additional finite element analyses in which different soil, pile and earthquake parameters were systematically varied. The numerical results were compiled into a database for calibrating a semi-empirical relationship which estimates the maximum bending moment in the pile based on a series of dimensionless terms.

The piles used by Subhadeep (2009) have prototype diameters of 0.9m and pile lengths of 13m. Ma (2010) carried out additional centrifuge tests to examine the performance of more flexible piles with 0.5m diameters.

2.6 Summary of Pile Group Effects under Earthquake Loading

Although pile groups have been quite widely studied in the literature (e.g., Blaney and O'neill, 1989; Toki *et al.*, 1991; Sakajo *et al.*, 1995; Meymand, 1998; Rollins *et al.*, 1998; Lu, 2006; Uzuoka *et al.*, 2007; Banerjee, 2009; Basile, 2010), the discussion about pile group effects under earthquake loading is still quite scarce. Hence, there are still many unclarified issues related to earthquake effects on pile groups, especially for large-scale pile groups involving 100 piles or more.

Only small pile groups have been studied to date. As previously stated, field and model tests are limited to small pile groups, due to input energy and container size constraints. Most finite element studies to date, with the exception of Lu (2006), are also limited to small groups owing to time and resource constraints. Pseudostatic approaches are more computationally economical, but require some assumptions with regard to the p-y values and p-multipliers, or the back-deduction of such information from model tests. P-multipliers remain controversial in their usage and validity. Previous studies also indicated that group interaction effects are more pronounced for pile groups with a larger number of piles (e.g. Kagawa, 1983c). While small pile groups may be commonly found in bridge piers and highway infrastructure, large high-rise buildings are often supported on large base slabs with tens or hundreds of piles.

The influence of pile spacing on group effect is still unclear. Kagawa (1983a) performed a series of parametric studies using integral equation method (Kagawa, 1981) and found that pile-to-pile dynamic interaction was pronounced at spacing

ratios of up to 30 for the lateral vibration mode. However, Gohl (1991) conducted 1-g shaking table tests and centrifuge shaking table tests on 1x2 pile group with different pile spacings and orientations. He reported that, for inline shaking, pile-to-pile interaction effects are significant within a spacing of three pile diameters, dissipate rapidly from three to six diameters, and can be neglected beyond six pile diameters. For out-of-line shaking, interaction effects are only significant within three pile diameters.

Other pile-group related research considered only a fixed pile spacing in the group and did not examine the effect of spacing (e.g., Meymand, 1998; Wilson, 1998; Dungca *et al.*, 2006; Lu, 2006; Ilankatharan, 2008; Banerjee, 2009).

Many high-rise buildings have lengths or width of up to 50m. For instance, the flats built by the Housing and Development Board (HDB) in Singapore for public housing are often in the form of long slabs. The wavelength of the shear wave in soft marine clay is typically in the order of about 70m. In areas where soil profiles are variable over the length of the building, pile lengths will vary along the building and different parts of the same building may be subjected to different amplification and phase excitations of the wave, leading to differential motion along the length of the building. Such whole-building response has not been well-studied. Similarly, foundations of buildings with more complex footprint shapes have also not been studied. Experimental and analytical tools for such problems are still not readily available.

Nikolaou *et al.* (2001) developed a simple formula to calculate the maximum bending moment of a single pile in layered soil subjected to harmonic SH seismic waves. Banerjee (2009) proposed a semi-analytical solution for the maximum bending moment of a single pile subjected to earthquake loading and structural inertial loading. Tabesh and Poulos (2007) proposed a series of design charts for single piles in clay subjected to earthquake loading. The charts can be used for the determination of the maximum bending moment and shear force in the pile. However, all these methods are for single pile response.

From the preceding discussion, it can be seen that no well-established design framework for earthquake response of large pile groups exists at present. Towards this end, the objective of this study is to investigate the performance of large soil-pile-structure systems in order to better understand the seismic interaction mechanisms between the soft clay, the pile group, and the superstructure. The study scope consists of the following:

(a) Developing and implementing an efficient, highly parallelized earthquake code for the analysis of large pile groups on a discrete memory PC cluster, so as to achieve a cost-effective and highly scalable way of solving very large finite element problems.

(b) Using this code to conduct detailed parametric studies involving the effects of pile group size, pile-to-pile spacing, pile stiffness and structural mass on the foundation performance.

(c) Conducting detailed parametric studies on the raft response and pile bending moments for stiff rafts supported on very large pile groups.

(d) Using dimensional analysis to derive simple relations for estimating the maximum bending moments and the moment distribution along the pile, based on the results of (c).

(e) Using the parallel code to examine some scenarios involving non-uniform or uneven soil stratigraphy and different earthquake motions.

Table 2-1 List of full-scale field pile tests

Reference	Brief description	Main conclusion	Remarks
Scott *et al.* (1982)	Both horizontal forced vibration and ring-down tests were conducted on a steel pipe pile in silty sand	Liquefaction was observed in the soil surrounding the pile. Damping and resonant frequencies were found to be dependent on the level loading	One of the first to conduct liquefaction test around pile
Crouse and Cheang (1987)	Quick-release vibration tests were performed at the Quwamish substation. The foundation consisted of a concrete pile cap with eight vertical and eight battered piles. All piles were embedded in 12.2m of loose sand overlying stiff glacial till.	The experimental and analytical results indicated that there was a lack of interaction between the pile cap and the supporting soil. The damping in this foundation model was shown to be substantially less than the one in the same foundation without piles.	The quick-release vibration test is easy to conduct and could provide some fundamental information about pile foundation.
Brown *et al.* (1987) and Brown *et al.* (1988)	Two-way, cyclic, lateral loading was conducted on a large-scale group. The piles were arranged in a 3 × 3 pattern spaced at three-time diameter in both directions. The sub-surface profile consisted of stiff, over consolidated clay to a depth of 13.1m with water above the ground surface.	The depth of the maximum bending moment increased from front row to back row. The bending moments were greater for the piles in the group than the single pile and occurred at greater depths. The front and middle row experienced similar maximum bending moments whereas the back row was lower in magnitude (see in Figure 2-1).	It provided a convenient way of expressing the soil resistance rduction due to group effect, “p-multiplier”.
Blaney and O'neill (1989)	A series of lateral dynamic loading tests on a single pile and a 3×3 group of steel pipe piles. All piles were driven into overconsolidated clay at centre-to-centre spacing of 3 times the pile diameter. The piles used were 0.237m in diameter and 13.7m in length. The load was applied horizontally through the pile head using an inertial mass vibrator.	Comparing the response of the pile group and a single pile, the equivalent per-pile response of the group was found to exhibit lower damping and more flexibility than a single pile. The deflected shape of the group piles at the system first mode resonance frequency resembled the single pile shape under static and dynamic load.	The fundamental characteristics of dynamic interaction between pile groups and soil was investigated. That could be used to evaluate the numerical simulation.
Kobori *et al.* (1991)	An extensive series of tests on a pile group were conducted with different pile cap contact/embedment conditions. It	The results indicated the backfill embedment has strong influence on group stiffness.	The forced vibration tests were actuated by dynamic loading on the pile caps.

	consisted of horizontal forced vibration tests and earthquake observations.		
Lam and Cheang (1995)	Slow-cyclic loading tests and fast-rate vibratory loading test were conducted on the same full-scale piles. The piles were 61cm in diameter and 10m in length, and were submerged in sand site.	For the lower loading amplitude, the loading rate didn't influence the $p-y$ curves; but for the higher loading amplitude, the pile stiffness tested from fast vibratory test was much lower than the one from slow cyclic tests.	The difference between cyclic loading tests and vibratory tests should be paid attention to, especially for the sandy site.
Rollins *et al.* (1998)	A static lateral load test was conducted on a 3x3 pile group with a 2.82 spacing ratio. The pile head is connected with a joint. The soil consisted of soft to medium-stiff clays overlaying dense sand.	The deflection of pile group was more than twice of the single pile, applying the same average loading. Bending moments for piles in a group were much larger than the isolated single pile.	The pile group effects were discussed based on the test results. These tests typically involved only one cycle of loading.
Snyder (2004)	Statnamic load test on 15-pile group were carried out in soft Salt Lake City clay which prevents the development of high compressive and tensile stresses that can potentially damage the test pile (see in Figure 2-2).	The average group load was 10 to 15% lower than the single pile load for deflections up to 38 mm, and approximately 20% lower for higher deflections. Maximum bending moments in the trailing rows were as much as 40% larger than the single pile, but occurred at similar depths. The maximum bending moments in the lead row occurred at shallower depths than the single pile and trailing rows.	The statnamic load test was conducted after 15 static cyclic loading tests on the same piles which caused gaps between soil and pile. So the results from statnamic load test may not reflect the virgin pile group.
Rollins *et al.* (2005)	Lateral loading test was conducted on a full-scale pile group following blast-induced. The 3x3 pile group at 3.3 pile diameter spacing was driven into loose to medium dense sand. Another single pile test was conducted for comparison.	In contrast to pre-liquefaction tests, group interaction effects were insignificant after liquefaction. The lateral resistance of each pile in the group was similar and about the same as that for the single pile test.	It provided information about soil resistance and pile group effect for post-liquefaction.
Agarwal *et al.* (2010)	Two, quarter scale, two-column, bridge bents were constructed. Two NEES mobile shakers were used to excite the surface of the ground and excite the bent cap, respectively. The loading histories used included (a) stepped sine, (b) chirp, and (c) fixed shine, for both shakers (see in Figure 2-3).	The response of the structure when excited directly was essentially the same as that when the ground was excited. However, the observed natural frequencies when the structure was excited directly were slightly less than those observed in when the ground was shaken.	The natural period of pile-soil system was discussed.

Table 2-2 Summary of 1-g shaking table pile tests

Reference	Brief description	Main conclusion	Remarks
Mizuno *et al.* (1984)	A 2x2 pile group with 1/30 similitude ratio embedded in two-layered clay was oscillated with records of Off Miyagi Prefecture Earthquake (1978) and Central Chiba Prefecture Earthquake (1980). The height of the building was ignored in the modeling. The cast-in-place piles were modeled with steel pipe pile with 71.7cm length. Pile head was fixed and its tip was hinged	The soil deformations may cause large bending moment in the pile. The bending moment at the interface of two layers is larger than that at the same depth of the one-layered subsoil. Effects of soil movement on piles during earthquake should be taken account into design of lateral resistance of piles.	The effects of the building inertia force and the soil movement on piles in the system was emphasized. The pile group was not clearly illustrated and the effects of pile group were not discussed.
Stanton *et al.* (1988)	The shaking table tests were conducted in University of Washington. The model pile was made of stainless steel tubing with 114mm length and 3.2 mm outer diameter. The specimen sand was contained in a flexible cylindrical shear bag with 122mm height and 122mm diameter. Sinusoidal base motions were used for tests.	The response of piles embedded in a soil deposit subjected to base excitation is controlled by the characteristics of the complete soil profile. To predict the response accurately the variation in shear modulus with depth must be accounted for, but a single value of damping for the whole soil mass is adequate.	The sand specimen might be too low to reflect the real stress status.
Gohl (1991)	Single and pile group (2 × 2) were subjected to sinusoidal and random earthquake excitation using University of British Columbia Earthquake Laboratory shaking table. C-109 Ottawa sand, an average particle size 0.4mm and a coefficient of uniformity 1.5, a peak friction angle 33°, was prepared as foundation in a rigid container bolted to the shake table. The model pile was hollow aluminum tubing with an outer diameter 6.35mm.	The seismic interaction between piles is significant during inline shaking for centre to centre pile spacing of up to six pile diameters, while during offline shaking, pile to pile interaction could be ignored for all practical purposes.	Although two 25mm thick Styrofoam pads were placed at each end of the container, the wave reflection from the sides of the rigid box still have significant influence to the results.
Meymand (1998)	The shaking table tests were performed on the earthquake simulator at the	Tests evaluating pile raft performance and the effects of impounded water souring the	The clay specimen may not be consolidated when the tests were

	Pacific Earthquake Engineering Research Center. A flexible wall container confines soil column 2.29m in diameter up to 2.13m in height. Single pile and pile group were driven into the soil after the soil was preloaded. Besides the seismic motion test, static lateral load tests, hammer blow test, sinesweep test were also conducted at the same piles. Earthquake records were input both in one direction and in two directions.	soil-pile gap and degrading resistance were somewhat inconclusive. The influences of 2-D shaking were seen to be minimal, as structural inertial forces tended to resolve the motion to a strong axis for the simple single degree of freedom models tested.	done. The consolidation degree has vital influence on the stiffness and strength of clay. Without suitable consolidation, the soil specimen may not reflect real properties. The pile and pile group were too close to the container wall which may influence the seismic response of piles (see in Figure 2-4).
Tao *et al.* (1998)	A real-size pile embedded in a sand layer with a thickness of over 5m was subjected to simulated seismic shaking using a large-scale shaking table. The model pile was a steel pipe with outer diameter of 0.32m and length of 6m, and was pinned to the laminar shear box.	The $p-y$ relationships were estimated using the strain gage data, and it was found that the $p-y$ stiffness, p/y, was approximately equal to the Young's modulus of soil.	It might be the largest-scale shaking table test, with equal size to prototype pile. However, it just conducted a single pile with free head and didn't illustrate and discuss the bending moment of pile.
Jakrapiyanun (2002)	The model piles of the pile group were made of aluminum with an outer diameter of 57.15mm, an inner diameter of 55.37mm, and a length of 863.6mm. The spacing between each pile is 171.45mm (3 pile diameters). The pile group was a skin-bearing foundation: the pile tips were neither fixed nor pinned to the container. To increase skin friction, sand was glued to the aluminum piles. The aluminum plates were welded to the pile head as pile cap, and the superstructures were inserted into the pile cap to investigate the inertia effect.	Horizontal soil-foundation stiffness is lower due to gap at pile gap level. The soil-pile cap stiffness is significant to total lateral soil-foundation stiffness. Pile cap side-soil contact has less influence to the rotational stiffness than pile cap base-soil contact. The soil-foundation-structure interaction effect could extend up to 35%, even for relatively low input motions.	The thesis mainly discussed about dynamic soil-shallow foundation-structure interaction and pile foundation shaking test was conducted and discussed simplified.
Wada *et al.* (2002)	A method was proposed to use two groups of piles supporting the building. One group has long-flexible piles for the building gravity weight and the other group has short-stiff piles resisting the	The decrease in shear force distribution factor obtained from the horizontal stiffness of the support piles and the capacity of the earthquake resistant piles to absorb additive energy in their vicinity decreases	The proposed method should be very useful for pile foundation design to earthquake force.

	lateral forces due to earthquake ground motion. A small shaking table test of soil-pile-structure interaction was used to verify the idea. The shaking table tests performed for 16 cases with different pile conditions, subjected to 3 earthquake ground motions.	the bending moment in the support piles and decreases the input power of earthquake to the superstructure.	
Tokimatsu *et al.* (2005)	A series large shaking table tests were conducted on pile-structure models with a foundation embedded in dry and liquefiable sand deposits. A2x2 steel pile group that supported a foundation with or without a superstructure was used. Each pile had a diameter of 165.2, and their tips were connected to the container base with pin joints and their heads were fixed to the foundation that was embedded in the ground.	If the natural period of the superstructure, T_b, is less than that of the ground, T_g, the ground displacement tends to be in phase with the inertial force from the superstructure, increasing the shear force transmitted to the pile. In contrast, if T_b is greater than T_g, the ground displacement tends to be out of phase with the inertial force, restraining the pile stress from increasing, as shown in Figure 2-5.	The results and discussion made it possible to estimate maximum pile bending moment from superstructure and earth pressure separately.
Shirato *et al.* (2008)	The experiments were conducted using a $4m \times 4m$ large-scale shaking table and a large flexible shear stack housed in Public Works Research Institute, Japan. The pile-group comprised a 3×3 box arrangement of nine steel piles. The piles were hollow steel pipes with a round-cornered rectangular section with $0.125m$ width and $3m$ length, and the nominal center-to-center distance was 2.5-times the pile diameter. The pile head was embedded into the pile cap and pile base was fixed on pinned supporting device. The soil specimen used was dry sand with internal friction angle 40.9°. Sinusoidal waves and an earthquake record from Kobe Earthquake (1995) were used as input.	The soil resistance intensities of the piles in different row differ markedly, even at the same displacement level, while those of the piles in the same row were very similar. The positive and negative amplitudes of soil resistance were different which rose from the group effect. The shape of single pile $p-y$ curve was soften together with the decrease in the ultimate soil resistance, accounting for the group effects on the lateral load transfer between soil and pile. The corner piles were expected to be less affected than other piles. The group efficiency decreases with increasing displacement level, and generally tends to converge to constant values at a displacement level of approximately of 5% of the pile diameter.	The paper proposed and validated a method that it's used measured bending moments to calculated soil resistance. With the soil resistance time history, the $p-y$ curves were discussed in details. The group effects and group efficiency were discussed and a method was proposed to incorporate the group effect during large earthquakes into any hysteretic $p-y$ curve models.

Ueng (2010)	Liquefaction model tests were conducted using a large biaxial laminar shear box on the shaking table. Clean Vietnam silica sand and Mailiao sand with silt were used. A single pile was placed inside the shear box to evaluate the pile performances and soil-pile interaction. The pile was fixed at the bottom of the shear box to simulate the condition of a pile foundation embedded in rock, and additional rigid steel adapters were fixed to pile head to simulate the inertia force from the superstructure.	Under small amplitude shakings, the pile response with small inertia force from superstructure was dominated by the kinematic force from the soil motion, but the one with a larger inertia force was mainly governed by the inertia force from the superstructure. Under large amplitude shakings, after the whole specimen liquefaction, the pile motions reduced in amplitude and remained steady to smaller vibrations of the same frequency as that of the input motion while the soil motions diminished.	The bending moment along the pile was measured but was not illustrated or discussed.

Table 2-3 Summary of centrifuge shaking table pile tests

Reference	Brief description	Main conclusion	Remarks
Gohl (1991)	Both two and four (2×2) pile tests were conducted at Caltech centrifuge, operating at $60g$. The soil container was $0.56m\ length \times 0.18m\ wideth \times 0.25m\ height$, with rigid wall. The specimen soil was Nevada 120 sand, with average particle size 0.13mm and coefficient of uniformity 1.6. The model pile was mad of 9.52mm outer diameter stainless steel tube. A mass was screwed to the pile head to simulate the influence of a superstructure. Sinusoidal motion and earthquake records were input via an electro-hydraulic system.	The location of maximum bending in a model pile tested in the 1-g shaking table is much greater relative to its diameter than that was observed for similar intensities of shaking on the centrifuge. For inline shaking, interaction effects are stronger than predicted using elastic theory for close pile spacing less than about 3 pile diameters. For larger pile spacing, interaction effects die off at a much quicker rate than predicted using elastic theory.	The study conducted and compared 1-g shaking table test and centrifuge test.
Wilson (1998)	A series of dynamic centrifuge test of pile supported structures were conducted on UC Davis centrifuge at a centrifugal acceleration of 30g. The soil profile consisted of two horizontal soil layers. The lower layer was dense sand while the upper layer was medium dense sand or normally consolidated clay. Foundation models included single pile foundations, four-pile group and nine-pile group. The pile tips were about 5.5 pile diameters above the container base.	It was found that changing the pore fluid viscosity by a factor of 10 to better simultaneously model dynamic and consolidation processes had apparently little effect on the seismic soil-structure interaction. The measured time histories of bending moments along pile and accelerations of soil profile and pile were used to back-calculate $p - y$ curves.	The study conducted quite comprehensive tests on dynamic response of pile foundations in soft clay and liquefying sand during strong shaking. However, it focused solely on the behavior of single-pile-supported structure, and seldom analyzed the pile-group-supported structures recorded.
Boulanger *et al.* (1999)	The centrifuge tests included two different single-pile-supported structures subjected to nine different earthquake events with peak accelerations ranging from 0.02 to 0.7g. Models were tested in a flexible shear beam container with a centrifugal acceleration of 30g at UC	The measured acceleration and bending moment were used to evaluate a dynamic beam on nonlinear Winkler foundation analysis method for analyzing seismic soil-pile-structure interaction. It obtained reasonably good agreement between	The results of the centrifuge tests provided experimental support for the use of dynamic $p - y$ analysis methods in seismic soil-pile-structure interaction problems.

	Davis centrifuge. The soil profile consisted of soft clay overlying dense sand.	calculated and recoded response for structural models in all earthquake events.	
Curras *et al.* (2001)	Centrifuge model tests on the seismic response of a pile-group-supported structure were conducted on the 9m radius centrifuge at UC Davis. Single and nine-pile group were founded in a profile of soft clay over dense sand. The pile group consisted of nine pile spaced at four diameters on center in a 3x3 gird. Each pile was equivalent to a 0.67m diameter steel pipe pile. Nine different earthquake motions having peak base accelerations of $0.02 - 0.7g$ were input from the shaking table.	The dynamic centrifuge model tests were used to evaluated a beam on nonlinear Winkler foundation analysis method for soil-pile-structure interaction. Reasonable agreement was obtained between calculated and recorded responses in all nine earthquakes when the interpolated recorded soil profile motions were used.	The results of the centrifuge tests provided experimental support for the use of dynamic BNWF analysis methods in seismic soil-pile-structure interaction problems involving pile groups.
Kagawa *et al.* (2004)	The authors conducted three cases using centrifuge shaking table test to simulate large-scale shaking table test(Tao *et al.*, 1998) about free field response and soil-pile-structure interaction. The centrifuge test treated the large-scale models as their prototypes. The sand from Lake Kasumigaura with mean particle diameter of 0.31mm and coefficient of uniformity of 3.0 was used.	It's found that carefully designed performed centrifuge tests could reproduce the key features of the response of the large-scale models. However, there were still some differences between the results from the two types of tests. The small-strain dynamic magnification factors of the sand layers were smaller in centrifuge models. The excess pore water pressure in the two systems was redistributed differently. And the response of the piles and the structural models were not in good agreement.	It might be the first study to involve extensive comparisons between the results from large-scale and dynamic centrifuge tests on geometrically similar soil-pile-structure models.
Chang (2007)	A series of eight dynamic centrifuge model experiments of pile foundations in liquefied and laterally spreading soil profiles was performed on UC Davis centrifuge. Soil profiles consisted of non-liquefiable clay crust overlying saturated loose sand over dense sand. A simple superstructure supported on a group of six prototype 1.17m diameter pipe piles.	It mainly studied the large crust load of lateral spreading crust on the pile foundation, and its relation with the inertial loads from the superstructure mass and pile cap mass. It was found that the crust load was a major driving force with low-frequency components, and it might act with inertial loads simultaneously on the pile cap.	The tests illustrated the dynamic loading of pile-supported structures in laterally spreading ground during earthquake shaking, and distilled the complex dynamic behavior into simple concepts for equivalent-static design methods.

	A sequence of scaled earthquake records was applied to the model base.		
Ilankatharan (2008)	Three series of centrifuge test about seismic soil-pile-bridge interaction were conducted in UC Davis. The model included four identical two-pile bents. All model piles were made of aluminum tubes of 19.05mm diameter. The soil used was dry Nevada sand, 80% relative density. Step displacement waves, frequency sweeps and scaled records of the 1994 Northridge Earthquake were input base.	A difference in prototype bent spacing between the centrifuge and 1-g shaking table models in addition to the interaction between the 1-g shake table bridge model caused some discrepancies between centrifuge results and 1-g shaking table result. There were also differences in spectral ratios that may be attributable to different energy dissipation mechanisms in centrifuge and 1-g shaking table tests.	One part of NEES collaborative research project to study soil-foundation-structure interaction. Agarwal *et al.* (2010) conducted field tests with quarter scale bridge, Johnson (2006) conducted 1-g shaking table test for two-span bridge with a quarter scale.
Banerjee (2009)	The shaking table tests for both pure kaolin clay beds and clay-pile-raft systems were conducted on NUS centrifuge. Remolded kaolin clay with inter friction angle 25° was placed and consolidated in a laminar box. The pile foundation consists of four piles and a steel pile cap. The piles were 1.8cm in diameter and 26cm in length. The pile-to-pile spacing is six and eleven times of pile diameter in two directions. Three earthquake accelerations of 0.022g-0.1g were input from shaking table.	The centrifuge test results indicated that the bending moment increase almost linearly with the scaled earthquake ground motion, and increase with the flexural rigidity of the pile material and additional mass on the pile raft. The measured acceleration and bending moment were used to validate finite element simulation on seismic clay-pile-raft interaction.	The tests indicated the influence of clay softening on the predominant period amplification of free-field ground motion and pile foundation during earthquake.

Table 2-4 Summary of beam-on-dynamic-Winkler-foundation approaches

Reference	Brief description	Main conclusion	Remarks
Meem *et al.* (1937)	A method was proposed for the analysis of Feagin's test data. The interaction between soil and pile were represented by elastic springs and the spring constant was assumed to be constant with depth.	The method could solve deflections, moments and shears in the piles. With the calculation results, Chang firstly introduced the concept of critical pile length.	Although the method is too simple to indicate the nonlinear characteristics of soil, it's still widely used today because its parameter is easy to determine.
Matlock *et al.* (1978)	A dynamic analysis for lateral soil-pile behavior was developed and implement in a beam-column computer program, SPASM (Seismic Pile Analysis with Support Motion). The single pile was discrete and restricted to linearly elastic. The superstructure was also simulated with increased stiffness beam, as shown in Figure 2-6.	The method was used to simulate three example and the results appeared to be consistent and reasonable in all respects.	It was a fully coupled method for analysis of single pile response. It was evaluated by Gohl (1991) with centrifuge shaking tests.
Gohl (1991)	Besides carried out a fully coupled analysis of single pile response using SPASM, the author also developed a computer model (PGDYNA) to analyze the dynamic response of a superstructure supported by a pile group.	The computed results indicated that prediction of pile group response were complicated by uncertainties in the degree of radiation damping to be expected in the system and by an inadequate knowledge of what effective input motions should be used in the analysis. The effects of kinematic interaction appeared to be more pronounced for pile groups than for single piles.	The kinematic interaction effects were neglected in PGDYNA, which appeared reasonable for small pile groups. However, for large pile groups, the effects of kinematic interaction could cause a significant reduction in effective motions transmitted to the pile group.
Kavvadas and Gazetas (1993)	A versatile beam-on-dynamic-Winkler-foundation model was developed and calibrated. The estimation of the spring stiffness was based on 3D finite element results. The viscosity of the associated Winkler dash-pots was used to reproduce the radiation and hysteretic damping of the system.	The model was used to simulate a free-head pile embedded in a multi-layered soil profile subjected vertically-propagating S-waves. The results indicated that the pile bending moment depends on the stiffness contrast of soil layers, pile rigidity, and excitation frequency.	Based on the results, a closed-form expression for pile bending moment at the interface of two layers soil was derived which is quite useful for seismic pile design. However, it ignored the inertia effects of structure and pile foundation.

Lok (1999)	A coupled model for the analysis of the seismic soil-pile-superstructure interaction was formulated, implemented and calibrated. The model included three parts, hysteretic model for site response analyses, nonlinear one-dimensional element for near field response, and the beam on nonlinear Winkler foundation model for the soil-pile-superstructure system.	The model was evaluated against the large-scale shaking table test by Meymand (1998). The calculated spectral accelerations of the superstructures, the pile bending moments and $p-y$ curves were comparable to the experimental data. The model was also applied to the analysis of pile groups using the equivalent pier concept and provided reasonably agreements with the observed responses of small pile group.	The proposed model could reproduce experimental shear modulus degradation and damping curves for clays, silts, and sands. It also had the capability to deal with the gap between pile and soil.

Table 2-5 Summary of Finite Element Methods

Reference	Brief description	Main conclusion	Remarks
Kuhlemeyer (1979)	An efficient finite element solution for static and dynamic pile response. A homogeneous soil profile was used for dynamic loading.		Linear elastic model was used for soil and pile.
Trochanis *et al.* (1988)	Three-dimensional analysis for single pile subjected lateral cyclic loading was performance with ABAQUS. 27-node quadratic isoparametric elements were used to model pile and soil, and 18-node thin-layer interface elements were placed around pile elements. Pile was elastic while soil was idealized as Drucker-Prager plastic material, as shown in Figure 2-7.	The results indicated that the inelastic soil behavior could affect the pile response significantly. Pile-soil separation and inelastic soil deformation were the crucial factors for lateral loading simulation. Based on the results, a simplified Winkler type model was developed.	Both slippage and gapping were considered at the soil-pile interface by using interface element with Coulomb's friction theory.
Wu (1994)	Based on a simplified 3-D wave equation, a quasi-3D finite element computer program PILE3D was developed for the analysis of non-linear response of pile foundations in the time domain. It simulated the 3D dynamic response by displacements in the horizontal shaking	Single pile and small pile group subject strong seismic shaking were simulated and validated with centrifuge tests. The analyses could reproduce the stiffness reduction and damping increment of the pile foundations with the increased level of shaking.	The method could greatly save computing space and computing time for the finite element analysis, and widely used by the author and others (e.g. Wu and Finn, 1997a; Wu and Finn, 1997b;

	direction, and neglected the displacements in the vertical direction and in the horizontal cross-shaking direction, as shown in Figure 2-8. The soil non-linearity was modeled using a modified equivalent linear method and yielding was taken into account.		Finn, 2005; Maiorano *et al.*, 2009).
Maheshwari *et al.* (2004b)	Single pile and 2-pile group embedded in clay subjected either harmonic or transient bedrock motions were simulated, a three-dimensional finite element program. The analyses involved a subsystem model and a successive-coupling incremental scheme, as shown in Figure 2-9.	Soil nonlinearity increased the responses at low and moderate frequencies, but at high frequencies, its effect could be negligible. The pile effect could reduce the effect of soil nonlinearity, and decrease the peak values of the pile foundation response.	The proposed successive-coupling incremental scheme could reduce the required computation space, which makes it possible to use small computer simulate relative large-scale problem.
Lu *et al.* (2005)	A shaking table model tests was simulated, three-dimensional finite element model, with ANSYS. Contact elements were used at soil-pile interface.	The comparison of calculated and test results indicated that the modeling calculation was rational. The bending moment is the largest at the corner pile, moderate at the middle pile in the side row, and smallest at the center pile.	The calculation was validated with the corresponding shaking table test. A small pile group with 9 piles was simulated and the pile group effect was briefly discussed.
Lu (2006)	A parallel finite element program was developed with incremental plasticity and coupling solid-fluid formulation. A large-scale simulation on pile-supported wharf system was conducted on a supercomputer, as shown in Figure 2-10.	Large-scale modeling on parallel computers was an effective way to simulate the dynamic soil-structure interaction. It could provide a better understanding of seismic behavior.	Parallel calculation was used in finite element analysis. It makes possible to simulate large-scale and complex soil-pile-structure interaction. The pile-supported wharf system was simulated very well, but the results were not discussed in details.
Chang (2007)	A two-dimensional nonlinear dynamic finite element model was developed on the OpenSees platform and calibrated with centrifuge shaking table tests. The saturated soil was modeled as a two-phase material with $u - p$ formulation based on the Biot theory. The dynamic soil-pile interactions were modeled with	The comparison indicated that the dynamic finite element analysis agreed well with the centrifuge tests for the overall soil and structural responses. The influences of liquefaction, pile stiffness structural mass and period, crust strength and displacement, and base motion were studied.	The developed two-dimensional finite element model with spring interface elements could capture the important mechanisms of load transfer and illustrate soil-pile interaction. However, it's quite difficult to determine the many parameters.

	zero-length nonlinear springs (see in Figure 2-11 and Figure 2-12).		
Uzuoka *et al.* (2007)	The damage process of a pile-group supported building in reclaimed land was simulated using three-dimensional finite element analysis. The coupling $u-p$ formulation was used to simulate the pore water pressure increment and liquefaction process.	pile yields before the complete liquefaction of reclaimed layer. The pile curvatures were mainly affected by inertial effects of superstructure before complete liquefaction, while the kinematic effect of foots on pile curvatures was considerable after complete liquefaction (see in Figure 2-13).	The liquefaction process and post-liquefaction were simulated, and evaluated against field records. The building was simplified and only twelve piles were modeled.
Javan *et al.* (2008)	Explicit dynamic finite element method, pile groups in saturated porous media, based on $u-w$ formation. A centrifuge shaking table test model (Wilson, 1998) was simulated and compared with measured data.	The effect of transmitting boundary was discussed by comparing the simulation using and without using transmitting boundary were compared	A new transmitting boundary was used to avoid wave reflection towards the structure.
Banerjee (2009)	Centrifuge model tests for soil-pile-raft system were back-analyzed using ABAQUS. Hyperbolic-hysteretic constitutive model was developed to model the dynamic properties of soft clay.	The computed results were evaluated with experimental observations. The numerical model could reasonably replicate the centrifuge tests. Based on the parametrical studies, a semi-analytical solution for the maximum bending moment was proposed.	The pile spacing is about eleven times of diameter, and the pile group effect was ignored. The detailed discussion on pile bending moment and the closed-form solution are very useful to study the seismic performance of pile foundation.
Dezi *et al.* (2009)	soil-structure kinematic interaction, single piles and pile groups, embedded in layered soil deposits, using elasto-dynamic Green's functions.	Rigid caps were modeled by constraining the displacements of the pile heads to those of a rigid body. The foundation impedances and the foundation input motion for the inertial interaction analysis of generic spatial superstructures.	The dynamic response of the soil-foundation system was evaluated and the stress resultants due to the ground motion in each pile were calculates.
Maheshwari and Sarkar (2011)	A finite element program was developed in MATLAB to model three-dimensional soil-pile-structure system. A 2x2 pile group in liquefiable soil was simulated.	Once the soil medium gets liquefied, the effect of relative rigidity of pile and soil loses its significance for the dynamic stiffness of the soil-pile system.	A simple model has powerful function.

Table 2-6 Summary of Pseudostatic Approaches

Reference	Brief description	Main conclusion	Remarks
Byrne *et al.* (1984)	A method was proposed to determine the pile response subjected to free-field soil displacement. The free-field displacement was applied to the pile via a series of springs. Then the pile was analyzed with Euler beam theory.	The method was used to analyze a casing within a caisson-retained island subjected to severe ice loading. The reasonable results showed the proposed method had promise.	Although this method did not take the inertial effects into account, it provides a methodology to analyze pile response which is widely used for pseudo static approaches.
Abghari and Chai (1995)	A pseudo static method was proposed to analyze a simplified soil-pile-structure interaction. The pile was subjected to maximum free field soil displacements and the part of superstructure inertial forces. The initial forces were calculated from the product of mass and spectral acceleration.	The pseudo static analysis could reasonably provide maximum pile bending moment and shear force, with maximum soil displacement plus 50% superstructure inertial forces.	The conclusion was based on only one simulation, which might lack persuasion. Actually, it's needed to further discuss how much structure inertial forces should be accounted for.
Wilson (1998)	Based on centrifuge test results, pseudo static analyses were conducted and compared with the recodes. The measured superstructure inertial forces were applied to the pile and measured soil deformations at the snapshot were applied to the ends of the $p-y$ springs. Baseline sets of $p-y$ springs were established using API(1993) recommended curves and the p-multipliers were calibrated via repeatedly analyses.	When the superstructure inertial loads were typically larger than the kinematic loads from soil profile displacements, the pseudo static analyses could give reasonable results for design. However, it's not clear for cases of large kinematic loading.	In the study, the measured inertial loads and soil deformations were available for input. However, in other cases, the estimation of inertial loads and soil deformation should be very challenging.
Tabesh and Poulos (2001)	Abghari and Chai (1995)'s method was developed to take the superstructure natural period into account. The lateral force was obtained from multiplication of cap-mass and the spectral acceleration corresponding to the structure natural period.	When the structure mass is small and the pile response is determined by the free-field movement, the method could give accurate result; on the contrary, when the pile response is dominant by cap-mass, the method would give underestimated results.	All calculations are based on elastic theory, and the nonlinear behavior of the soil is not considered.

Liyanapathirana and Poulos (2005)	Pseudo static approach was developed for analysis of pile in liquefying soil. The influence of soil liquefaction was considered in both stages. At first stage, the free-field response analysis was based on effective stress. And the nonlinear springs based on degraded soil stiffness was used to connect pile and free-field soil.	The computed results of several examples could agree well with the results from another dynamic method, which might indicated the proposed pseudo static method had promise in practical applications. And the method was evaluated with the pile performance observed in a centrifuge test and a real earthquake.	The method did not take the superstructure natural period into account, and all the cases to verify the method were free head piles or light head piles, so it should be careful to use this method for analysis of piles with heavy head.
Castelli and Maugeri (2009)	Liyanapathirana and Poulos (2005)'s method was developed to calculate the response of single pile and pile group. A hyperbolic p-y relationship was proposed based on horizontal subgrade reaction. And an empirical factor was used to simulate the influence of pile group effect on p-y curves.	Among all factors influencing pile bending, the most important is the pile deflection, especially when the soil is homogeneous or the stiffness ratio of the soil layers is low. The maximum moments can be also underestimated if a linear elastic analysis is carried out instead of a nonlinear analysis, to take into account that the lateral pile response to static and dynamic loading is typically nonlinear.	The proposed method could successfully provide the response of a single pile and pile group during earthquake.
(Elahi *et al.*, 2010)	Tabesh and Poulos (2001)'s work was extended for elastoplastic pseudo static analysis of pile group. The static pile-soil-pile interaction was reproduced using a matrix of soil-displacement-influence factors. An elastic-perfectly-plastic model was used for p-y curves to illustrate soil yielding behavior (see in). The method was developed a computer program, PSPG, and was verified with centrifuge tests results and instrumented real pile-supported structure.	When the inertial force is larger than the kinematic force, group effects have less contribution to pile group response. While if kinematic force becomes dominant, group effects have more influence on the response. The proposed method was reliable when the pile cap natural period was larger than twice period of maximum spectral acceleration of surface motion.	It provided an efficient approach to study the seismic soil-pile group-structure interaction using static pile-soil-pile influence factors. It should be cautious to use this method when the natural period of structure is close to the one of the field.

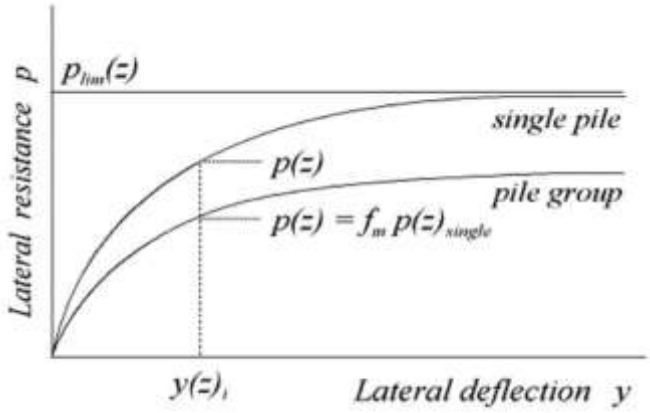

Figure 2-1 p-y multipliers for group effects (Brown *et al.*, 1988)

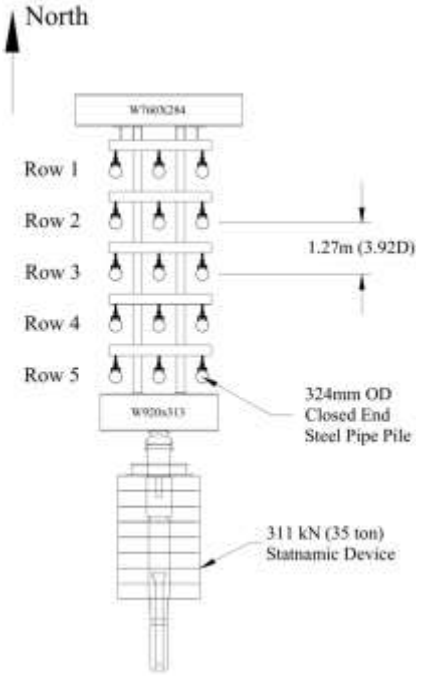

Figure 2-2 The layout of statnamic lateral load tests(Snyder, 2004)

Figure 2-3 Harmonic excitation using shaker from Thumper (Agarwal *et al.*, 2010)

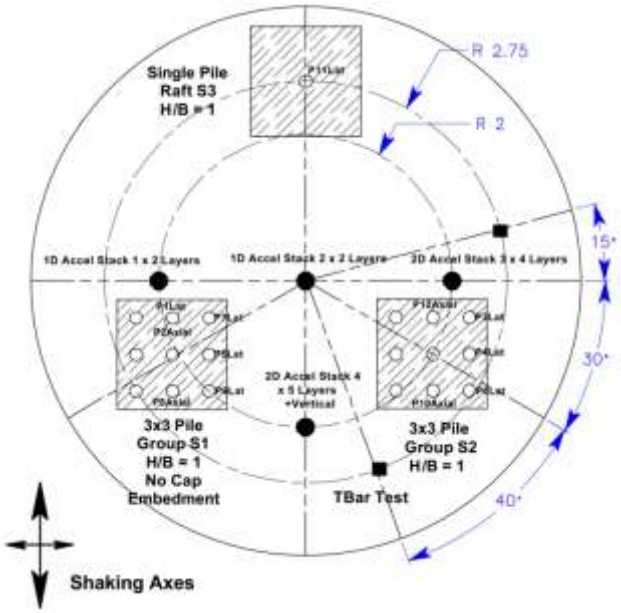

Figure 2-4 Layout of multi test in one soil specimen (Meymand, 1998)

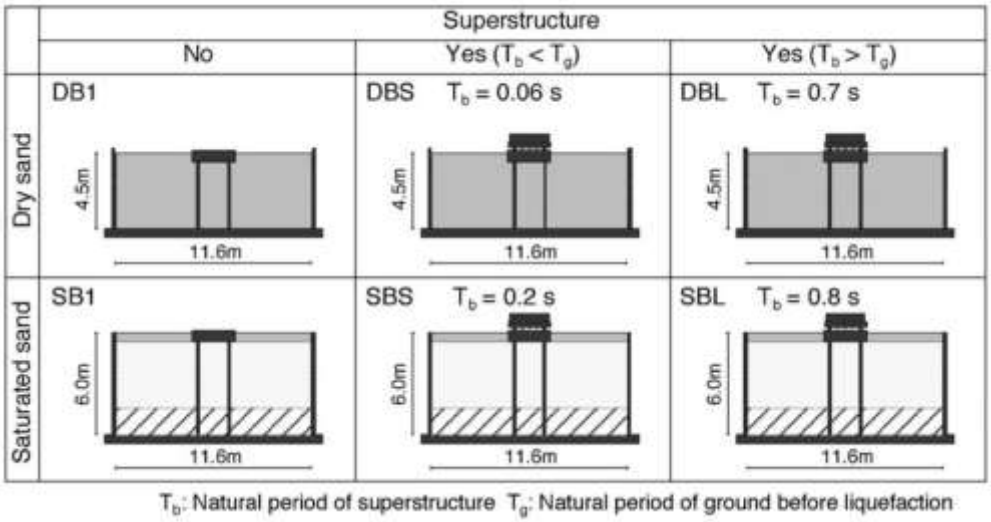

Figure 2-5 Soil-pile-structure model series in shaking table tests (Tokimatsu *et al.*, 2005)

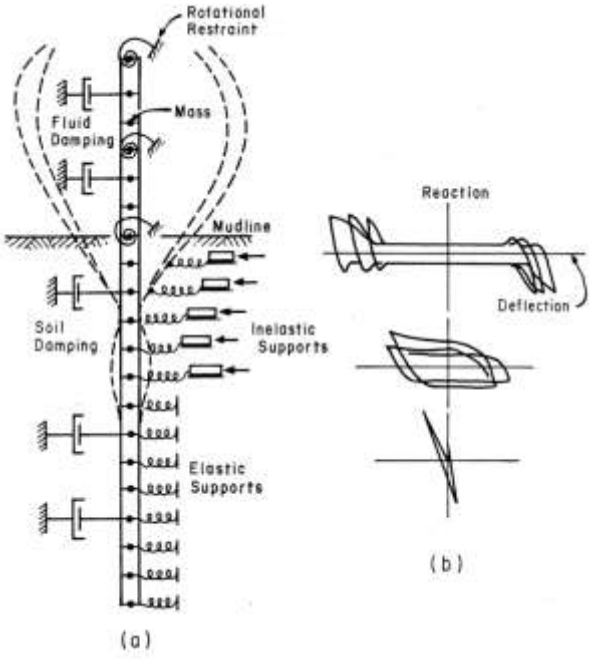

(a) Simulation of structure-pile-soil system
(b) Typical observed cyclic reaction-deflection characteristics

Figure 2-6 The diagrammatic sketch for beam-on-dynamic-Winkler foundation approach(Matlock *et al.*, 1978)

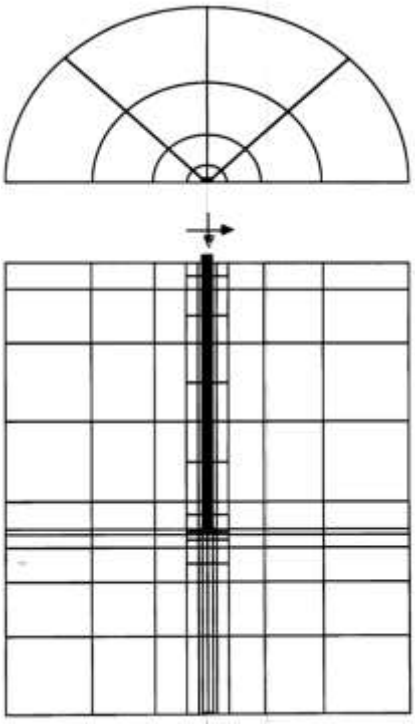

Figure 2-7 Finite element mesh in early days (Trochanis *et al.*, 1988)

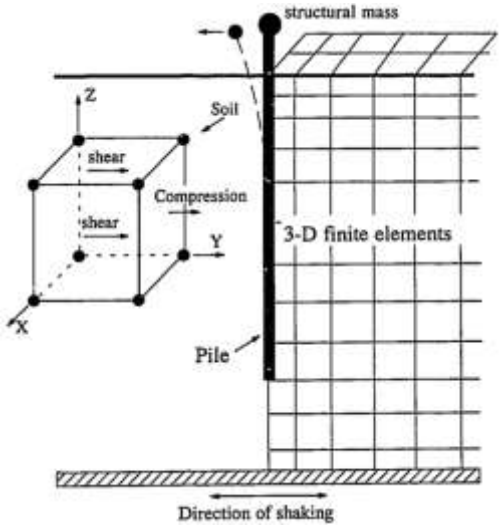

Figure 2-8 The principle of quasi-3D dynamic pile-soil interaction (Wu, 1994)

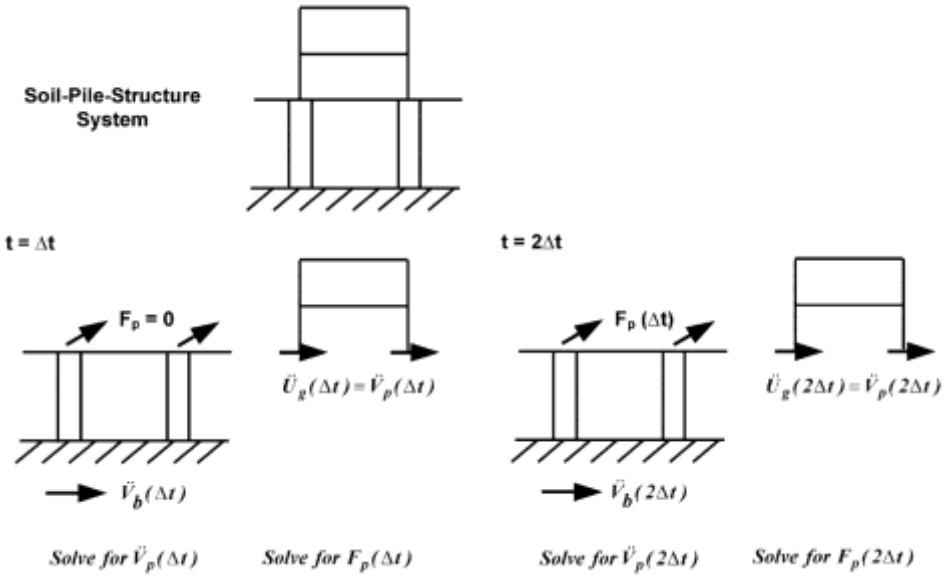

Figure 2-9 Schematic of successive-coupling scheme (Maheshwari *et al.*, 2004b)

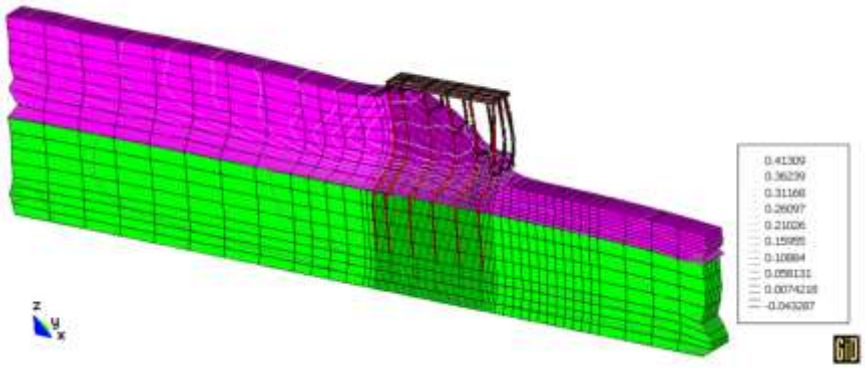

Figure 2-10 Final deformation of pile-supported wharf model (Lu, 2006)

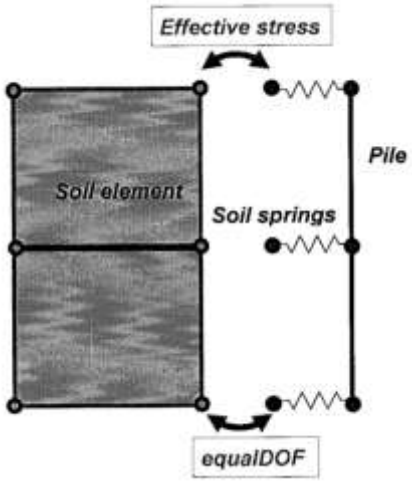

Figure 2-11 Schematic of soil-pile $p - y$ springs connections (Chang, 2007)

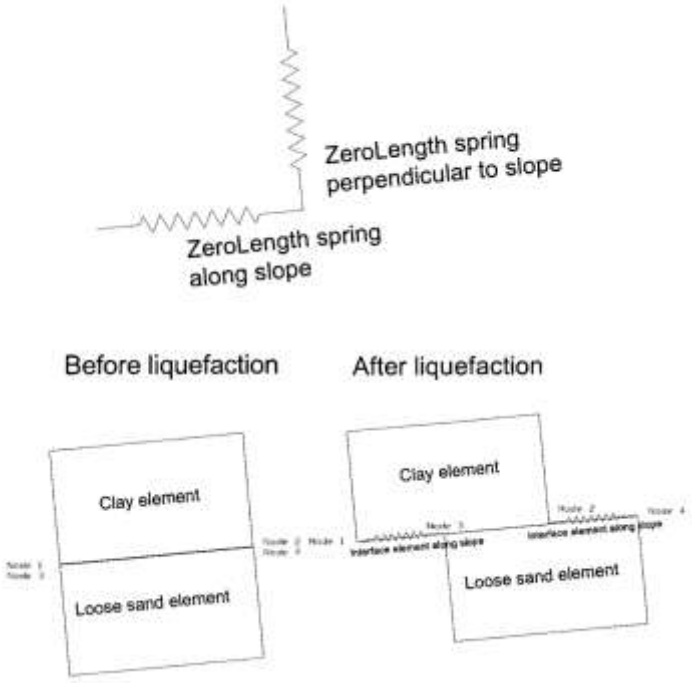

Figure 2-12 Interface elements between non-liquefiable soil and liquefiable soil (Chang, 2007)

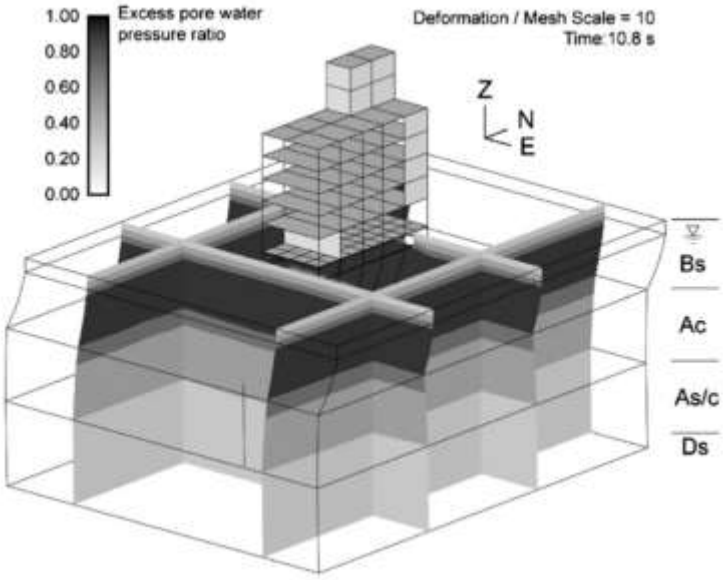

Figure 2-13 the computed deformation of soil-pile-structure system and the distribution of excess pore water pressure (Uzuoka *et al.*, 2007)

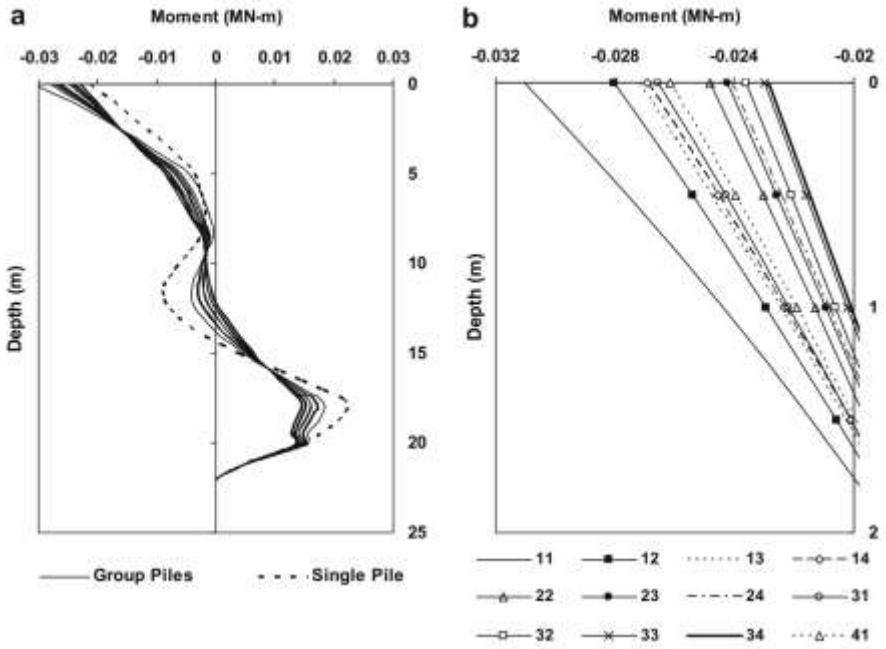

(a) Variation of moment distribution along the piles
(b) Focused on top 2m piles' length

Figure 2-14 Range of maximum moments along different piles in the group (Elahi *et al.*, 2010)

Chapter 3 Parallel Finite Element Method Using a PC Cluster

3.1 Introduction

As discussed in Chapter 2, most dynamic soil-structure interaction problems analyzed to date are relatively small scale, involving individual foundations, pile group or small clusters of these (e.g., Cai, 1995; Chu, 2006; Tafreshi, 2008). The largest dynamic soil-structure problem known to be attempted is a fully-coupled effective stress analysis which examined the effect of stone columns for mitigation of liquefaction hazards (Elgamal *et al.*, 2008). This was solved using the ParCYCLIC code, which used a parallel sparse direct solver and was implemented on Itanium 64 processors. However, the model considered by Elgamal *et al.* (2008) only involved 8 pile caps, each with 2×2 piles, resulting in 90,780 degrees-of-freedom for the total soil-pile-cap system. This is unlikely to be sufficient for modeling a very large pile group system.

In contrast, if one thinks of an urban environment such as a public housing estate in Singapore, where many blocks of high-rise flats are built by the Housing and Development Board (HDB) within a limited plot of land, each HDB block is likely to have much more than 8 pile caps with 2x2 or 3x3 pile configuration. Hence, the foundation is likely to consist of a large number of piles closely spaced together. With the closer spacing of the foundation elements, small element sizes will be required. While one can of course analyze each pile group separately, this will

ignore any "whole-building" effects. To see how such "whole-building" effects can arise, one need to take a historical perspective.

In conventional earthquake design philosophy, pioneered largely by Seed *et al.* (1975), the building is considered to be much lighter in mass than the surrounding ground. As a result, soil-structure interaction effects are largely insignificant, and the design was based largely on site-response effects; hence "green-field" ground motion was used as base input for earthquake structural analysis. However, with larger and more massive buildings, several new considerations enter into the picture. Firstly, interaction effects will increase in importance and may not be negligible. Secondly, the shear wave velocity in soft Singapore marine clay is about 70m/s to about 150m/s(Leong *et al.*, 2003). If one considers a frequency of 1Hz, which is well within earthquake frequency range, then the corresponding shear wave length ranges from about 70m to 100m. For a frequency of 2Hz, the shear wave length ranges from about 35m to 75m. On the other hand, the shear wave length in the bedrock is of the order of kilometers. If one considers a long slab-type of HDB flat as an example, the length of building is still much shorter than the shear wave length in bedrock, but it is of the same order of magnitude as the shear wave length, and therefore Rayleigh wave length, in soft marine clay. Thus, such buildings sitting on top of soft marine clay strata may distort during an earthquake, especially if the sub-soil profile is non-uniform. Such a phenomenon cannot be captured in small-scale analysis of individual pile or pile group.

In addition, the lateral boundaries of the finite simulation domain not only have to support static earth pressure, but should also simultaneously absorb the reflected waves from the pile foundation while imposing the base excitation from bedrock. The need to satisfy these often conflicting boundary conditions is a big challenge for finite element simulation and will be discussed in detail in the next chapter. In order to decrease the influence of the lateral boundary condition, the calculated domain is always required to be much larger than the soil domain of interest, which will further increase the computational workload. Furthermore, compared with several or dozens of time steps for static simulation, the number of time steps for seismic simulation is usually in the order of several thousands.

All these requirements put large-scale soil-structure interaction analysis beyond the capability of conventional finite element calculations. The finite element model for the whole building with large soil domain will be huge, which means that a large amount of memory is required for the analysis. The amount of random access memory (RAM) needed is likely to be well beyond the range of normal desktop PCs and even workstations. Another daunting challenge is the computational time required for a typical earthquake event simulation, which will likely take up to several weeks or months or even more, on a normal desktop computer.

This section discusses the development of a parallel computation scheme based on a class of Krylov sub-space iterative solvers. The feature of this class of solvers is that they do not need the global matrices to be assembled, thereby yielding significant savings in memory requirement. Furthermore, as will be shown below,

the algorithm is easily parallelizable using Message Passing Interface (MPI) protocol, hyper-threading using OpenMP or even a combination of both.

3.2 Literature Review on Parallel Computation

Parallel computing has already been in used in computational studies over the past two decades (e.g. Erhel *et al.*, 1991; Yagawa *et al.*, 1991; Gullerud and Dodds, 2001; Sato *et al.*, 2001; Sihota, 2004; Liu *et al.*, 2007; Petropoulos, 2008; Stavroulakis and Papadrakakis, 2009). Most of the earlier works deal mainly with vector and shared memory machines (e.g., George *et al.*, 1986; Adeli and Kamal, 1992; Gummadi and Palazotto, 1997). While memory management in such machines is relatively straightforward, such machines suffer from the disadvantage that they are not readily scalable. In recent years, the trend in parallel computing has been towards distributed memory computing such as cluster computing with high speed data network to facilitate data interchange, which can be easily up-scaled by adding nodes onto the data highway. Such distributed parallel computing schemes usually involve some form of domain decomposition process wherein the domain is broken down into sub-domains, each of which is then analyzed by a node or a processor.

Distributed parallel computing had been used in dynamic geophysical problems such as those dealing with the propagation of seismic waves through the Earth's crust (e.g. Komatitsch and Tromp, 2001; Kashiyama *et al.*, 2002; Komatitsch *et al.*, 2003). However, most of these implementations are based on explicit time integration schemes. In dynamic soil-structure interaction problems, explicit time integration schemes often cannot be applied because mass lumping gives rise to

unacceptable phase errors (Guin and Banerjee, 1998) and damping is often strain rate-, rather than velocity-, dependent (Yang, 1992).

Hsieh (2004) implemented a variant of the Domain Decomposition Method with the sparse direct solver on ABAQUS 5.8 to simulate tunnel heading excavation. The finite element domain in his analysis was 150m long x 80m wide x 30m deep and involved about 380,000 degrees-of-freedom. Domain decomposition was implemented explicitly by sub-dividing the entire domain into separate sub-domains. Data interchange between sub-domains was implemented using message passing interface (MPI) protocol. With Windows XP or Vista 64-bit operating systems and 8GB RAM, such a problem can now be solved on a single high-end personal computer.

Peng *et al.* (2004), Lu (2006) and Elgamal *et al.* (2008) used the ParCYCLIC code to study large-scale liquefaction problems using the Blue Horizon and Datastar supercomputers. The ParCYCLIC code employs a parallel row-oriented direct sparse solution solver which was developed by Law and Mackay (1993) and is based on explicit domain decomposition with MPI. The largest problem solved by their algorithm involved approximately 365,000 degrees-of-freedom, which is of the same order of magnitude as that of Hsieh (2004).

In recent years, Krylov subspace iterative algorithms have been increasingly used for large finite element problems (e.g. Lee *et al.*, 2002; Phoon *et al.*, 2002; Phoon *et al.*, 2003; Phoon, 2004; Chen and Phoon, 2009). For very large problems on a single computer, Krylov subspace algorithms such as preconditioned conjugate

gradient (PCG) and quasi-minimal residual (QMR) methods have been demonstrated to be significantly faster than direct solution methods, and the speed-up increases with the size of the problem (e.g. Wang, 1996; Phoon, 2004; Chen, 2006). In addition, Krylov subspace algorithm can be readily implemented on an element-by-element basis, thereby obviating the assembly of the global stiffness matrix and its accompanying memory requirements. Thus, for a given random-access memory (RAM) size, much larger problems can be solved using an element-by-element implementation of Krylov subspace methods than direct solution algorithms (Wang, 1996).

MPI-based implementation of pre-conditioned conjugate gradient (PCG) solver using element-by-element (EBE) scheme has also been used in geotechnical analysis (e.g., Gullerud and Dodds, 2001; Liu *et al.*, 2007). Gullerud and Dodds (2001)'s study was conducted on an SGI/Cray Origin 2000 supercomputer. They used a dual-level mesh decomposition scheme, with a coarse-level decomposition using the METIS graph-partitioning software to sub-divide the domain into sub-domains, each sub-domain being assigned to a processor. A second fine-level decomposition sub-divides every sub-domain into blocks of elements for parallel computing on each processor. Liu *et al.* (2007)'s parallel PCG scheme was implemented on a cluster of 36 nodes, each being a shared memory machine consisting of four PIII Xeon 700MHz processors. MPI was used for data interchange between processors. Liu *et al.* (2007) also used the METIS software to sub-divide the domain. Both Gullerud and Dodds (2001) and Liu *et al.* (2007)

utilized a system of identifying shared nodes so that only information on shared nodes are exchanged between processors.

In spite of the similarity of their approaches, Gullerud and Dodds (2001) and Liu *et al.* (2007) obtained very different speedup efficiency values, defined herein as the ratio of the speedup to the number of processors used. Using 48 processors, Gullerud and Dodds (2001) obtained a maximum speedup efficiency of about 71% using a PCG solver with diagonal pre-conditioner. With a direct sparse solver, the speedup efficiency decreases drastically to below 24%. Liu *et al.* (2007)'s diagonally-preconditioned PCG solver, on the other hand, was only able to obtain a speedup efficiency of about 70% with 4 processors. With 16 processors, their speedup efficiency fell to about 43%, in simulating Ertan arch dam-foundation system with 20,879 nodes and 17,980 elements.

This comparison shows that while speedup is indeed achievable, in principle, with parallel computing on cluster machines, the level of efficiency which can be achieved with different algorithms do differ significantly. As shown above, some of these differences are explainable in terms of the solution algorithm, but other differences are not so readily explained. Possible reasons include differences in hardware platform, especially data interchange speed between processors, detailed procedures and programming with respect to data interchange and even the degree of optimality in domain sub-division using METIS. In terms of hardware comparison, Liu *et al.* (2007)'s cluster is probably newer but not much information was provided on the speed of the data highway.

3.3 Computer Resources and Architecture

3.3.1 Setup of PC cluster in EIT lab, NUS

The current PC cluster in the NUS Civil Engineering Educational and Information Technology (EIT) laboratory comprises 128 desktop computers that are linked using a Myri-10G Modular Switch, as shown in Figure 3-1. All computers have 64-bit architecture and operating systems, but were bought in three batches with different specifications, listed in Table 3-1. 64-bit representation was used to improve precision and access more memory. The operating system, Windows HPC server 2008, is installed on all computers and Linux Fedora is also installed on some of the computers, which allow users to choose the OS respectively. This study uses only the Windows HPC Server 2008 operating system.

The processors on all PCs are standard Intel CORE processors with quad-core architecture. The use of standard PC allows scaling up to be achieved with minimal incremental cost. Each core is an individual calculation unit, and could process scientific calculation separately. All four cores on the same processor share the same memory and could access the whole memory individually. This makes it possible to use hyper-threading to speed up the calculation by distributing the calculation work to all cores. This architecture is named as shared memory, as different calculating units share the same memory. It is readily adapted for parallel calculation, without requirement of additional equipment. The access of shared memory could efficiently reduce the communication among different cores. One core stores data at a certain location for other cores to collect them, without explicit

send-receive communication. The standard protocol for hyper-threading, OpenMP, was used to split the computation workload among the different cores. However, there exist several limitations with shared memory configuration:

(1) All four cores access shared memory through the same front side bus (FSB) which is either the older north bridge or current QPI. This FSB can become a bottle neck for the calculation speed. This will be discussed further in section 3.8.2.

(2) The four cores could read from & write to the same memory location simultaneously, which may lead to some conflict between cores updating the same data. This can lead to computation errors.

Parallel computation amongst different computers is also possible with high speed network. All the 128 computers are connected using Myri-10g network which offer 10Gbps data transfer speed between any two computers. The Myri-10g network consists of the following components:

- Myri-10G dual-protocol network interface cards (NICs), as shown in Figure 3-2. Myri-10G NICs connect to hosts through PCI-Express x8, a 2+2 Gigabytes/s full-duplex IO fabric that is fast enough to keep up with the 1.25 + 1.25 Gigabyte/s network port. A PCI-X bus, with a speed of 1 Gigabytes/s at best, has only 40% of the 2.5 Gigabyte/s peak data rate needed for 10-Gigabit networking. Myri-10g NICs is the first near-wire-speed 10-Gigabit NICs.
- The 128-port Myri-10G multi-protocol switch box.

- The 10G base-SR fiber cables, which connect the NIC and switch. The transmission speed is almost independent on cable length. Based on the distance between PC and switch, the cable length used in this study varies from 2 meters to 15 meters.

The 128 computers are connected with the Myri-10g network to form a local network, and could access internet via head node, as shown in Figure 3-3. The head node, with the same specification as other nodes, takes charge of assigning IP address for other nodes, distributing calculation load, and monitoring the resources of the whole cluster.

For large-scale modeling, the biggest advantage of adopting a PC cluster over the supercomputer is the much lower startup and operating costs and higher degree of scalability. This makes parallel computations more readily available to research centers or engineering companies, which would otherwise not have access to supercomputing facilities.

3.3.2 Message Exchange Using MPI

The critical problem in performing parallel computations using a PC cluster is communication between processors or different nodes. All computers have to synchronize their operations and exchange data with one another. The inter-processor communication is commonly achieved using MPI (Message Passing Interface) protocol (Snir and Gropp, 1998), which is a language-independent communications protocol for message passing. MPI was defined by the MPI Forum,

a broadly based group of parallel computer vendors, library developers, and applications specialists. One advantage of MPI is its portability, which makes it suitable to develop programs to run on a wide range of parallel computers and workstation clusters. Another advantage of MPI is its performance, because each MPI implementation is optimized for the hardware it runs on. Generally, MPI code can be developed for an arbitrary number of processors. It is up to the user to decide, at runtime, the number of processors to be invoked for the execution.

The MPI library consists of a large set of message passing primitives (functions) to support efficient parallel processes running on a large number of processors interconnected over a network. Such processes can be divided into two types: point-to-point communication and collective communication. The point-to-point communication in MPI involves transmittal of data between two processors, typically using *MPI_Send* to send data on one node and using *MPI_Recv* to receive the data on another node. The collective communications, on the other hand, transmit data among all processors in a group, typically using *MPI_Bcast* to broadcast data from a head node to all other nodes, and using *MPI_Reduce* to collect data from all nodes to the head node. The performance of these commands on this PC cluster was evaluated prior to the development of the parallel code. This will be discussed below.

Figure 3-4 (a) shows the time needed to transmit relatively short data segments with lengths ranging from 10,000 to 70,000 64-bit double precision numbers between two PCs using the commands *MPI_Send* and *MPI_Recv*, in a 1send-1received configuration. As this figure shows, the average transmission speed is

about 4.92Gbits/s and there is an apparent latency of about 13.8μs. This transmission rate lies well below the specified maximum of 10Gbits/s. Figure 3-4 (b-d) shows the corresponding times for 2send-2receive, 4send-4receive and 8send-8receive configurations. As can be seen, the average transmission speed remains roughly the same, but the latency increases slightly as the switch is busy. Figure 3-4 (e) and (d) also show the time for 1send-1receive and 2send-2receive operation involving cores on the same PC. As can be seen, for the Core i7 940 machines, the core-core transmission requires the same amount of time as the PC-PC transmission. For the Core2 Quad Q9550 machines, the core-core transmission speed is even lower, less than half of that of the Corei7 machines, as shown in Figure 3-4 (g). Thus, the bottleneck lies within the PC rather than the network switch.

Figure 3-5 (a) shows similar data volume sent in longer segments, ranging from 1,000,000 to 5,000,000. As can be seen, the transmission rate is significantly closer to the specified maximum and the apparent latency time significantly shorter. Hence, it is more efficient to send data in longer bursts, and this phenomenon is also found to apply for data transmission among cores, as shown in Figure 3-5 (b). As in the case for shorter data burst, core-core transmission requires the same amount of time as the PC-PC transmission, indicating that the bottleneck lies within the PC rather than the network switch.

Figure 3-6 shows the time taken for broadcast operations involving different number of PCs, normalized by the time needed for a 1send-1receive operation. As

can be seen, where only 2 PCs are involved, the broadcast operation is slightly faster than the 1send-1receive operation. When 16 PCs are involved, that is, one PC broadcasting to 15 PCs, the entire operation takes about 2½ times as long as a 1send-1receive operation. Hence, when the same data has to be transmitted to a large number of PCs, the broadcast operation is much quicker than the send-receive operation. Besides, higher efficiency can be obtained when the number of PCs involved is a perfect power of 2, and the similar features were noted by other researchers and the number of PCs involved was always a perfect power of 2 (e.g. Lu, 2006; Dupros *et al.*, 2010).

Figure 3-7 shows the corresponding time for a reduce operation, in which all PCs send their respective data to the head node PC to be summed up. As can be seen, when only 2 PCs are involved, the all-reduce operation is slower than the 1send-1receive operation. However, when 16 PCs are involved, the entire operation remains much quicker than that needed by 15 1send-1receive operations. As Figure 3-7 shows, the reduce operation is faster when the number of PCs in a cluster is a perfect power of 2.

So far, the performance of the hardware components and the message passing features have been discussed in terms of the data transmission speed. The performance of the computer cluster for simulating large-scale geotechnical problems, together with considerations of the parallel architecture, will be discussed later in Sections 3.5 to the end of the chapter. Before this, Section 3.4 introduces the governing equations, the finite element formulation and solution

schemes for the analysis of undrained seismic soil-structure interaction problems. This information is combined with the analysis flow chart for typical finite element simulations to provide a better appreciation of the parallel features and software architecture for carrying out such parallel computations.

3.4 Finite element analyses for undrained nonlinear dynamic simulation

3.4.1 Finite element formulation for undrained dynamic analysis

The equation of dynamic equilibrium of a small solid element within a solid medium can be written as follows:

$$\sigma_{ij,j} + \rho f_i = \rho \ddot{u}_i \tag{3.1}$$

in which

σ_{ij} is the total stress vector, which is the sum of the effective stress and water pore pressure.

$$\sigma_{ij} = \sigma'_{ij} + \delta_{ij} p \tag{3.2}$$

σ'_{ij} is the effective stress vector of the soil.

p is the pore water pressure

f_i is the body force vector

$\ddot{u}_i$ is the acceleration vector of solid. In an undrained analysis, the displacements u, velocity $\dot{u}$ and acceleration $\ddot{u}$ of both the soil and the water phases are assumed to be the same.

ρ is the bulk density of the soil, that is, the total density of the soil and water.

Instead of solving Eq (3.1) exactly over the whole domain, the finite element method involves subdividing the domain into a series of smaller elements, each defined by a set of nodes which serve to connect the elements together. Approximate solutions to Eq (3.1) are then obtained for all the nodes in the system. The displacements at these nodes are usually chosen to be the primary variables. The values of these variables at any other point within the element are related to the nodal values by means of approximating or shape functions (Zienkiewicz and Taylor, 1989).

By applying a weighted residual method, a weak formulation of the problem can be obtained. The essence of this method, which is an optimization process, is the multiplication of weighting functions w_i to the governing differential equations and minimizing the errors thus obtained over the volume of the element while satisfying the essential boundary conditions. The resulting integral for the element equilibrium can be written as

$$\iiint_v w_i \left(\sigma_{ij,j} + \rho f_i - \rho \ddot{u}_i \right) dV = 0 \qquad (3.3)$$

which, upon expansion, leads to

$$\iiint_v w_i \sigma_{ij,j} dV + \iiint_v w_i \rho f dV - \iiint_v w_i \rho \ddot{u}_i dV = 0 \tag{3.4}$$

Using Gauss' Divergence Theorem,

$$\iiint_v w_i \sigma_{ij,j} dV = \iint_s w_i \sigma_{ij} n_j dS - \iiint_v w_{i,j} \sigma_{ij} dV \tag{3.5}$$

The Generalized Hooke's Law for a solid allows σ_{ij} to be expressed as

$$\sigma'_{ij} = D'_{ijkl} \varepsilon_{kl} + E'_{ijkl} \dot{\varepsilon}_{kl} = D'_{ijkl} \frac{\partial u_k}{\partial x_l} + E'_{ijkl} \frac{\partial \dot{u}_k}{\partial x_l} \tag{3.6}$$

in which D'_{ijkl} is the constitutive tensor governing the deformation response, and E'_{ijkl} is the constitutive tensor governing the viscous response. The pore pressure can be expressed as

$$p = K_w \varepsilon_v = K_w \frac{\partial u_i}{\partial x_i} \tag{3.7}$$

in which K_w is the bulk modulus of pore water.

Substituting Eqs (3.2), (3.5), (3.6), (3.7) into Eq (3.4), the following equation is obtained

$$\iint_s w_i \sigma_{ij} n_j dS - \iiint_v w_{i,j} \left(D'_{ijkl} \frac{\partial u_k}{\partial x_l} + E'_{ijkl} \frac{\partial \dot{u}_k}{\partial x_l} \right) dV - \iiint_v w_{i,j} \delta_{ij} K_w \frac{\partial u_k}{\partial x_k} dV + \iiint_v w_i \rho f dV - \iiint_v w_i \rho \ddot{u}_i dV = 0 \tag{3.8}$$

Upon expansion of the term in brackets and rearranging,

$$\iiint_v w_{i,j} D'_{ijkl} \frac{\partial u_k}{\partial x_l} dV + \iiint_v w_{i,j} E'_{ijkl} \frac{\partial \dot{u}_k}{\partial x_l} dV + \iiint_v w_{i,j} \delta_{ij} K_w \frac{\partial u_k}{\partial x_k} dV - \iiint_v w_i \rho f dV = \iint_s w_i \sigma_{ij} n_j dS - \iiint_v w_i \rho \ddot{u}_i dV \tag{3.9}$$

In order to solve Eq (3.9), it is necessary to choose a suitable weighting function w_i. In this study, the Galerkin's weighted residual method (Finlayson, 1972), in which the weighting function is chosen to be the same as the shape function N_i of the element, is used to obtain approximate solutions to Eq (3.9). This leads to

$$\iiint_v N_{i,j} D'_{ijkl} \frac{\partial u_k}{\partial x_l} dV + \iiint_v N_{i,j} E'_{ijkl} \frac{\partial \dot{u}_k}{\partial x_l} dV + \iiint_v N_{i,j} \delta_{ij} K_w \frac{\partial u_k}{\partial x_k} dV - \iiint_v N_i \rho f dV = \iint_s N_i \sigma_{ij} n_j dS - \iiint_v N_i \rho \ddot{u}_i dV \tag{3.10}$$

In typical finite element matrix formulation, this can be written as

$$\sum_{nel} \iiint_{v_e} [B]^T [E'][B]\{\dot{u}\} dV + \sum_{nel} \iiint_{v_e} [B]^T ([D'] + [I_u])[B]\{u\} dV + \sum_{nel} \iiint_{v_e} [N]^T \rho \{\ddot{u}\} dV = \sum_{nes} \iint_{s_e} [N]\{\sigma\} dS - \sum_{nel} \iiint_{v_e} \rho [N]^T \{f\} dV \tag{3.11}$$

or simply

$$[M]\{\ddot{u}\} + [C]\{\dot{u}\} + [K]\{u\} = \{F\} \tag{3.12}$$

where

$[M]=\sum_{nel}\iiint_{v_e}[N]^T\rho_d[N]dV$ is the global mass matrix

$[C]=\sum_{nel}\iiint_{v_e}[B]^T[E'][B]dV$ is the global viscosity matrix

$[K]=\sum_{nel}\iiint_{v_e}[B]^T\left([D']+K_w[I_u]\right)[B]dV$ is the stiffness matrix, and

$\{F\}=\sum_{nes}\iint_{s_e}[N]^T\{f_s\}dS-\sum_{nel}\iiint_{v_e}\rho_d[N]^T\{f\}dV$ is the resultant applied load

due to the surface applied tractions and the body forces respectively.

$\{u\}=\begin{pmatrix}u_1 & v_1 & w_1 & \cdots & u_n & v_n & w_n\end{pmatrix}^T$ is the displacement vector,

$[B]=\left[N_{i,j}\right]$ is the strain-displacement transformation matrix,

$[I_u]=diag(1\quad 1\quad 1\quad 0\quad 0\quad 0)^T$

Eq (3.12) is analogous to the equation of motion commonly encountered in structural dynamics, i.e.

$$Ma+Cv+Ku=F \tag{3.13}$$

in which a is the acceleration vector, v is the velocity vector, and u is the displacement vector. Eq.(3.13) is an undrained finite equation system which is different from the $u\sim p$ formula (Chan, 1982) and $u\sim v$ formula (Ye, 2013). It's

assumed that the water does not diffuse during seismic shaking which is reasonable to soft clay and has been widely used.

In non-linear dynamic analysis, Eq (3.13) is often integrated over time domain in a series of steps. One of the most widely used families of direct methods for solving Eq (3.13) is the Newmark method (Newmark, 1959), which consists of the following equations:

$$M\ddot{u}_{n+1} + C\dot{u}_{n+1} + Ku_{n+1} = F_{n+1} \tag{3.14}$$

$$u_{n+1} = u_n + \Delta t\dot{u} + \Delta t^2[(1-2\beta)\ddot{u}_n + 2\beta\ddot{u}_{n+1}]/2 \tag{3.15}$$

$$\dot{u}_{n+1} = \dot{u}_n + \Delta t[(1-\gamma)\ddot{u}_n + \gamma\ddot{u}_{n+1}] \tag{3.16}$$

in which Δt is the incremental time-step, and β, γ are dynamic integration constants. The subscripts n and $n+1$ denote successive points in time. The parameters β and γ also determine the stability and accuracy characteristics of the algorithm under consideration.

The implementation to be adopted here is the a-form, in which the primary variable is the incremental acceleration $\Delta\ddot{u}_{n+1}$. This form of implementation is convenient for generalizations to algorithms that employ 'mesh partitions' but is not the most efficient implementation (Hughes, 1990). Although the concept of mesh-partitioning into implicit and explicit zones is not used in this study, it is envisaged that the need for such an algorithm to solve soil-structure interaction will arise in the future, which is why this implementation is chosen.

By writing $u_{n+1} = u_n + \Delta u_{n+1}$, $\dot{u}_{n+1} = \dot{u}_n + \Delta \dot{u}_{n+1}$, and $\ddot{u}_{n+1} = \ddot{u}_n + \Delta \ddot{u}_{n+1}$, Eqs (3.14), (3.15) and (3.16) can be written in the following incremental forms:

$$M\Delta \ddot{u}_{n+1} + C\Delta \dot{u}_{n+1} + K\Delta u_{n+1} = \Delta F_{n+1} \tag{3.17}$$

$$\Delta u_{n+1} = \Delta t \dot{u}_n + \Delta t^2 [\ddot{u}_n + 2\beta \Delta \ddot{u}_{n+1}] / 2 \tag{3.18}$$

$$\Delta \dot{u}_{n+1} = \ddot{u}_n \Delta t + \gamma \Delta \ddot{u}_{n+1} \Delta t \tag{3.19}$$

Substituting Eqs (3.18) and (3.19) into Eq (3.17),

$$\left[M + \gamma \Delta t C + \beta \Delta t^2 K \right] \Delta \ddot{u}_{n+1} = \Delta F_{n+1} - \left[(\ddot{u}_n \Delta t) C + \left(\dot{u}_n \Delta t + \frac{\ddot{u}_n \Delta t^2}{2} \right) K \right] \tag{3.20}$$

is obtained. This is the recursion relation used in this study to determine $\Delta \ddot{u}_{n+1}$. Once $\Delta \ddot{u}_{n+1}$ is determined, Δu_{n+1} and $\Delta \dot{u}_{n+1}$ can be obtained using Eqs (3.18) and (3.19) respectively.

The Newmark family of time integration schemes encompasses, as special cases, many well-known and widely used methods, depending on the choice of values for β and γ. The values of β and γ allow the numerical dissipation to be continuously controlled by a parameter other than the time step. For example, by setting $\beta = \left(\gamma + \frac{1}{2} \right)^2 / 4$ and $\gamma \geq \frac{1}{2}$, the amount of dissipation for a fixed time step can be increased by increasing γ. On the other hand, the dissipative properties of this

family are considered to be inferior to both the Houbolt (1950) and the Wilson-θ (Wilson, 1968) methods, since the lower modes are affected too strongly.

The linear acceleration and Fox-Goodwin methods are conditionally stable; hence they are not economically competitive for large-scale systems when compared to unconditionally stable techniques such as the average acceleration method, which is obtained when $\beta = 0.25$ and $\gamma = 0.5$.

Although the average acceleration method is unconditionally stable for linear problems and generally permits the use of a larger time-step size, accuracy considerations may require that the time-step used should be reasonably small. The commonly used rule-of-thumb for non-dissipative algorithms requires at least ten time steps per period be taken for accuracy (Hilber, 1977). This requirement becomes even more stringent for elasto-plastic materials, since the numerical computations in the plastic region usually involve some form of approximation of the stress-strain relationship, such as the tangent stiffness method. For numerical codes that do not perform any iterative stress correction, such as in CRISP92, it is necessary to use time steps or load steps that are sufficiently small so that the drift from the correct stress-strain behavior is reduced (Britto and Gunn, 1987; Potts and Ganendra, 1991). This is usually done by performing preliminary studies to check the convergence characteristics of different time-step sizes.

3.4.2 Newton-Raphson method for dynamic analyses

The Newton-Raphson algorithm for drift correction has been widely used in non-linear static problems. However, its formulation for non-linear dynamic problems

is less widely documented. For this reason, the Newton-Raphson formulation which is used in this study is presented below.

In nonlinear computations, the material stiffness and damping at the end of the current time step (n+1) is not available at the start of the time step. As a result, their values at the end of the time step n are often taken as being representative of those over the entire time step (n+1), that is

$$[M]\{\Delta\hat{a}\}_{n+1}+\left[\hat{C}\right]\{\Delta\hat{v}\}_{n+1}+\left[\hat{K}\right]\{\Delta\hat{u}\}_{n+1}=\{\Delta F\}_{n+1} \tag{3.21}$$

$$\{\Delta\hat{u}\}_{n+1}=\Delta t\{v\}_n+\frac{\Delta t^2}{2}\left(\{a\}_n+2\beta\{\Delta\hat{a}\}_{n+1}\right) \tag{3.22}$$

$$\{\Delta\hat{v}\}_{n+1}=\Delta t\left(\{a\}_n+\gamma\{\Delta\hat{a}\}_{n+1}\right) \tag{3.23}$$

in which $\left[\hat{K}\right]$, $\left[\hat{C}\right]$ are the initial tangent value of stiffness & damping matrix at $(n+1)$ time step respectively, and $\{\Delta\hat{a}\}_{n+1}$, $\{\Delta\hat{v}\}_{n+1}$, $\{\Delta\hat{u}\}_{n+1}$ are the corresponding approximate solutions, as shown in Figure 3-8.

Let

$$\{\Delta u\}_{n+1}=\{\Delta\hat{u}\}_{n+1}+\{\delta u\}_{n+1} \tag{3.24}$$

$$\{\Delta v\}_{n+1}=\{\Delta\hat{v}\}_{n+1}+\{\delta v\}_{n+1} \tag{3.25}$$

$$\{\Delta a\}_{n+1}=\{\Delta\hat{a}\}_{n+1}+\{\delta a\}_{n+1} \tag{3.26}$$

in which $\{\delta u\}_{n+1}$, $\{\delta v\}_{n+1}$, $\{\delta a\}_{n+1}$ are the errors of incremental displacement, velocity and acceleration due to the initial tangent value assumption.

Substituting Eqs (3.24), (3.25) and (3.26) into Eq (3.17) leads to

$$\begin{aligned}[M]\left(\{\Delta\hat{a}\}_{n+1}+\{\delta a\}_{n+1}\right)+[C]\left(\{\Delta\hat{v}\}_{n+1}+\{\delta v\}_{n+1}\right)\\ +[K]\left(\{\Delta\hat{u}\}_{n+1}+\{\delta u\}_{n+1}\right)=\{\Delta F\}_{n+1}\end{aligned} \tag{3.27}$$

Rearranging,

$$\begin{aligned}[M]\{\delta a\}_{n+1}+[C]\{\delta v\}_{n+1}+[K]\{\delta u\}_{n+1}=\{\Delta F\}_{n+1}\\ -\left([M]\{\Delta\hat{a}\}_{n+1}+[C]\{\Delta\hat{v}\}_{n+1}+[K]\{\Delta\hat{u}\}_{n+1}\right)\end{aligned} \tag{3.28}$$

Substituting Eqs (3.25) and (3.26) into Eq (3.19) leads to

$$\{\Delta\hat{v}\}_{n+1}+\{\delta v\}_{n+1}=\Delta t\left(\{a\}_n+\gamma\{\Delta\hat{a}\}_{n+1}+\gamma\{\delta a\}_{n+1}\right) \tag{3.29}$$

Subtracting Eq (3.23) from Eq (3.29) leads to

$$\{\delta v\}_{n+1}=\gamma\Delta t\{\delta a\}_{n+1} \tag{3.30}$$

Substituting Eq (3.24) and (3.26) into Eq (3.18) leads to

$$\{\Delta\hat{u}\}_{n+1}+\{\delta u\}_{n+1}=\Delta t\{v\}_n+\frac{\Delta t^2}{2}\left(\{a\}_n+2\beta\{\Delta\hat{a}\}_{n+1}+2\beta\{\delta a\}_{n+1}\right) \tag{3.31}$$

Subtracting Eq (3.22) from Eq (3.31), leads to

$$\{\delta u\}_{n+1}=\beta t^2\{\delta a\}_{n+1} \tag{3.32}$$

Substituting Eqs (3.30) and (3.32) into Eq (3.28), leads to

$$\left([M]+\gamma\Delta t[C]+\beta\Delta t^2[K]\right)\{\delta a\}_{n+1}=\{\Delta F\}_{n+1} -\left([M]\{\Delta\hat{a}\}_{n+1}+[C]\{\Delta\hat{v}\}_{n+1}+[K]\{\Delta\hat{u}\}_{n+1}\right) \tag{3.33}$$

Since the values of $[C]$ and $[K]$ matrices used are those at the beginning of the time step n+1, $\{\delta\tilde{a}\}_{n+1}$ so obtained is only an approximate value.

$$\left([M]+\gamma\Delta t[C]^{(i-1)}+\beta\Delta t^2[K]^{(i-1)}\right)\{\delta a\}_{n+1}^{(i)}=\{\Delta F\}_{n+1} -\left([M]\{\Delta\hat{a}\}_{n+1}^{(i-1)}+[C]^{(i-1)}\{\Delta\hat{v}\}_{n+1}^{(i-1)}+[K]^{(i-1)}\left\{\Delta\hat{d}\right\}_{n+1}^{(i-1)}\right) \tag{3.33}$$

The Newton-Raphson method is often used to correct the errors so incurred. In this method, the errors in the displacement, velocity and acceleration are converted into out-of-balance stresses and thereby forces

$$\{\Delta F_b\}_{n+1}^{(i-1)}=[M]\left(\{\Delta\hat{a}\}_{n+1}^{(i-1)}+\alpha\{\Delta\hat{v}\}_{n+1}^{(i-1)}\right)+\sum\int_v[B]^T\left(\{\Delta\sigma\}^g+\beta\{\Delta\upsilon\}^g\right)dV \tag{3.34}$$

in which

$$\{\Delta\sigma\}^g=[D][B]\left\{\Delta\hat{d}\right\}_{n+1}^{(i-1)} \quad \text{at Gauss point} \tag{3.35}$$

$$\{\Delta\upsilon\}^g=[D][B]\{\Delta\hat{v}\}_{n+1}^{(i-1)} \quad \text{at Gauss point} \tag{3.36}$$

Then

$$\left([M]+\gamma\Delta t[C]^{(i-1)}+\beta\Delta t^2[K]^{(i-1)}\right)\{\delta a\}_{n+1}^{(i)}=\{\Delta F\}_{n+1}-\{\Delta F_b\}_{n+1}^{(i-1)} \tag{3.37}$$

in which

$$\{\Delta\hat{a}\}_{n+1}^{(0)} = \{\Delta\hat{a}\}_{n+1} \qquad \{\Delta\hat{v}\}_{n+1}^{(0)} = \{\Delta\hat{v}\}_{n+1} \qquad \left\{\Delta\hat{d}\right\}_{n+1}^{(0)} = \left\{\Delta\hat{d}\right\}_{n+1} \tag{3.38}$$

According to Eq (3.30) and (3.32)

$$\{\delta v\}_{n+1}^{(i)} = \gamma\Delta t\{\delta a\}_{n+1}^{(i)} \tag{3.39}$$

$$\{\delta d\}_{n+1}^{(i)} = \beta t^2\{\delta a\}_{n+1}^{(i)} \tag{3.40}$$

Then

$$\left\{\Delta\hat{d}\right\}_{n+1}^{(i)} = \left\{\Delta\hat{d}\right\}_{n+1}^{(i-1)} + \{\delta d\}_{n+1}^{(i)} \tag{3.41}$$

$$\{\Delta\hat{v}\}_{n+1}^{(i)} = \{\Delta\hat{v}\}_{n+1}^{(i-1)} + \{\delta v\}_{n+1}^{(i)} \tag{3.42}$$

$$\{\Delta\hat{a}\}_{n+1}^{(i)} = \{\Delta\hat{a}\}_{n+1}^{(i-1)} + \{\delta a\}_{n+1}^{(i)} \tag{3.43}$$

$$\{d\}_{n+1}^{(i)} = \{d\}_{n+1} + \left\{\Delta\hat{d}\right\}_{n+1}^{(i)} \tag{3.44}$$

and $[K]^{(i)}$, $[C]^{(i)}$ can be calculated from the latest $\{d\}_{n+1}^{(i)}$. The iterations are repeated until $\{\delta a\}_{n+1}^{(i)}$ is small enough.

3.4.3 EBE-MJPCG iterative solver

As shown by Eqs (3.20) and (3.37), the solution of the soil-pore water-pile-superstructure interaction problem involves solving a system of linear equations of the form

$$[A]\{x\} = \{b\} \tag{3.45}$$

The most widely used algorithms for solving Eq (3.45) are refined variants of the Gaussian elimination approach, such as the bandwidth solver (Zienkiewicz and Taylor, 1999), frontal solver (e.g. Irons, 1970; Britto and Gunn, 1987; Zienkiewicz and Taylor, 1999) and the multi-frontal solver (Hibbitt, 1997). Such solvers are very efficient for small to medium-sized problems where the matrix is still fairly dense and the time spent on factoring is less than or equivalent to the time spent on solving the system iteratively. However, for 3D problems involving large matrices, the storage of the front or semi-bandwidth alone can require a large amount of memory. Even with out-of-core access, the memory capacity may still be inadequate to cope with the minimum storage required to run the analysis. In addition, in multi-clocked hierarchical computer systems such as PCs, the large amount of indirect addressing used by such algorithms tends to lead to a rather low cache data re-use rate, thereby causing a drop in processor efficiency.

In contrast to Gaussian elimination methods, iterative methods may not require assembly of the global stiffness matrix, thereby significantly reducing computer memory usage. Barrett *et al.* (1994) showed that the combination of

preconditioning and Krylov subspace iterations could provide efficient and simple "general purpose" procedures that are viable alternatives to direct solvers. In contrast to direct methods, iterative methods converge iteratively towards the correct answer, the iterations being terminated when the required accuracy is reached. Many iterative methods have convergence characteristics which vary substantially with condition number. In general, the larger the condition number, the poorer will be the convergence characteristics. To accelerate convergence, iterative methods usually incorporate a preconditioning process with a preconditioner matrix. A commonly used, simple and inexpensive preconditioner is the Jacobi Preconditioner (Saad, 1996; Smith, 2000), which is a collection of the diagonal terms in the stiffness matrix. Lee *et al.* (2002) examined the performance of the Jacobi preconditioner when the iterative method was used to solve drained, undrained and consolidation problems, while Chan *et al.* (2001) proposed a modified Jacobi preconditioner for solving ill-conditioned Biot's consolidation equation.

Fox and Stanton (1968) and Fried (1969) pointed out that the assembly of the global stiffness matrix is not essential in conjugate gradient (CG) methods and that the matrix-vector operations can be performed at the element level. This opened the way for element-by-element (EBE) implementation of CG methods, which can drastically reduce memory requirements in large 3-D finite element analyses. An efficient element-by-element preconditioned conjugate gradient (EBE-PCG) algorithm was developed by Hughes *et al.* (1987) by combining the element-by-element method (Hughes *et al.*, 1983a; 1983b) with the traditional PCG method.

Later this method was improved by Papadrakakis and Dracopoulos (1991) and Tezduyar (1992). Lim (2003) combined the modified Jacobi preconditioned conjugate gradient (MJPCG) method and EBE-PCG algorithm to come up with the EBE-MJPCG iteration solver, as shown in Figure 3-9.

As can be seen, there are four types of calculations in each iteration of the EBE-MJPCG solution process, as follows:

(1) Type 1 Calculation: Pre-multiplication of a n-component vector with a pre-conditioner (in this case diagonal matrix) to give another n-component vector, where n is the number of degrees-of-freedom.
(2) Type 2 Calculation: Matrix-vector multiplication (once for each element).
(3) Type 2a Calculation: Formation of element stiffness matrix (done once in each time or load step for each element).
(4) Type 3 Calculation: Two dot-product calculations between two n-component vectors.
(5) Type 4 Calculation: Three calculations involving addition of an n-component vector to the scaled version of another.

For a problem involving *m* elements, each with *l* degrees-of-freedoms and a total of *n* degrees-of-freedoms, the number of fetch, store, multiplication and summation operations are shown in Table 3-2.

For an 8-noded brick element with 24 degrees-of-freedom, $l^2 = 576$. For a 20-noded brick element, $l^2 = 3600$. For most problems, *n* is either of the same order

of magnitude as m or at most about 1 order larger, hence the Type 2 calculations clearly dominate the operations and would benefit most from parallel processing. For Type 2a calculations, the number of operations is difficult to estimate and depends upon a number of factors such as the type of element, constitutive model and number of integration points.

Table 3-3 shows the time taken by an Intel Core2 Quad Q9550 2.83GHz desktop PC to complete 50 time steps for a simple example of an idealized elastic cubical domain subjected to bottom horizontal excitation, as shown in Figure 3-10. Hyper-threading was disabled to ensure fully serial computation. Twenty-node brick elements are used in all the calculations.

As Table 3-3 shows, when the number of degrees-of-freedom is less than about 350,000, the time taken for the Types 2 and 2a calculations are of the same order of magnitude. In the example shown, the cases are well-conditioned and convergence is quite rapid. As Table 3-3 shows, the average number of iterations per time step is only a small fraction of the number of degrees-of-freedom. For more ill-conditioned problems, the number of iterations is likely to increase. Thus, in general, one may surmise that the Types 2 and 2a calculations are likely to require roughly the same amount of time. For larger problems, the time needed for the Type 2a calculations rapidly outstrips that of the Type 2 calculation. The combined time taken for the Types 1, 3 and 4 calculations is far less than that taken for the Types 2 and 2a calculations. In other words, Type 2 and 2a are the critical players in terms of the total computational time consumed. Hence, for

parallelization purposes, these two types of calculations will be divided and distributed on multi-PCs or multi-cores to speed up the calculation.

3.5 Domain Decomposition Scheme

Numerous domain decomposition schemes have been proposed in the past (e.g. Kumar and Adeli, 1995; Deng, 2003; Komatitsch *et al.*, 2003; Laemmer *et al.*, 2003; Wang *et al.*, 2005). The main objective of these domain decomposition schemes is to reduce the volume of data transmission required between sub-domains and thereby to reduce the data transmission time. Gullerud and Dodds (2001) and Liu *et al.* (2007) used the METIS graph partitioning software to partition their domain. With this, as well as most of the methods proposed thus far, the sub-domains have to be pre-divided and then ported manually into each computer. To date, no single method has been shown to be optimal or superior compared to the others.

Most domain decomposition schemes are aimed at minimizing the amount of data that need to be transmitted over the network, even at the expense of an increase in the volume of housekeeping which needs to be done within each of the computers. This is based on the assumption that network data transmission speed is far slower than data processing and transmission speed within a node. However, the benchmarking results presented above show that this is not necessarily true, at least for the hardware used in this study; the network transmission speed is at least as high as the core-to-core transmission speed. This is supported by the fact that the element stiffness formation process takes, by far, the most time in each time

step. In such a situation, decreasing the volume of data transmission over the network may result in an increase in housekeeping work, which would have the opposite effect. Thus, instead of merely minimizing the volume of network data transmission, one may need to find an optimal balance between the volume of network data and internal housekeeping work.

This motivates an alternative approach to domain decomposition and data transmission which is explored in this study. Before finite element calculation, the meshed elements are renumbered in such a way as to reduce the front width, this numbering being achieved using Duff *et al.* (1989)'s method. Preliminary trials show that the numbering of the nodal degrees-of-freedom is also largely contiguous (i.e. with relatively few gaps in numbering) and relatively compact. This is consistent with the fact that some amount of optimization has been made to the element numbering in order to achieve an efficient frontwidth. This implies that if the domain is now sub-divided based on its element numbering sequence, the degree-of-freedom numbering within each sub-domain will be largely contiguous and the number of shared nodes will be reasonably reduced. This method of sub-dividing the mesh, based directly on element numbering, is used herein. It has several advantages. Firstly, it is easily automated so that the user does not have to be involved in the decomposition. Secondly, it is easy to trace which sub-domain a particular element resides in as this depends purely on its number. Thirdly, balancing the computational workload of each node is relatively straightforward. Since much of the time is taken up by the formation of the element stiffness matrices and the pre-multiplication of the element stiffness matrix into the $\{p\}$

vector (see Figure 3-9 and Table 3-3), a simple method of balancing computational workload is to sub-divide the domain into sub-domains, each having an equal number of contiguously-numbered elements.

3.6 Data Interchange Schemes

The data interchange schemes used by Gullerud and Dodds (2001) and Liu *et al.* (2007) involves identifying nodal points which are shared by two or more sub-domains and transmitting the data for these shared nodal points over the network. While this is consistent with the objective of minimizing the volume of data transmission over the network, it also increases the volume of housekeeping work on each node significantly since each data item has to be individually pointed to its correct destination. Moreover, it is difficult to balance data transmission workload and synchronize the data transmission process since some sub-domains will have more shared nodes and some nodes may be shared amongst more than two sub-domains. Thirdly, since specific items of data are only interchanged between specific computers, it is difficult to exploit the efficiency of the broadcast and reduce operations. Thus, while some vectors will need to be reduced, the reduction processes will have to be done manually and perhaps by more than one node.

Three data interchange schemes are studied herein and they are as follows:

Scheme 1 – using the broadcast (sending necessary information from head node to other nodes) and reduce (collecting calculated results from all nodes to head node) MPI operations. The individual element matrices, $[A_e]$, are formed by different

processes and stored separately, as shown in Figure 3-11. The matrix-vector multiplication operations $[A_e]\{x_0\}$ between the element matrices and the appropriately segments of the trial solution vector are also carried out on each process simultaneously, and the resultant vector for each sub-domain is computed by its corresponding process. When this is completed, all processors transfer the respective resultant vectors to the first process (Proc 0), where they will be further summed to obtain the global vector for the whole domain; this utilizes the reduce operation. Proc 0 will perform the following computations serially while the other processors wait.

(1) Summation of two vectors, $\{r\} = \{b\} - \{f\}$

(2) Multiplication of two vectors, $\{z\} = [M]^{-1} \times \{r\}$, in which $[M]$, a diagonal matrix, is the modified Jacobi preconditioner.

(3) Dot product of two vectors, $\rho = \{r\} \cdot \{z\}$

(4) Comparison and check $\sqrt{\rho} \le \delta, i > 1$, where δ is the critical tolerance for the iteration and i is the iteration number.

(5) Division of two scalar, $\beta^{(i-1)} = \rho^{(i-1)} / \rho^{(i-2)}$

(6) $\{p\}^{(i)} = \{z\}^{(i-1)} + \beta^{(i-1)} \times \{p\}^{(i-1)}$

After evaluating $\{p\}^{(i)}$, Proc 0 will broadcast it to all other processors, whereupon each processor carries out the multiplication of the matrix $\{p\}^{(i)}$ and the vector $[A_e]$ for each element in its subdomain concurrently, and sums the resulting $[A_e]\{p\}^{(i)}$

for all degrees of freedom in the subdomain. When this is completed, all the processors transfer their respective product vector to Proc 0 (as shown in Figure 3-13 (a)), which then proceeds to execute the following serial code:

(7) Dot product, $c^{(i)} = \{p\}^{(i)} \cdot \{q\}^{(i)}$

(8) Division of two scalars, $\alpha^{(i)} = \rho^{(i-1)} / c^{(i)}$

(9) Updating $\{x\}^{(i)} = \{x\}^{(i-1)} + \alpha^{(i)} \times \{p\}^{(i)}$ and $\{r\}^{(i)} = \{r\}^{(i-1)} + \alpha^{(i)} \times \{q\}^{(i)}$

Proc 0 will then broadcast $\{x\}^{(i)}$ and $\{r\}^{(i)}$ to all other processors to perform the next iteration, until convergence is achieved. The program flow chart is shown on Figure 3-12, in which the parallel calculations are highlighted in green and serial calculations in yellow. This scheme involves the largest volume of data interchange but also the least amount of internal housekeeping.

Scheme 2. This Scheme is similar to Scheme 1 in sequence. However, instead of the broadcast and reduce operations, only data relevant to the active degrees-of-freedom in each sub-domain is transmitted and this is achieved using a few parallel, synchronized send-receive operations as shown in Figure 3-13 (b). As this Figure shows, for a total of N-processors, the first parallel send-receive operation involves N/2 pairs of processors, namely Proc N➦Proc (N-1), Proc (N-2)➦Proc (N-3), Proc (N-4)➦Proc (N-5)….Proc 1➦Proc 0. The next operation involves Proc (N-1)➦Proc (N-3), Proc(N-5)➦ Proc (N-7) …. Proc 2➦Proc 0 and so on. Data corresponding to inactive degrees-of-freedom which are interspersed between the active degrees-of-freedom are not transmitted. The serial operations in Scheme 1 remain as serial

operations. This scheme involved much less data transmission than Scheme 1 but also more internal housekeeping to correlate the data sent and received to its correct degree-of-freedom.

Scheme 3. This Scheme is similar to Scheme 2 except that data corresponding to inactive degrees-of-freedom which are interspersed between the active degrees-of-freedom are also transmitted. This results in less housekeeping than Scheme 2 since the data vector is now contiguous (see Figure 3-13 (c)) and can be added up once the beginning and end points are known. However, it also results in more data transmission than Scheme 2. Compared to Scheme 1, it involves more housekeeping but less data transmission.

The simple model in Figure 3-10 is used to evaluate the efficiency of the three data interchange schemes, and the time taken for 50 time steps is compared in Table 3-1. It is seen that Scheme 1 performs best in terms of time-savings, which may be due to the merit of the *MPI_Reduce* operation compared to send-receive operations. Hence, Scheme 1 is employed in the following parallel computations.

3.7 Parallel Computation Architecture

As discussed in the previous section, in carrying out the finite element analyses, the largest amount of time is spent on (i) calculating the element stiffness & mass matrices, (ii) multiplying matrix and vector, and (iii) updating strain & stress vectors. The main objective of parallel computations is to improve the execution speed of these three calculation types, which may take up to 97% of the solution time in serial calculations. For each element, the calculation of its stiffness & mass

matrices, as well as the updating of the strain & stress vectors, can be carried out independently of all other elements. Thus, such tasks are 'stand-alone' activities that can be directly distributed among the various processors in the group. On the other hand, the solution of the linear system of equations involves all degrees of freedom, which requires a large volume of communication and data transfer among the different processors, and significantly increases the complexity of the parallel computations. Hence, the parallel solution of a large system of linear equations will be discussed separately in the next section.

Apart from the abovementioned processes, the remaining code makes up 80% of the program but executes in less than 3% of the overall solution time. This code will still be executed in the serial mode, so as to retain compatibility with the original serial program.

As shown in Figure 3-11, the first processor (Proc 0) reads geometric data, control parameters, material properties, boundary conditions and seismic excitation from the hard disk, and broadcast the information to other processors. After this, all processors are 'called' to commence preparatory work for the entire calculation domain, such as setting up the in-situ stresses and initializing displacement and load vectors. In forming the element stiffness & mass matrices, each processor deals only with a specific number of elements assigned to it, following a systematic order as shown:

Proc 0 --- element 1 to n_1

Proc 1 --- element n_1+1 to $2n_1$

Proc 2 --- element $2n_1+1$ to $3n_1$

--- --- ---- ---

Proc (n-1) --- element $(n-1)n_1+1$ to n_{el}

in which n is the number of processors involved in the parallel computations, n_{el} is the total number of elements, and n_1 is the quotient of n_{el} and n. In this phase, each processor performs its own set of calculations, which is approximately $1/n$ of the total calculations required for the full domain. Hence the speed-up of the parallel calculations will be n, that is to say, the time required to form the element stiffness & mass matrices for the whole domain is $1/n$ of that required for the serial code.

Besides the speed-up, this phase also exploits another advantage of parallel calculations, in that it allows each processor to store only the matrices corresponding to the elements present in its sub-domain. Hence, the random access memory (RAM) required in each processor is also approximately $1/n$ that of the memory required if the serial code is used. In this way, it is possible for a cluster of linked PCs, each with its own relatively small RAM, to work together to solve large problems.

After the solution of the assembled global system of linear equations (which will be discussed in the next section), the computed nodal acceleration & displacement

vectors are used to update the strain & stress vectors in each element. This process, which is similar to the earlier phase for calculating the element matrices, offers similar speed-up and memory advantages when parallel computations are executed. After each processor updates the strain & stress vectors for the elements corresponding to its sub-domain, it transfers the data back to the first processor (Proc 0) for output, as shown in Figure 3-15.

With the latest strain & stress vectors, the program can either carry out Newton-Raphson iteration, or proceed to the next time step.

3.8 Hyper-threading Parallel Calculation Using OpenMP

Besides the above parallel architecture that uses the MPI platform to link different computers, another lower level parallel architecture, which uses hyper-threading technology, can be utilized among different cores in the same processor. Hyper-threading is different from MPI in that it allows different threads to share the same memory within the same PC and does not require a network to communicate, which can reduce the memory storage requirements and facilitate the execution of the parallel code. However, special attention should be paid to the individual variables in each thread, as such variables may be modified by other threads if they are not declared as private.

The OpenMP (Open Multi-Processing) is the application program standard that provides an easy method for threading applications without burdening the programmer with the complications of creating, synchronizing, load balancing,

and destroying threads (Akhter and Roberts, 2007). In this way, the programmer can spend more time determining which loops should be threaded and how best to structure the algorithms for performance. The full potential of OpenMP is realized when it is used to thread the most time-consuming loops, that is, the hot spots.

By using statements that begin with *!$omp*, the large time-consuming loops in GeoFEA are threaded using OpenMP as follows:

```
!$omp  parallel default(shared)
        !$omp  do private(i),schedule(static,chunksize)
                do i=1,nit
                        … … ! Iteration body
                enddo
        !$omp  end do
!$omp  end parallel
```

in which *nit* is the number of iterations. The iteration body will be distributed to different threads for execution. Once the loops are completed, the parallel threads are terminated using the statement '!$omp end parallel', and the program then reverts to serial execution using one thread.

When using OpenMP for hyper-threading parallel calculations, care should be taken when dealing with the following issues:

- Flow dependencies, which exist when previous iterations of a loop write data that will be read in future iterations, or two iterations write the same value, or a read occurs before a write.
- Race conditions, in which multiple threads attempt to update the same variable at the same point of time.
- Computational overheads, as in the initialization & ending of hyper-threading processes and distribution of the work, all of which require computational time. If the number of iterations is not sufficiently large, the use of hyper-threading may result in a longer execution time compared to a single thread.

3.9 Parallel Hybrid Computations Using MPI and OpenMP

A parallelization combining threads and message passing, compared to just pure message passing, is a promising way to reduce the computational overheads with respect to memory and performance. Hybrid parallelization (Hipp and Rosenstiel, 2004) is the combination of a thread-based programming model for parallelization on shared memory nodes together with message passing based parallelization between the PCs. The hybrid implementation reduces the amount of transferred data because the communication of shared data on each PC takes place internally.

For the hybrid implementation, OpenMP is used for the inner intra-node parallelization and MPI is used for inter-node communication. To achieve better portability, only the master thread calls the MPI functions, because not all MPI

implementation calls are thread safe. So the hyper-threading technology is inserted in the MPI parallel architecture as follows:

```
CALL MPI_INIT(ierr)
    ...    ...
    !$omp  parallel default(shared)
        ...    ...                    ! for hyper-threading technology
    !$omp  end parallel
        ...    ...
CALL MPI_...        ! for inter-node communication
    ...    ...
    !$omp  parallel default(shared)
        ...    ...                    ! for hyper-threading technology
    !$omp  end parallel
    ...    ...
CALL MPI_FINALIZE(ierr)
```

In this way, hyper-threading is performed within each node (PC), and message passing communication is performed among different nodes (PCs) using the Myri-10G network, as shown in Figure 3-16.

3.10 Parallel Performance

The methods and algorithm discussed in the previous sections have been incorporated into the geotechnical finite element code GeoFEA (http://www.geosoft.sg/products/geofea.php). The parallelized, dynamic version

of the code has been successfully ported onto the NUS EIT Lab PC cluster. The parallel performance is presented in the following sections. Section 3.10.1 describes the basic concepts of performance evaluation for parallel software, followed by the performance results measured on the PC cluster.

3.10.1 Parallel Performance Evaluation

The performance of a parallel application is usually evaluated by using the speedup factor, $S(n)$, defined as (Amdahl, 1968)

$$S(n) = \frac{t_s}{t_p} \tag{3.46}$$

where t_s is the execution time on a single processor and t_p is the execution time on a multiprocessor. $S(n)$ gives the increase in speed in using a multiprocessor. The maximum speedup is n with n PC nodes (linear speedup). Super-linear speedup, where $S(n) > n$, may be encountered on occasions, such as when a sequential algorithm needs to use virtual memory due to insufficient RAM, or some unique feature of the architecture that favors the parallel formation.

3.10.2 Performance of Parallel Computation

This section deals with the parallel finite element solution for three pile foundation configurations (2x2, 21x9, 41x11) with sizes ranging from 129,444 to 2,259,345 degree of freedoms (dofs), as shown in Figure 3-17. All the three models are calculated on 1, 2, 4, 8, 16 and 32 PC nodes with and without hyper-threading, and

the computational run-times are summarized in Table 3-6. The PCs used in this exercise run on the Intel CORE i7-950 processor, which has 4 cores and supports a maximum of 8 hyper-threads. However, preliminary studies show that using 8 hyper-threads confers no speed-up compared to 4 hyper-threads. This is not surprising. Using 8 hyper-threads means that every core has to support 2 hyper-threads. This is effective if each hyper-thread only uses a core intermittently, which is often the case in software involving a lot of user interaction. However, in heavily computational work such as finite element analysis, each core is utilized virtually continuously on each hyper-thread. If each core is further required to support 2 hyper-threads, then the core will have to split up its time and resources and incur additional housekeeping work to co-ordinate the two hyper-threads. On this basis, using one hyper-thread per core will be more effective, and hence this is the configuration adopted for hyper-threading in this study. For the quad-core processors used in this study, this implies 4 hyper-threads per PC.

The material properties, boundary conditions, base input motion and calculation results will be discussed later in Chapters 4 and 5. A complete analysis consists of 5000 time steps, which will take too long time on one PC running in serial mode. Hence, the complete calculations are only carried out in Chapters 4 and 5 using eight or sixteen PC nodes with hyper-threading. For the parallel performance study considered in this section, only the first 50 time steps are carried out using different parallel PC configurations ranging from 1 to 32 nodes. Besides GeoFEA, the three same models were also analyzed using ABAQUS v6.11 with user subroutine, so that their respective run-times can be compared.

The processing workload is distributed such that each processor is responsible for approximately the same number of elements and hence, computational operations. When there is good load balance, each processor will complete its tasks at about the same time and synchronization costs will be minimized.

The calculation results from different computation schemes are compared in Figure 3-18. The acceleration response at pile raft of model 1, calculated by both sequential computation and different parallel schemes, are visually the same. There is difference from the sixth significant digit at the last time step, as shown in Table 3-5. The difference is due to the round-off error, and will be discussed in section 3.11.1.

Table 3-6 summarizes the execution times of the solution phase for each model required for the first 50 time steps. It is seen that, for the small-scale model, i.e. Model 1, GeoFEA on one PC node without hyper-threading takes about twice as long as ABAQUS; but for the medium-scale model, i.e. Model 2, GeoFEA on one PC node without hyper-threading could save about 42% off the run-time of ABAQUS. This illustrates the speed advantage of iterative solvers on medium-scale problems. The large-scale model, i.e. model 3 could not be calculated with both GeoFEA and ABAQUS on one PC because the 12GB memory is insufficient for such an analysis. However, when GeoFEA is run in the parallel mode with four PC nodes, this large-scale model could be analyzed by distributing the data to the individual memories on each PC node.

Table 3-5 also highlights that, when more PC nodes are used, additional savings in the computational run-times using GeoFEA can be achieved. By extrapolating the run-time for Model 2, it is expected that the full analysis of 5000 time steps will take about 1703 hours, or almost 2½ months, on one PC node. For most practical purposes, this is probably not acceptable. However, the same analysis for Model 2 takes 153.61 hours to complete when implemented on eight PC nodes with hyper-threading. Similarly, it takes 618.42 hours to complete the Model 3 calculations on sixteen PC nodes with 4 hyper-threading. These run-time results indicate that the parallelized version of GeoFEA provides a feasible and efficient efficient approach for solving large-scale analysis on a normal PC cluster.

The parallel speedup factors for the different node configurations are calculated with respect to the calculation time on one PC node without hyper-threading, as shown in Table 3-7 and Figure 3-19. It is seen that increasing the number of PC nodes could efficiently shorten the calculation times for all three models, with a speedup factor of more than 30 achieved when 32 PC nodes are used with hyper-threading for Models 1 and 2. However, the increase of speedup factors is not linear, and may slow down with too many PC nodes, as can be seen in Figure 3-18 for Models 1 and 2. This may be due to the additional time expended to transfer data among more PC nodes. Compared with the non-hyper-threaded calculations, the use of 4 hyper-threads only increased the speed-up from 1.26 to 2.05. This suggests that the speedup efficiency due of hyper-threading is not very high, which may be caused by congestion on the front-side bus; this will be discussed further in a separate section below. Overall, however, compared to the speedup factor of 15.4

on 64 processors reported by Lu (2006), the speedup factors in Table 3-7 indicates that element-by-element iterative solvers may provide a relatively straightforward, promising and efficient method for the parallelization of large-scale finite element analyses.

3.11 Some Technical Issues about Parallel Computation

This section briefly discussed some of the problems and issues that were encountered in the parallel implementation of GeoFEA on the EIT PC cluster, and how these were addressed, or in some cases, avoided.

3.11.1 Round-off Errors for Parallel Computation

Due to round-off errors from digital computation, the floating-point associative law of addition is not necessarily satisfied. In other words, $a+b+c+d$ is not necessarily equal to $(a+b)+(c+d)$. An example is illustrated below for the case where a = 1234.567, b = 45.67844, c = 0.0004 and d = 0.0003.

The calculation of $a+b+c+d$ is carried out as follows:

1234.567+45.67844=1280.245

1280.245+0.0004=1280.245

1280.245+0.0003=**1280.245**

On the other hand, $(a+b)+(c+d)=$

1234.567+45.67844=1280.245

0.0004+0.0003=0.0007

1280.245+0.0007=**1280.246**

In parallel calculations, the associative law of addition is used extensively to split $a+b+c+d$ into $(a+b)$ and $(c+d)$, which are then distributed to different processes or threads. Hence, the results from parallel calculations will not strictly agree with those from sequential calculations. To overcome this problem, longer format data and stable algorithms are needed. The former is achieved by declaring all floating-point data used in this study as double precision. The increased precision using the double precision format also helps to enhance the stability of the calculations by slowing down the rate of error accumulation.

3.11.2 Limitation of the Front Side Bus in Personal Computer

In personal computers, the Front Side Bus (FSB) is the 'vehicle' (or the connecting path) that carries data between the CPU and the Northbridge (Figure 3-20). The bandwidth or maximum theoretical throughput of the front side bus is determined by the product of the width of its data path, its clock frequency (cycles per second) and the number of data transfers it performs per clock cycle. In PCs and many workstations, the FSB operates at a much lower clock rate and speed than the CPU (http://www.wisegeek.org/what-is-a-front-side-bus.htm). To speed up burst-mode data transfer, motherboards feature a separate bus that directly connects the CPU to special cache (memory) reserves. However, the cache is only effective if high-speed transfer is only needed intermittently e.g. when starting up a software. In continuous high-speed data transfer, such as that required in this study, the

cache is rapidly exhausted and the data transfer rate falls to that limited by the front-side bus.

The lower speed of the FSB, compared to the CPU, means that the FSB is unable to keep with the data demand of the 4 cores if the computations on all four cores require continuous high-speed data transfer. For example, in calculating the following floating-point data operation, the speedup of hyper-threading with 4 cores is still smaller than 2, as shown in Table 3-8. This is because the data transfer rate through the FSB reaches its maximum when 2 threads are used. When more than 2 threads are running, the FSB will experience a bottle neck that affects the overall parallel computations. This explains why, as noted above, the speed-up efficiency when using 4 hyper-threads is not high.

```
do j=1,1000
!$omp  parallel default(shared)
!$omp  do private(i,j),schedule(static)
  do i=1,4000000
     C(i)=A(i)*B(i)     ! A, B, C are double precision
  enddo
!$omp  end do nowait
!$omp  end parallel
enddo
```

To overcome this problem, the algorithm should be improved so as to maximize the re-use of data stored in the cache, which will then reduce the data transfer

through the FSB. As the L2 cache is shared among all the cores, the data in the L2 cache should be used as often as possible.

3.11.3 MPI on Windows Operating System

Windows is an operating system that is built upon the super-threading architecture, which weaves together the execution of different threads in a single processor without truly executing them at the same time. This qualifies it as time-sliced or temporal multithreading, rather than simultaneous multithreading. It is motivated by the observation that the processor is occasionally left idle while executing an instruction from one thread. Super-threading seeks to make use of unused processor cycles by applying them to the execution of an instruction from another thread. In this approach, a task cannot be processed immediately when it is submitted, but needs to wait for its turn. Hence, when a MPI protocol wants to transfer data from one PC to another, both processes which send or receive data need to wait for their turn to do so on their own processor. The transfer cannot be carried out until both processors are available. The waiting time may be longer than the transfer time, even for a small amount of data. Due to this limitation, the highest transfer speed between two PCs is still lower than 700Mbps, even though the network hardware is capable of a transfer rate of 10Gbps. In order to achieve the full network transfer speed, the data transfer operations was promoted to kernel level and directly handled by the processor on the network card.

3.12 Summary

In this chapter, the need for carrying out realistic large-scale finite element analyses involving big piled foundations supporting a multi-storey structure is first highlighted and discussed. However, due to their tremendous computational requirements, such analyses cannot be readily performed using many of the commercial serial-based finite element codes currently available to practicing engineers. While some progress in this area have been made over the past ten years, the reported works in the literature pertaining to soil-pile-structure interaction are still quite limited, with the largest problem size not exceeding half a million degrees of freedom. A comparison of the published studies shows that, while speedup is achievable with parallel computing on cluster machines, the level of efficiency which can be achieved with different algorithms differ significantly.

In this study, a parallelized version of the finite element code GeoFEA was developed and implemented on the PC cluster that has been set up in the NUS Civil Engineering Educational and Information Technology laboratory. Key features of the code, such as the use of hyperthreading and MPI protocols, the element-by-element modified Jacobi preconditioned conjugate gradient iterative solver, and the domain decomposition scheme for distributing the workload to the different nodes, are presented and discussed. The hardware and software factors affecting the computational performance of the finite element analyses are highlighted and discussed.

The performance of the parallelized code as implemented on the NUS PC cluster was tested for three soil-pile foundation models with configurations of 2x2, 21x9 and 41x11 respectively. The runs were carried out using different numbers of PC nodes, ranging from 1 to 32, with and without hyperthreading. The identical models were also analyzed using ABAQUS v6.11 for comparison. The largest model involving 41x11 piles contained about 2.3 million degrees of freedom, and could not be run on both GeoFEA and ABAQUS using one PC node. This model could be analyzed in GeoFEA using 4 PC nodes in about 12 hours with 4 hyper-threads. In all cases, the reduction in computational times achieved by using more PC nodes was clearly demonstrated. Using less than 20 nodes, the increase in speed-up is approximately linear in all cases. With additional nodes, there is a slow-down in the speed-up obtained for Models 1 and 2 with hyperthreading. Such a trend points toward diminishing returns with an increasing number of nodes. The reasons for such diminishing returns are discussed.

In the next chapter, a formal validation of the parallelized finite element code GeoFEA for soil-pile interaction analyses will be carried out using the results from centrifuge experiments. Following this, the analyses will be extended to larger soil-pile-superstructure systems for which systematic parametric studies will be performed.

Table 3-1 Hardware specifications for the cluster PCs

Batch No.	1	2	3	4
Date	2007.3	2008.10	2009.4	2010.7
Number	16	16	48	48
Processor	Intel QX6700	Intel Q9550	Intel i7-950	Intel i7-950
Number of cores	4	4	4	4
Clock speed	2.66GHz	2.83GHz	3.06GHz	3.06GHz
FSB/QPI speed	1066MHz	1333MHz	4.8GT/s	4.8GT/s
Memory size	8GB	8GB	12GB	12GB
Memory speed	333MHz DDR2	533MHz DDR2	533MHZ DDR3	533MHZ DDR3
Hard disk	750GB	750GB	750GB	750GB
OS	Fedora/Windows HPC server 2008	Windows HPC server 2008	Windows HPC server 2008	Fedora/Windows HPC server 2008

Table 3-2 Different operations for EBE-MJPCG calculation

Calculation Type	Fetch Operations	Store Operations	Multiplication Operations	Summation Operations
1	$2n$	n	n	0
2	$2ml^2$	ml	ml^2	ml^2
3	$2n$	0	n	N
4	$2n$	n	n	N

Table 3-3 Time consumed by each calculation type for different model size

Number of Elements	Number of DOF	Time (min)/50 steps	Time (s) for forming matrix. Type 2a Calculation.	Time (s) for multiply of matrix and vector. Type 2 Calculation	Time (s) for vectors calculation. Types 1, 3 and 4 Calculation
1,000	14,883	0.68	17.285	10.327	0.250
8,000	107,163	6.45	170.618	111.104	2.246
27,000	348,843	30.39	903.043	532.899	15.850
64,000	811,923	195.25	8992.132	1668.399	56.722
125,000	1,568,403	1035.45	53903.850	4122.753	141.962
216,000	2,690,283	3763.25	156721.325	4685.100	162.250

Table 3-4 Comparison of time taken for different data interchange schemes (Time in minutes, for 50 time-steps, Intel i7-950 processor, 12GB DDR3 memory per node)

Number of Elements	Number of DOF	Number of PCs involved	Scheme 1	Scheme 2	Scheme 3
8,000	107,163	4	0.81	0.82	0.85
		16	0.23	0.24	0.26
64,000	811,923	4	47.32	50.11	47.48
		16	14.16	14.72	14.52
216,000	2,690,283	4	927.75	969.31	932.76
		16	285.13	295.23	325.57

Table 3-5 Comparison of calculated results from different parallel schemes

Parallel schemes	Acceleration at t=25sec
Sequential Computation	0.87102741005284D-01
1 node with 4 hyper-threading	0.87102749506282D-01
8 nodes w/o hyper-threading	0.87102801138298D-01
8 node with 4 hyper-threading	0.87102830164165D-01

Table 3-6 Execution times of solution phase for soil-pile foundation model (Time in hours, for 50 time-steps, Intel i7-950 processor, 12GB DDR3 memory per node)

Number of PC node	With or without Hyper-threading	Model 1	Model 2	Model 3
Number of equations		129,444	1,338,093	2,259,345
ABAQUS®	--	0.34	29.37**	--*
1	w/o hyper-threading	1.09	17.03	--*
	with 4 hyper-threads	0.64	13.46	--*
2	w/o hyper-threading	0.68	12.76	--*
	with 4 hyper-threads	0.33	8.28	--*
4	w/o hyper-threading	0.32	5.80	15.72
	with 4 hyper-threads	0.15	3.28	12.48
8	w/o hyper-threading	0.17	2.59	10.63
	with 4 hyper-threads	0.08	1.52	6.62
16	w/o hyper-threading	0.10	1.31	5.16
	with 4 hyper-threads	0.05	0.80	3.08
32	w/o hyper-threading	0.06	0.69	2.66
	with 4 hyper-threads	0.04	0.49	1.41

Note: * Due to insufficient RAM, the model cannot be calculated.

** Virtual memory is used for UMAT subroutine.

Table 3-7 Speedup factors of solution phase for soil-pile foundation model

Number of PC node	With or without Hyper-threading	Model 1	Model 2	Model 3
Number of equations		129,444	1,338,093	2,259,345
1	w/o hyper-threading	1.00	1.00	--
	with 4 hyper-threads	1.70	1.27	--
2	w/o hyper-threading	1.60	1.33	--
	with 4 hyper-threads	3.28	2.06	--
4	w/o hyper-threading	3.47	2.94	1.00*
	with 4 hyper-threads	7.49	5.19	1.26*
8	w/o hyper-threading	6.50	6.59	1.48*
	with 4 hyper-threads	13.26	11.21	2.38*
16	w/o hyper-threading	11.67	12.99	3.05*
	with 4 hyper-threads	22.84	21.39	5.12*
32	w/o hyper-threading	20.28	24.56	5.92*
	with 4 hyper-threads	33.56	34.90	11.18*

Note: * Relative to 4 PC nodes.

Table 3-8 Time and speedup factors for hyper-threading (1,000,000,000 times floating-point data operation)

Number of threads	1	2	3	4
Time (s)	50	27	27	27
Speedup	1.00	1.85	1.85	1.85

Figure 3-1 Snapshot of PC cluster in NUS EIT lab

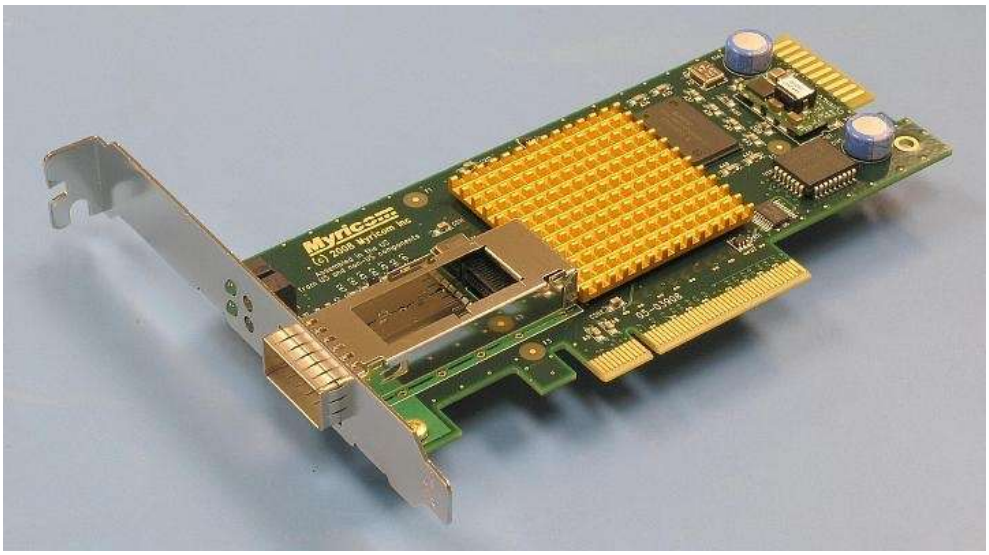

Figure 3-2 Myri-10g network interface card

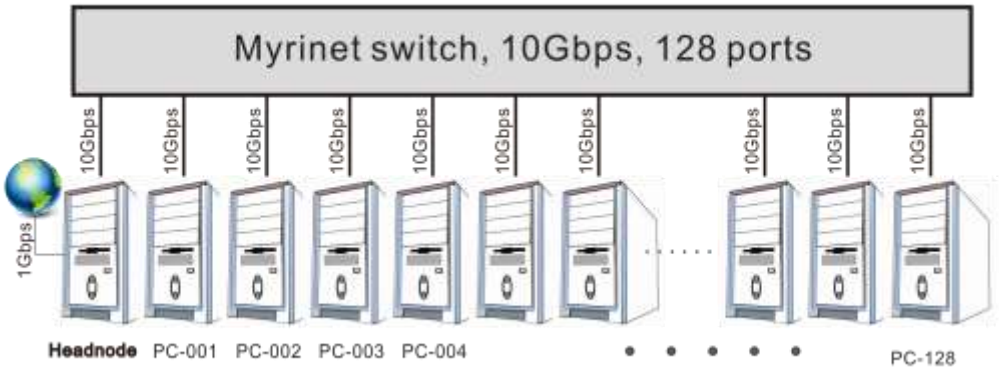

Figure 3-3 Architecture of NUS EIT PC cluster

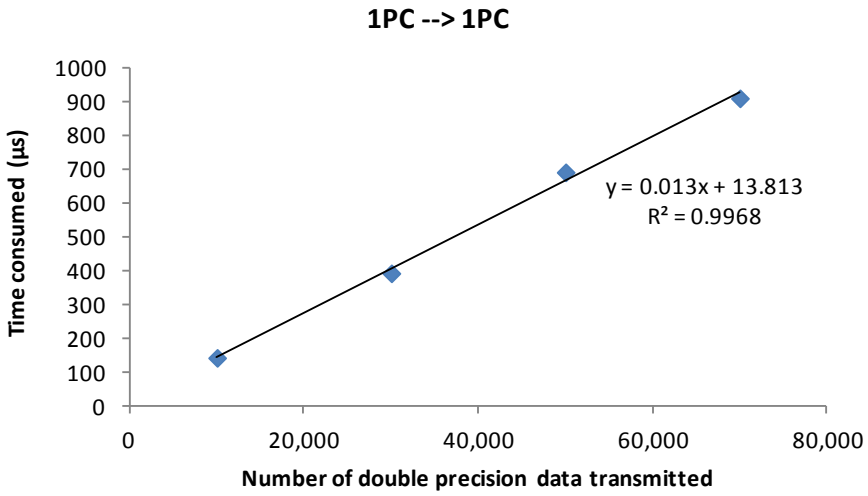

(a) One PC sends and another PC receives

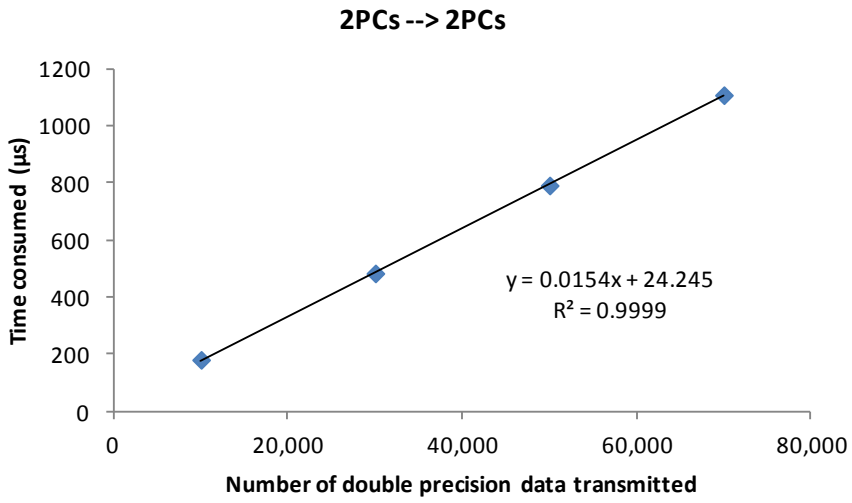

(b) Two PCs send data to another two PCs simultaneously

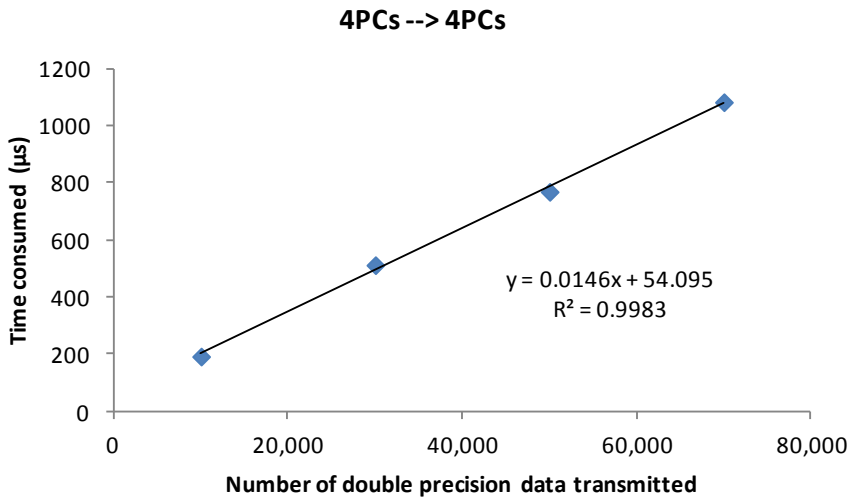

(c) Four PCs send data to another four PCs simultaneously

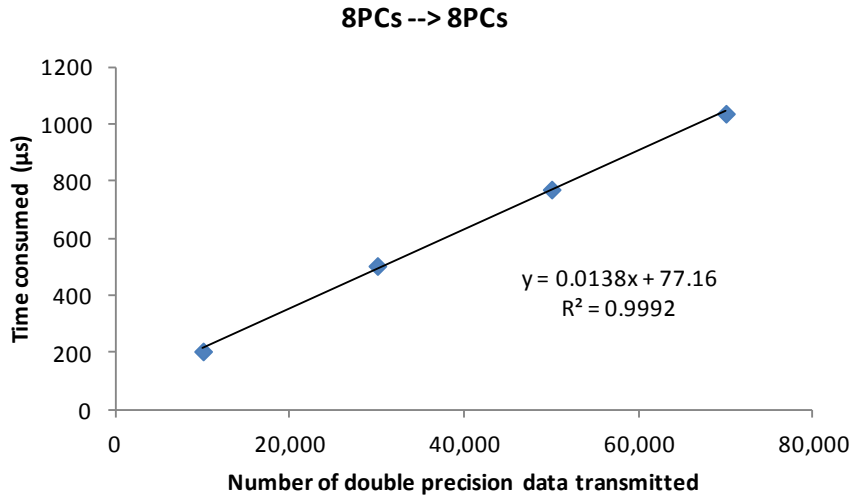

(d) Eight PCs send data to another eight PCs simultaneously

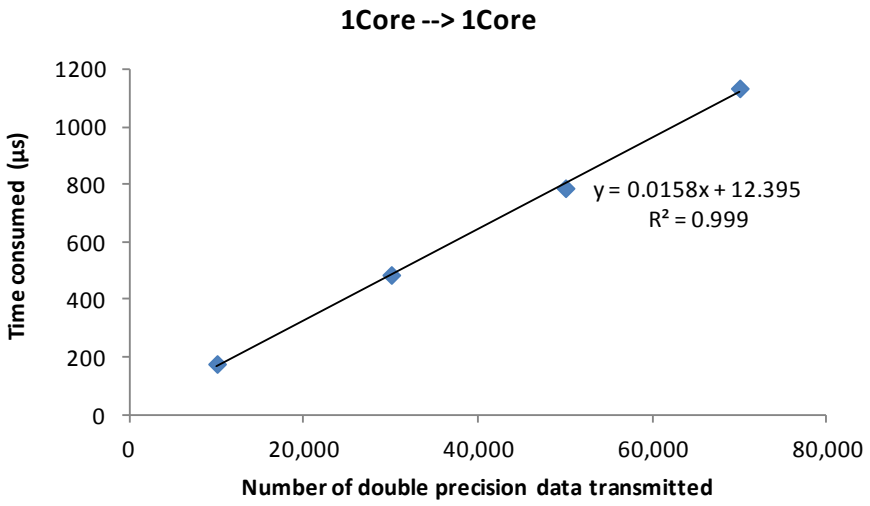

(e) One core sends and another core receives in the same PC (i7-950 processor)

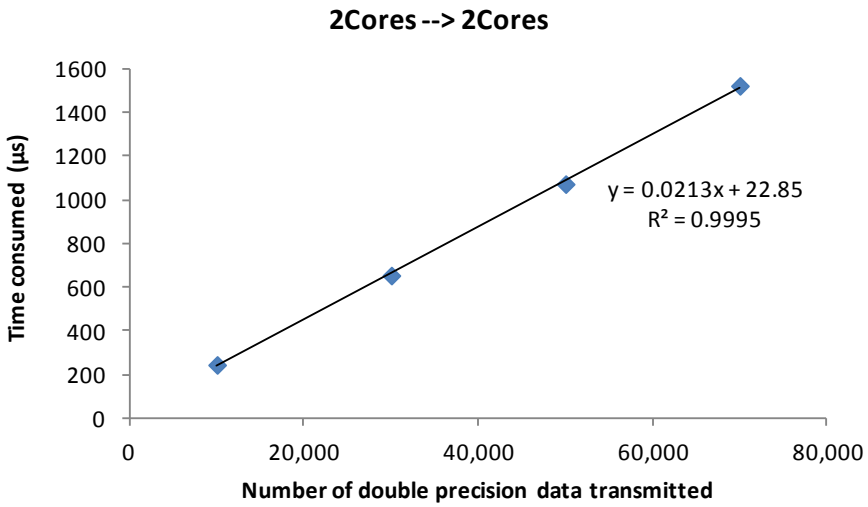

(f) Two cores send data to the other two cores in the same PC simultaneously (i7-950 processor)

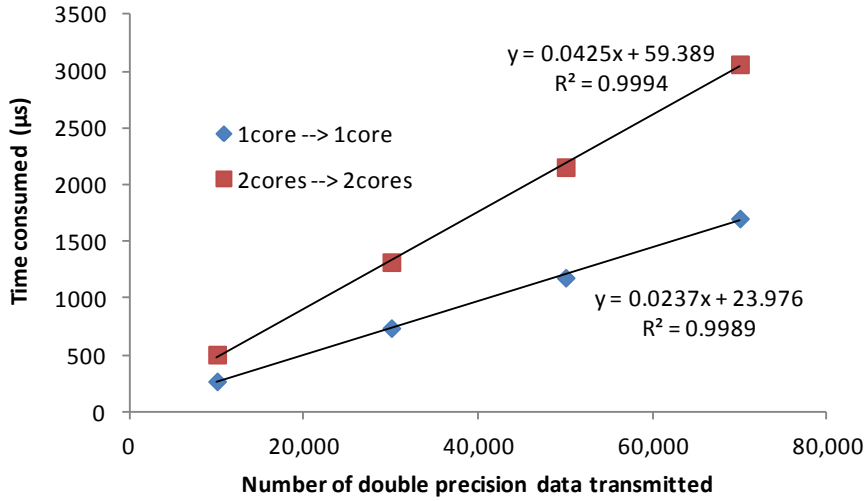

(g) Data transmitting among cores in the same PC (Q9550 processor)

Figure 3-4 Performance of transmitting relatively short data segments

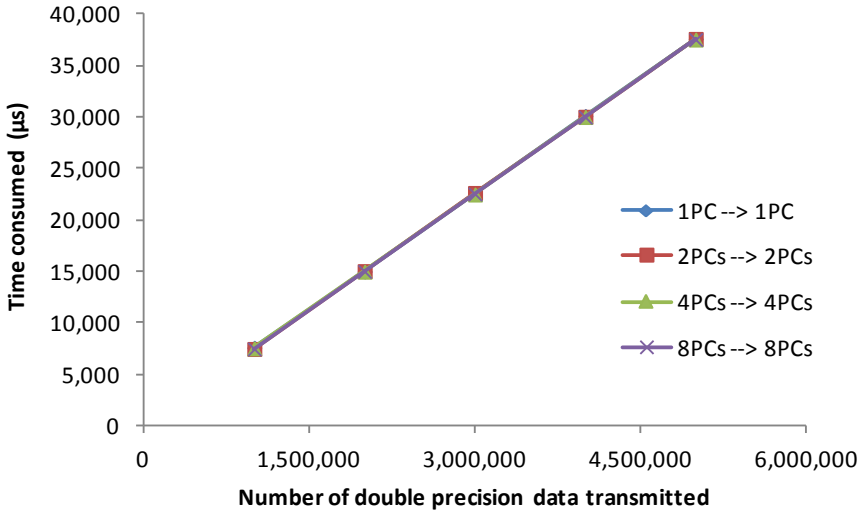

(a) Data transmitting among PCs

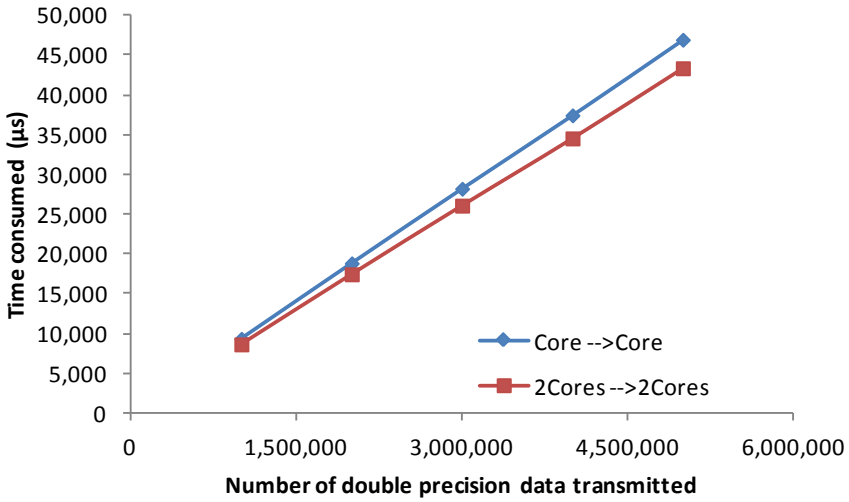

(b) Data transmitting among cores in the same PC (i7-950 processor)

Figure 3-5 Performance of transmitting relatively long data segments

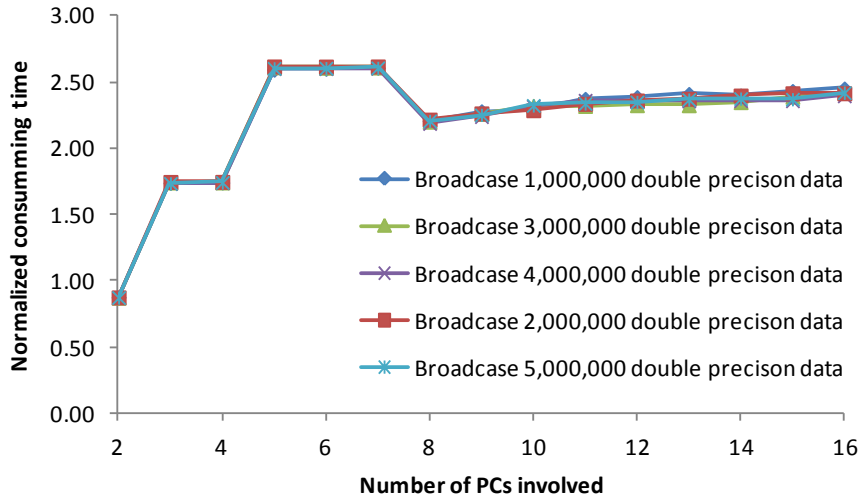

Figure 3-6 Performance of *MPI_Bcast* among PC cluster

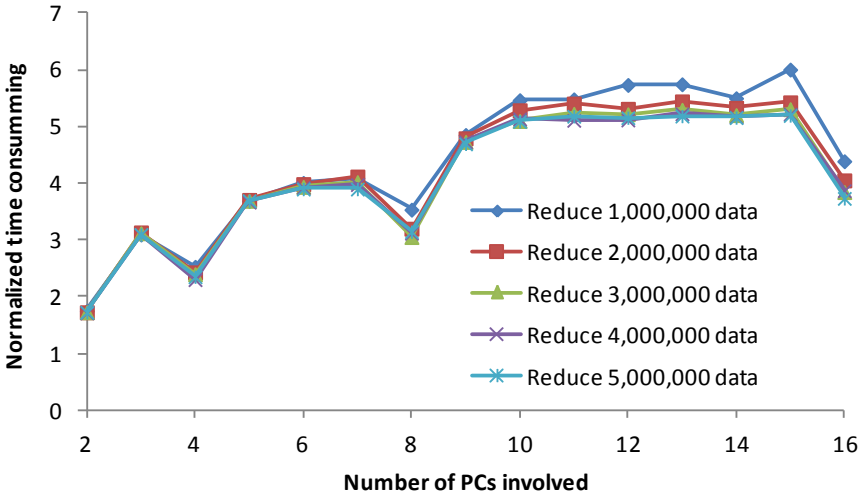

Figure 3-7 Performance of *MPI_Reduce* among PC cluster

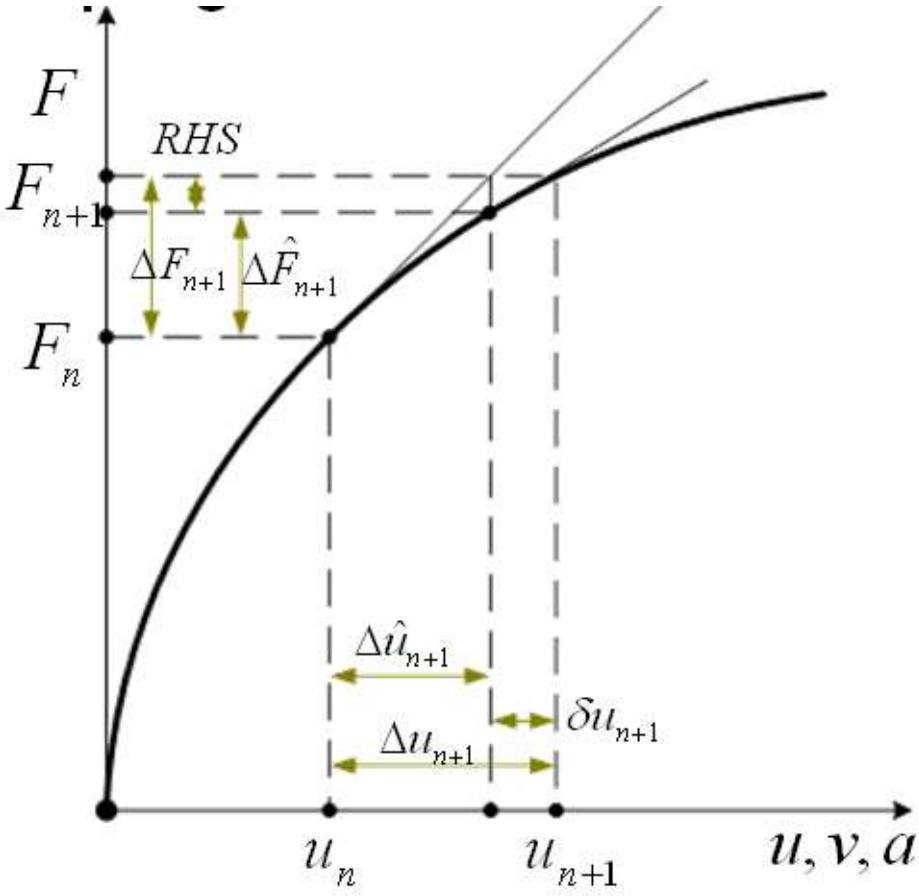

Figure 3-8 Newton-Raphson scheme for dynamic analyses

Compute $r^{(0)} = b - \sum_{e=1}^{nel} A_e x^{(0)}$ *for some initial guess* $x^{(0)}$

For $i = 1, 2, ...$

$Mz^{(i-1)} = r^{(i-1)}$

$\rho_{i-1} = r^{(i-1)} z^{(i-1)}$

if $i = 1$

$p^{(1)} = z^{(0)}$

else

$\beta_{i-1} = \rho_{i-1} / \rho_{i-2}$

$p^{(i)} = z^{(i-1)} + \beta_{i-1} p^{(i-1)}$

endif

$q^{(i)} = \sum_{e=1}^{nel} A_e p^{(i)}$

$\alpha_i = \rho_{i-1} / p^{(i)T} q^{(i)}$

$x^{(i)} = x^{(i-1)} + \alpha_i p^{(i)}$

$r^{(i)} = r^{(i-1)} - \alpha_i q^{(i)}$

Check convergence; *continue if necessary*

end

NOTE : M is the preconditioner; nel is the total number of elements

Figure 3-9 Pseudo-code for EBE-MJPCG (Lim, 2003)

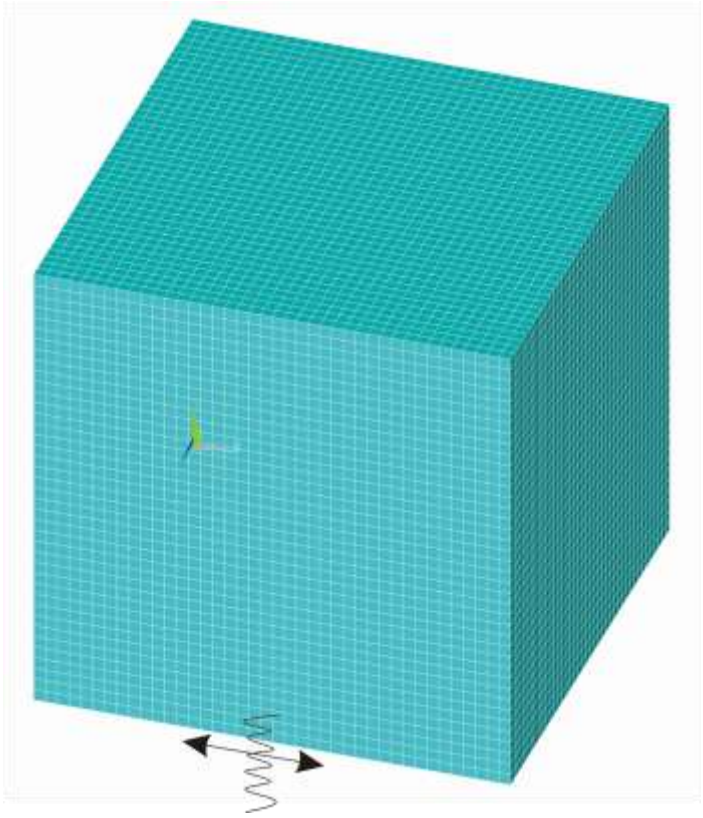

Figure 3-10 Simple model for vertical propagation of shear wave

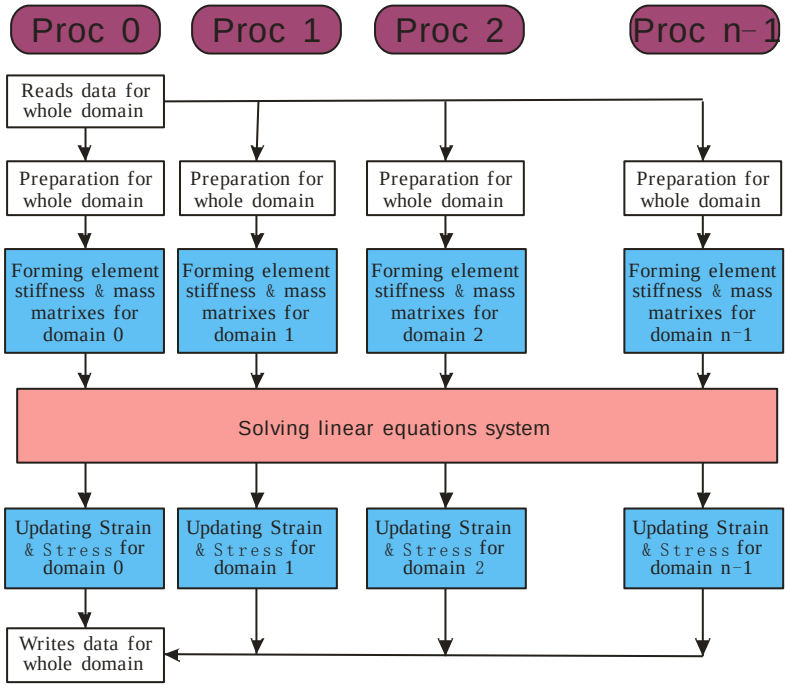

Figure 3-11 Parallel computation architecture

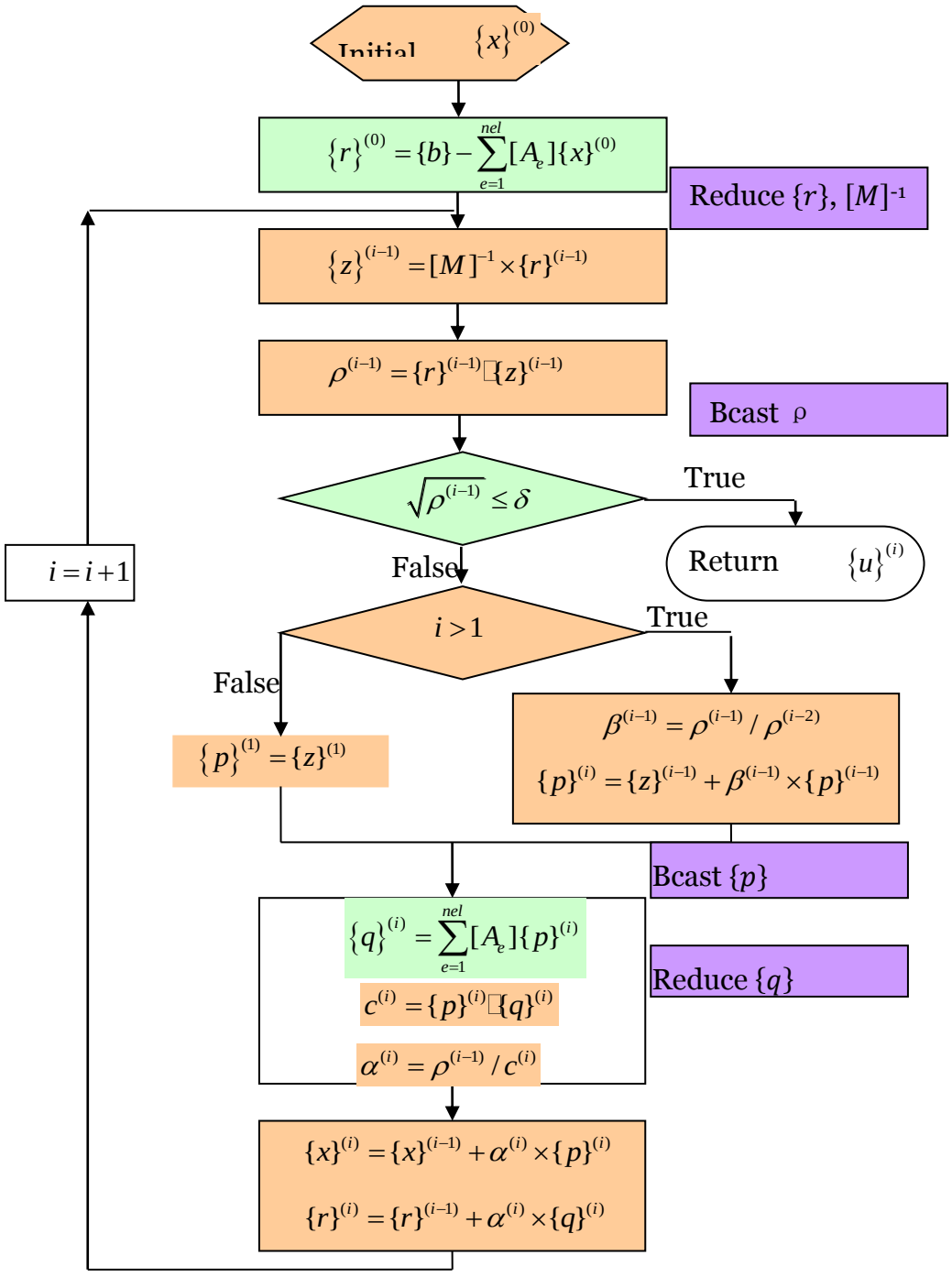

Separate executed on each processor
Time (s) for multiplication of matrix and vector
Executed on processor 0 while other processors are waiting
Time (s) for vectors calculation
Communication among each processor
Time (s) for data transfer

Figure 3-12 Flow chart for parallel EBE-MJPCG method

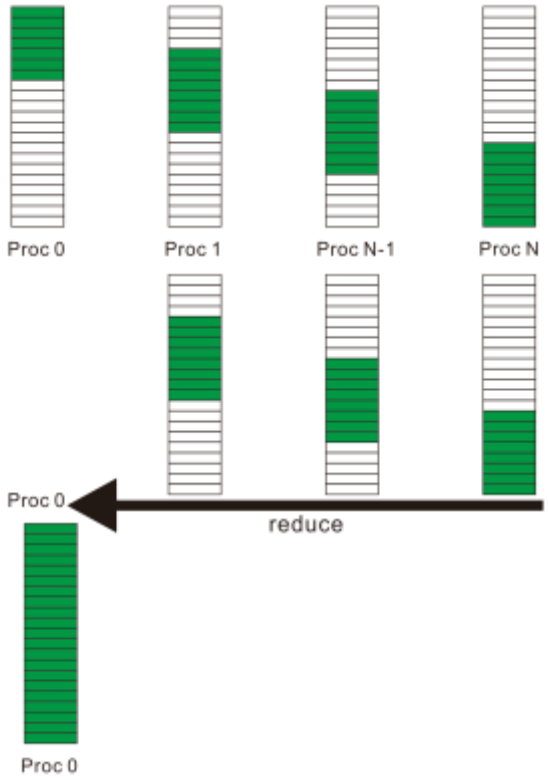

(a) Scheme 1

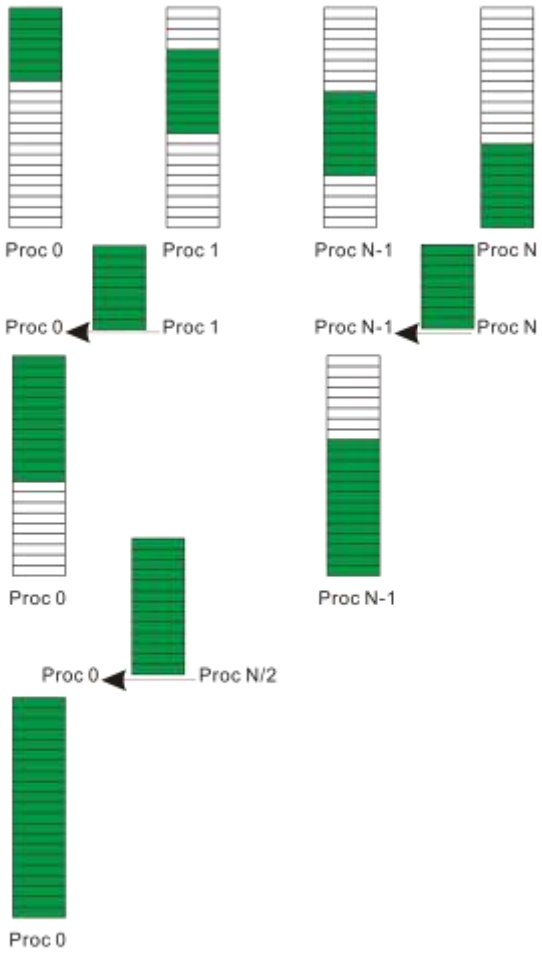
Proc 0
Proc 1
Proc N-1
Proc N
Proc 0
Proc 1
Proc N-1
Proc N
Proc 0
Proc N-1
Proc 0
Proc N/2
Proc 0

(b) Scheme 2

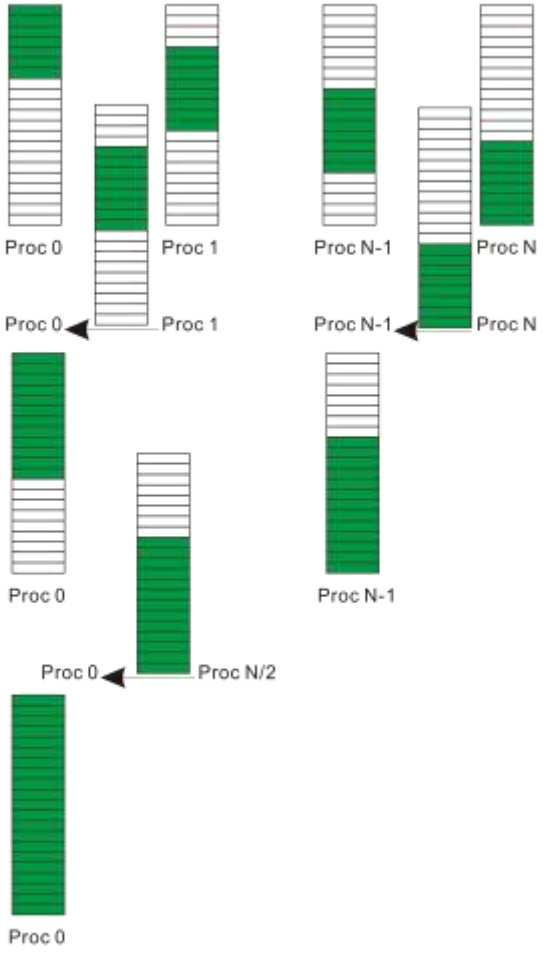

(c) Scheme 3

Figure 3-13 Data interchange schemes

```
CALL MPI_INIT(ierr)
CALL MPI_COMM_RANK(MPI_COMM_WORLD, myid, ierr)
CALL MPI_COMM_SIZE(MPI_COMM_WORLD, numprocs, ierr)
......
CALL MPI_BCAST(BUFFER, COUNT, DATATYPE, ROOT, COMM, ierr)
      ......
CALL MPI_ALLREDUCE(SENDBUF, RECVBUF, COUNT, DATATYPE, OP,
COMM, ierr)
```

Figure 3-14 Sample MPI code for message passing in GeoFEA

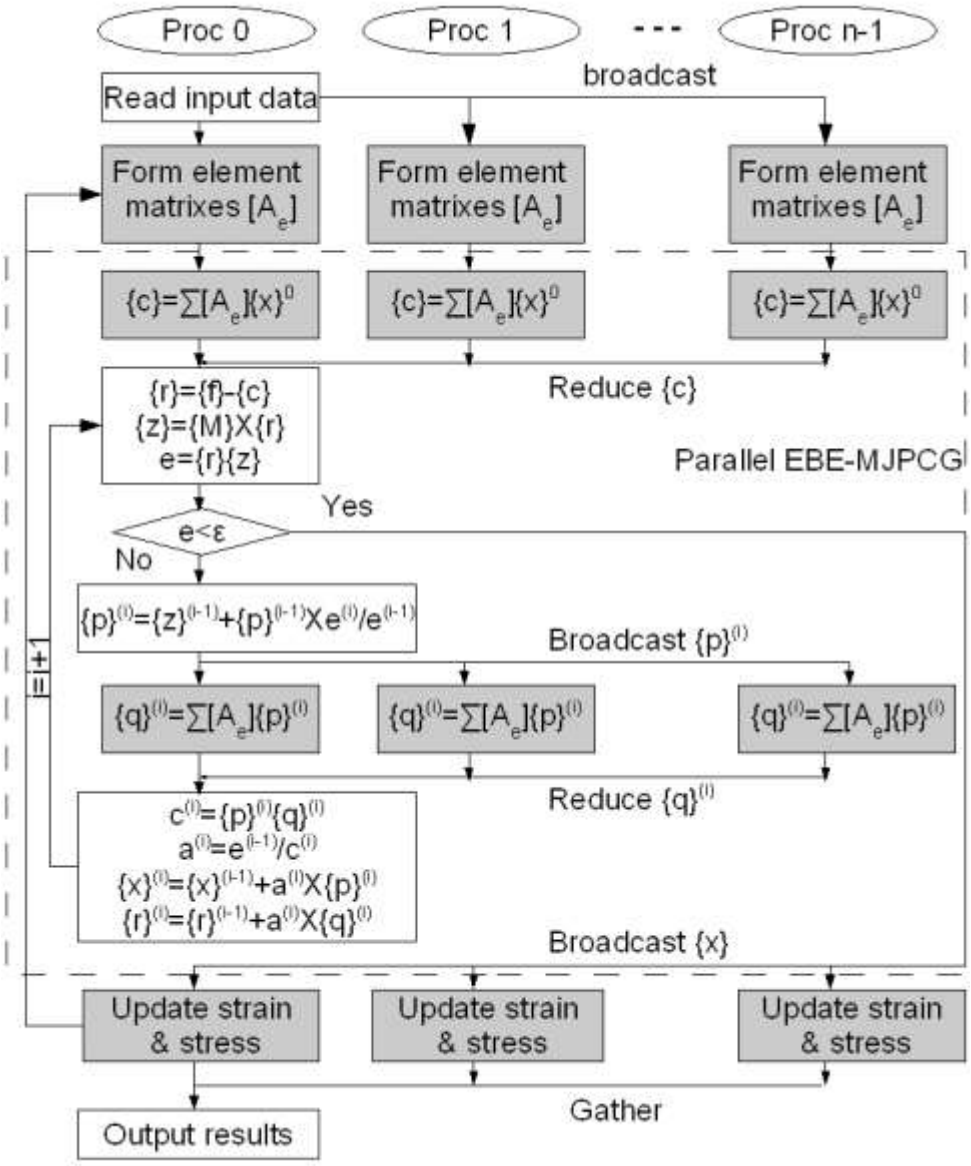

Figure 3-15 Flowchart for parallel program

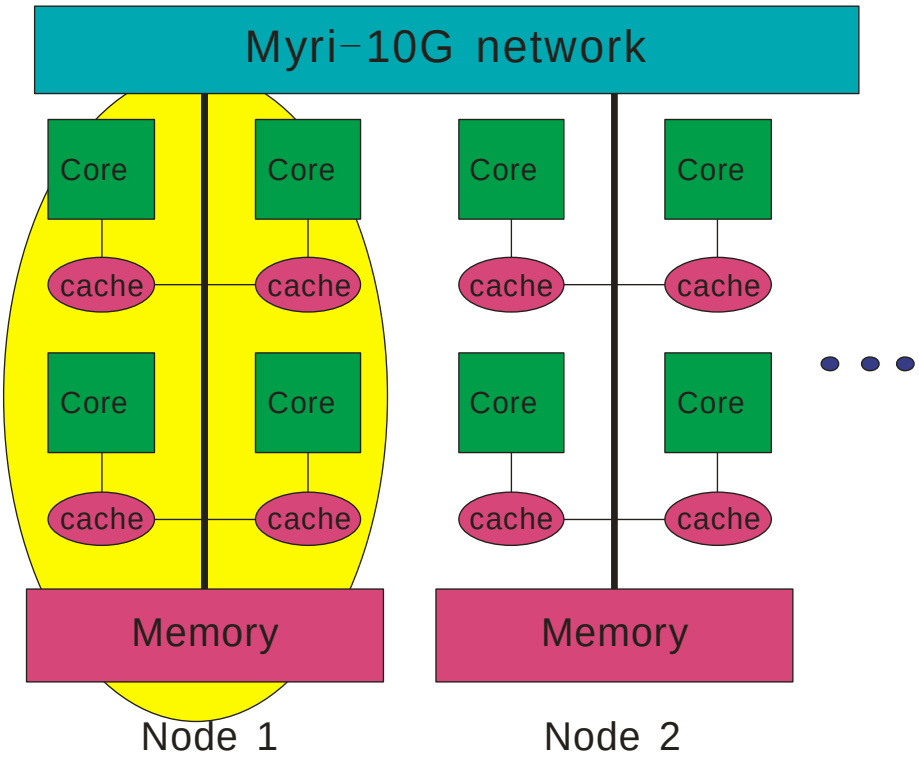

Figure 3-16 Physical model of hybrid parallel architecture

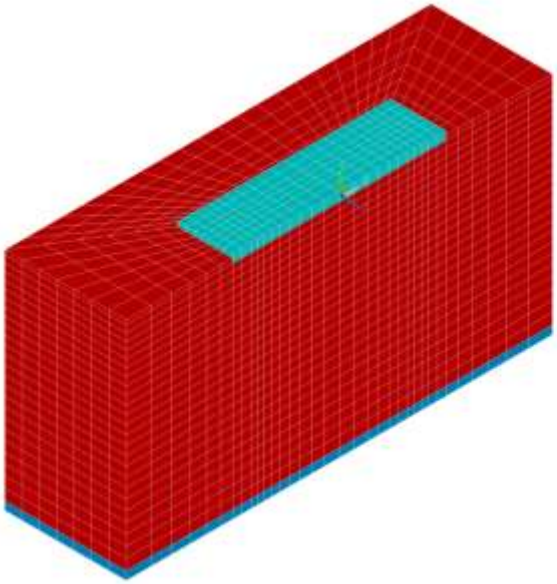

a. Model 1—2x2 piles group (half), with 9,774 elements with 129,444 dofs

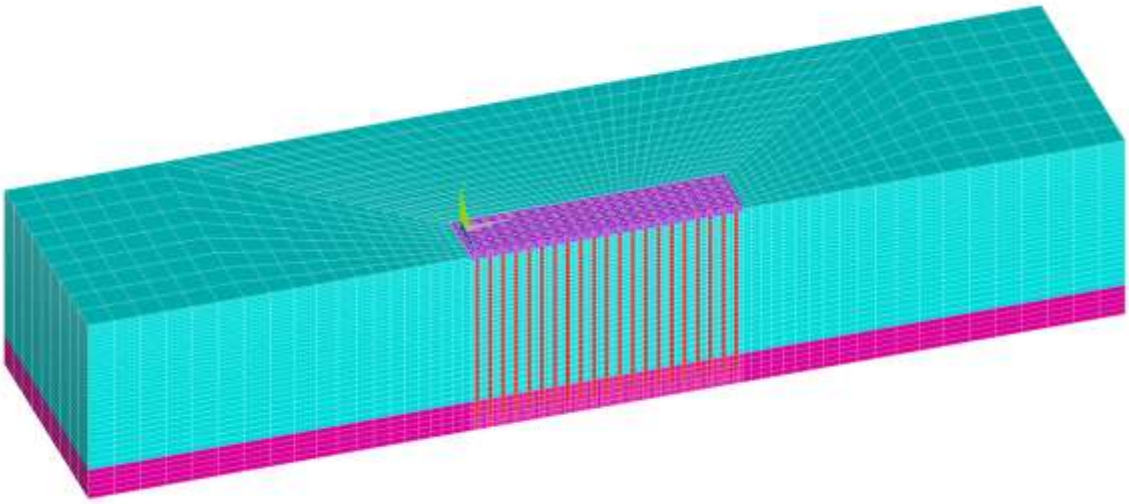

b. Model 2—21x9 piles group (half), with 109,623 elements 1,338,093 dofs

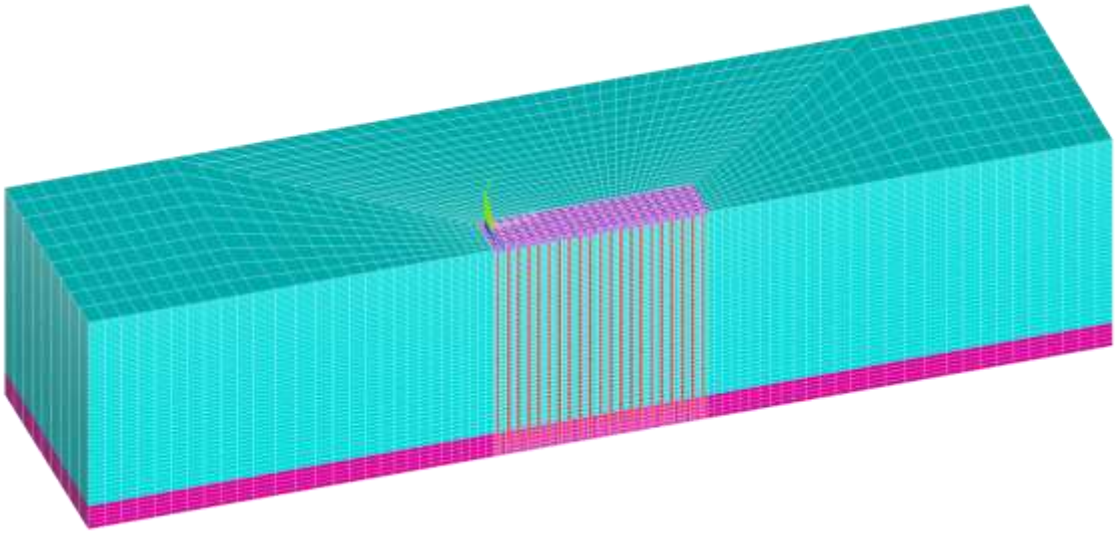

c. Model 3—41x11 piles group (half), with 186,060 elements 2,259,345 dofs

Figure 3-17 Finite element models for different scales of soil-pile foundation-structure systems

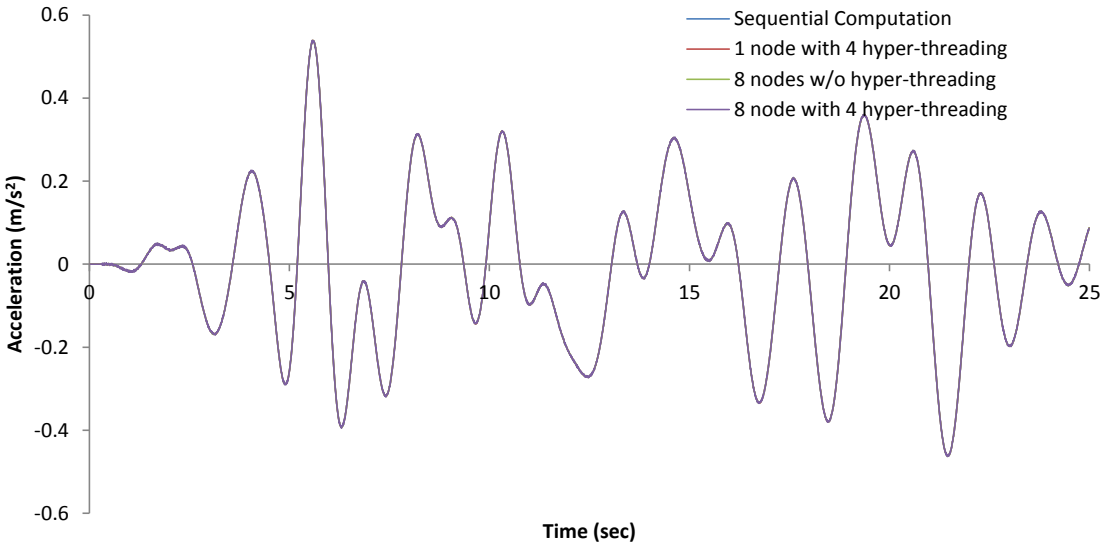

Figure 3-18 Comparison of pile raft response from different computation schemes

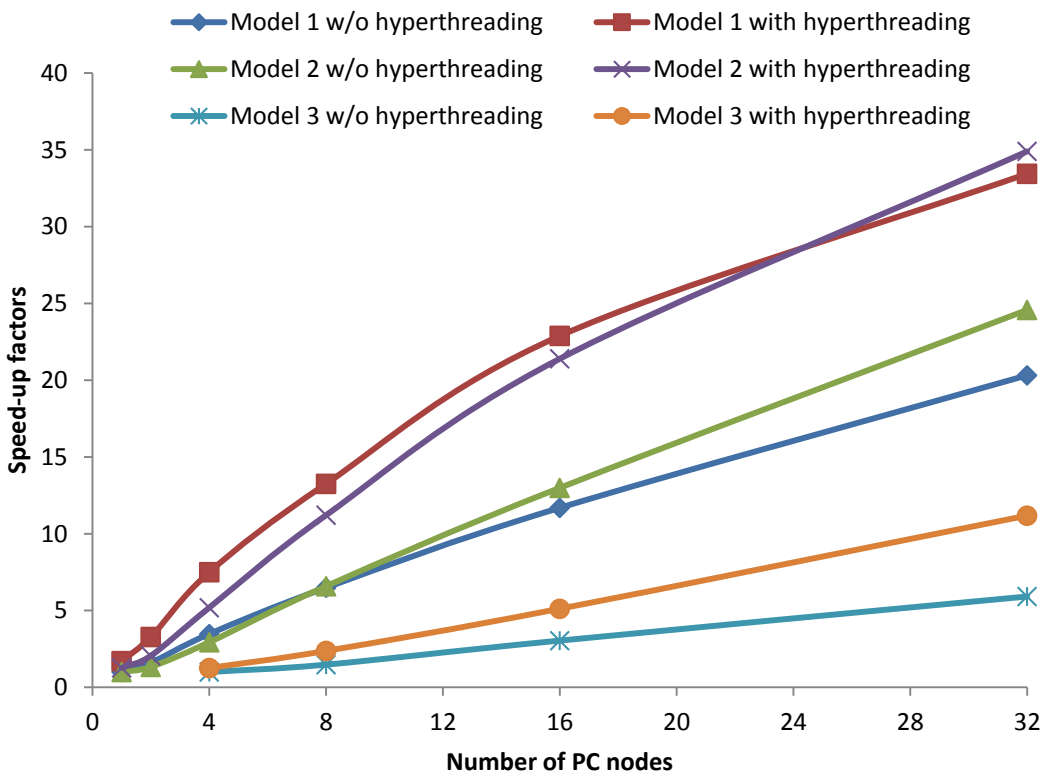

Figure 3-19 Speedup factors of solution phase for soil-pile foundation model

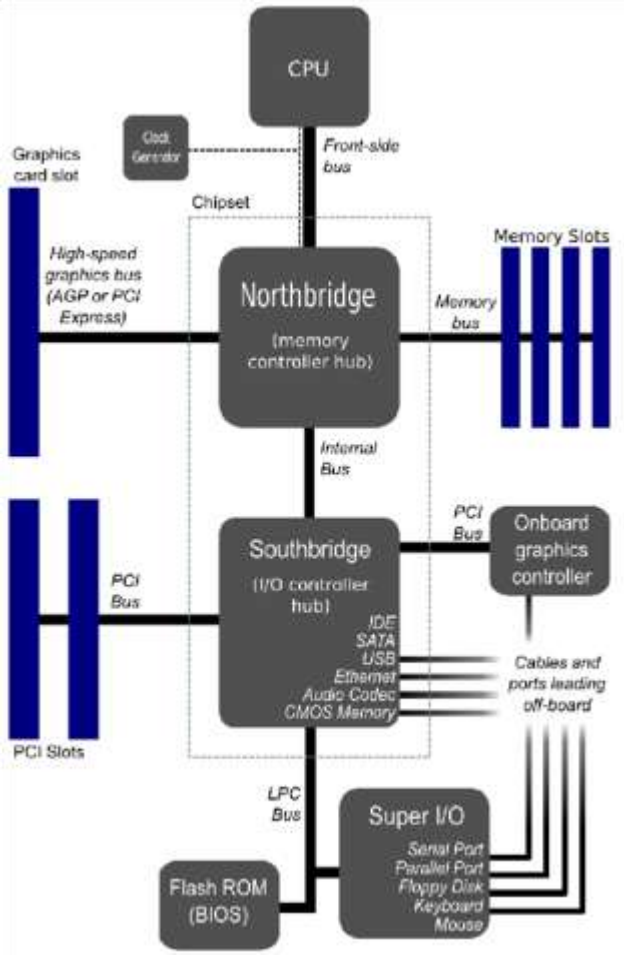

Figure 3-20 A typical north/south bridge layout (Wikipedia, 2007)

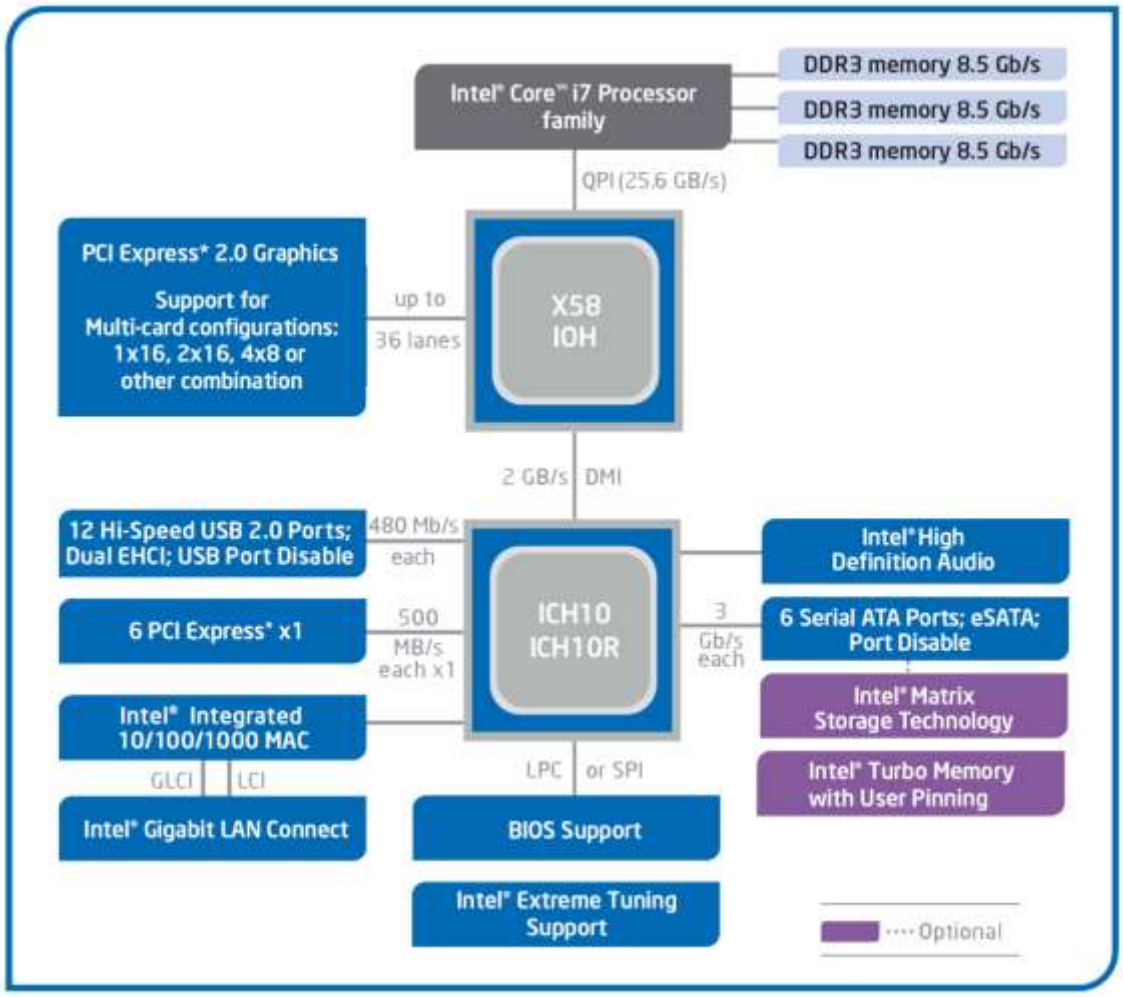

Figure 3-21 A typical layout for QPI and X58 chipset (Mitrofanov, 2008)

Chapter 4 Numerical Simulation of Soil-Pile-Structure Interaction

4.1 Introduction

In the previous chapter, the feasibility of carrying out realistic, large-scale 3-D finite element modeling of a soil-pile-superstructure system was examined, using the computational resources of the PC cluster described in Section 3.3. The analyses were carried out using the parallelized dynamic version of the finite element code GeoFEA, the formulation of which was presented in Section 3.4.

In this chapter, details of the nonlinear hysteretic soil model, as well as its implementation in GeoFEA, are presented. Other features related to the numerical modeling of seismic soil-pile interaction in GeoFEA, such as the pile element type, the pile-soil interface, boundary conditions and the input base motion, are also highlighted and discussed. The finite element code was then validated against the soil and pile response measurements obtained from centrifuge shaking table tests involving small pile foundations. Upon validation, a much larger model involving 21x9 piles of longer length was set up to study the seismic response of more realistic soil-pile-structure systems. The results are presented and discussed, and some comparisons are made with those obtained using the linear elastic model and the pseudostatic approach.

4.2 Numerical Implementation of the Key Features in GeoFEA

The analysis theory, equations, and the numerical formulation underlying the dynamic finite element code GeoFEA were discussed in Chapter 3. For realistic

modeling of seismic soil-pile interaction problems, there are other key considerations related to the constitutive soil model, pile element type, lateral boundary conditions and base motion excitation. These will be discussed in this section.

4.2.1 Soft Soil Constitutive Model for Dynamic Soil-Pile Interaction

From the preceding literature review of Chapter 2, it is quite clear that the seismic performance of pile foundations is significantly affected by the dynamic properties of the soil in which it is installed (e.g., Maheshwari *et al.*, 2004a; Miwa *et al.*, 2006; Shamsabadi, 2007). The dynamic characteristics of soft clay can be summarized as:

- At very small strains (about $\varepsilon_s \leq 0.01\%$), the soil behavior is linearly elastic, and the shear modulus is nearly constant (e.g. Jardine *et al.*, 1986; Dasari, 1996).
- The maximum shear modulus may be approximated as a power function of the soil's mean effective stress p', $G_0 = A \cdot (p')^n$ (e.g. Viggiani and Atkinson, 1995; Banerjee, 2009).
- The shear modulus reduces significantly from G_0 to about $0.1G_0$ as the shear strain increases from 0.01% to 1%, with the typical normalized shear modulus exhibiting the inverse S-shape, as shown in Figure 4-1 (e.g. Hardin and Drnevich, 1972; Vucetic and Dobry, 1991; Kagawa, 1992; Ishibashi and Zhang, 1993; Banerjee, 2009).

- The shear modulus increases with frequency, but the effect is quite insignificant compared to that of the strain (e.g. Zanvoral and Campanella, 1994; Teachavorasinskun *et al.*, 2002).
- The damping ratio in clay increases from about 3% to about 30% as the shear strain increases from 0.01% to 1%, following an S-shape curve, as shown in Figure 4-2 (e.g. Hardin and Drnevich, 1972; Vucetic and Dobry, 1991; Kagawa, 1992; Ishibashi and Zhang, 1993; Banerjee, 2009).
- At small strains, the shear modulus is independent of the number of load cycles. However, when the strain amplitude exceeds a threshold level, typically about 0.1%, the soil stiffness will decrease under repeated loading (Kokusho *et al.*, 1982; Matasovic and Vucetic, 1995), a phenomenon known as "stiffness degradation". This is also usually accompanied by a decrease in strength, the decrease being dependent on the strain level and the number of cycles applied (e.g. Zhou and Gong, 2001; Nishimura *et al.*, 2007; Banerjee, 2009).

Following these characteristics, many constitutive models have been proposed to replicate the stress-strain relationship of soft clay. Pyke (1979) combined the nonlinear hyperbolic model proposed by (Duncan and Chang, 1970) and Masing's rules to develop a hysteresis model for one-dimensional simple shear-type loading. The model was applicable to soils that do not exhibit cyclic degradation. Vucetic (1990) extended it to the behavior of cyclically degradable clays. Hyodo *et al.* (1994) proposed a semi-empirical model to evaluate the residual shear strain under cyclic loading. Pastor *et al.* (1990) redefined the loading-unloading-reloading directions

in the boundary surface model and proposed a generalized plasticity model to simulate the cyclic behavior of sands and clays. Yu *et al.* (2007) developed a simple unified bounding surface plasticity theory to model the stress-strain behavior of sand and clay under both drained and undrained cyclic loading conditions. Masin (2012) developed the hypo-plastic model to simulate the clay behavior under cyclic loading. However, these models could only reproduce parts of the characteristics listed above. More importantly, their performance and applicability have not been evaluated for Singapore Marine Clay.

Based on the results of resonant column tests and cyclic triaxial tests on Malaysian kaolin clay, Banerjee (2009) proposed a hyperbolic-hysteretic constitutive relationship for three-dimensional finite element analysis; this is essentially a three-dimensional generalization of the one-dimensional hyperbolic model. The model is based on nonlinear elastic theory and cannot reproduce the generation of excess pore pressure during cyclic loading, but it was able to capture most features of cyclic behavior of soft clays. The maximum shear modulus for the normally consolidated kaolin used by Banerjee (2009) may be estimated using

$$G_0 = 2060\left(p'\right)^{0.653} \tag{4.1}$$

in which p' is the mean effective stress; this allows the shear modulus to vary with effective stress in a nonlinear manner. The shear stress-strain relationship is shown in Figure 4-3 and may be mathematically described as follows:

$$q=\begin{cases} q_f-\dfrac{1}{3G_0/q_f}\left[\dfrac{3G_0}{1+3G_0\varepsilon_s/q_f}\right] & \text{loading path} \\ -2q_f+\dfrac{2}{3G_0/q_f}\left[\dfrac{3G_0}{1+3G_0\left(\varepsilon_{r1}-\varepsilon_s\right)/\left(2q_f\right)}\right]+q_{r1} & \text{unloading path} \\ 2q_f-\dfrac{2}{3G_0/q_f}\left[\dfrac{3G_0}{1+3G_0\left(\varepsilon_s-\varepsilon_{r2}\right)/\left(2q_f\right)}\right]-q_{r2} & \text{reloading path} \end{cases} \quad (4.2)$$

in which, q_f is the undrained deviator stress at failure, which can be calculated using the modified Cam clay model as

$$q_f=\frac{6\sin\varphi}{3-\sin\varphi}p'\left(\frac{1}{2}\right)^{\frac{\lambda-\kappa}{\lambda}} \quad (4.3)$$

The degradation for soil stiffness and strength during cyclic loading follows the exponential decay model proposed by (Idriss *et al.*, 1978). For kaolin clay, Banerjee (2009) proposed the following fitted equation to characterize the cyclic degradation response:

$$\frac{G_{\max,N}}{G_{\max,1}}=\frac{q_{f,N}}{q_{f,1}}=N^{-(0.0536\log\varepsilon_r+0.1285)} \quad (4.4)$$

To some extent, this degradation feature serves to make up for the limitation of the model in not explicitly evaluating the excess pore pressure. More details about this model are available in Banerjee (2009)'s thesis. This model is adopted herein to simulate the behavior of the soft clay considered in this study.

4.2.2 Pile simulation

In finite element analysis of soil-pile interaction, the piles are often modeled as linear elastic structures; this being consistent with the fact that, structurally, piles

are usually designed to operate within their elastic range (Eurocode 8, 2006; IBC 2009). The proper simulation of piles is an important aspect in seismic soil-pile interaction analyses. One approach is to use 2-node or 3-node beam elements to model piles (e.g. Uzuoka *et al.*, 2007; Gu, 2008; Dezi *et al.*, 2010). With this method, it's easy to mesh the soil domain and obtain the bending moments and shear forces in the piles. This approach was also adopted in the initial phase of this study (Zhao *et al.*, 2010), but it was subsequently abandoned due to the following limitations:

- The beam element could not represent the finite cross-sectional area of the pile which has a significant influence on the stress field of the soil around the pile. In many instances, this can result in overestimation of the stresses in the soil elements connected to the beams, which may lead to errors when stress-dependent soil models are used.
- The connection between the beam element and the solid element could not adequately represent the pile-soil interface.

Alternatively, solid elements are also used to model the piles (e.g. Trochanis *et al.*, 1988; Lu *et al.*, 2005; Mahboubi and Panaghi, 2010). This approach captures the pile dimensions more realistically. However, it often requires many more elements and degrees-of-freedom, and therefore increased computational resources, especially for large-scale problems. Furthermore, it is difficult to compute the pile bending moment and shear force directly. Hence, pile bending moments are often

not computed directly using this approach (e.g. Maheshwari *et al.*, 2004c; Miao *et al.*, 2006; Chau *et al.*, 2009).

In order to determine the bending moment along the piles, several approaches have been proposed and adopted in previous studies. Lu (2006) used 20-node brick elements for all materials, including piles, to simulate the seismic soil-pile-wharf interaction. After solving the equations, the computed profile of the pile displacements along its central axis was mapped to an equivalent column of beam elements representing the pile to calculate the axial forces and bending moments using SAP 2000. Banerjee (2009) used a line of very flexible beam elements along the discretized pile axis (as shown in Figure 4-4) and calculated the pile bending moments by upscaling the bending moments of the flexible beam. This is equivalent to using the beam elements to capture the curvature of the pile and then using the correct flexural rigidity to obtain the bending moments. Similarly, Zhang *et al.* (2000) used a hybrid element consisting of a beam element and several solid elements to simulate the pile. The bending stiffness of the pile is the weighted average sum of the bending stiffness of the beam and solid elements, based on a 9:1 ratio. All these three methods assume that the pile behaves as an Euler–Bernoulli beam wherein all planar cross-sections remain plane and perpendicular to the neutral axis during bending. However, this approach may lead to significant underestimation of bending moments in the vicinity of the pile–raft joint where the Euler-Bernoulli beam assumption could not be satisfied and the pile curvature does not follow that of an Euler beam. This is readily illustrated by fixing the raft and applying a transverse point load at the pile tip, as shown in Figure 4-4. In

Figure 4-5, the theoretical bending moment is obtained by treating the pile as a cantilever. As can be seen, the bending moment obtained using the embedded beam element is accurate along much of the pile length, but is underestimated in the vicinity of the pile-raft joint, as shown in Figure 4-5. The length of the segment where large errors are incurred is about twice the pile diameter, which is also the critical portion of the pile near the joint where the maximum pile bending moment usually occurs. This phenomenon was also alluded to in Banerjee (2009)'s results. Hence, the use of embedded beam elements to simulate the pile may yield a maximum bending moment which is smaller than the cantilever solution.

Figure 4-5 also shows the computed bending moments obtained by integrating the stresses across the cross-section of the pile simulated using solid elements; this obviates the need to replicate the curvature of the beam accurately. This study also uses the 20-node hexahedral element to model both pile and soil. The pile is assumed to have a square cross-section, which is commonly assumed in pile studies (e.g. Trochanis *et al.*, 1988; Lu *et al.*, 2005; Lu, 2006; Maheshwari and Sarkar, 2011). The square pile sections are discretized into 2x2 hexahedral elements, as shown in Figure 4-4, Figure 4-6, and Figure 4-14. The pile bending moment can be calculated by integrating the normal stresses with respect to the area at all the Gauss points within the cross-section, as shown in Figure 4-6. Each 20-node hexahedral element has 27 Gauss points located over three layers. The neutral axis of the cross-section formed by the four elements coincides with the

pile axis and is perpendicular to the loading direction. Accordingly, the bending moment is given by

$$M = \sum_{elem} \int_{area} \left(\sigma - \sigma_{avg} \right) \cdot s \cdot dA \tag{4.5}$$

in which σ_{avg} is the average of the axial stress within the whole pile cross-section, and s is the distance from the Gauss point to the natural axis. More details about the stress integration can be found in Hearn (1997). As shown in Figure 4-5, this method yields accurate bending moments along the whole pile, right up to the pile-raft joint.

4.2.3 Pile-Soil Interface

Under earthquake loading, sliding and separation may occur between the piles and soil, due to their different characteristics. Pile-soil gapping has been observed in post-earthquake surveys (e.g. Horikoshi *et al.*, 2000) and shaking table tests (e.g. Meymand, 1998; Wei *et al.*, 2001). The significance of soil-pile interface was also discussed in previous studies involving beam-on-dynamic-Winkler-foundation approach (e.g. Lok, 1999) as well as the finite element method (e.g. Lu *et al.*, 2005; Chang, 2007).

Lok (1999) simulated the nonlinear p-y curve with gapping using a configuration that comprises a friction element in parallel with the gap element and nonlinear spring. In many finite element analysis, the pile elements and soil elements share the same nodes at the interface, so that the pile and soil are constrained to have same displacement (Lu, 2006; Banerjee, 2009). This approach ignores the possible

pile-soil gap and may produce tensile stresses in the soil during strong shaking. Chang (2007) proposed zero-length soil springs to connect pile and soil in all three directions. The strengths of these springs were dependent on the effective stress level, and hence could degrade with increasing excess pore water pressure. Chau *et al.* (2009) used the *NNLink* element in "SAP 2000 Nonlinear" to simulate the gap between soil and pile. The gap elements were applied between the pile and soil only in the shallower soil where the pile-soil gap might appear. In the closed mode, the gap element transfers the normal stress between pile and soil, while in the opened model, no force is transmitted across the gap element. Lu *et al.* (2005) used the surface-surface contact element in ANSYS to simulate the pile-soil interface. The pile surface was set as the target while the soil surface was taken as the contact. The contact pair could transfer compression and shear stress, and eliminate extension stress between pile and soil.

These studies suggest that pile-soil interface behavior is dominated by the gapping effect. Before gapping occurs, the stress and strain response follows the general principles of mechanics, satisfying compatibility of deformation and equilibrium of forces. This phase could be calculated with conventional finite element analysis which uses regular solid elements. However, when the pile and soil separate and the gap occurs, such analysis might produce extensional forces between the pile and soil, which is incorrect. While the idea of contact elements is attractive, such an element is highly non-linear. It will also increase the number of elements and degrees-of-freedom significantly, thereby increasing the amount of computation.

As a large number of piles is modeled in this study, it is felt that such an approach is not feasible. Instead, a simplified "no-tension" approach is used (e.g. Desai *et al.*, 1984; Day and Potts, 1994), whereby the tensile stresses in parts of the pile are nullified. This involves developing a modified elastic constitutive model for piles to simulate the gapping effects.

In this approach, the normal stresses in the direction of shaking in the pile elements adjacent to the interface are checked in each time step. If the normal stress is positive, the pile-soil interface is considered to be in compression and no gap occurs. If the normal stress is negative, the pile-soil interface is considered to be in tension and a gap is then assumed to exist between pile and soil. In order to replicate this gapping effect, the negative normal stress in the corresponding integration point of the pile element is set to zero. The resulting unbalanced force at the pile-soil interface nodes will then be equilibrated using Newton-Raphson iteration. This approach was validated in this study using Zhang *et al.* (2011)'s centrifuge model pile test data, as shown in Figure 4-8.

4.2.4 Lateral boundary conditions

In finite element analysis involving wave propagation, boundary reflection is often an important aspect which needs to be addressed. Wave energy reflection at the artificially truncated boundaries can lead to a build-up of wave energy within the finite element domain, which would reduce the accuracy of the simulation or produce erroneous results. Numerous types of infinite or transmitting boundaries have been proposed to simulate the energy radiation through the truncated

boundary toward the infinite domain. Uzdensky and Kulsrud (1998) and Bosello *et al.* (2007) proposed a viscous boundary to absorb the wave energy at the lateral boundary. Kim *et al.* (2000) and Javan *et al.* (2008) proposed transmitting boundaries to transmit waves outward without reflection. Tzong and Penzien (1983) used an impedance model to represent the far-field soil that lies beyond the finite element domain. Rizos and Wang (2002) and Wijaya (2009) coupled finite elements and boundary elements to simulate the near-field and far-field regions respectively. Yerli *et al.* (2003) and Seo *et al.* (2007) developed infinite elements using approximate expressions of multiple wave components for the wave function to model the exterior soil region. Chu (2006) used dashpots to simulate radiation damping on the cut off boundary in both normal and tangential directions. One common shortcoming of these methods is that their parameters are frequency-dependent, and hence difficult to determine in time domain analysis.

Another simple approach commonly used in seismic finite element analyses is to constrain the base and side nodes from moving in all directions except for the direction of shaking, which is unconstrained. This approach is commonly used in liquefaction and soft soil problems. Its rationale is derived from the assumption that the soft soil layer is underlain by a much stiffer soil or rock layer which is reasonably simulated by a rigid boundary constrained in the vertical direction but imparts earthquake motion in the lateral direction. Secondly, if the side boundaries are sufficiently far from the object of analysis, the former will experience conditions that is similar to that caused by one-dimensional vertically propagating

shear wave (e.g. Lysmer and Kuhlemeyer, 1969; Seed and Lysmer, 1975). Under such conditions, there is no lateral constraint between adjacent vertical planes. One disadvantage of this approach is that the side boundaries have to be sufficiently far from the object of analysis, which is also commonly the source of wave scattering. However, it should be noted that none of the infinite or transmitting boundaries discussed earlier approximates the one-dimensional vertically propagating shear wave scenario even if they are placed very far from the object of analysis. For this reason, this simple approach remains commonly used if it is desired to approximate a one-dimensional vertically propagating shear wave scenario in the far-field.

One variant of this approach is to tie the corresponding degree of freedom at the opposite ends of the truncated model perpendicular to the shaking direction (i.e. Parra *et al.*, 1996; Lu, 2006; Banerjee, 2009) as illustrated in Figure 4-9. This variant is often used to replicate the conditions in a laminar box, wherein the presence of laminar rings ensures that points at the same depth have the same displacement at any point of time. Theoretically, it also satisfies the vertical propagation of shear wave in uniform or horizontal-layered soil. However, the lateral boundary may also exert some influence on the wave close to the boundary (Takahashi, 2002). Jakrapiyanun (2002) pointed out that the lateral boundary influence zone was about half of the model depth as shown in Figure 4-10. Lu (2006) also noted this phenomenon and advised that the model domain should be large enough in the shaking direction. In this study, this approach was adopted.

4.2.5 Base excitation

Earthquake ground motion is highly dependent on the region of interest. In this study, the earthquake motions considered are representative of far-field events measured in Singapore from previous Sumatran earthquakes. Based on the characteristics of previously recorded earthquake data, synthetic ground motions have been generated for use in small-scale model tests performed at the NUS Geotechnical Centrifuge Laboratory (e.g. Yu and Lee, 2002; Banerjee, 2009), as shown in Figure 4-11. In order to study the influence from the ground vibration amplitude, the maximum acceleration in these records was scaled to 0.022g, 0.07g and 0.1g, corresponding to a small earthquake, a medium earthquake and a large earthquake (in the Singapore context), respectively. The peak acceleration in the large earthquake used for the current study is significantly higher than that recorded in Singapore from previous earthquakes (Banerjee, 2009). Besides these long-period earthquake motions, the 1940 El Centro Earthquake, which is a near-field large earthquake rich in short period components, is also used for comparison in Chapter 6.

4.3 Comparison with centrifuge data

Before studying the large-scale seismic interaction of soil-pile-structure systems, numerical simulations using GeoFEA were carried out for comparison with a series of centrifuge shaking table tests conducted by Banerjee (2009). In Banerjee's experiments, the remolded kaolin clay was consolidated in a laminar box on a unidirectional shaking platform. The pile foundation consists of a 2x2 pile group

connected by a stiff raft. The piles have a diameter of 0.9m and a length of 13m under prototype conditions. The pile-to-pile spacing ratio is about eleven in the direction of shaking and six in the transverse direction; these spacings were chosen to minimize the interaction between piles. The pile head was welded on the pile raft and the pile tip was placed on a thin layer of sand at the base of a laminar box (see Figure 4-12). More details about the tests are available in Banerjee (2009). Besides the physical tests, the soil-pile-raft model was also simulated by Banerjee (2009) using ABAQUS v6.8 with the hyperbolic-hysteretic constitutive model. In this study, the same problem is simulated using the parallelized dynamic version of GeoFEA and compared with Banerjee's measured and numerical results.

Banerjee (2009) conducted two series of tests, one involving free field simulation in the absence of piles and the other involving the soil-pile-raft system. In the first series, the model only contains soft clay and bottom sand, without the pile-raft system, as shown in Figure 4-13. Because of symmetry, only a half-model needs to be analyzed. A similar model is adopted for the second series with the soil-pile-raft system, as shown in Figure 4-14. The discretized finite element model contains 9,774 20-noded hexahedron elements and 43,148 nodes.

The boundary conditions imposed by the laminar box are simulated using the method discussed in Section 4.2.4, that is, by tying the corresponding edge nodes at the same depth on opposite ends of the model to simulate the laminar box motion and constraining movements in all directions other than the direction of shaking. The nodes at the symmetrical plane are restrained against out-of-plane motion. The shaking table is assumed to be rigid and the shaking acceleration is

input from the bottom face of the model. The nodes at the bottom are restrained vertically. The soft clay behavior is modeled using the hyperbolic-hysteretic model described in section 4.2.1. The bottom sand is modeled using Mohr-Coulomb model. Both pile and raft are modeled using linear elastic materials. The parameters for all these materials are fundamentally consistent with those used by Banerjee (2009), as listed in Table 4-1.

For the free-field model with peak base acceleration of 0.07g, the GeoFEA computed time histories at the clay surface are compared with the centrifuge measurements and the ABAQUS results in Figure 4-15. The time histories from the GeoFEA analysis agree well with Banerjee (2009)'s ABAQUS analysis. However, both show smaller peak accelerations compared to the centrifuge data. This may be attributed to the limitation of the hysteretic model, which has been shown to over-predict the damping ratio of soils at large strains (Banerjee, 2009). The response spectra in Figure 4-16 show that the dominant accelerations between the 1 and 2-sec period band are well replicated by both analysis. For the longer period components, the ABAQUS results generally over-estimate the centrifuge data while the GeoFEA results tend to under-estimate.

Figure 4-17 compares the computed and measured raft accelerations in the pile-raft model. Due to the complication of the tests and noise of measurement system, it's difficult to get complete match for numerical simulation and centrifuge shaking table tests. In previous studies, such discrepancies in the acceleration time histories between the numerical simulation and tests are popular and acceptable

(e.g., Lu *et al.*, 2005; Chang, 2007). There is greater divergence between Banerjee (2009)'s results and the current computed results using GeoFEA. Subjectively, however, the current results appear to capture the maximum accelerations better than Banerjee's analysis. Banerjee's analysis was carried out with the ABAQUS code combined with a user subroutine (UMAT). Due to the limitation of the user subroutine, the Newton-Raphson scheme could not be used. Coupled with the nonlinear nature of the soil model and soil-structure interaction calculations, it is likely that Banerjee's analysis contains some unavoidable numerical errors, which may accumulate over time. The GeoFEA calculations performed in this study were carried out using a code that was mostly developed in-house, which allows us to minimize possible errors associated with the problem nonlinearity. On the other hand, as Figure 4-18 shows, all three response spectra are in close agreement. This suggests that both sets of analyses give a good account of the energy distribution; what appears to be different is the phase relationship between the various frequency components. This may be attributed to differences arising from the time step integration scheme used in the analyses. The computed and measured pile bending moment envelopes are shown in Figure 4-19. As can be seen, there is good agreement between the computed and measured results. Banerjee (2009)'s computed bending moment envelope shows a leveling off near the pile head whereas the bending moment computed in this analysis continues to increase. This demonstrates the effect of the different methods of computing the bending moment, as discussed earlier.

Besides the medium earthquake with a peak base acceleration (PBA) of 0.7m/s^2, analyses were also conducted for two similar earthquakes with the PBA scaled to 0.22m/s^2 and 1.0m/s^2 respectively. The computed accelerations at the clay surface and pile raft, as well as the pile bending moment, are compared in Table 4-2. Because the bending moments are measured at discrete depths in the centrifuge tests, bending moments are compared at a depth of 1.25m in Table 4-2 corresponding to the strain-gauge location nearest to the pile head. The envelopes are compared in Figure 4-20. In all the cases, the response of the clay surface accelerations and pile foundation are well replicated using the dynamic GeoFEA code.

4.4 Scale effect of pile foundation

As stated in chapter 2, previous studies were focused mainly on single pile and small pile groups. Although Sakajo *et al.* (1995)and Lu (2006) analyzed pile groups, they did not investigate the scale or size effect of the pile group. Hence, there is still relatively little information on scale effects associated with large pile groups, or the relationship, if any, between the response of small and large pile groups. In this section, a preliminary study of the scale effect due to pile group size is carried out using finite element modelling. The numerical simulations are performed for pile groups of different sizes and pile spacings.

Soft soil conditions are quite common in coastal and estuarine areas around the world such as Singapore, Bangkok and Jarkata. In Singapore, the most common soft soil formation is the Kallang Formation, as shown in Figure 4-21 and Figure

4-22. Figure 4-23 shows some typical finite element models for the single pile and small pile groups considered in this study. The soil layer is idealized into two horizontal layers; the upper layer is soft clay and the lower layer is stiff clay or rock. The upper soft clay is assumed to have a thickness of 25m, and is modeled using Banerjee (2009)'s hyperbolic-hysteretic constitutive model. The bottom hard layer is modeled as a Mohr-Coulomb material. The pile and raft are reinforced concrete structures modeled as linear elastic materials, because the piles' response is often required to be elastic with minor or no residual deformation when subjected to design earthquakes (e.g. Eurocode 8 2006; IBC 2009). Each pile is 28m long and is modeled as a 0.6mx0.6m square cross section. The raft has a thickness of 1m with the lower 0.4m embedded in the clay. The influence of the superstructure is simplified to that of an equivalent mass resting on the raft. The material characterization and parameters for all these components are listed in Table 4-3.

The influence of pile length, pile diameter, pile raft and additional mass will be discussed in chapter 5. The influence of the superstructure's natural period, and its simplification as an added mass, will be discussed in chapter 6. In this chapter, the focus is on the pile spacing and the pile-group size.

4.4.1 Effect of pile spacing

The effect of pile spacing on pile-to-pile interaction was studied by Kagawa (1983a) and Gohl (1991), both of whom reached quite different conclusions. Kagawa (1983a) found that the pile-to-pile interaction was significant even up to a spacing of sixty

pile diameters, while Gohl (1991) concluded that pile-to-pile interaction could be negligible beyond a spacing of six pile diameters.

In this study, the critical spacing for pile-to-pile interaction was examined by carrying out finite element analyses of a 3x3 pile group using GeoFEA. Different models were set up for pile-to-pile spacings of three, five, seven, nine and eleven pile diameters respectively, as shown in Figure 4-23. Also included in this series is the analysis of a single pile with a raft or cap, which serves as a benchmark. In all cases, the vertical displacement of the raft is restrained to prevent rocking. In order to minimize the influence of structural mass, the combined mass of the superstructure and the raft in each analysis is such that average mass supported by each pile is the same for all six cases.

Figure 4-24 plots the computed pile raft displacement obtained from the single pile analysis and the 3 × 3 pile group analysis with three diameters spacing. For this case, the total mass of the raft and superstructure is taken as 81.6 tons, and the peak base acceleration is 0.7 m/s^2. The results show that the maximum raft displacement of the 3x3 pile group is larger than that of the single pile, which was also noted by Gohl (1991) and Sakajo *et al.* (1995), the difference being attributable to pile-pile interaction. When the pile spacing increases, the difference in the raft displacement decreases, as shown in Figure 4-25. For this case, when the pile spacing is larger than seven pile diameters, the pile-pile interaction appears to be negligible.

Pile-to-pile interaction effects are also reflected in the computed pile bending moments, as shown in Figure 4-26(a). For the 3x3 pile group with 3d spacing, all the piles have the same horizontal displacement at the pile heads, since they are rigidly connected to the raft; however, their bending moment profiles are different. For all the piles within the group, the maximum bending moment occurs at the pile head. Near the pile tip, there is a locally minimum negative bending moment at the depth of 25m, which corresponds to the interface between the soft clay and the hard bedrock. Comparatively, it is observed that the bending moments of the corner and exterior piles are generally larger than those of the interior piles. Figure 4-26(b) shows that the corner or exterior pile (e.g. A1) has a larger bending moment at the pile head compared to a single pile, and that the converse is true for the interior pile (e.g. C2).

Referring to Figure 4-27(a), the ratio of the largest (Pile A1) to the smallest (Pile C2) bending moment computed at the pile head, M_{max}/M_{min}, is about 1.38. This is shown in Figure 4-28, which also plots the corresponding ratios for similar 3x3 pile groups with different spacings. It is seen that the bending moment ratio approaches one with increasing pile spacing. These results suggest that pile-to-pile interaction effects are present for pile spacings of up to about 9.

The effects of pile spacing on the raft displacement and pile bending moments are shown on Figures 4-29 and 4-30 for a larger and smaller superstructural mass of 117.6 tons and 45.6 tons respectively. Figure 4-29 shows that the larger structural mass results in greater raft displacements. Nonetheless, the overall trend for all three masses is similar in that the raft displacements approach constant values as

the pile spacing increases. Similar trends are obtained for the bending moment ratios for different structural masses, as shown in Figure 4-30 Figure 4-28 and Figure 4-29 appear to show a slight decrease in the pile-pile interaction distance with increasing structural mass. This can be explained by the fact that a larger structural mass will induce larger relative pile-soil movement, which in turn gives rise to larger strains in the soil, leading to more severe stiffness degradation. As the stiffness of the soil decreases, so does pile-pile interaction effects.

Figure 4-30 and Figure 4-31 illustrates the influence of the peak base acceleration (PBA) on pile-pile interaction distance. As can be seen, the effect is similar to that of increasing the super-structural mass and can be attributed to the same cause. As the PBA increases, so does the strain level in the soil, causing more severe degradation, with consequent decrease in the pile-pile interaction distance.

In all cases analysed, pile-pile interaction was found to be negligible when the pile-pile spacing is larger than nine pile diameters. This influence distance is slightly larger than the one proposed by Gohl (1991) but much smaller than that proposed by Kagawa (1983a).

The pile-pile influence distance is dependent on lots of factors, such as structural mass, base shaking amplitude and frequency feature, pile dimensions and pile stiffness, soil profiles, etc. In this study, it was discussed with several specific cases and the obtained conclusion is qualitative. More extensive studies are required for general and quantitative conclusions in future.

4.4.2 Effect of pile foundation size

As stated in chapter 2, most existing studies on seismic pile foundation response deal with single piles or small-scale pile groups (Fan *et al.*, 1991; Gazetas *et al.*, 1991; Toki *et al.*, 1991; Meymand, 1998; Uzuoka *et al.*, 2007; Javan *et al.*, 2008; Dezi *et al.*, 2009; Tang *et al.*, 2009; Elahi *et al.*, 2010; Motamed and Towhata, 2010; Kong *et al.*, 2011). Although Lu (2006) and Shirato *et al.* (2008) used a relative large-scale pile group in their studies, they did not examine the effect of pile group size. In this section, finite element analyses are carried out for several pile groups of different sizes subjected to the same conditions, and their responses analyzed and compared to examine the effect of pile group size. A uniform pile spacing of three pile diameters is used in all the analyses, which may be expected to introduce pile-to-pile interaction effects based on the results of Section 4.4.1. The pile group size ranges from 1x1 pile (single pile), 3x3 piles, 5x5 piles, 7x7 piles and 9x9 piles, as shown in Figure 4-32. In order to minimize the influence of the superstructure, the super-structural mass is assumed to increase proportionally with the number of piles in the group; that is, the super-structural mass averaged over the number of piles is the same for all cases. The material properties adopted in these analyses are listed in Table 4-3. The peak base acceleration is 0.7 m/s^2.

Figure 4-33 plots the computed maximum raft displacement versus the pile group size. As can be seen, the horizontal raft motion generally increases as the pile group becomes larger. This trend has also been noted by other researchers (e.g. Gohl, 1991; Brown *et al.*, 2001) for group size of up to 3x3. As shown in Figure 4-34, a somewhat similar trend is also reflected in the bending moment envelope; however,

the increase in the bending moment is proportionately smaller than the increase in raft displacement. This may be due to the fact that the soil between adjacent piles tends to move together with the piles. Similar trends in the raft and bending moment responses are observed for different super-structural masses and peak base accelerations, as shown in Figure 4-35 to Figure 4-38.

4.5 Large Pile Foundation (9x21 piles)

In addition to the above cases, a very large pile foundation consisting of 9x21 piles, each with 0.6mx0.6m square cross section and length 25m, is also analyzed (Figure 4-40). The pile center-to-center spacing is 2m, which is roughly 3 times the pile width. According to Jakrapiyanun (2002), the lateral extent of the influence zone of the pile foundation is about three times the raft length, while the lateral extent of the influence region of the side boundaries is about half the model depth. Taking these requirements into consideration leads to a model length of 180m used in this study, as shown in Figure 4-40.

The pile raft has dimensions $42m \times 18m \times 1m$, as shown in Figure 4-41. All other geometric parameters are the same as the cases studied above.

The dynamic response of the superstructure is likely to be very complex. Since the focus of this study is on the pile foundation, the superstructure is simplified as an equivalent lumped mass on the raft, which is an approach widely used in construction codes (e.g. Eurocode 8, 2006; API, 2006; IBC, 2009). All other materials properties are the same as those used in section 4.4, as listed in Table

4-3. The applied earthquake motion is shown on Figure 4-12. The analysis was carried out using the parallel dynamic version of GeoFEA on eight PC nodes, which took about 150 hours. Besides the large-scale soil-pile foundation system, a similar free-field model with the same dimensions and soil parameters, was also simulated for comparison, as shown in Figure 4-42.

4.5.1 Acceleration response

Figure 4-43 shows the computed acceleration histories at different locations A to F on the ground surface. Referring to Figures 4-40 and 4-41, Point A is located close to the model boundary, point C is located close to the raft, and point B is located at a distance of 42m from pile raft and 26m from the model boundary. Point F is located on the soil surface of the free field model as shown in Figure 4-42.

Figure 4-44 plots their corresponding spectra with 5% damping. Amongst the three points, only point B has a response that is similar to that of the free field obtained by analyzing an identical soil model without the pile foundation. The response at point A is evidently influenced by lateral boundary while the response at point C is influenced by pile foundation. These results indicate that the model length is acceptable for minimizing the influence of the lateral boundary.

The computed acceleration histories at various other points in the domain are shown in Figure 4-45. It is seen that the accelerations at the soil layer interface (point E in Figure 4-40) is quite similar to the input motion at the base of the model. Figure 4.47 shows the response spectra at different locations of the model, as well as the amplification spectrum. The amplification spectra of the far-field soil and

pile foundation, obtained by dividing the response spectra of the far-field soil and the pile raft by the corresponding spectrum of the base input motion, are also plotted in Figure 4-46. It can be seen that the long-period response (2 to 3s) of the raft is generally similar to that of the free-field, but its short-period response (~1s) is smaller than that of the free-field. Hence, the common engineering practice of using the free-field ground surface accelerations as the input acceleration to the base of the structure may lead to errors.

4.5.2 Deformation

The computed displacements of the pile raft and far-field soil, relative to the model base, are similar except for the amplitudes, as shown in Figure 4-47. The maximum displacement occurs at t=11.85 sec. At this instant, the horizontal soil deformation profiles at point B (far-field) and point D (near-field) are plotted in Figure 4-47.

The computed shear-stress and strain hysteresis loops at different depths below point D are shown in Figure 4-48. The shear strains & stresses at the surface are very small but increase dramatically with depth. The maximum shear strain profile with depth is plotted in Figure 4-49. The maximum shear strain is 0.83% at the depth of 19.8m from the soil surface.

4.5.3 Bending Moment

The computed bending moment histories at four depths along the pile are plotted in Figure 4-50. It can be seen that significant moments are generated near the pile head (depth 0.8m) over the entire duration of shaking. At intermediate depths of

10m and 20m, the moment responses are much smaller. The moment response picks up at a depth 24.2m, which is very near to the interface (at 25m depth) between the soft and stiff soil layers. As shown on Figure 4-50, the maximum moments at these 4 points occur at time t = 11.95 s. Figure 4-51 shows the computed instantaneous bending moment distributions for all the piles (considering symmetry) at time t = 11.95 s. Despite differences in the maximum positive moments near the pile head and maximum negative moments near the interface between the soft and stiff soils, the overall profiles are very similar in all the piles. This is also reflected in Figure 4-52, which plots the contours of the pile head moment for each pile.

4.5.3 Comparison with analysis using linear elastic model

In this section, the effect of using the hyperbolic soil model is examined by comparing the results with those obtained using a linear elastic model. In the hyperbolic model, the maximum shear modulus of the soft clay G_{max} at small strains is solely a function of the initial effective stress p', and may be prescribed using Eq(4.1). The G_{max} profile thus obtained is shown on Figure 4-54. The G_{min} profile shown on the same figure is obtained by substituting the maximum strain values shown on Figure 4-49 into Eq(4.2). Also shown on the same figure is the shear modulus profile obtained using the method proposed by Duncan and Buchignani (1987), which lies between G_{max} and G_{min} for much of the depth.

For the linear elastic analysis, the shear modulus is assumed to increase linearly with depth, that is

$$G(y) = A \cdot y + B \tag{4.6}$$

in which y is the depth in meters, and $G(y)$ is the corresponding shear modulus in kPa. For a given linearly increasing shear modulus profile, the natural period of the uniform soil layer with this relationship can be determined. By using A=160 and B=300, a good match on the first two natural periods of the free-field soil response can be obtained with those computed using the hyperbolic model shown on Figure 4-46 for point B. The resulting shear modulus profile may be adopted for use in the "equivalent" linear elastic model. This gives a shear modulus variation with depth that is also very close to Duncan and Buchignani (1987)'s recommendation. The Rayleigh damping was set at 16% as this was found to give roughly the same level of response as the hyperbolic model. All other materials are kept the same as listed in Table 4-3.

As Figure 4-56, Figure 4-57 and Figure 4-58 show, despite the above attempts to match the response, significant differences nevertheless remain. This indicates that it may be difficult to "tune" an elastic model to give similar response to a nonlinear model.

4.5.4 Comparison with pseudostatic approach

The pseudostatic approach was proposed by Tabesh and Poulos (2001) and Elahi *et al.* (2010) as a possible method to evaluate large pile-group response under earthquake loading. In this approach, a static analysis is conducted on a pile foundation based on the maximum free-field soil movements and a static lateral loading on the pile raft to simulate the effect of superstructure (Tabesh and Poulos,

2001). Tabesh and Poulos (2001) and Elahi *et al.* (2010) used Winkler springs to represent the near-field soil and pile-soil-pile interaction. In large pile foundation, the spring constants can be very difficult to ascertain. The maximum pile group size in their study is 3x3.

In this study, the finite element method using ANSYS 13 is employed to simulate the near-field soil and pile-soil-pile interaction, as shown in Figure 4-59. The model is the same as the one used in the previous dynamic simulations except for the size of the soil domain. In order to eliminate the horizontal resistance of the soil, an orthotropic material is used to simulate the soil. For this material, the G_{xz} values are obtained using the linearly increasing elastic G profile shown on Figure 4-53, and $G_{xy} = G_{zy} \cong 0$. The far-field soil displacement profile, as shown in Figure 4-47 for point B, is applied to the nodes on the four vertical faces of the model in the x-direction, and a horizontal force, obtained by multiplying the equivalent structure and raft mass to the acceleration at $t = 11.85\ sec$, is uniformly applied to the pile raft. The static analysis using ANSYS 13 takes about 9 minutes.

The computed deformation from the static calculation is shown in Figure 4-60, with a magnification factor of 30. The bending moment of the corner pile is plotted in Figure 4-61, and compared with the maximum bending moment profile from the GeoFEA dynamic analysis. As can be seen, although the trend is well-replicated by the pseudostatic analysis, discrepancy nonetheless still remains. In general, the pile head moment appears to be under-estimated by the pseudo-static analysis. It is not recommended to use such an analysis for detailed design. Nonetheless, the

pseudo-static analysis, as a simplified method, might provide approximate bending moments as preliminary estimates for design practice.

4.6 Summary

The first part of this chapter presents details of the numerical implementation and modeling of seismic soil-pile-structure interaction using the finite element method. A nonlinear material model is adopted which incorporates the hysteresis behavior of soft soil response under cyclic loadings. Different methods of modeling the piles are discussed, and an approach is proposed using 3-D solid elements which can yield accurate values of the bending moments along the whole pile. Other issues examined include (i) the occurrence of pile-soil interface effects such as gapping, and how these may be approximately captured by modifying the stress-strain behavior of the soil elements in contact with the pile, (ii) the implementation of lateral boundary conditions which can accurately capture the free-field seismic soil response away from the foundation and structure using the finite domain, (iii) the method of prescribing the ground motion via base excitation.

For validation, the GeoFEA numerical simulations were first carried out to analyze the small-scale centrifuge tests involving a small 2x2 pile group subjected to shake table excitation under 50g. Favorable agreement was obtained between the computed and measured soil and raft accelerations, as well as the pile bending moment profiles.

Larger finite element models were set up to study the effects of pile spacing and pile group size. The results show that both the raft accelerations and the maximum bending moments decrease with increasing pile-to-pile spacing of up to about 9 diameters. This suggests that pile-to-pile interaction effects are significant up to this distance. The effect of pile group size is less obvious. For the same pile-to-pile spacing and the same structural mass carried per pile, the raft displacements increase as the pile group becomes larger. However, the increase in the maximum pile bending moments with pile group size is not so significant. This may be due to the fact that the soil between adjacent piles tends to move together with the piles.

Finally, finite element analyses were carried out for a large-scale problem involving a 9x21 pile group. The acceleration responses at various soil and raft locations in the model are presented and discussed. The bending moment response was also examined. Although the shapes of the computed bending moment distributions in all the piles are highly similar, there are differences in the maximum positive moments at the pile-head and maximum negative moments at the interface between the soft clay and the harder underlying soil. Comparisons of the raft response and pile bending moments were also made with the results obtained using an equivalent linear elastic soil model and a simplified pseudo-static approach.

In Chapter 5, additional large-scale analyses involving the 9x21 pile foundation will be carried out as part of a series of detailed parametric studies. The parameters of interest include the pile length, the shear modulus of the soft soil, the structural mass as well as the peak base acceleration. The results will be processed and

interpreted using dimensional analysis to obtain expressions for the maximum bending moment at both the pile head and near the pile tip where the pile is socketed into the underlying stiffer soil.

Table 4-1 Material properties for modeling centrifuge shaking table test

Component	Constitutive behavior	Parameter	Adopted value
Bottom sand	Mohr-Coulomb	Young modulus	220MPa
		Poisson's ratio	0.25
		cohesion	30kPa
		internal friction	30°
		density	2000kg/m^3
Soft clay	hyperbolic-hysteretic	Effective stress exponent	0.635
		frictional constant M	0.9
		Slope κ	0.05287
		Slope λ	0.244
		Poisson's ratio	0.3
		Density	1600kg/m^3
Pile & raft	Linear elastic	Young modulus	21GPa
		Poisson's ratio	0.2
		density	7800kg/m^3
Additional plate	Lumped mass	mass	605 ton

Table 4-2 Comparison of Computed and Measured Results for Similar Earthquakes with Different Scaled Peak Base Acceleration

Item	Components	Method	PBA=0.22m/s²	PBA=0.7m/s²	PBA=1.0m/s²
Free-field surface response	Maximum acceleration (m/s²)	GeoFEA	0.12	0.39	0.97
		ABAQUS	0.13	0.37	0.96
		Centrifuge	0.16	0.52	1.08
	Resonance period (sec)	GeoFEA	1.2	1.3	1.7
		ABAQUS	1.2	1.4	1.7
		Centrifuge	1.3	1.5	1.9
Pile raft response	Maximum acceleration (m/s²)	GeoFEA	0.21	0.54	0.81
		ABAQUS	0.27	0.42	0.77
		Centrifuge	0.24	0.56	0.83
	Resonance period (sec)	GeoFEA	1.6	1.4	1.5
		ABAQUS	1.6	1.4	1.6
		Centrifuge	1.6	1.5	1.5
Pile bending moment	Bending moment @-1.25m (kN.m)	GeoFEA	689	1775	2661
		ABAQUS	728	1778	2855
		Centrifuge	622	1880	2610

Table 4-3 Material properties of model components in the large-scale analyses

Component	Constitutive behavior	Parameter	Adopted value
Hard layer soil	Mohr-Coulomb	Young modulus	450MPa
		Poisson's ratio	0.25
		cohesion	30kPa
		internal friction	30°
		density	2000kg/m^3
Soft clay	hyperbolic-hysteretic	Effective stress exponent	0.635
		frictional constant M	0.9
		Slope κ	0.05287
		Slope λ	0.244
		Poisson's ratio	0.3
		Density	1600kg/m^3
Pile & raft	Linear elastic	Young modulus	3000MPa
		Poisson's ratio	0.25
		density	2400kg/m^3
Superstructure	Lumped mass	mass	72 ton per pile

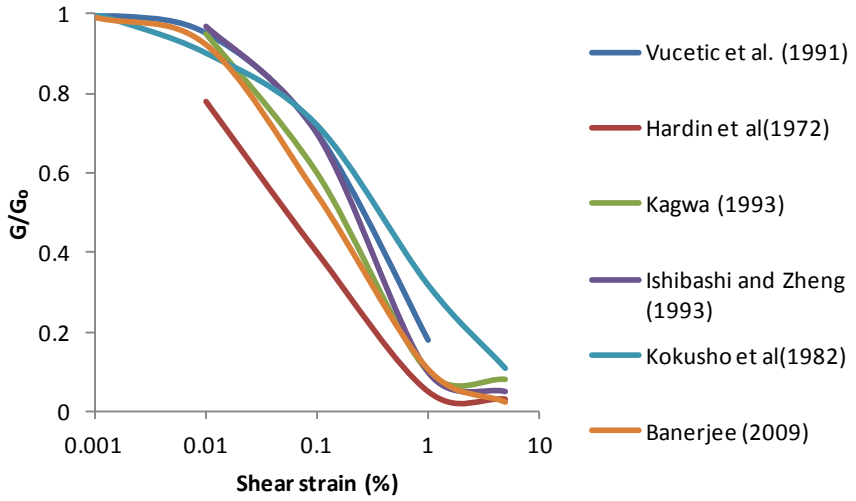

Figure 4-1 Variation of G/G_0 with shear strain from published literature

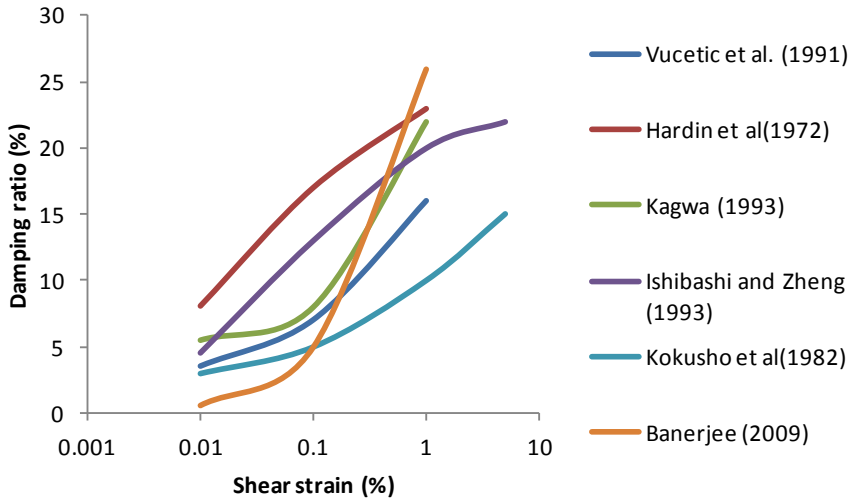

Figure 4-2 Variation of damping ratio with shear strain from published literature

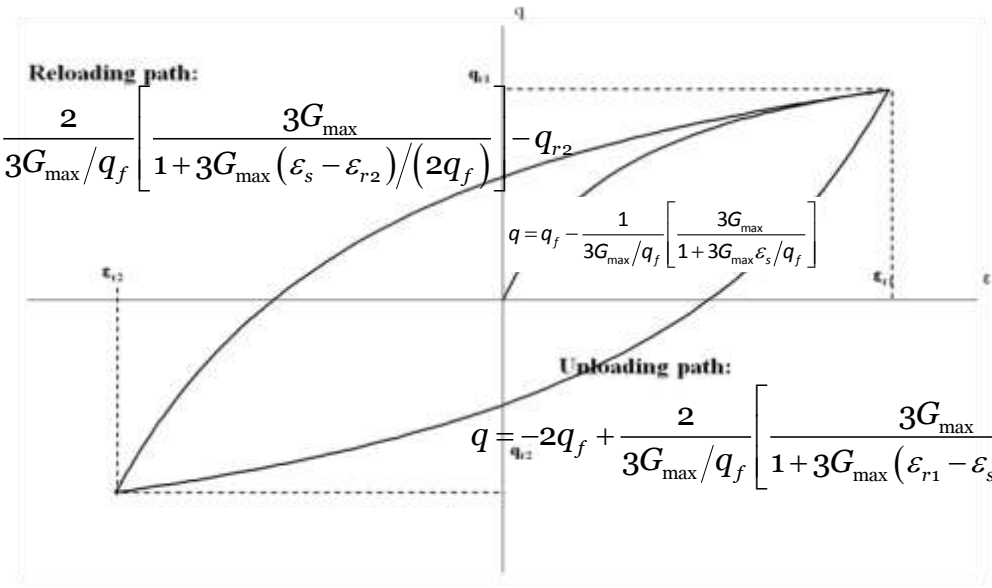

Figure 4-3 A typical unload-reload cycle for soft clay based on the combined hyperbolic and Masing's rules (Banerjee, 2009)

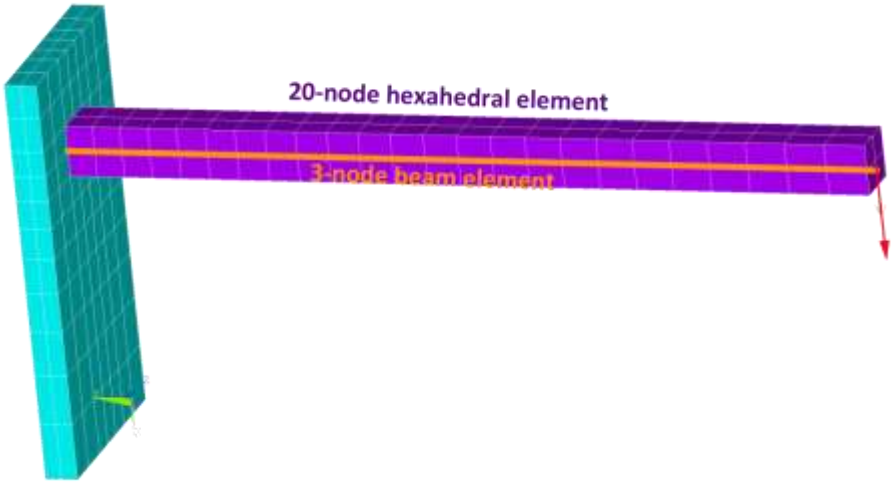

Figure 4-4 Use of a flexible beam along the pile central axis to capture the bending moment

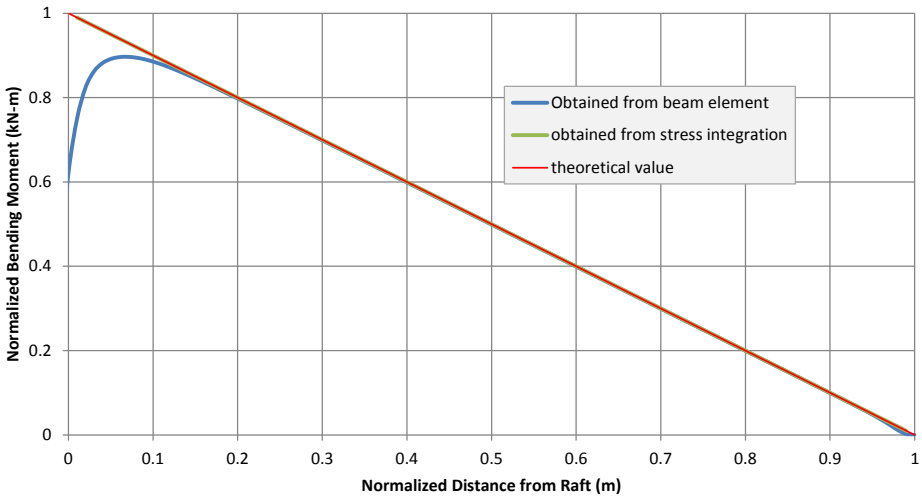

Figure 4-5 Comparison of bending moment along cantilever

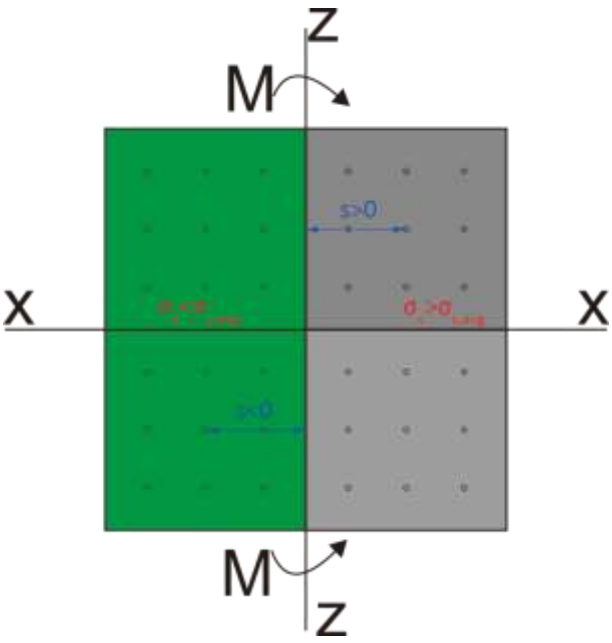

Figure 4-6 Determination of pile bending moment via integration of axial stress with respect to distance from the neutral axis

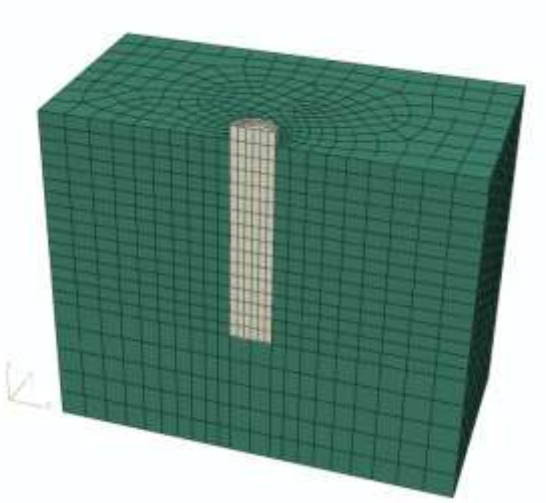

Figure 4-7 Finite element model for a laterally loaded pile test

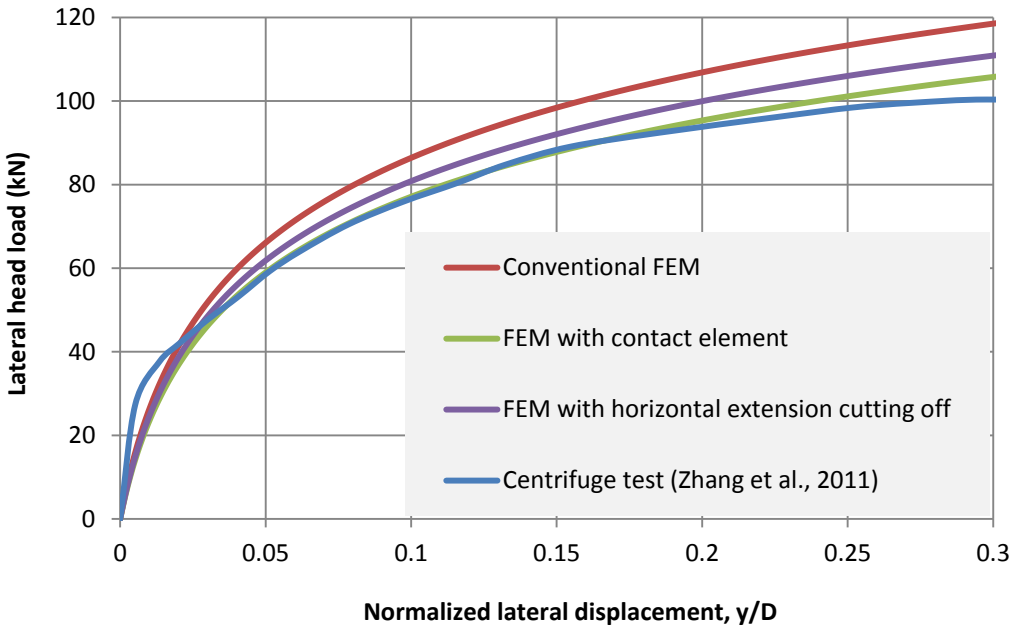

Figure 4-8 Comparison of lateral pile capacity with different soil-pile interface assumptions

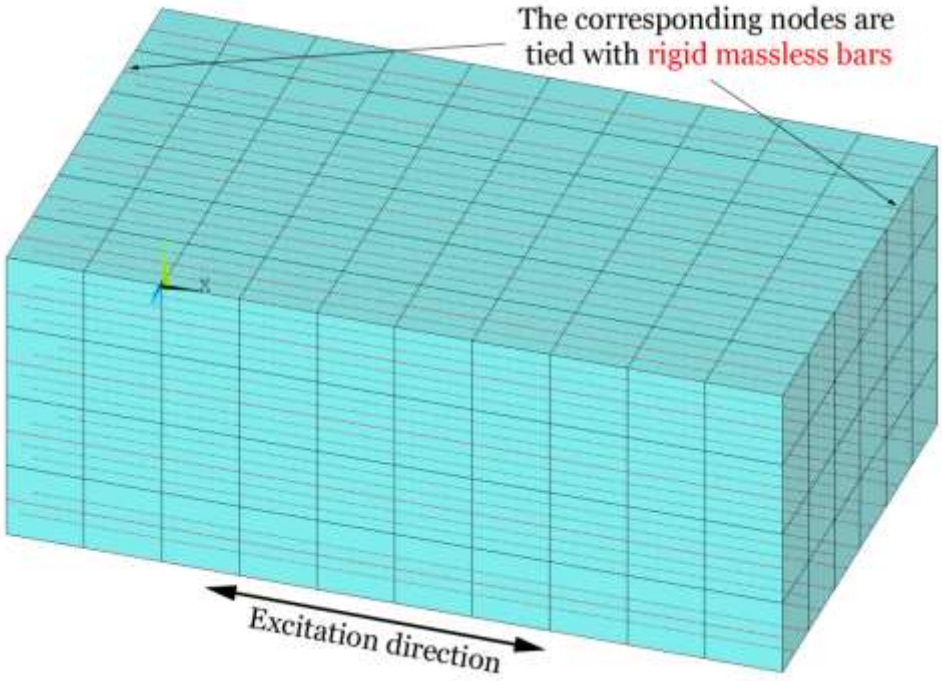

Figure 4-9 Illustration of tied nodes for lateral boundary condition

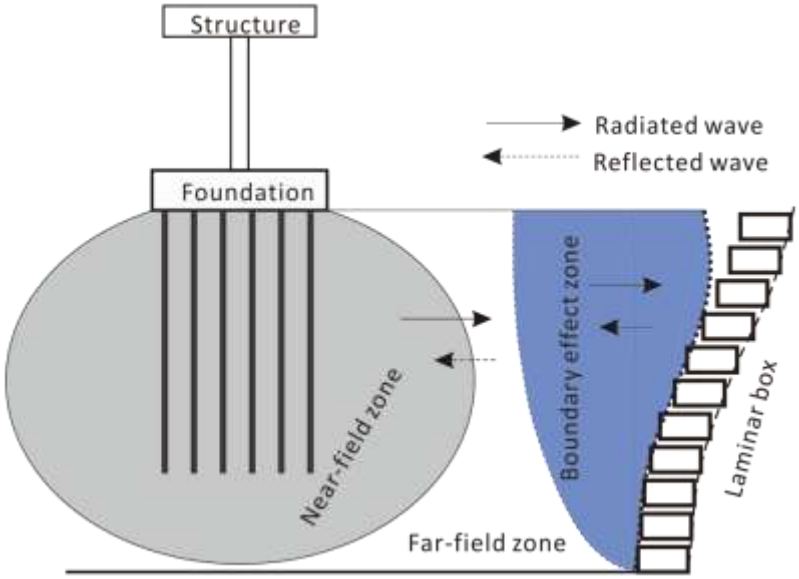

Figure 4-10 Structure and pile foundation model in laminar container

(Jakrapiyanun, 2002)

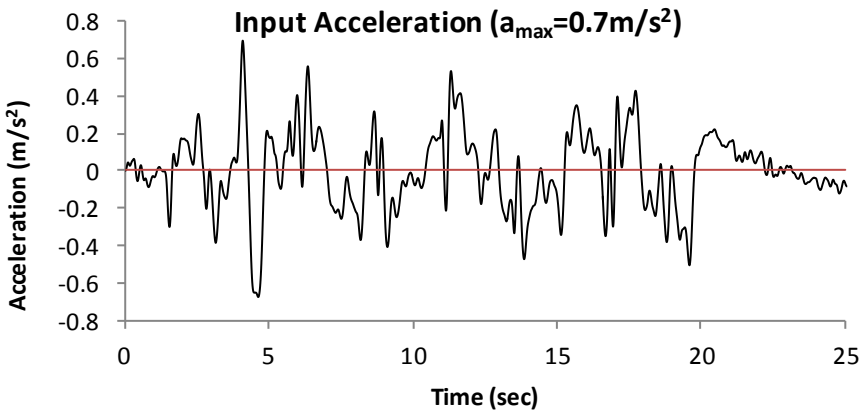

(a) Time Series

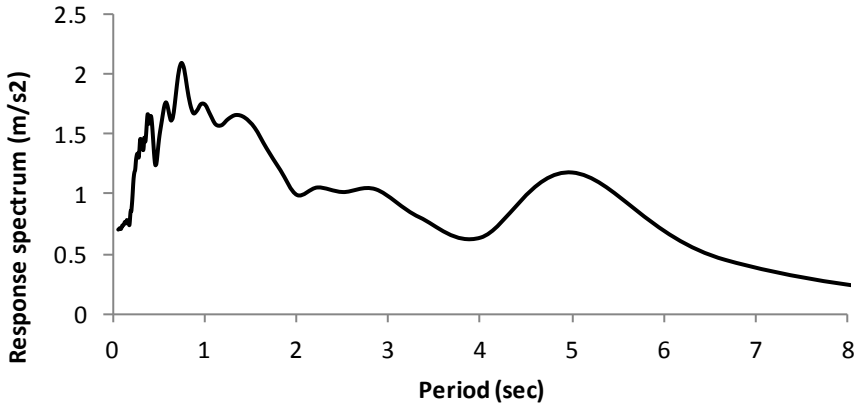

(b) Response Spectrum

Figure 4-11 Typical earthquake acceleration series and response spectrum used in this study (Banerjee, 2009)

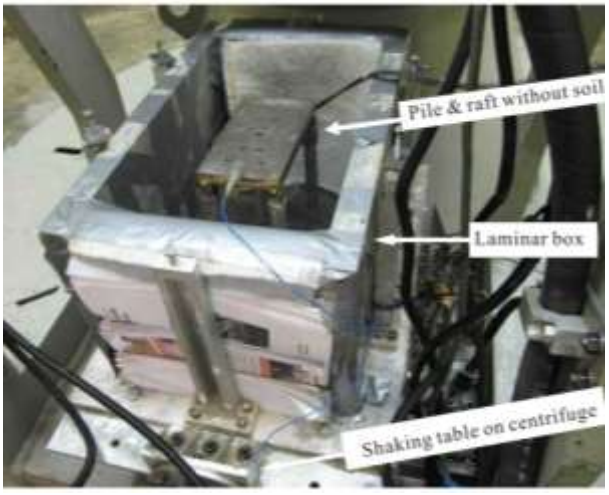

Figure 4-12 Centrifuge shaking table model for soil-pile-structure interaction (Banerjee, 2009)

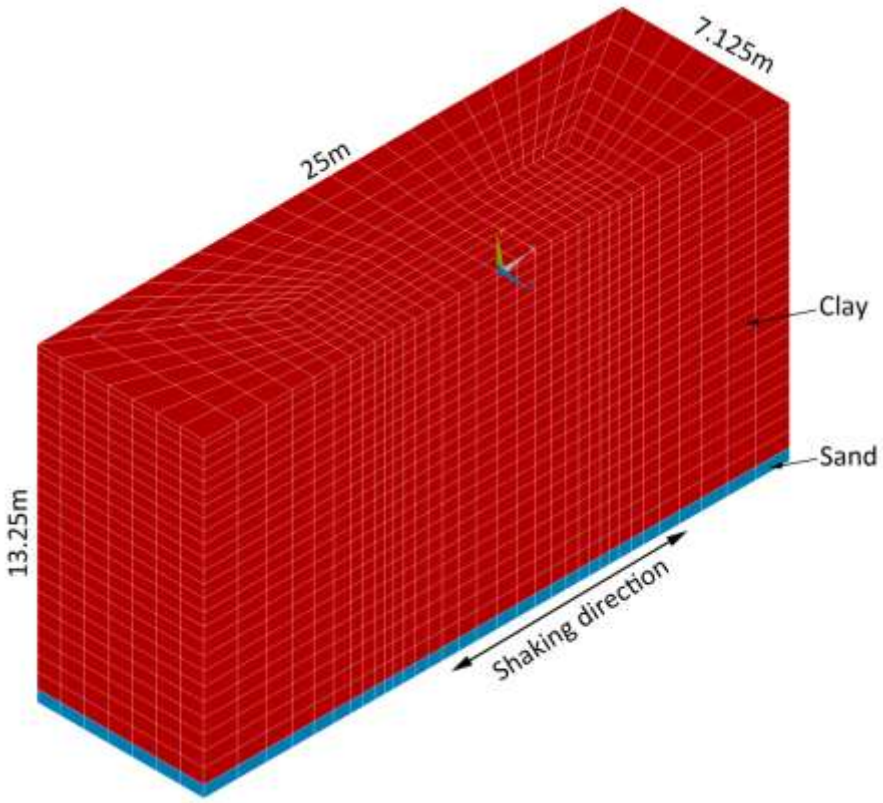

Figure 4-13 Symmetrical finite element model for simulating centrifuge clay bed tests

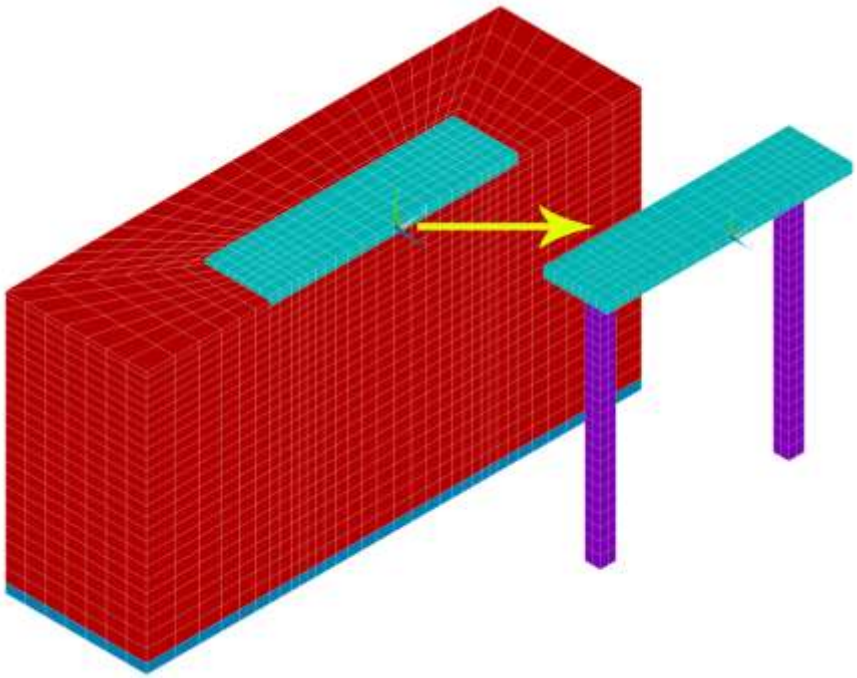

Figure 4-14 Symmetrical finite element model for simulating centrifuge soil-pile tests

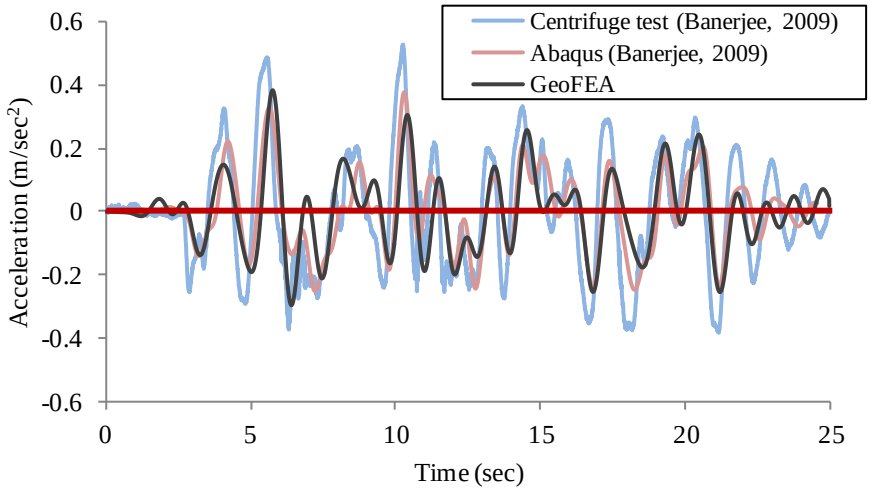

Figure 4-15 Comparisons of computed and measured acceleration histories at the clay surface, for the free field model ($PBA = 0.70\,m/s^2$)

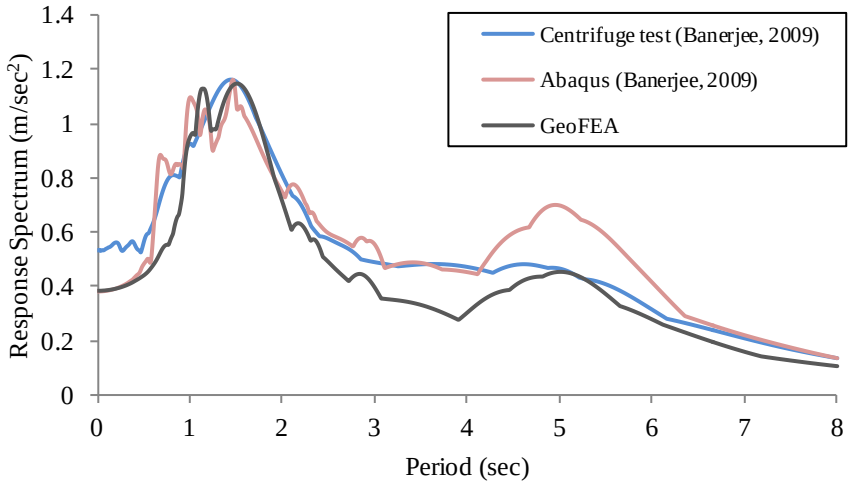

Figure 4-16 Computed and measured response spectra at the clay surface of the free-field model ($PBA = 0.70\,m/s^2$)

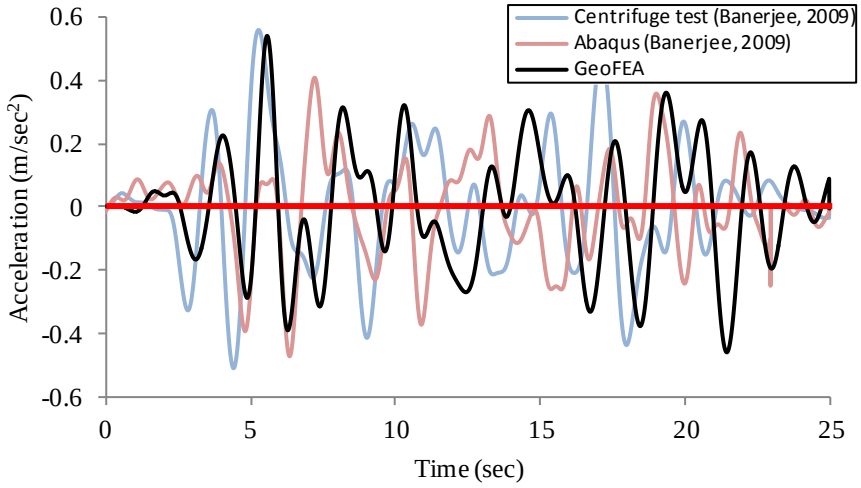

Figure 4-17 Comparison of raft accelerations for the centrifuge model ($PBA = 0.70\,m/s^2$)

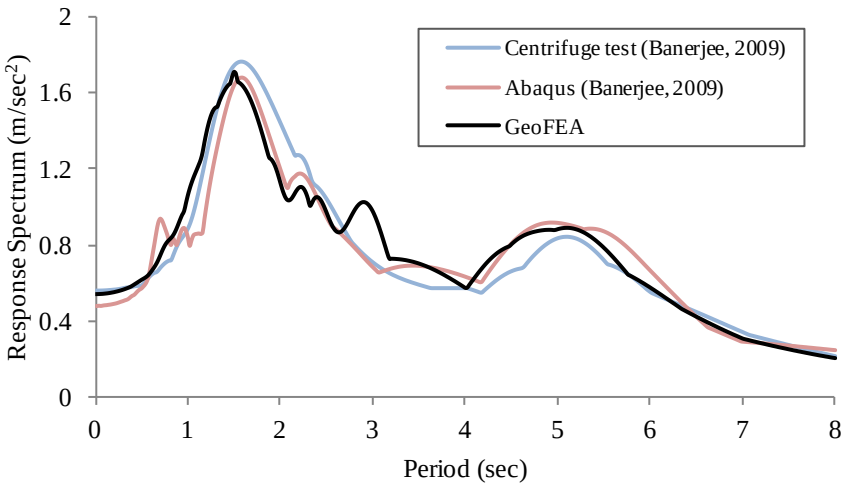

Figure 4-18 Comparison of raft response spectrum for the centrifuge model ($PBA = 0.70\,m/s^2$)

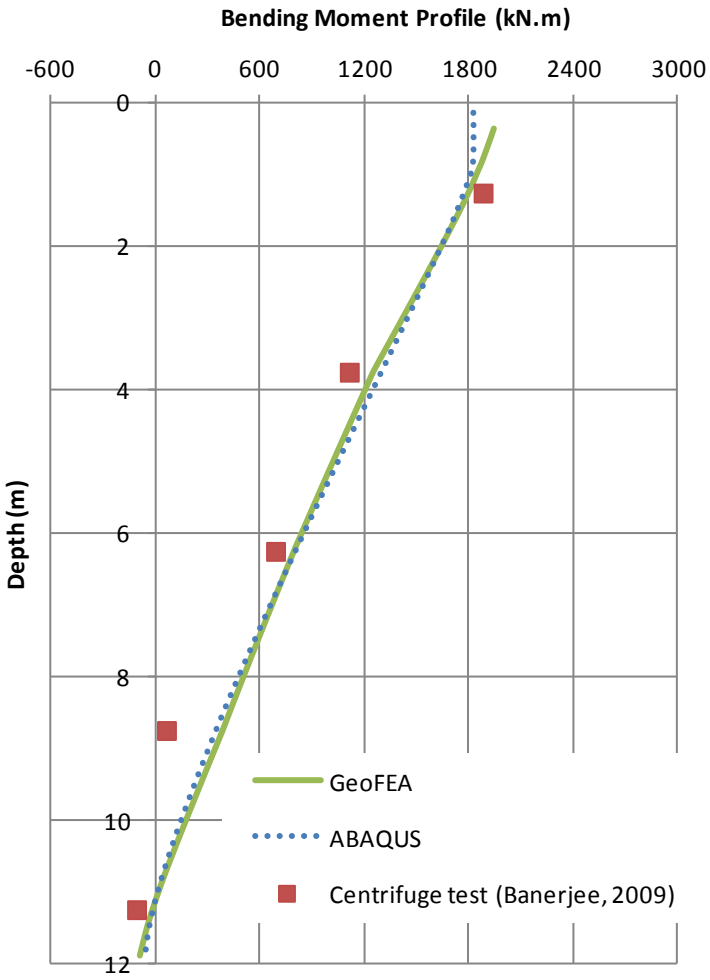

Figure 4-19 Comparison of maximum pile bending moment ($PBA = 0.70\,m/s^2$)

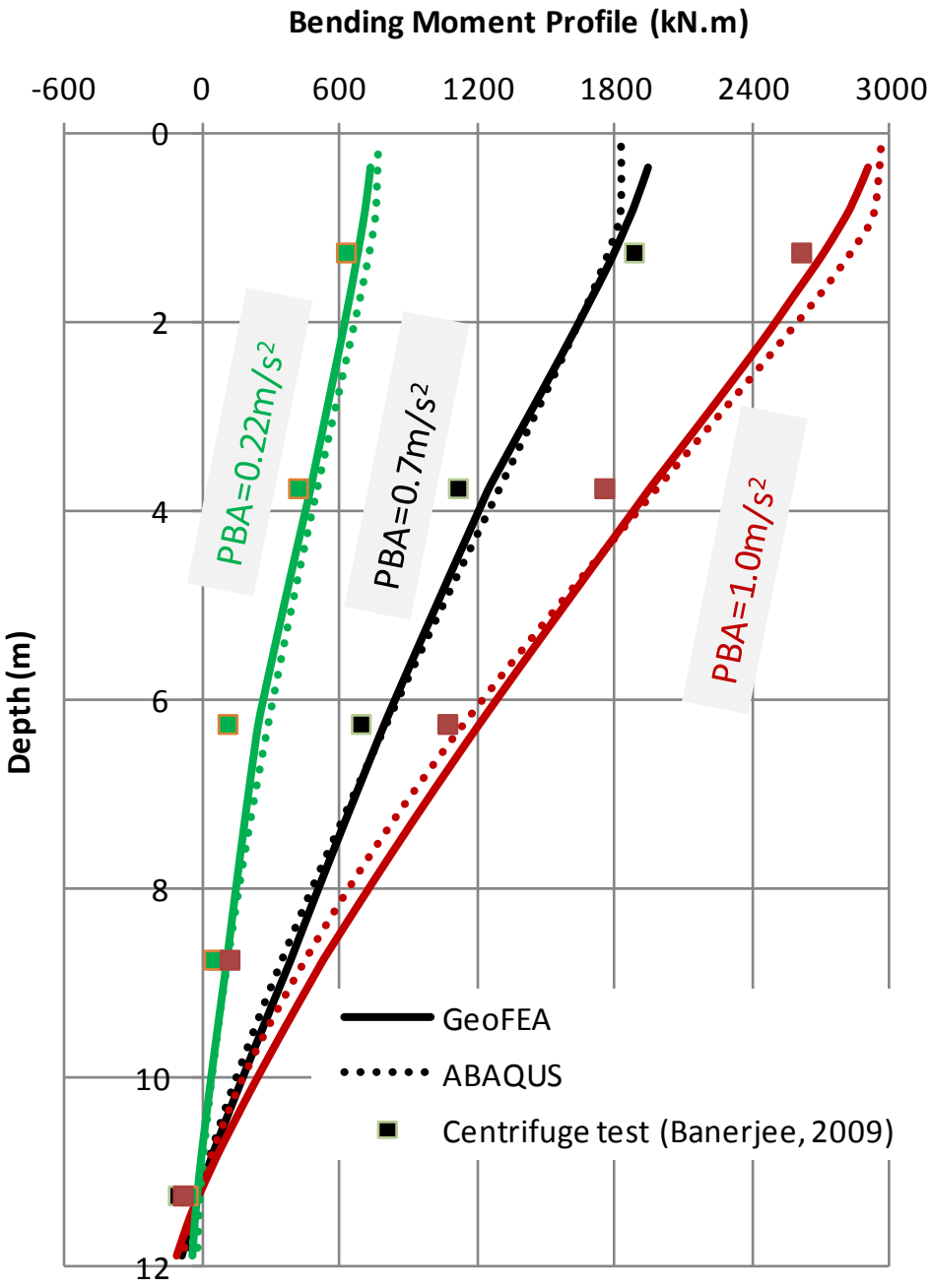

Figure 4-20 Comparison of maximum pile bending moment for three scaled earthquakes

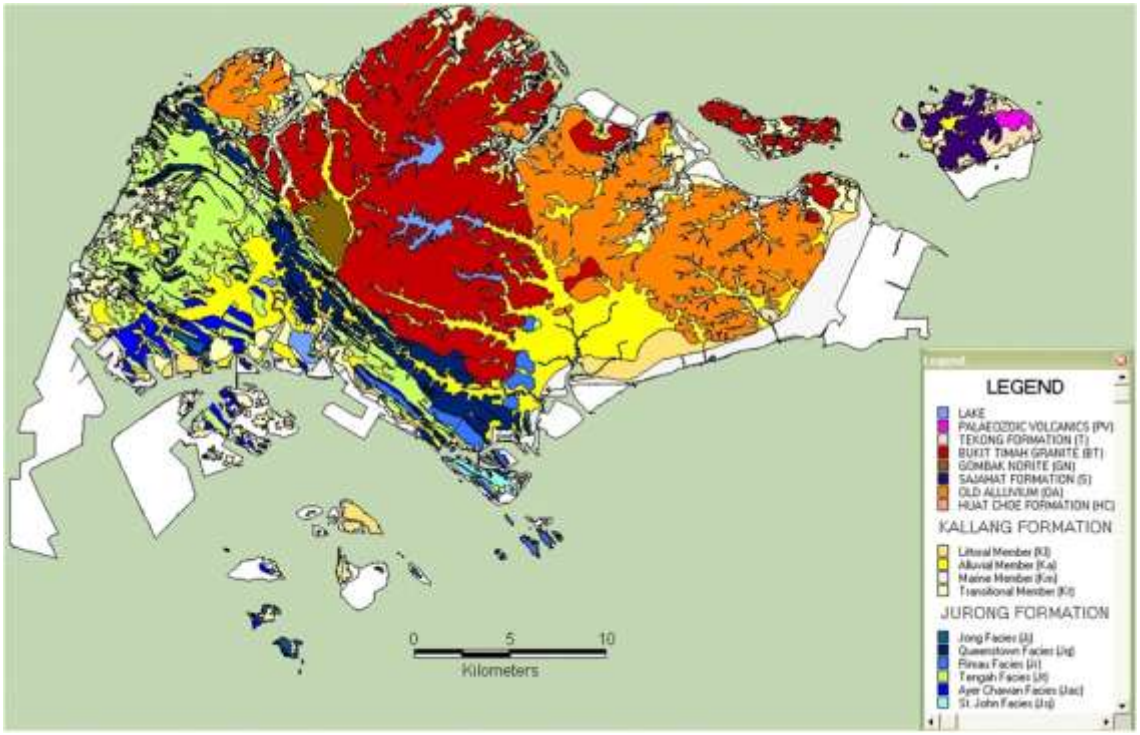

Figure 4-21 Geological formations in Singapore

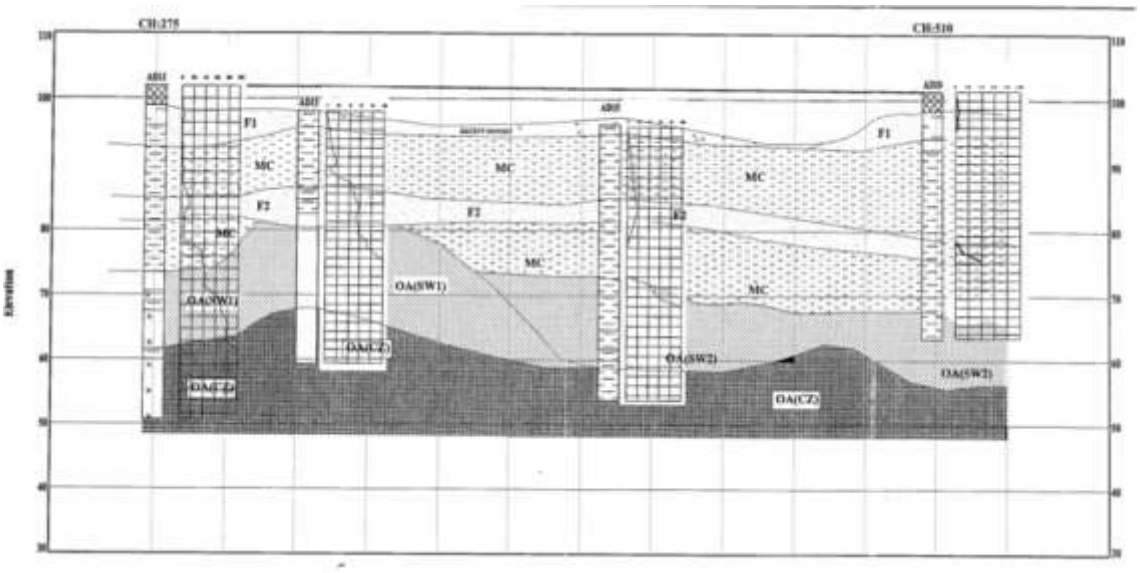

Figure 4-22 A typical soil profile in Singapore

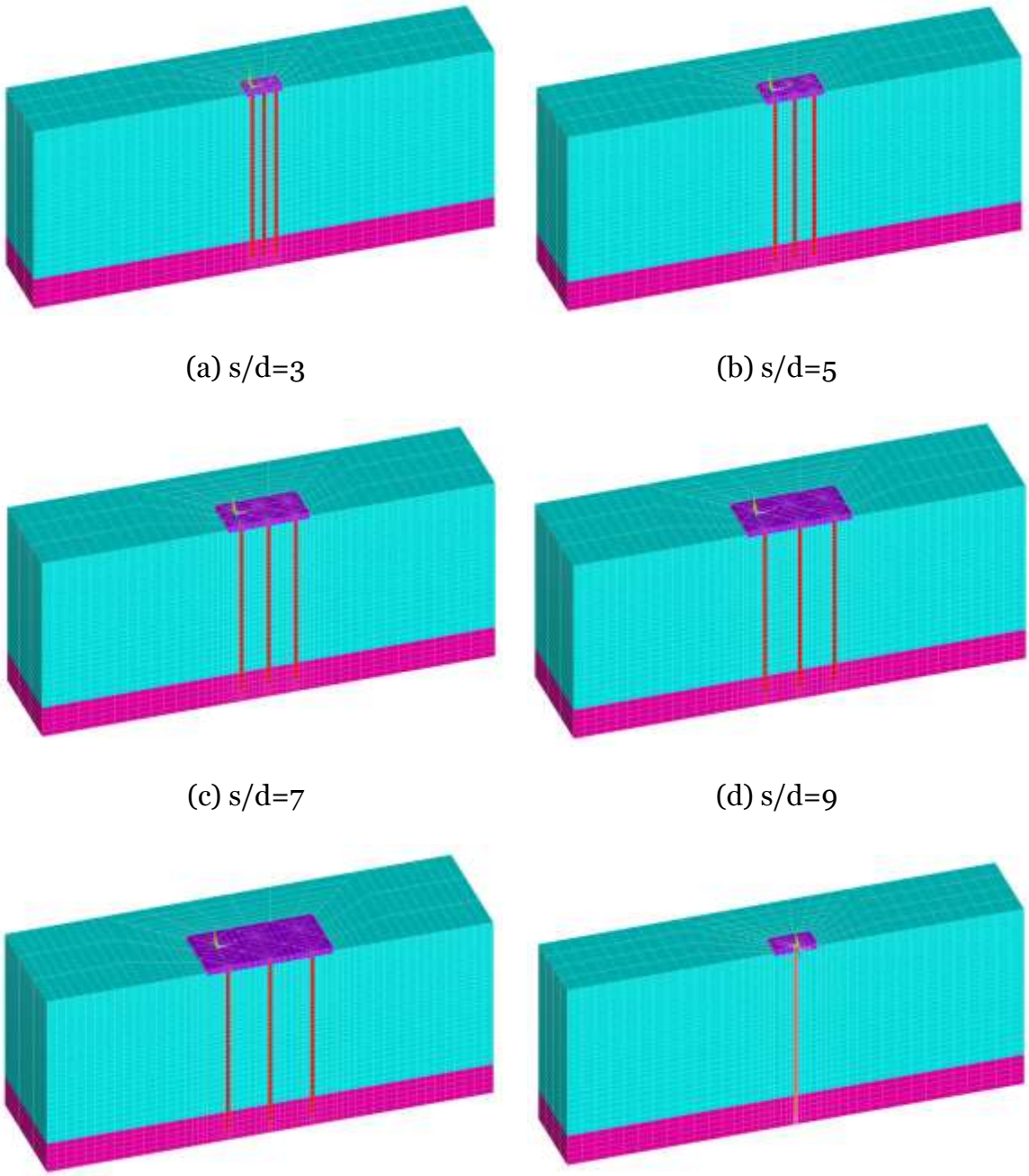

(a) s/d=3

(b) s/d=5

(c) s/d=7

(d) s/d=9

(e) s/d=11

(f) single pile (vertical displacement of pile raft is fixed)

Figure 4-23 Pile foundation models with different pile spacing

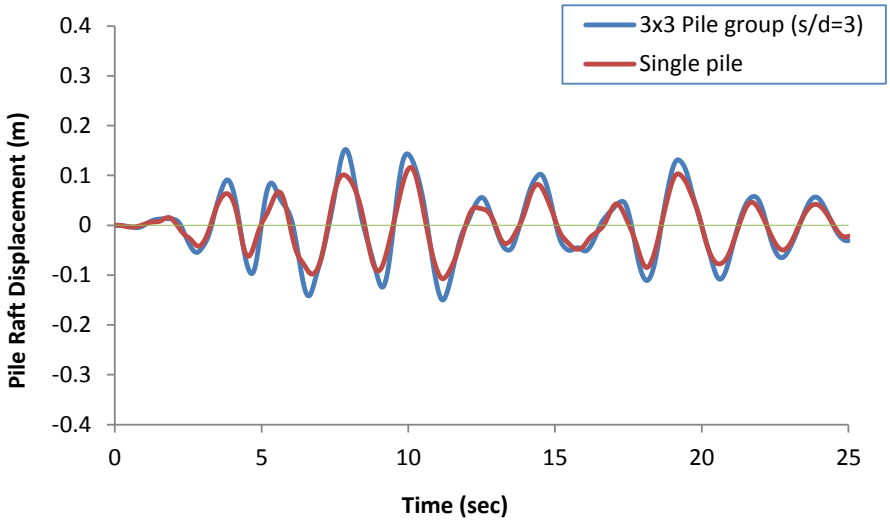

Figure 4-24 Comparison of the pile cap displacement: 3x3 pile group vs single pile

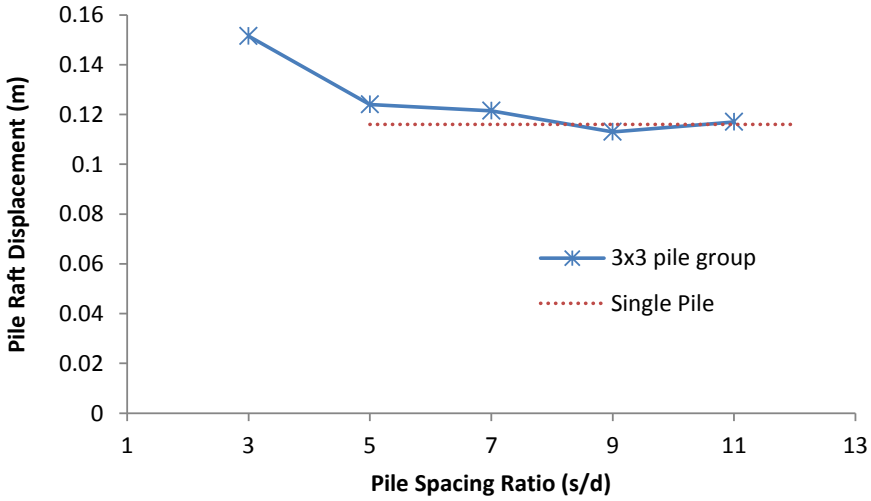

Figure 4-25 Maximum pile raft displacement versus pile spacing ratio

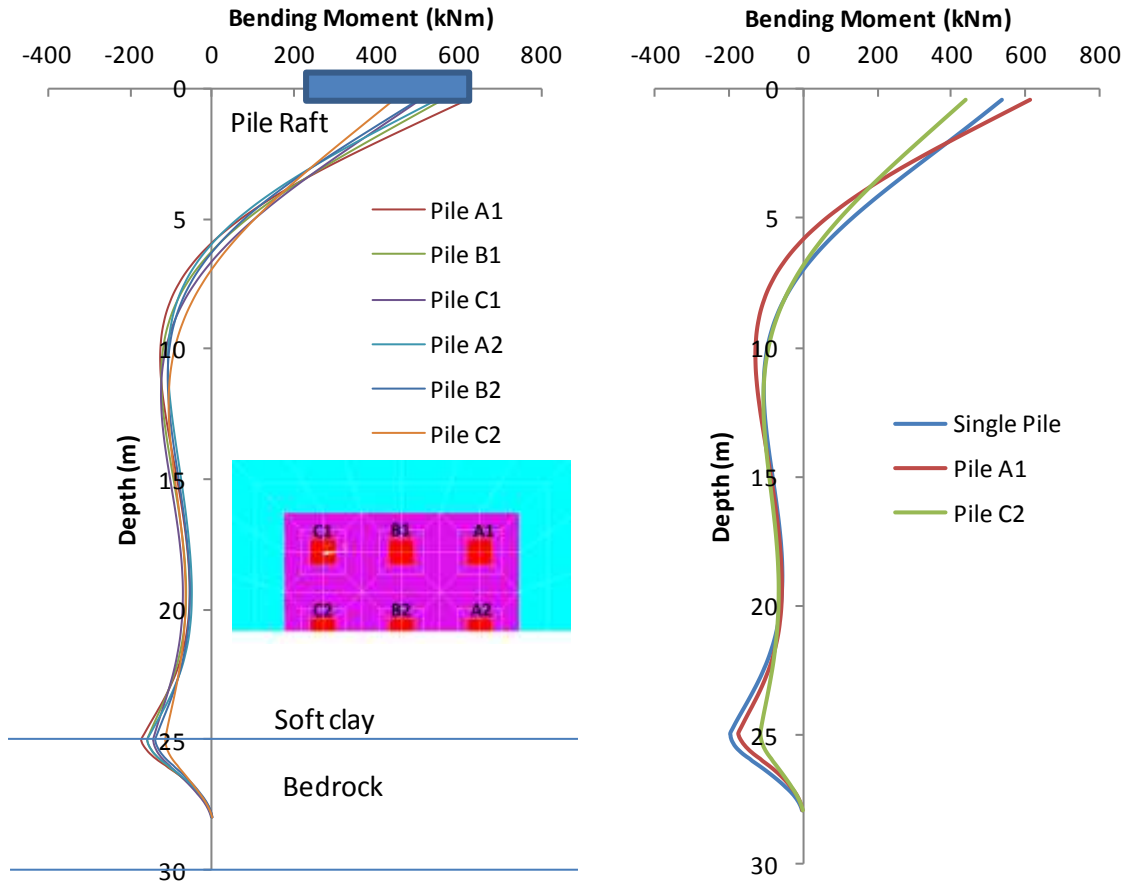

(a) All piles within the pile group (b) Comparison with single pile

Figure 4-26 Pile bending moment profiles in a 3x3 group with 3d spacing

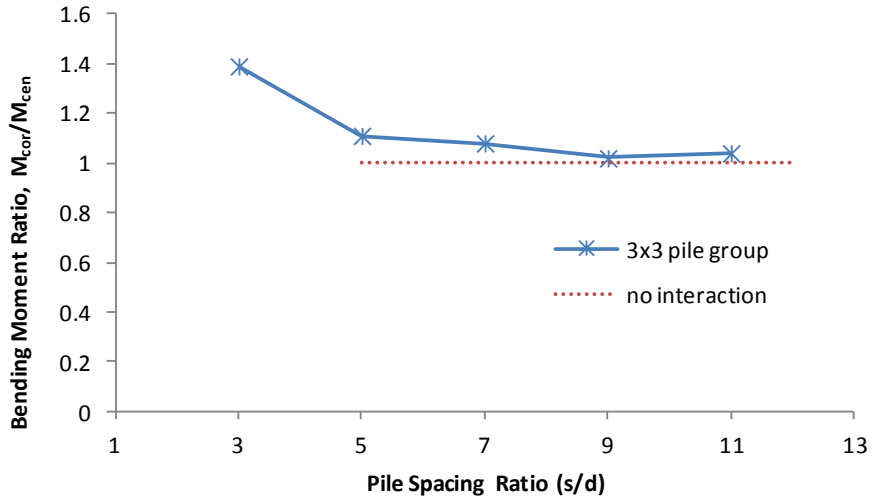

Figure 4-27 Pile bending moment ratio versus pile spacing ratio

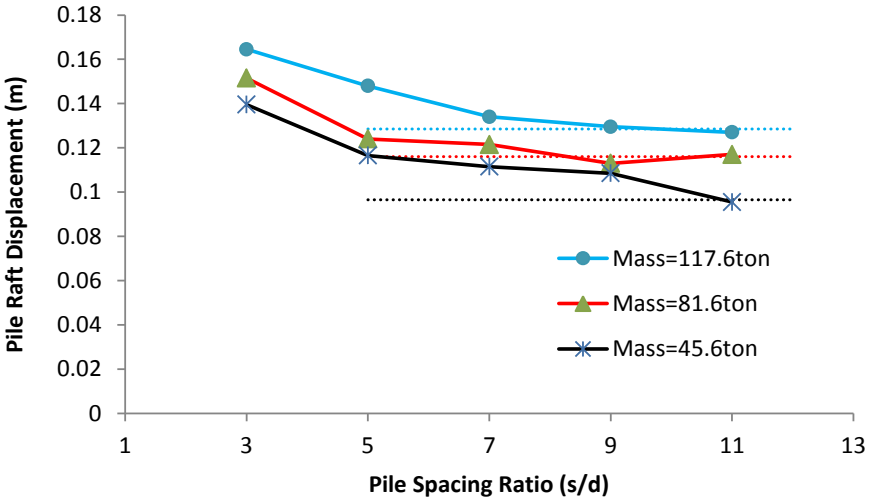

Figure 4-28 Maximum pile raft displacement versus pile spacing ratio with different structural mass

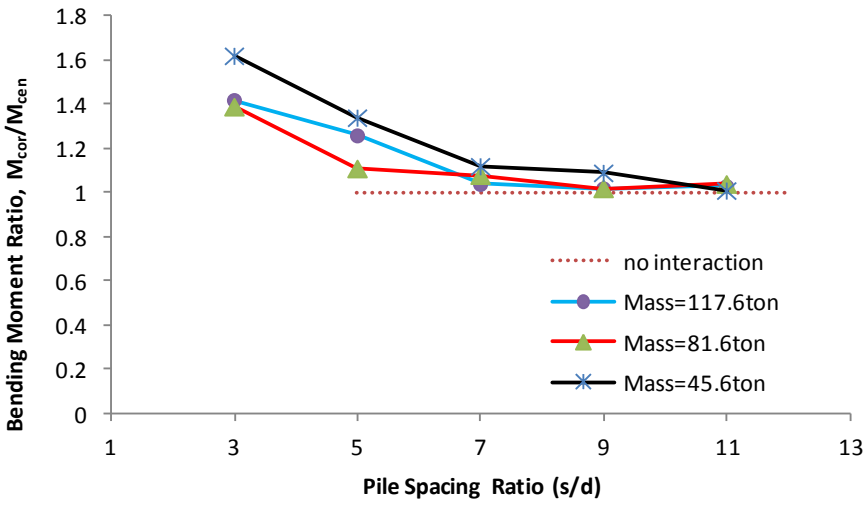

Figure 4-29 Pile bending moment ratio versus pile spacing ratio with different structural mass

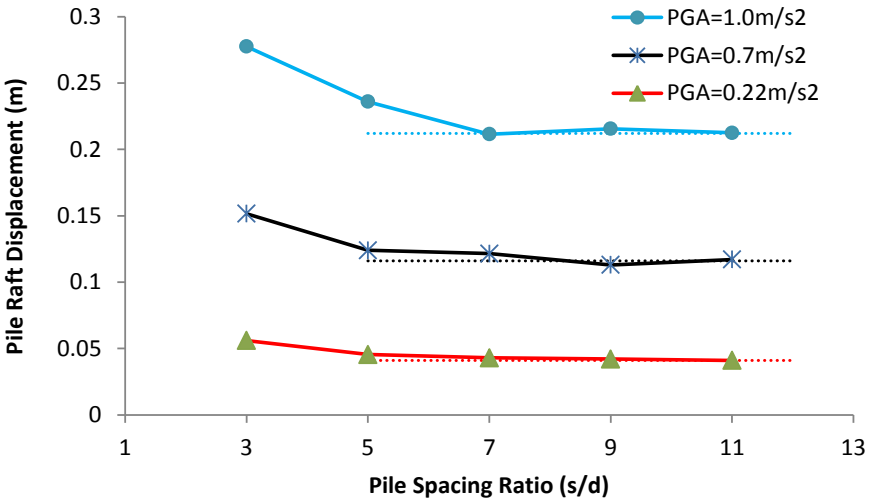

Figure 4-30 Maximum pile raft displacement versus pile spacing ratio with different peak base acceleration

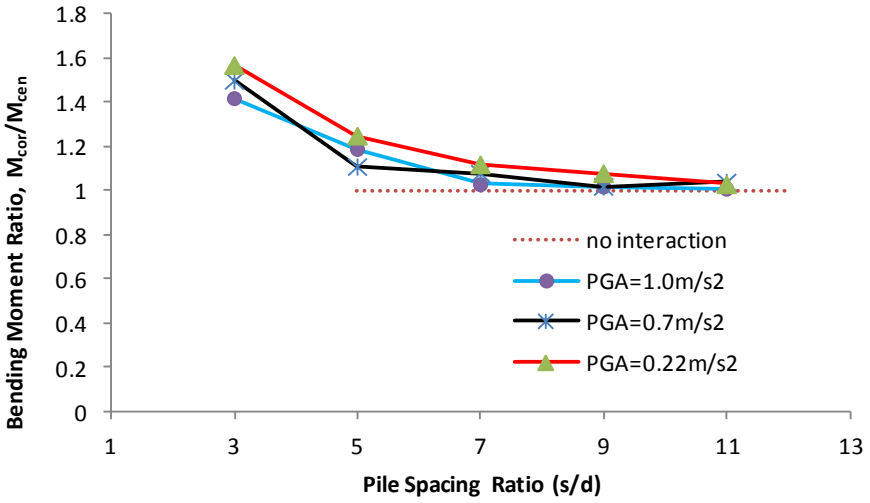

Figure 4-31 Pile bending moment ratio versus pile spacing ratio with different peak base acceleration

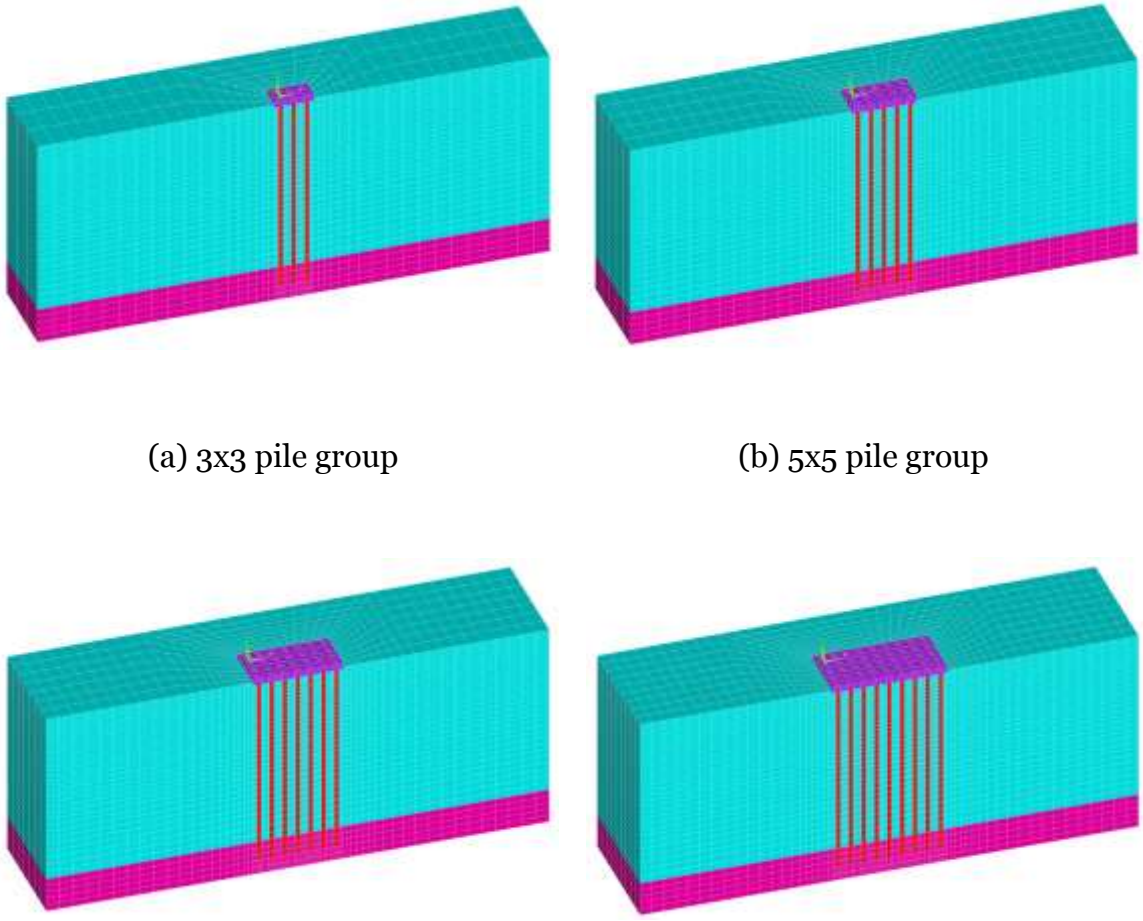

(a) 3x3 pile group

(b) 5x5 pile group

(c) 7x7 pile group

(d) 9x9 pile group

Figure 4-32 Pile group models with different pile group sizes

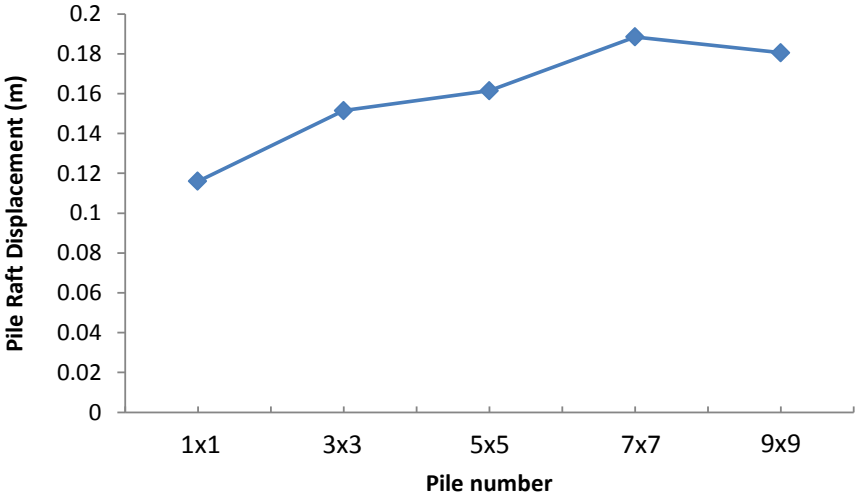

Figure 4-33 Maximum pile raft displacement versus pile group size

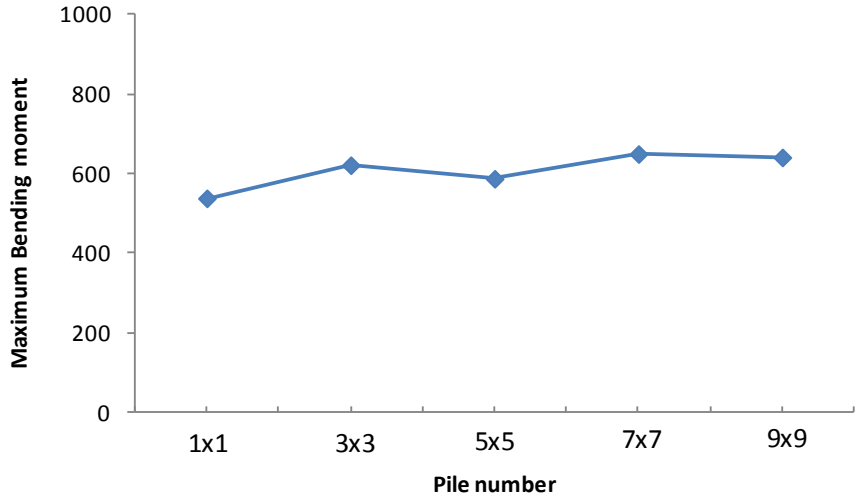

Figure 4-34 Maximum pile bending moment versus pile group size

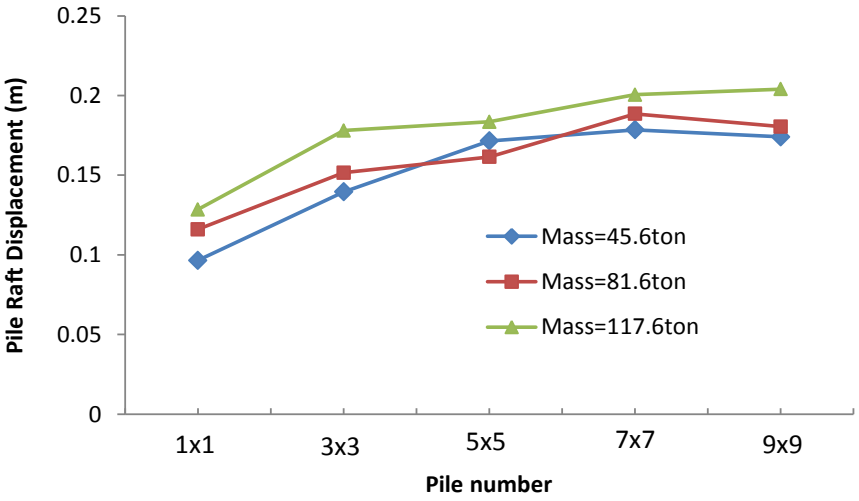

Figure 4-35 Maximum pile raft displacement versus pile group size for different structural masses

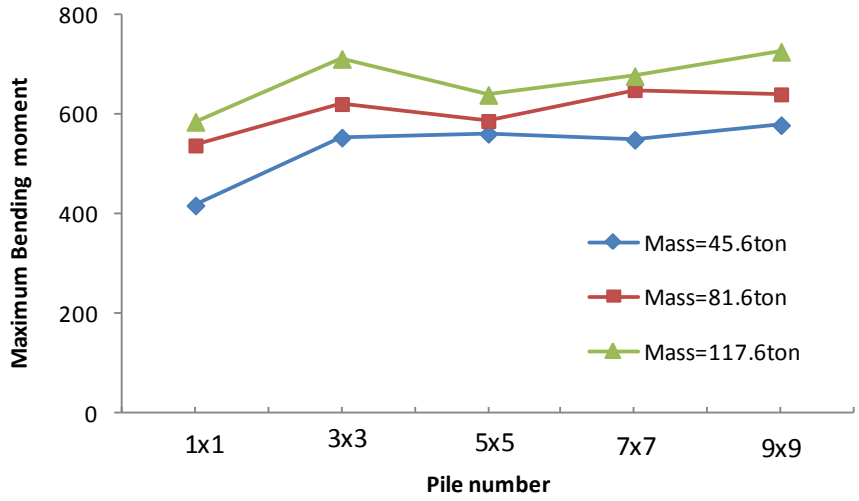

Figure 4-36 Maximum pile bending moment versus pile group size for different structural masses

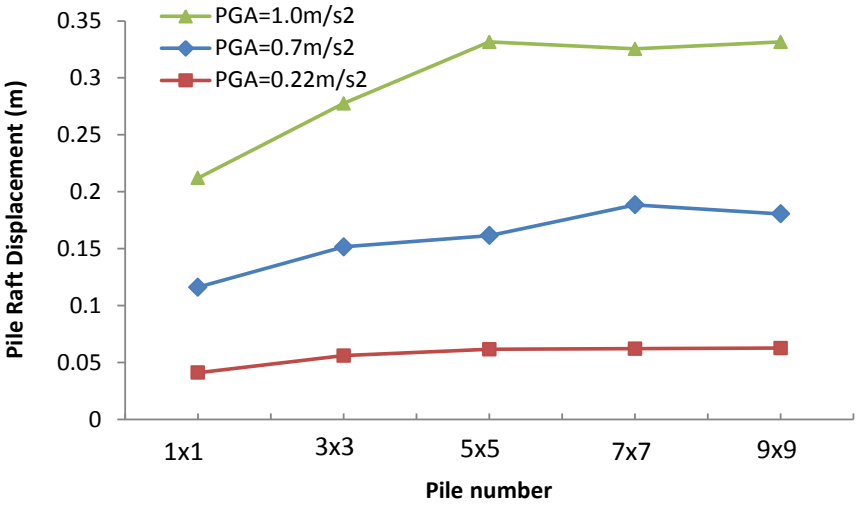

Figure 4-37 Maximum pile raft displacement versus pile group size for different peak base acceleration

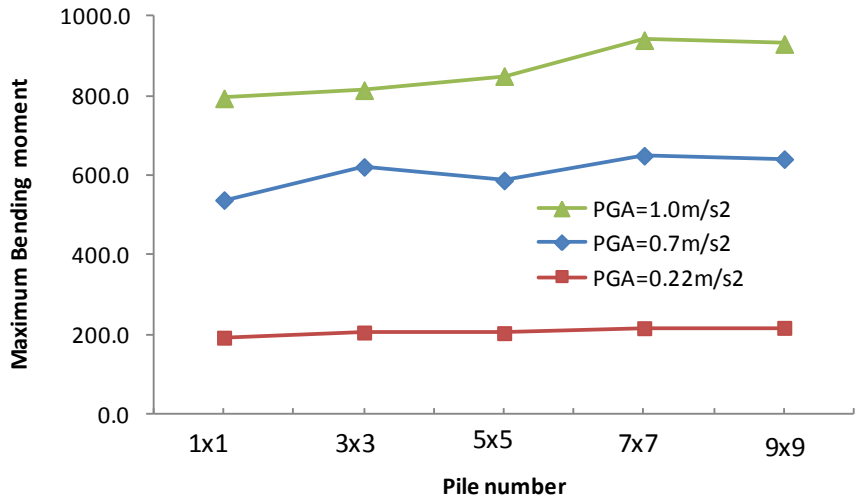

Figure 4-38 Maximum pile bending moment versus pile group size for different peak base acceleration

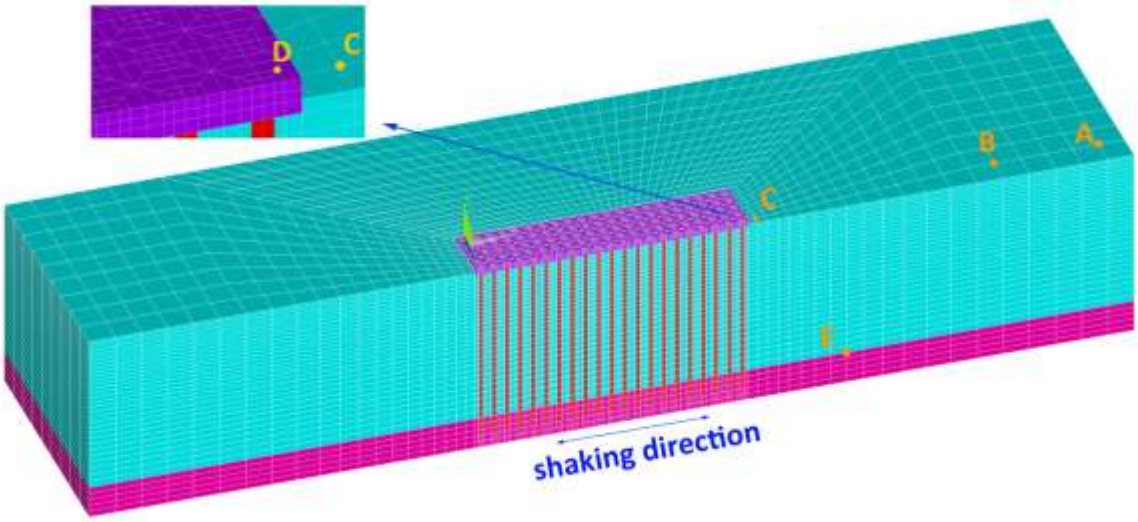

Figure 4-39 Finite element model for large-scale soil-pile group-raft system

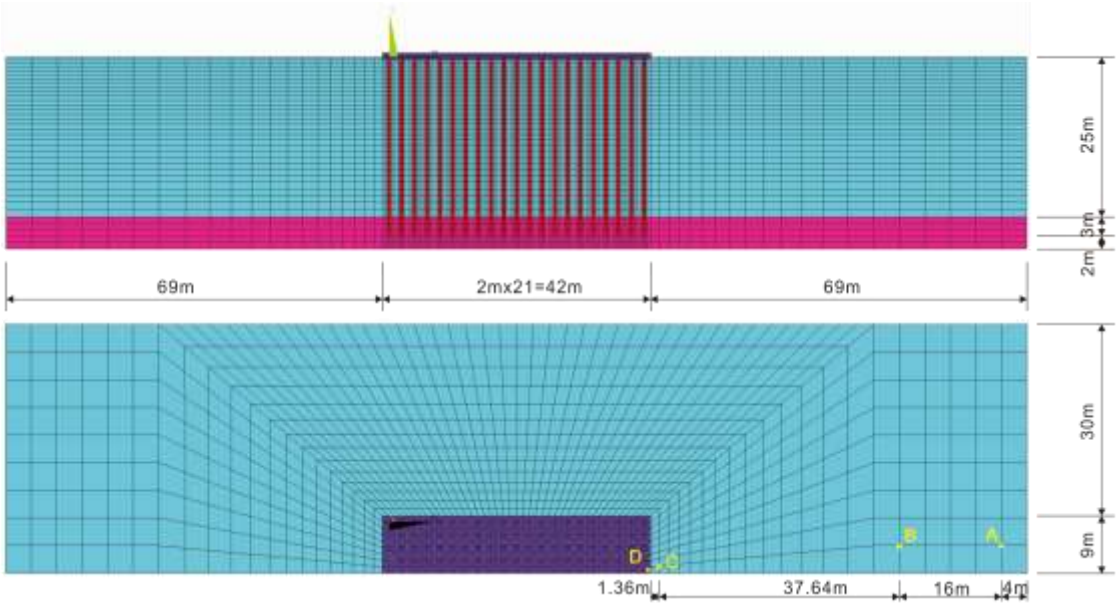

Figure 4-40 Model dimensions of the large-scale soil-pile foundation system

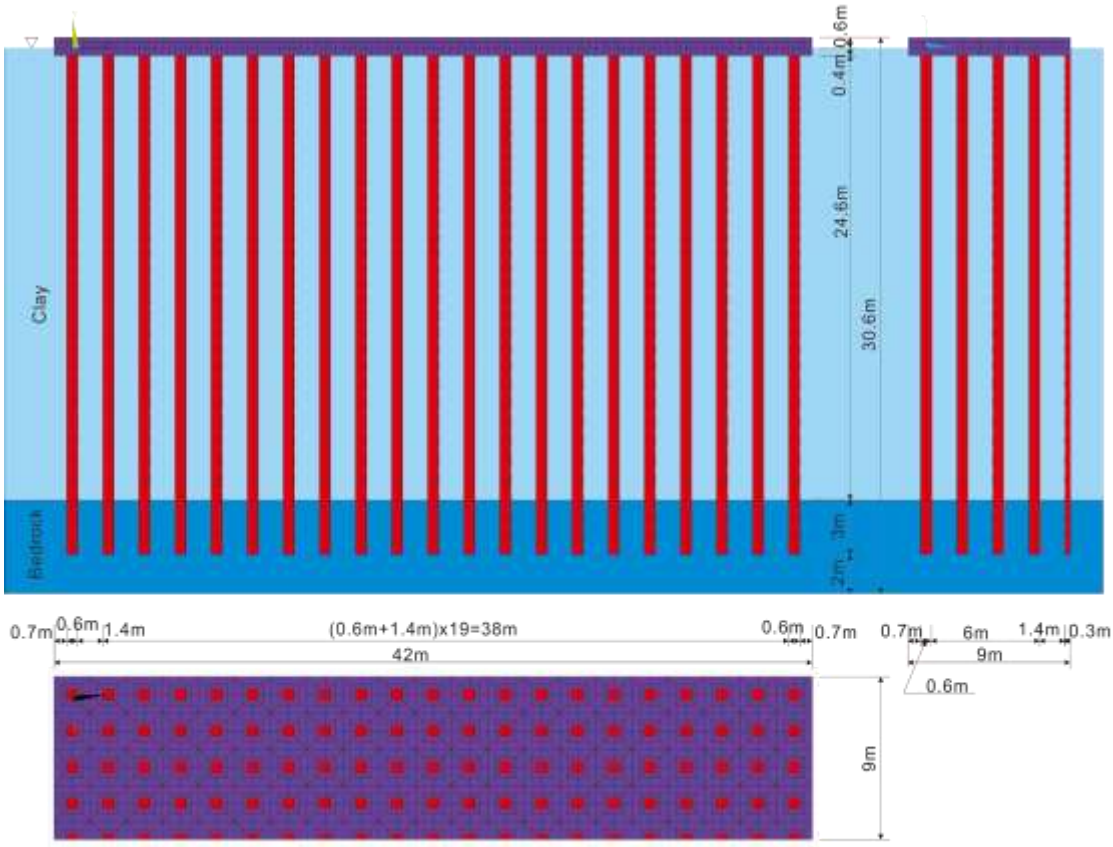

Figure 4-41 Model dimensions of the pile foundation

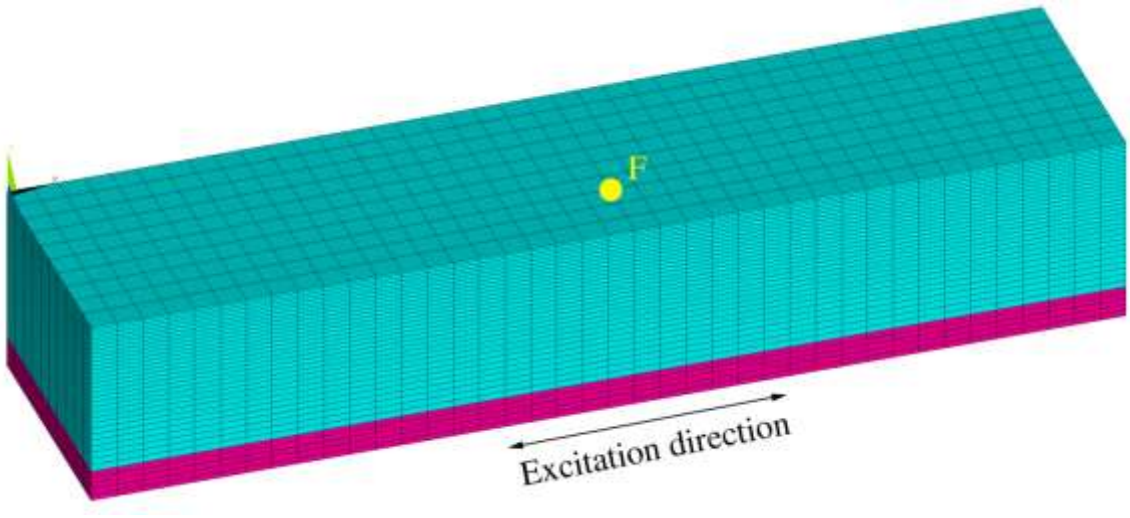

Figure 4-42 Finite element model for free field simulation with the same dimensions

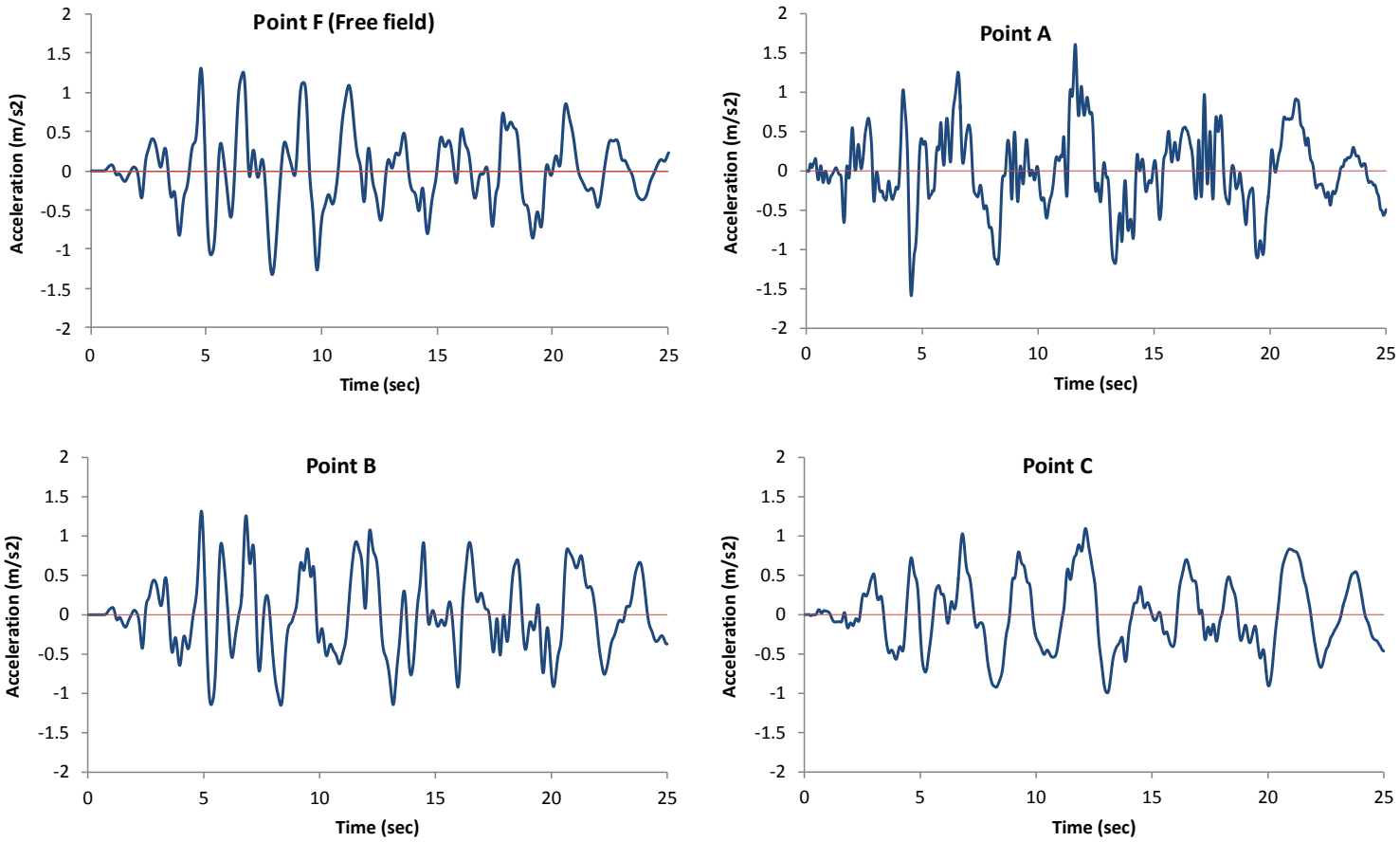

Figure 4-43 Computed acceleration histories at different surface locations

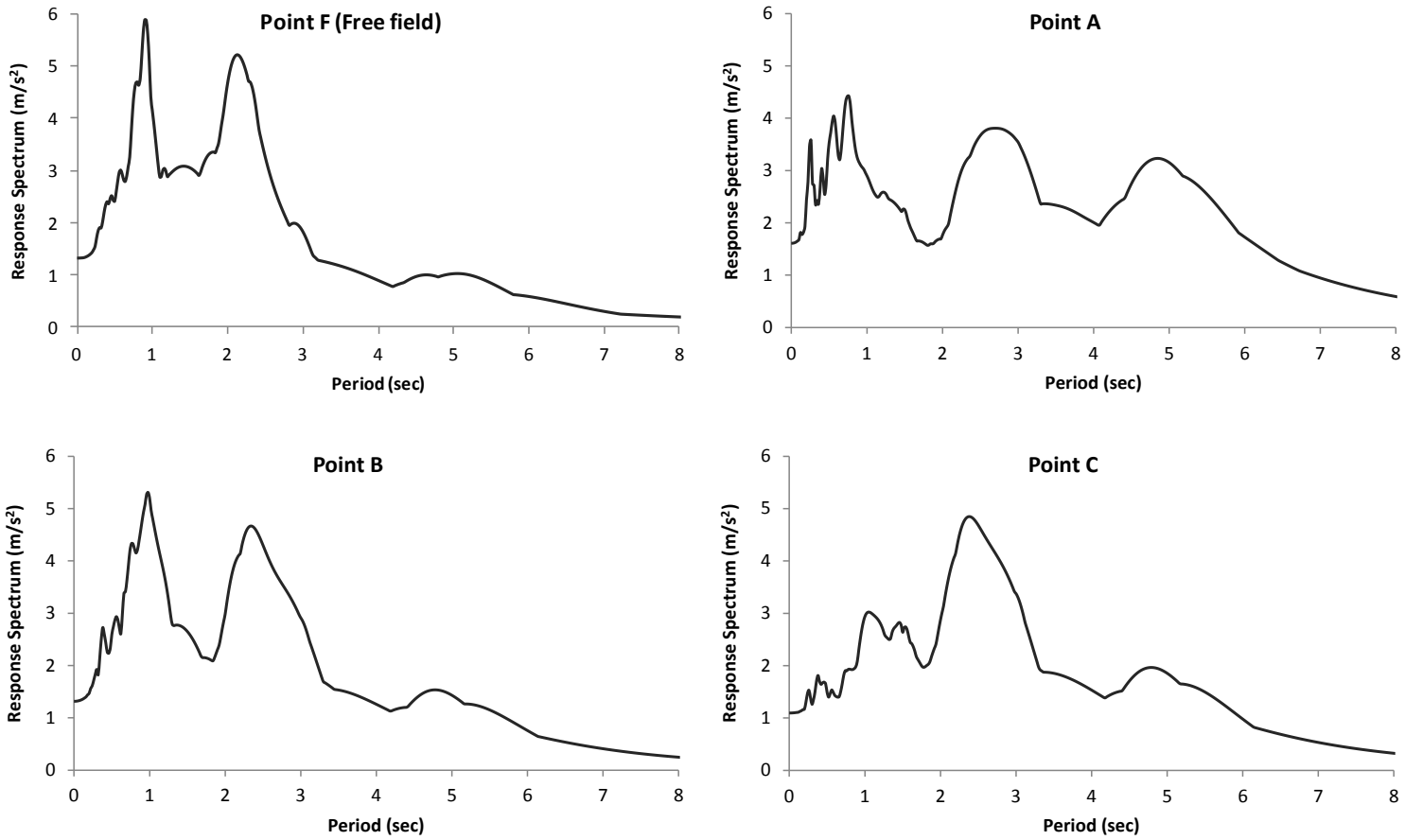

Figure 4-44 Computed response spectrum at different surface locations

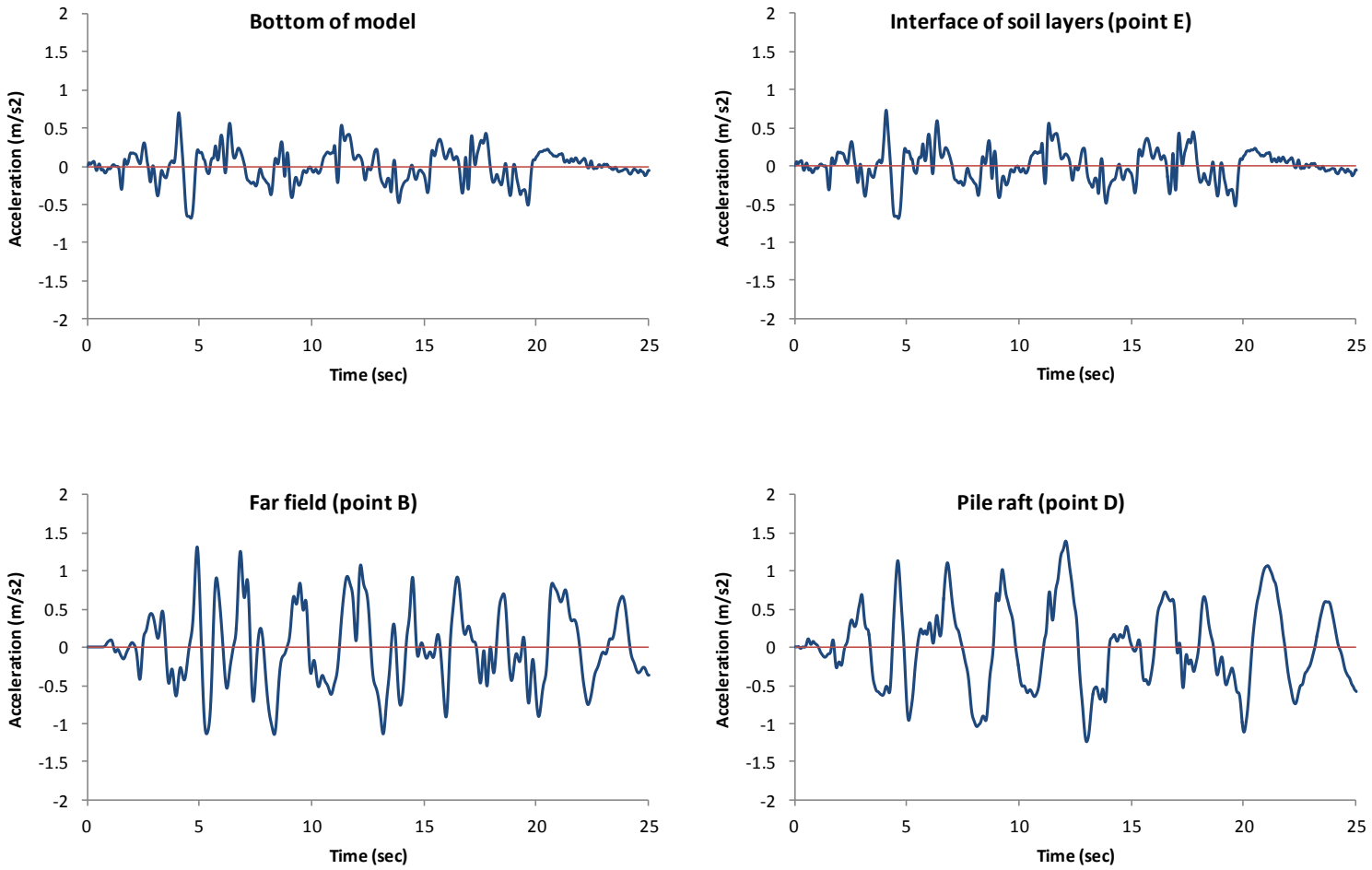

Figure 4-45 Computed acceleration time histories at different locations of the soil-pile-structure system

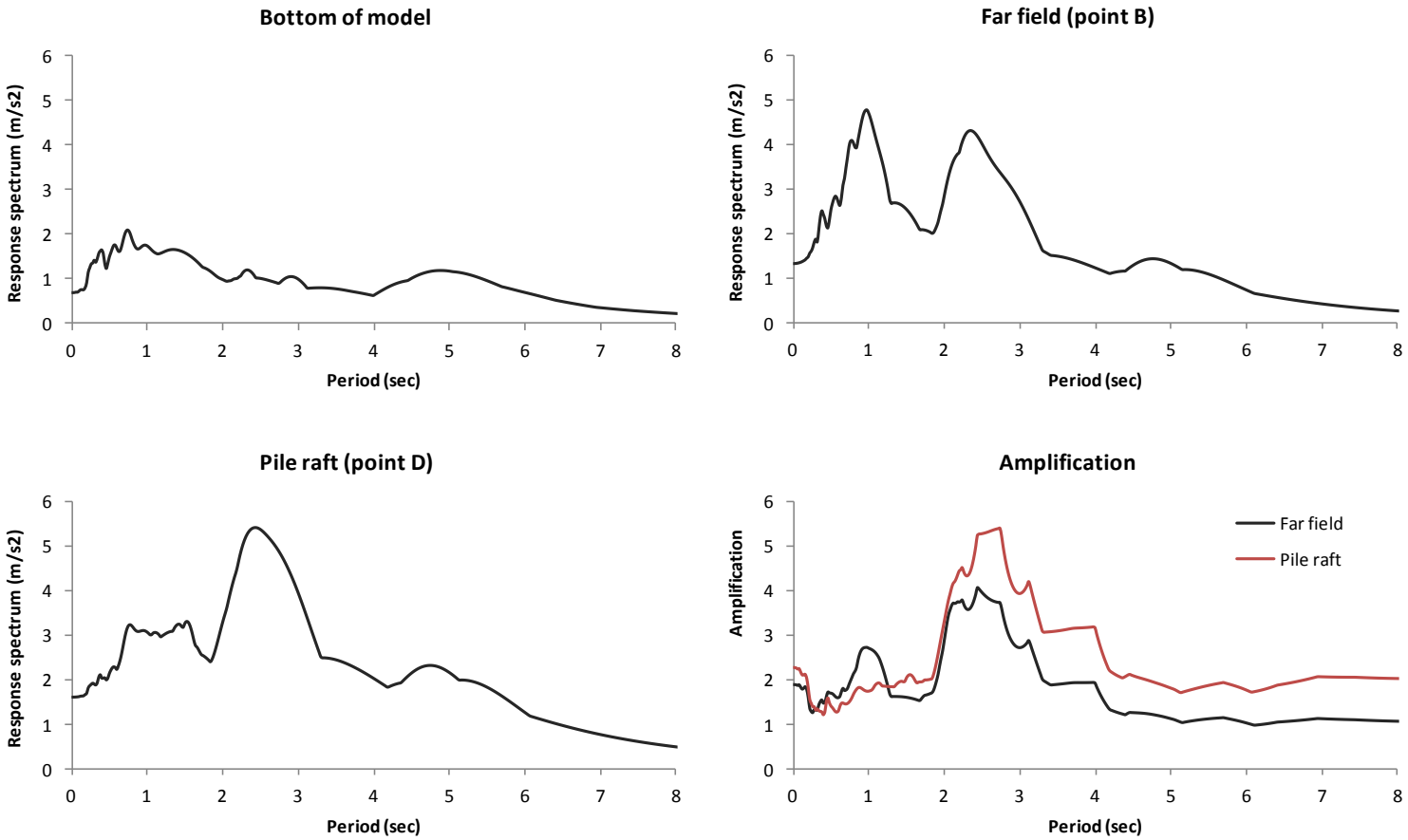

Figure 4-46 Response spectra and amplification at the far field and the raft

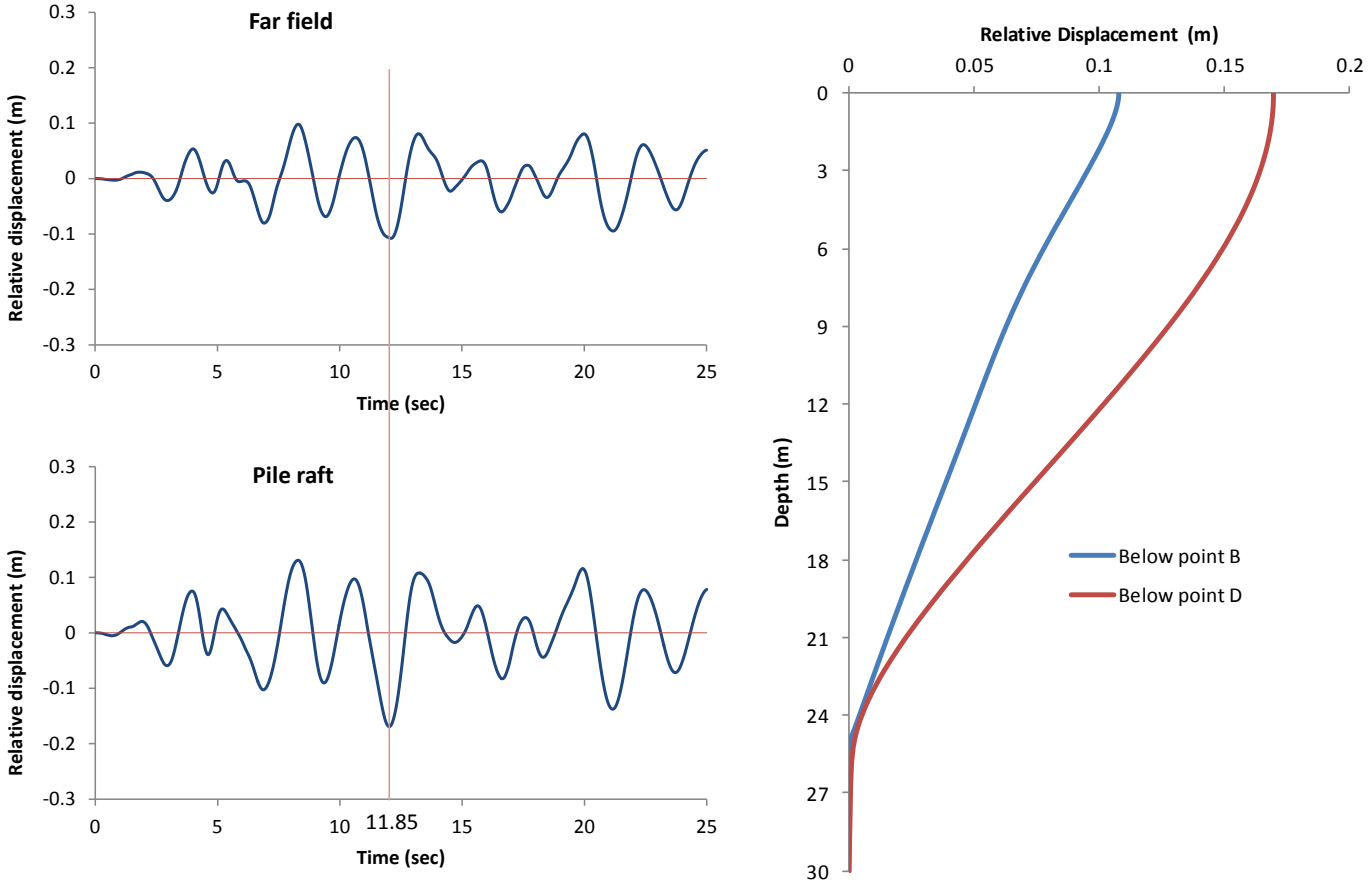

Figure 4-47 Comparison of displacement profiles for the far field and near field

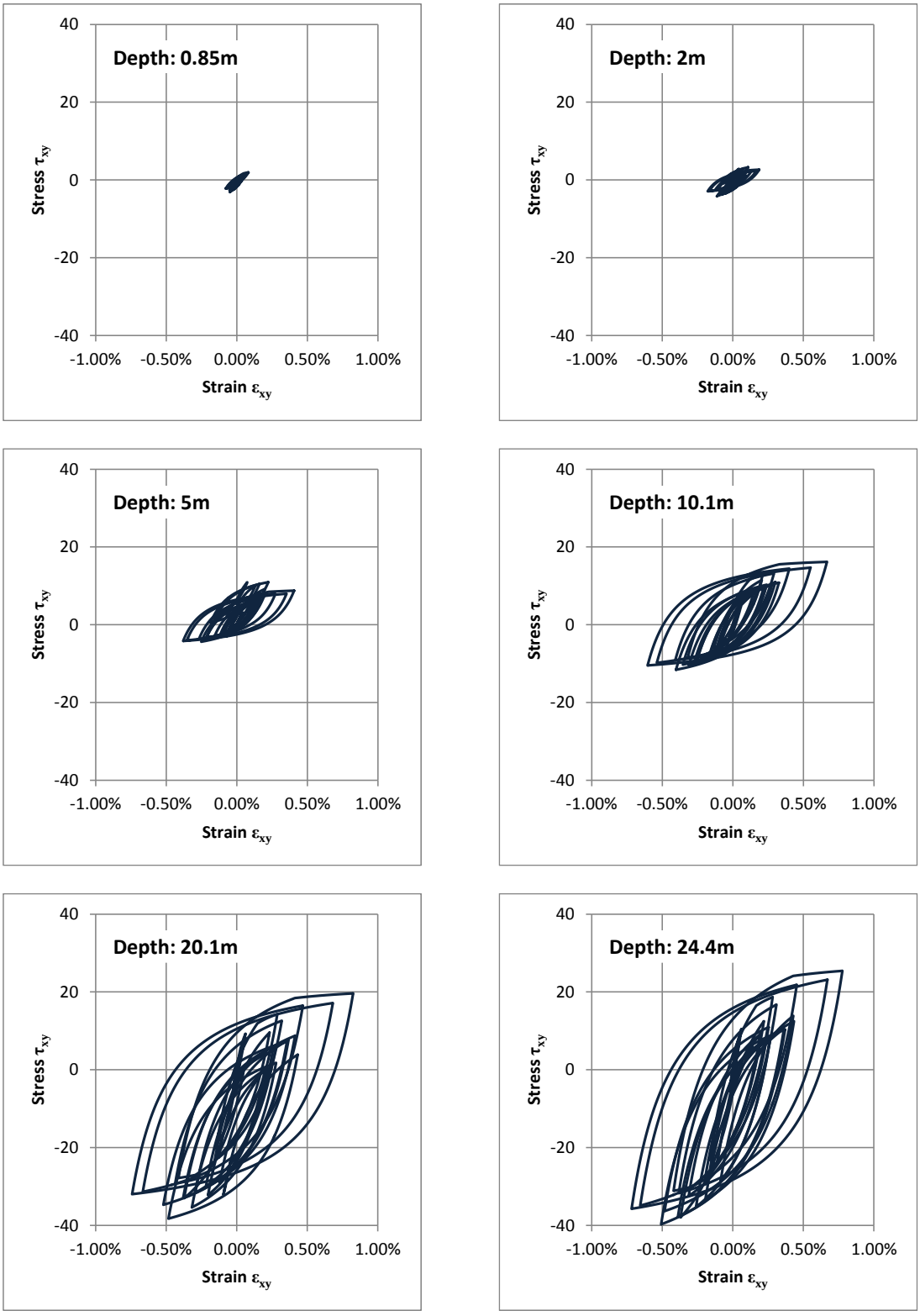

Figure 4-48 Shear stress-strain relationships at different depths (below point D)

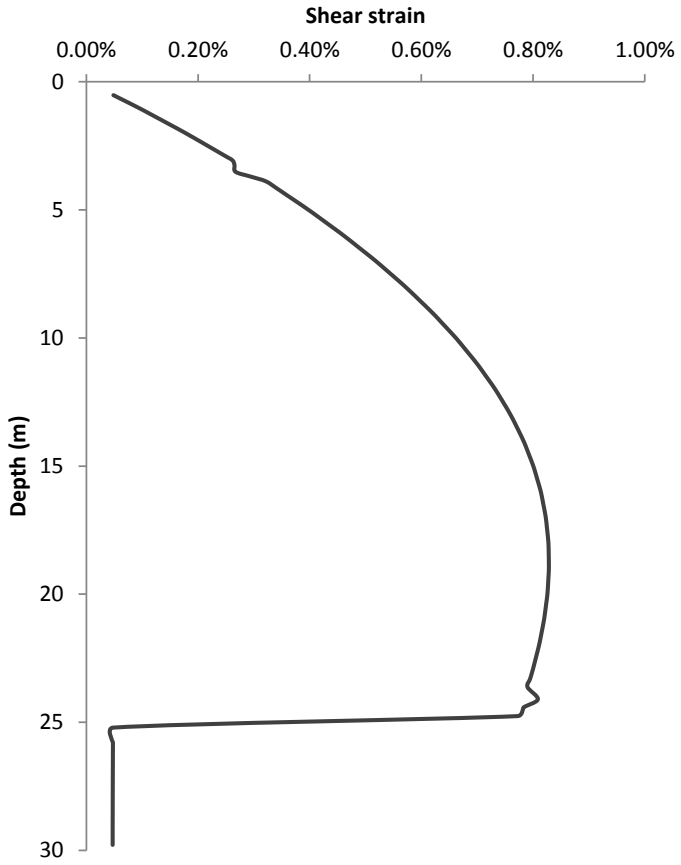

Figure 4-49 Shear strain profile with depth (below point D, at t=11.85 sec)

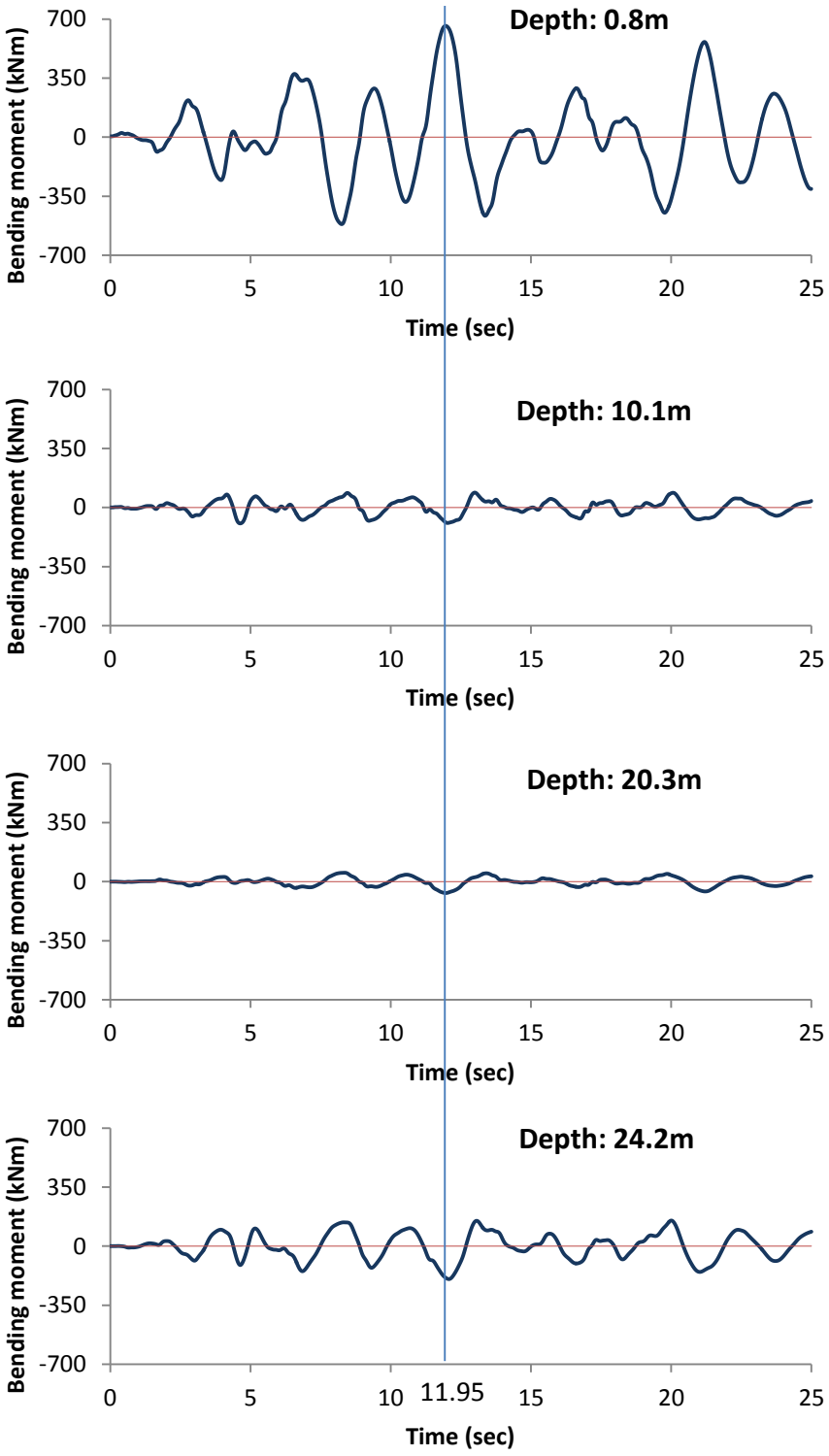

Figure 4-50 Typical bending moment histories at different depths (below corner pile)

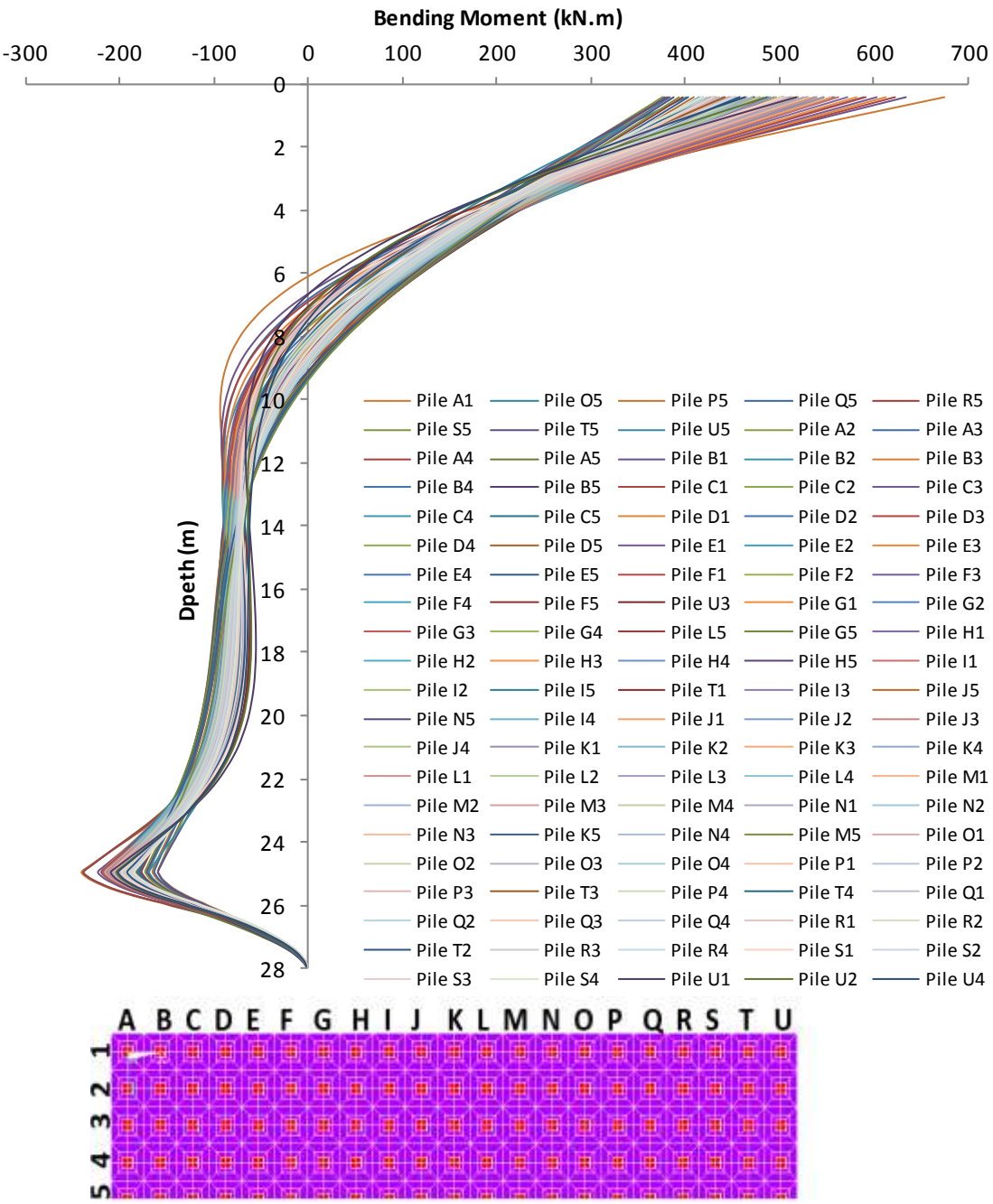

Figure 4-51 Bending moment profiles for all piles at time t = 11.95 s.

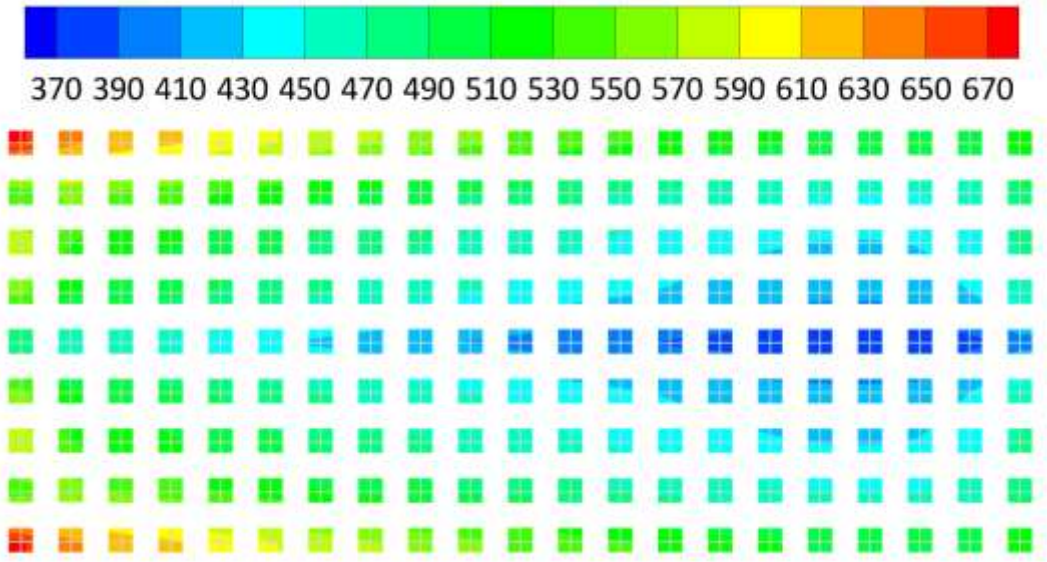

Figure 4-52 Distribution of maximum bending moment at the pile head for all piles within the group

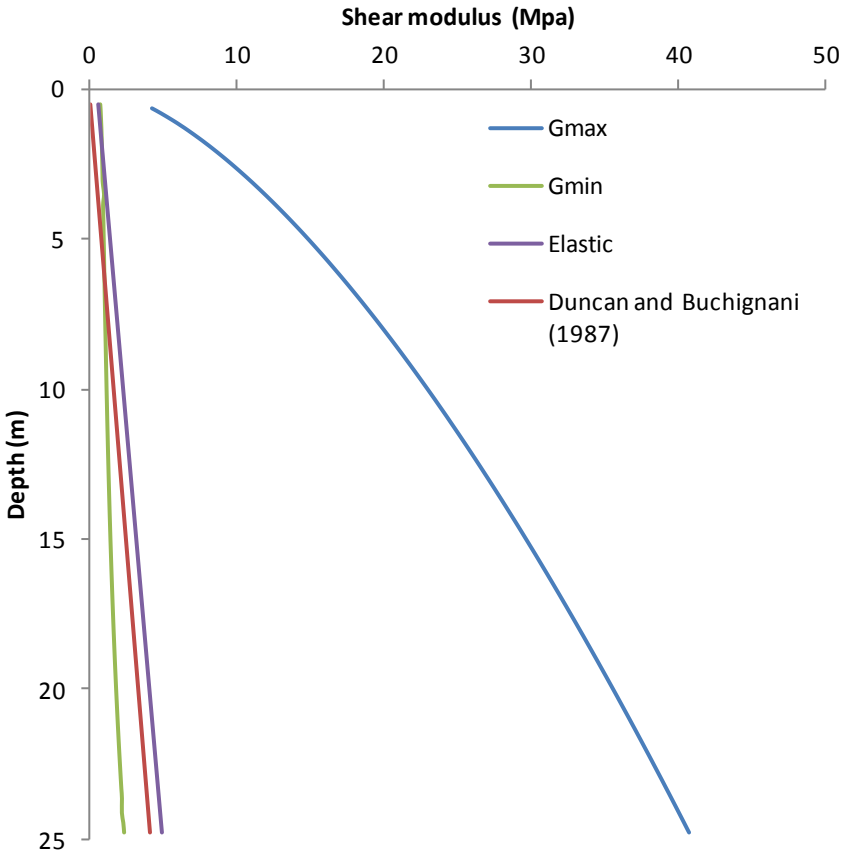

Figure 4-53 Shear modulus profile of the soft soil with depth

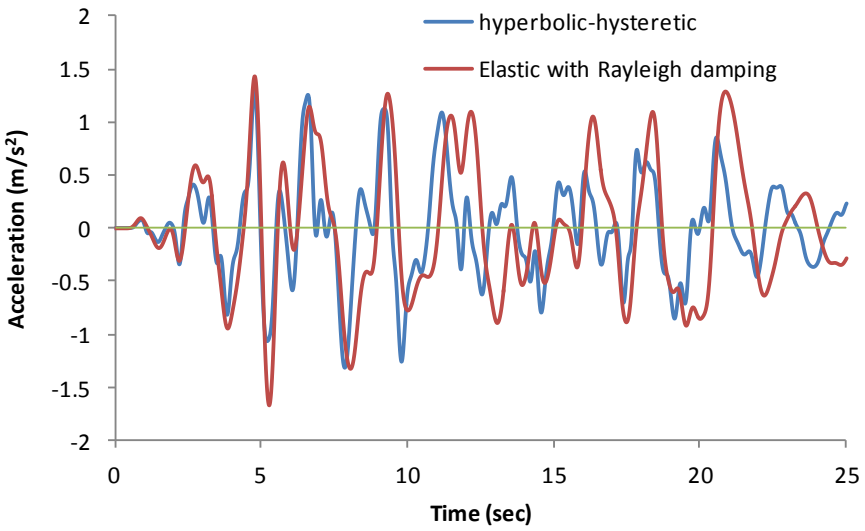

Figure 4-54 Comparison of the free field acceleration histories computed using the hyperbolic-hysteretic model and the elastic model with Rayleigh damping.

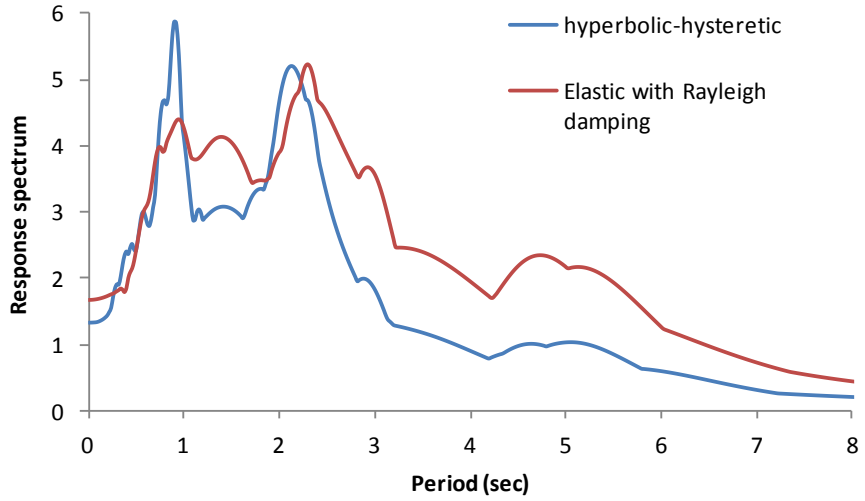

Figure 4-55 Comparison of the free field response spectrum computed using the hyperbolic-hysteretic model and the elastic model with Rayleigh damping.

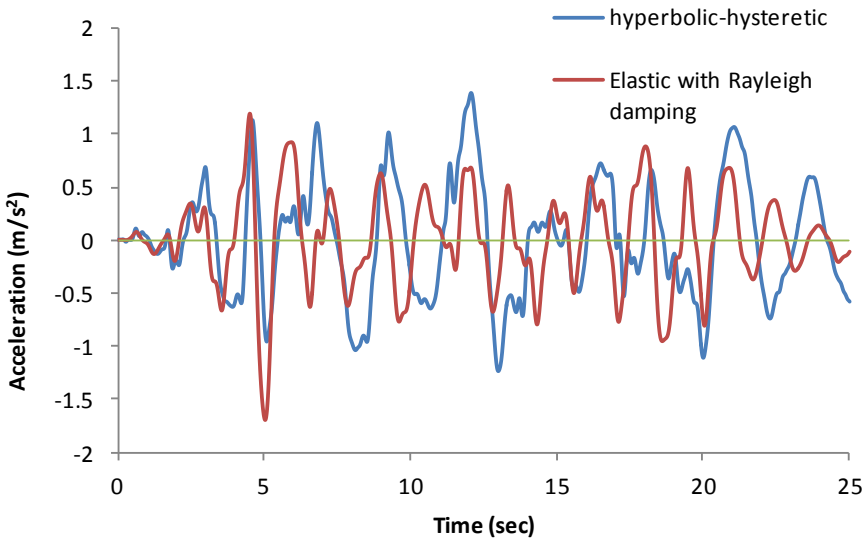

Figure 4-56 Comparison of the pile raft acceleration histories computed using the hyperbolic-hysteretic model and the elastic model with Rayleigh damping.

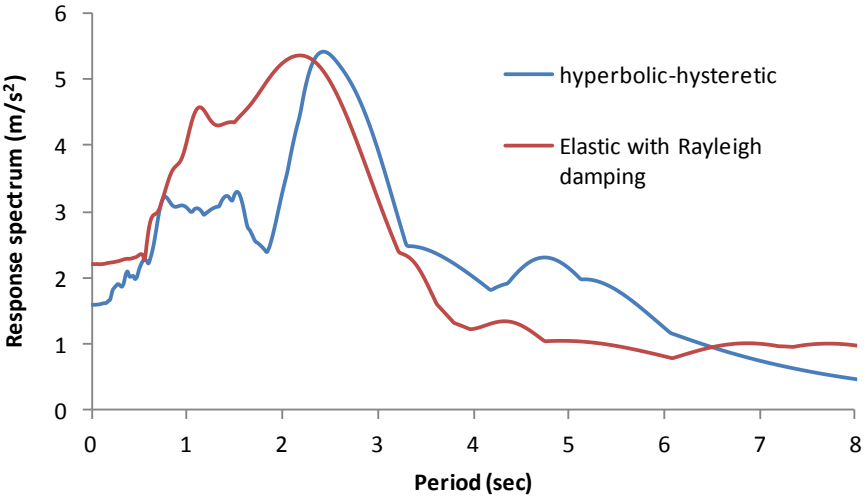

Figure 4-57 Comparison of the pile raft response spectrum computed using the hyperbolic-hysteretic model and the elastic model with Rayleigh damping.

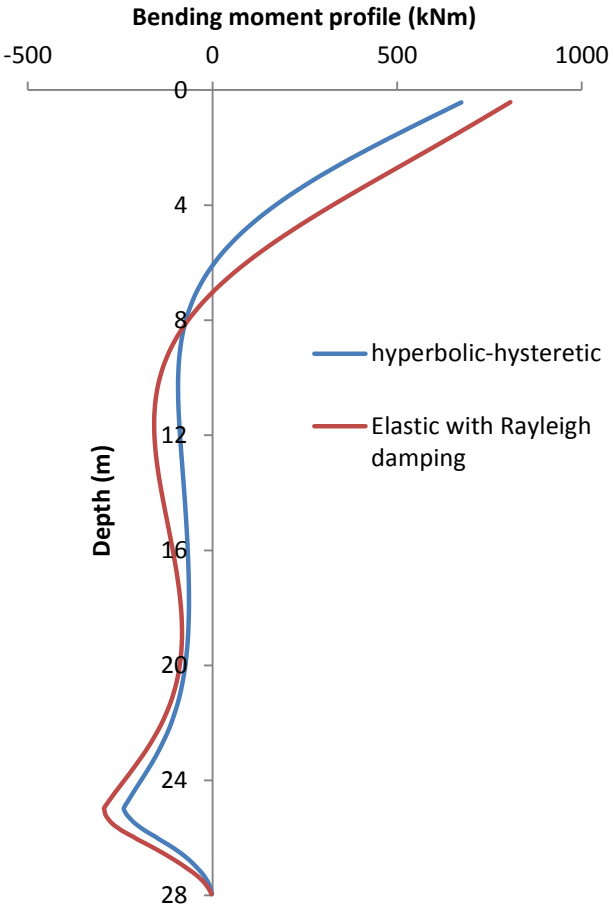

Figure 4-58 Comparison of the maximum bending moment profiles computed using the hyperbolic-hysteretic model and the elastic model with Rayleigh damping (corner pile A1).

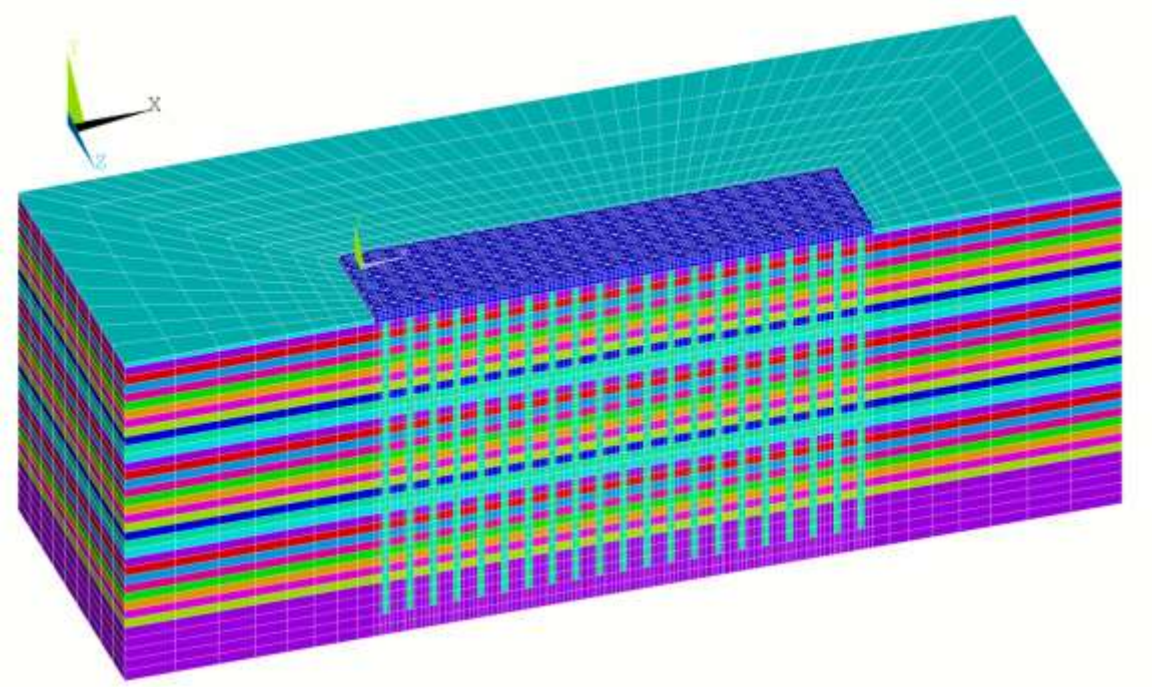

Figure 4-59 Finite element model for pseudo static analysis

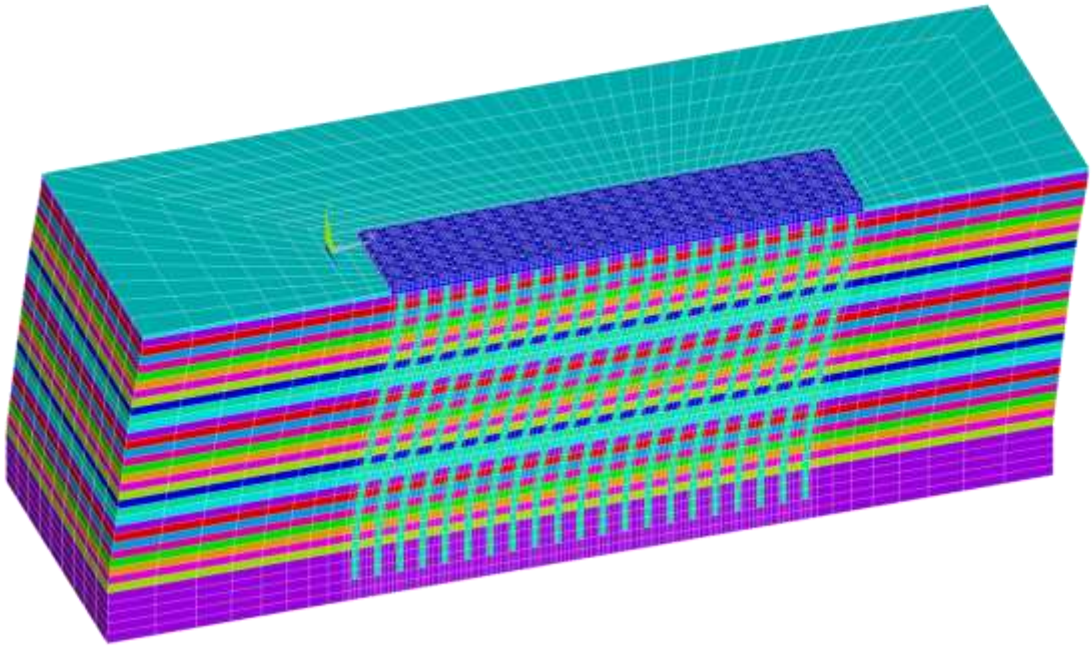

Figure 4-60 Deformed mesh of the model after the pseudo static analysis

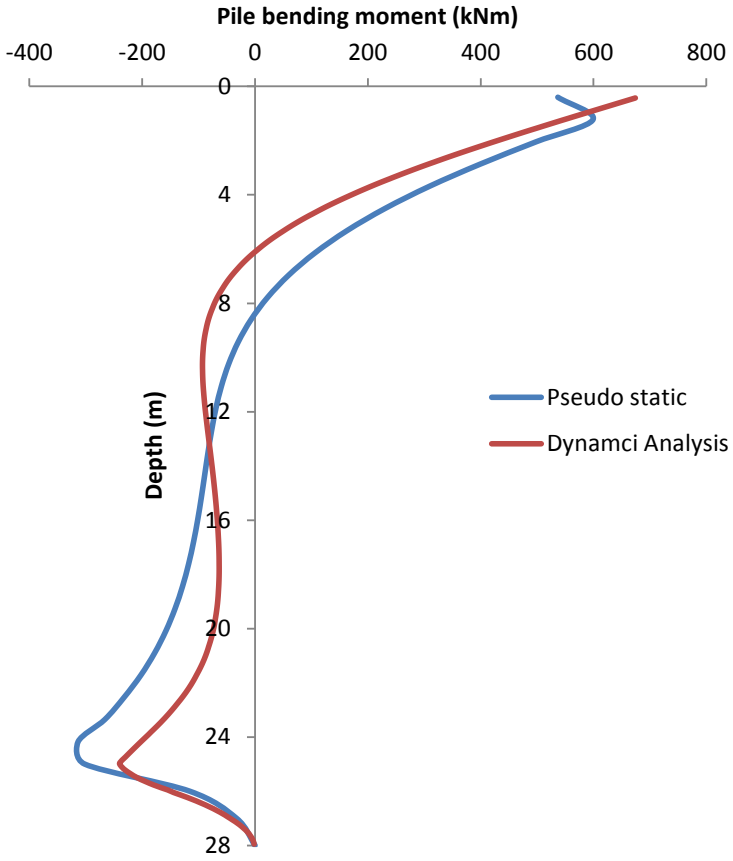

Figure 4-61 Comparison of the maximum bending moment profiles computed using the rigorous dynamic analysis and pseudostatic analysis (corner pile A1).

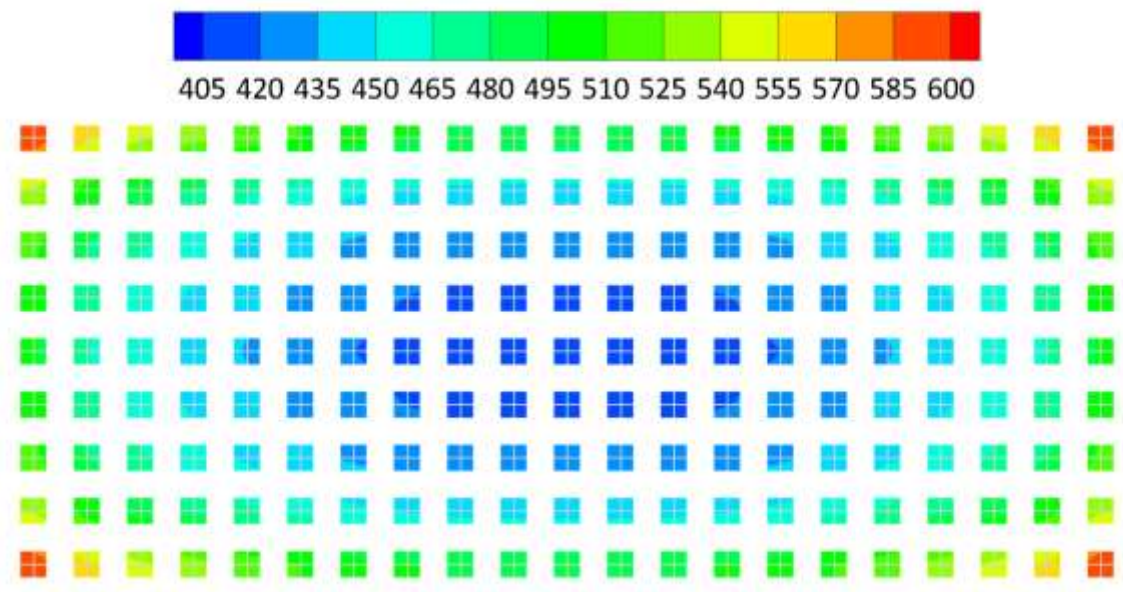

Figure 4-62 Distribution of the maximum pile bending moment at the pile heads from pseudo static analysis

Chapter 5 Parametric Studies for Seismic Pile Foundation

5.1 Introduction

In chapter 4, a large-scale soil-pile foundation -superstructure model subjected to earthquake loading was analyzed using a parallel nonlinear finite element program. Due to the size of the problem, the computational time required for the analysis of a single earthquake event is about 7 days, even when running on eight parallel computer processors. Hence, it is very difficult for other researchers or engineers to carry out similar analyses without advanced computational resources such as supercomputers or PC clusters.

In general geotechnical earthquake engineering design, similar large-scale problems are commonly encountered, although the number and type of piles, soft soil properties and thickness, and earthquake motions may vary from site to site. Due to the costly computational requirements, site-specific analysis for such a large-scale problem is still not a practical option for most engineers. In many cases, design charts or hand calculations are still commonly used. It would thus be beneficial if design charts or equations are available to facilitate at least an approximate analysis.

In this chapter, a suite of large-scale soil-pile foundation -superstructure analyses will be conducted in which the pile foundation dimensions, material properties, and earthquake amplitudes are systematically studied. The influence of the various parameters on the bending moment response of the pile is examined using

the dimensional analysis approach, through which a dimensionless equation for the maximum bending moment in the pile may be obtained. The bending moment profiles in the piles are also examined to obtain the bounding envelope. The results thus obtained, when properly generalized in the form of a dimensionless equation for the maximum bending moment as well as a bounding envelope for the moment profile, will provide a useful tool for geotechnical engineers to design pile foundations under earthquake loading.

5.2 Previous studies on design approach for seismic pile foundation

Previous studies have provided simple methods to predict the kinematic bending moment at the interface between two soil layers (e.g. Margason, 1975; Dobry and O'rourke, 1983; Kavvadas and Gazetas, 1993; Mylonakis, 2001; Nikolaou *et al.*, 2001; Saitoh, 2005) and that at or near the pile head (e.g. Banerjee, 2009; Dezi *et al.*, 2010; Sanctis *et al.*, 2010).

Margason (1975) assumed that a long pile follows the motion of the surrounding soil, and proposed the following simple formula for kinematic bending moments by considering the peak curvature the develops in the free-field soil

$$M = E_p I_p \left(1/R\right) \tag{5.1}$$

where $E_p I_p$ is the flexural rigidity of the pile, and R is the peak curvature generated in the free-field soil due to the earthquake shaking. While this equation provides a quick and simplified method of estimating the maximum pile bending moment,

it has a major limitation in that the interaction between pile and soil was not considered.

Dobry and O'rourke (1983) derived an explicit solution for the pile bending strain at the interface of two soil

$$\varepsilon_p = 2r\gamma_1\left(\frac{k_1}{4E_pI_p}\right)^{1/4}\left[c^{-3}(c-1)\left(c^2-c+1\right)\right] \tag{5.2}$$

in which $c = (G_2/G_1)^{1/4}$ expresses the ratio of the shear moduli of the two layers, and r the pile radius, γ_1 the soil shear stress at the interface and k_1 the modulus of the Winkler springs in the top layer, taken by Dobry and O'rourke (1983) to be three times the shear modulus of the material, i.e. $k_1 = 3G_1$.

Nikolaou *et al.* (2001) also derived a closed-form solution of the maximum bending moment as a function of depth and density of the soil stratum, soil and pile moduli, PGA of the ground motion, and length and diameter of the pile.

$$M \cong 0.042\tau_c d^3\left(\frac{L}{d}\right)^{0.3}\left(\frac{E_p}{E_1}\right)^{0.65}\left(\frac{V_2}{V_1}\right)^{0.5} \tag{5.3}$$

in which a_s is the surface soil acceleration, ρ_1 is the mass density of upper layer soil, h_1 is the upper layer soil thickness, d is the pile diameter, L is the total pile length, E_p is the Young's modulus of the pile, E_1 is the Young's modulus of the upper layer soil, and $V_1$and V_2 are the shear wave velocities in upper and lower soil layers.

While all these methods provide useful estimates of the maximum bending moment for a pile in a two-layered soil, they assume a free-head pile condition with

no super-structural masses involved. The effect of super-structural masses on the bending moment profiles was not considered.

Saitoh (2005) studied the earthquake response of cylindrical fixed-head piles embedded in a homogeneous elastic stratum using three-dimensional wave propagation theory. He derived a closed-form formula for the bending strain ε_p at the pile head, where

$$\varepsilon_p = \frac{\gamma_s P_r}{\frac{100 - P_r}{(d/H)_{\max} - (d/H)_{\max}}\left[(d/H) - (d/H)_{\max}\right] + 100} \tag{5.4}$$

in which P_r is the ratio of the normalized bending strain at the local minimum to that at the local maximum, d/H is the slenderness ratio of the pile, $(d/H)_{min}$ and $(d/H)_{min}$ are the slenderness ratio of pile at local minimum and maximum bending strain respectively, γ_s is the unit weight of the soil. This formula could be used to optimize the pile diameter to minimize the bending strains of the pile.

Tabesh and Poulos (2007) produced charts of seismically-induced maximum bending moment in single fixed-head piles embedded in a linearly elastic homogeneous clay layer, by considering the pile-soil system as Winkler soil-beam combination. Super-structural mass were considered by applying an axial load on the pile head.

Banerjee (2009) performed parametric studies of the kinematic bending moment of stiff piles in soft clay using centrifuge shaking table tests and 3-dimensional

finite element analyses. He proposed a semi-analytical solution for the maximum bending moment

$$M_{\max} = \frac{9.7656}{10^4} \frac{E_p I_p}{d} \frac{a}{g} \left(\frac{E_p I_p \rho}{G M l_p} \right)^{0.1} \left(\frac{l_p}{d} \right)^{0.6} \left(\frac{\rho r_0^3}{M} \right)^{-0.8} \tag{5.5}$$

where $E_p I_p$ is the pile flexural rigidity, d is the pile diameter, a_{max} is the maximum acceleration at the bedrock, ρ is the soil mass density, M is the mass of the raft, and G is the equivalent shear modulus of soft soil. However, Banerjee's (2009) tests and analyses were conducted on relatively stiff piles which showed bending moment extending right to the pile tip. This may not be the case for more flexible piles.

Ma (2010) also studied the kinematic bending moment of more slender and flexible piles in soft clay using centrifuge shaking table tests and 3-dimensional finite element simulation. He proposed an active pile length

$$l_a = 1.5d \left(\frac{E_p}{E_s} \right)^{0.25} \tag{5.6}$$

to divide the piles into short, stiff piles and long, slender piles. For the long, slender piles, the active pile length was used to calculate the maximum bending moment at pile head instead of the whole pile length. A fitted formula was proposed to predict the maximum pile bending moment

$$M_{\max} = 1.2 \times 10^{-8} E_p^{1.12} M^{0.6} a_{\max}^{0.9} d^{0.7} l_p^{0.5} E_s^{-0.12} \rho_p^{0.1} \rho_s^{-0.7} \qquad l_p \le l_a \tag{5.7}$$

$$M_{\max} = 1.2 \times 10^{-8} E_p^{1.12} M^{0.6} a_{\max}^{0.9} d^{0.7} l_a^{0.5} E_s^{-0.12} \rho_p^{0.1} \rho_s^{-0.7} \qquad l_p > l_a \tag{5.8}$$

in which E_p and $E_s$are the Young's modulus of pile and soil, ρ_p and $\rho_s$are the mass density of pile and soil, d and l_p are the pile diameter and pile length, and M is the raft mass.

Using three-dimensional finite element analysis, Dezi *et al.* (2010) studied the response of a fixed-head single pile in a two-layered soil. From their parametric studies, they obtained an empirical expression for the maximum bending moment at the interface between the bedrock and the upper soil layer

$$M \cong \frac{\ddot{u}_g}{0.25g} M_{400}(D,h) e^{f(D,h)(V_s-400)} \tag{5.9}$$

in which M_{400} is the absolute bending moment obtained with $V_s = 400m/s$, where V_s is the shear wave velocity of the upper soil layer, and the function $f(D,h)$ characterizes the dependency of the exponential regression on the pile diameter D and the upper layer soil depth h. The functions $M_{400}(D,h)$ and $f(D,h)$ were calibrated with a nonlinear least square procedure by fitting the finite element data obtained from the parametric analysis.

For the maximum bending moment at the interface between the bedrock and overlying soil layer,

$$M_{400}(D,h) = \left(77.7D^3 + 409D^2 - 192D + 24.5\right) \times \left(-0.0009h^2 + 0.068h - 0.2\right) \tag{5.10}$$

$$f(D,h) = \left(0.000124h - 0.01106\right)\left(-0.05D + 0.864\right) \tag{5.11}$$

For the maximum bending moment at the pile head

$$M_{400}(D,h) = \left(85D^3 + 85.75D^2 - 30.93D + 3.37\right) \times \left(0.000133h^2 - 0.00042h + 1.091\right) \tag{5.12}$$

$$f(D,h)=(0.000067h-0.0113)(-0.07D+1.002) \quad (5.13)$$

It should be noted that Equations(5.10)-(5.13) do not account for the influence of the super-structural mass and the pile stiffness.

Sanctis *et al.* (2010) performed an extensive parametric study using three-dimensional finite element analyses, and proposed an expression to predict the maximum kinematic bending moment at the pile head

$$M_{\max}=0.141\frac{a_{\max}}{g}\gamma d^4\frac{E_p}{E_1} \quad (5.14)$$

where a_{max} is the maximum acceleration at the soil surface, E_p and E_1 is the Young's modulus of the pile and upper layer soil, and γ is the unit weight of the soil.

The above survey of the previous studies involving the seismic response of piles shows that, with the exception of Banerjee (2009) and Ma (2010) most of the works do not consider the effect of the super-structural mass on the pile's bending moment. Also, these studies only consider a single pile, and hence do not account for the effect of pile-group interaction in a piled raft system when many piles are located at close spacing.

5.3 Parametric Studies

In this section, parametric studies using 3-D finite element analyses are carried out for large pile-group systems installed in a soft clay layers. These analyses examine the influence of the soft clay depth (or pile length), pile diameter, soil stiffness, super-structural mass and peak bedrock acceleration on the bending moment

profiles and the maximum bending moment induced within the piles in a large pile foundation.

The baseline soil-pile foundation model adopted for the parametric studies is the same as that considered in Section 4.5, in which a 9x21 pile foundation is installed in a 28m thick soft clay layer. The pile tips are embedded to a depth of 3 x pile diameter in a stiff soil or rock layer. The pile and soil properties, together with the earthquake information, for the baseline analysis are summarized as Case No. 1 in Table 5-1.

Figure 5-2 shows the computed pile bending moment distribution at different instances during the simulated earthquake event for the baseline analysis. The results are shown for the corner pile. It is seen that, while the bending moment distribution changes continuously with time due to the transient earthquake loading, the depths at which the bending moment changes from positive to negative (or vice versa) falls within the a narrow range of between 6 to 7m. This suggests that, for this particular analysis, the depth of the point of contraflexure in the pile remains relatively constant throughout the duration of earthquake shaking. In other words, the pile behaves like there is a pinned support at this relatively constant depth of contraflexure, which can significantly affect the maximum bending moment response near the pile head. In this study, the depth of contraflexure, at which the pile bending moment is zero, will be termed the critical depth. It's different with the term 'critical pile length' defined by Randolph (1981) which is to divide long pile and short pile.

Given that the critical depth may vary over a small range (as shown on Figure 5-2), its value will be defined more specifically as the contraflexure depth corresponding to the instant when the maximum bending moment develops near the rigid connection between the pile and raft. For the baseline analysis, the critical depth of 7.08m occurs at time $t = 5.05\ s$, when the maximum pile bending moment is about 700 kNm.

As shown on Figure 5-2, besides the maximum bending moment which occurs at the pile head, the moment response also shows a local maximum value which develops at the interface between the upper soft clay layer and the underlying stiffer soil in which the pile is shallowly embedded. At any given instant, the two maximum bending moments have opposite signs.

These features are also present in the bending moment time histories at three selected depths, as shown on Figure 5-3. These depths correspond approximately to (i) the pile head location where the maximum moment in the pile occurs, (ii) the critical depth where the point of contraflexure occurs at time t=5.05s, and (iii) the interface between the soft clay and underlying stiff soil. It is noted that the bending moment at the critical depth of 7.08m is very small throughout the entire earthquake event, and for all purposes, is negligible compared with the two locally maximum bending moments near the pile head and the clay-stiff soil interface. It is also noted that, while the two maximum bending moment histories always have opposite signs, they attain their corresponding peak values at the same instance $t = 5.05s$. Hence, the bending moment profile in Figure 5-2 corresponding to $t =$

5.05*s* may be used to characterize the maximum pile bending moment response for the baseline case.

Figure 5-4 shows, for the same 25m thick soft clay layer with different super-structural mass, clay shear stiffness and peak base acceleration, the bending moment profiles corresponding to the instance when the maximum moment is generated near the pile head and at the clay-stiff soil interface. As can be seen, the characteristic bending moment profiles for these different cases are generally similar to that obtained from the baseline analysis. However, the critical depths for these cases vary from about 4m to 10m due to the different parameters adopted in the analyses. Between the critical depth and the clay-stiff soil interface, the negative bending moments are relatively small and quite constant with depth.

Figure 5-6 shows, for a 40m thick soft clay layer, the computed bending moment profiles from various analyses with different parameters. The characteristic shapes are similar to those shown on Figure 5-4 for the 25m thick clay layer, with critical depths varying from about 4m to 15m.

Figure 5-5 shows the computed bending moment profiles for the case when the soft clay layer is only 10m thick. The general shape is still characterized by a maximum bending moment near the pile head, with another smaller local maximum of opposite sign at the interface between the clay and the underlying stiff soil, and a point of contraflexure at the critical depth where the bending moment changes sign. However, due to the small thickness of the clay layer, the zone of relatively small, the segment of nearly constant and small negative moment between the critical

depth and the clay-stiff soil interface is not present. Instead, it is replaced by a larger negative maxima in the bending moment, which can be readily attributed to the fixed-end moment of the stiff soil or rock layer, into which the pile is socketed. Hence the bending moment exhibits a slightly curvilinear variation from the maximum near the pile head to the smaller negative maximum at the clay-stiff soil interface.

Based on the foregoing results for earthquake loading conditions, Figure 5-7 shows the typical bending moment envelopes for a fixed head pile within a large pile foundation installed in a predominantly soft clay layer, the tip of which is nominally embedded to a depth of 3 pile diameters. The profile consists of three key features: (i) a maximum pile bending moment M_1 at or near the pile head, (ii) the critical pile length $\boldsymbol{\ell_c}$ (this length is referred to the distance from pile head to the inflection point, and is different from the one defined by Randolph (1981)) and (iii) the smaller negative maxima M_2 at the clay-stiff soil interface. These features will be examined in greater detail in the subsequent sections, in which the parametric results from the large-scale finite element analyses will be processed and interpreted using dimensional analysis to arrive at proposed equations for estimating these quantities given the soil, pile and earthquake information.

In the following parametric study, the influence of (i) the soft soil layer thickness H, (ii) the pile radius r, (iii) the super-structural mass m_{str}, (iv) the clay modulus G_0 and (v) the peak base acceleration a_{max}on the maximum pile bending moment response is examined. The large-scale model of section 4.5 involving a 9x21 pile foundation is used as the baseline analysis, with the following baseline parameters:

$$H = 25m \quad r = 0.343m \quad m_{str} = 13,608ton \quad G_0 = 2060p'^{0.653} \quad a_{\max} = 0.70\,m/s^2 \quad (5.15)$$

The effects of changing these baseline parameters are presented and discussed in the following subsections.

5.3.1 The effect of soft soil thickness *H*

Three soft soil layer thicknesses, viz. 10m, 25m and 40m, are considered, while all other baseline parameters are kept constant. As shown on Figure 5-8, the thicker the soft soil layer, the smaller will be the maximum bending moment induced at both the pile head (M_1) and the soft soil-stiff soil layer interface (M_2). On the other hand, the critical pile length increases with the soft soil layer thickness.

Figure 5-8 shows the effect of soft soil layer thickness on the critical pile length, for other combinations of the soil, pile and earthquake parameters. Overall, it can be seen that the critical pile length generally increases with increasing thickness of the clay layer, the trend being especially significant for the larger pile ($r = 0.457m$) subjected to the stronger earthquake ($a_{max} = 1.0\ m/s^2$).

Figure 5-10 shows the effect of soft soil layer thickness H on the maximum moment M_1 at the pile head, for different combinations of the soil, pile and earthquake parameters. While many of the cases considered show that M_1 is quite insensitive to the clay layer thickness, the results from other cases show a tendency for M_1 to decrease with increasing clay layer thickness.

Figure 5-11 shows the effect of soft soil layer thickness H on the negative maximum moment M_2 that develops at the clay-stiff soil interface. Compared to the pile head

moment, the tendency for the interface moment M_2 to reduce with increasing clay layer thickness is much stronger. This may be attributed to the stress-dependent stiffness of the clay layer, which leads to a higher clay stiffness or modulus at a greater depth. Hence, with increasing depth, the stiffness contrast between the clay and the underlying stiffer soil becomes less significant, thus resulting in a smaller bending moment M_2 at the interface.

5.3.2 The effect of pile radius *r*

The parametric studies were carried out for three values of the pile radius, i.e. 0.229m, 0.343m and 0.457m. Figure 5-12 compares the maximum bending moment profiles corresponding to the three pile radii, with all other baseline parameters kept constant. $H_{soi} = 25m, m_{str} = 13{,}608ton$, $G_0 = 20600p'^{0.653}$, $a_{max} = 0.70\, m/s^2$

Figure 5-13 shows the effect of the pile radius on the critical pile length, for various combinations of the soil, pile and earthquake parameters. In all cases, the critical pile length increases with the pile radius. The increase is especially significant for the longer piles in the thick clay layer of 40m subjected to the larger earthquake shaking, e.g. when $a_{max} = 1.0\, m/s^2$.

Figure 5-14 shows the effect of the pile radius on the pile head moment, for various combinations of the soil, pile and earthquake parameters. Figure 5-15 shows the corresponding effect on the interface moment. Both figures exhibit a clear trend in which the pile head and interface moments increase with the pile radius.

5.3.3 The effect of structural mass, m_{str}

The parametric studies were carried out for three values of the structural masses m_{str}: 6,804 tons, 13,608 tons and 20,412 tons. Figure 5-16 compares the maximum bending moment profiles corresponding to the three structural masses, with all other baseline parameters kept constant. The larger the structural mass supported by the piles, the greater is the inertial force imposed on the piles by the raft, which gives rise to a larger pile head moment. On the other hand, the interface moment remains relatively unchanged with increasing structural masses. In fact, the results of Figure 5-16 suggest that, for the 25m thick clay layer, the effect of the structural masses is felt mainly in the upper 15m of the pile. Below 15m, the pile bending moment response does not change with increasing structural masses. The critical pile length decreases with increasing structural mass.

Figure 5-17 shows the effect of the structural mass m_{str} on the critical pile length, for various combinations of the soil, pile and earthquake parameters. While the change is generally not too drastic, there is an overall trend for the critical pile length to reduce with increasing structure mass.

Figure 5-18 shows the effect of the structural mass on the pile head moment, for various combinations of the soil, pile and earthquake parameters. Overall, there is a clearly discernable tendency for the pile head moment to increase with increasing structural mass in almost all the cases considered.

The corresponding results for the effect of the structural mass on the interface moment are shown on Figure 5-19. In most cases, the interface moment appears to be quite insensitive to the structural mass, as previously noted in Figure 5-16. The exception is the suite of analyses involving the smallest clay layer thickness H of 10m, where the interface moment increases slightly with increasing structural mass.

5.3.4 The effect of soil stiffness G_0

In this study, the stiffness of the soil is characterized by its initial shear modulus. The variation of initial shear modulus G_0 with mean effective stress p' is adopted from Banerjee (2009) relationship for normally consolidated kaolin clay and follows the form proposed by Viggiani and Atkinson (1995)

$$G_0 = C \cdot p'^{0.653} \tag{5.16}$$

In this equation, the coefficient C varies depending upon the soil type. $C = 2060$ for the kaolin clay used by Banerjee (2009) and Ma (2010). In this section, the effect of the clay stiffness, characterized by its initial shear modulus, is varied by changing the coefficient C to 1030 and 3090, respectively.

Figure 5-20 compares the bending moment envelopes associated with the three small-strain clay moduli, with all other baseline parameters kept constant. With increasing clay stiffness, both the critical pile length and the two maximum bending moments M_1 and M_2 decrease.

Figure 5-21 shows the effect of the clay stiffness G_0 on the critical pile length ℓ_c, for various combinations of the soil, pile and earthquake parameters. It is seen that, for some combinations of the parameters, the critical length is relatively insensitive to changes in G_0. However, for other combinations involving the larger earthquake acceleration a_{max} = 1.0 m/s^2, there is a noticeable decrease of the critical pile length with increasing G_0.

Generally similar trends are observed in Figure 5-22 and Figure 5-23, which shows the effect of G_0 on the maximum bending moments M_1 and M_2 for various combinations of the soil, pile and earthquake parameters.

5.3.5 The effect of peak base acceleration, a_{max}

Parametric studies were carried out for three scaled earthquake ground motions, corresponding to peak base accelerations a_{max} of 0.22m/s^2, 0.7m/s^2 and 1.0m/s^2. Figure 5-24 compares the bending moment envelopes associated with the three peak base accelerations, with all other baseline parameters kept constant. The pile head and interface moments both increase with the peak base acceleration, while the critical pile length remains relatively unchanged.

Figure 5-25 shows the effect of the peak base acceleration a_{max} on the critical pile length ℓ_c, for various combinations of the soil and pile parameters. While the change in critical length is generally small, there is an overall trend for the critical pile length to increase with increasing structure mass. The influence is more conspicuous for the 40m long piles installed in the softest clay of $G_0 = 1030\,(p')^{0.653}$.

Figure 5-26 shows the effect of the peak base acceleration a_{max} on the maximum bending moment M_1 at the pile head, for various combinations of the soil and pile parameters. It can be clearly seen that M_1 increases with increasing peak base acceleration in all the cases considered.

Figure 5-27 shows the corresponding effect of the peak base acceleration a_{max} on the maximum bending moment M_2 at the clay-stiff soil interface. Like the pile head moment M_1, the interface moment M_2 also shows a distinct increase in magnitude with the peak base acceleration a_{max}.

5.4 Dimensional Analysis of Pile Bending Moment Response

Under seismic loading, the factors influencing the bending moment in a fixed head pile can be organized into dimensionless groups, taking into account inertial effects, earthquake loading, increase in soil modulus with depth and, in an approximate manner, non-linearity in stress-strain behavior of the soil.

First, the combined lateral stiffness of the piles in the pile foundation above the contraflexure or inflection point is given by

$$k_p = \sum_{\text{all piles}} \frac{E_p I_p}{l_c^3} \tag{5.17}$$

while the corresponding lateral stiffness of the near-field soil may be expressed as

$$k_s = \frac{G_{soi} A_{raf}}{l_c} \tag{5.18}$$

in which A_{raf} is the horizontal area of the pile raft, ℓ_c is the critical pile length, and $\tilde{G}_{soi}$ is an equivalent shear modulus of the clay over the depth ℓ_c, which is adopted in place of the actual shear modulus G(z, ε) which varies with depth and strain level. In the infinitesimal strain case, the soil shear modulus takes the maximum value G_{max}, which is a function of depth. For normally consolidated Malaysian kaolin clay, Banerjee (2009) proposed that the maximum shear modulus G_{max} can be correlated to the mean effective stress using Viggiani and Atkinson (1995)'s relationship

$$G_{\max}\left(\text{in } kPa\right) = c_1\left(p'\right)^{0.653} \tag{5.19}$$

in which $c_1 = 2060$ was obtained from resonant column test results.

In this study, the water table is coincident with the ground surface, so that

$$p' = \frac{1+2K_0}{3}\gamma' z \tag{5.20}$$

in which K_o is the at-rest earth pressure coefficient, γ' is the effective unit weight and z is the depth below ground surface. This leads to

$$G_{\max} = c_1 \cdot \left(\frac{1+2K_0}{3}\gamma' z\right)^{0.653} = c_1 \cdot \left(\frac{1+2K_0}{3}\gamma'\right)^{0.653} z^{0.653} = c_2 z^{0.653} \tag{5.21}$$

in which $c_2 = c_1 \cdot \left(\frac{1+2K_0}{3}\gamma'\right)^{0.653}$

Under a unit horizontal force applied at the ground surface, the lateral displacement δ of the soil layer over the critical pile depth is given by,

$$\delta = \int_0^{l_c} \frac{1/A_{raf}}{G(z)}\,dz = \int_0^{l_c} \frac{1/A_{raf}}{c_2 z^{0.653}}\,dz = \frac{1}{A_{raf}} \frac{l_c}{0.347 c_2 l_c^{0.653}} \tag{5.22}$$

The corresponding lateral soil stiffness, for the infinitesimal strain condition, can be expressed as

$$k_s\big|_{\varepsilon \to 0} = \frac{1}{\delta} = \frac{0.347 c_2 l_c^{0.653} \cdot A_{raf}}{l_c} \tag{5.23}$$

The parameter l_c in Eq.(5.23) represents the average critical length for the piles within the pile foundation. The critical length for each pile may vary slightly based on the pile foundation size and geometry. However, trying to account for the individual ℓ_c values will make the problem very complicated and detract from the simplified approach proposed herein.

A comparison of Eq (5.18) and Eq (5.23) yields, for the infinitesimal strain condition, the following expression for the equivalent maximum shear modulus over the critical length ℓ_c:

$$G_{\max} = 0.347 c_2 l_c^{0.653} \tag{5.24}$$

Referring to Eq.(5.24), it is seen that the equivalent shear modulus G_{max} is 0.347 times the maximum shear modulus at depth z = ℓ_c.

It is assumed herein that an equivalent shear modulus G_{soi} could be obtained by the product of the equivalent maximum shear modulus and a function of strain level H(ε), that is

$$G_{soi} = G_{\max} \cdot H(\varepsilon) \tag{5.25}$$

However, the effect of strain level is difficult to quantify since strains are non-uniform around the pile and soil behavior is non-linear and hysteretic. Nevertheless, all other factors being equal, the strain level in the soil is likely to increase with the peak base acceleration a_{max}. Hence, the peak base acceleration a_{max} is proposed as an approximate indicator of strain.

$$H(\varepsilon) \approx B\left(\frac{a_{\max}}{g}\right)^{m} \tag{5.26}$$

in which B and m are coefficients to be determined in the following fitting procedure. B > 0 and m < 0 indicate that the soil modulus decreases as the peak base acceleration increases.

Hence, for strain levels associated with a peak earthquake acceleration of a_{max}, the soil lateral stiffness over the depth ℓ_c may be expressed as

$$k_s = \frac{0.347 c_2 l_c^{0.653} \cdot A_{raf}}{l_c} \cdot B\left(\frac{a_{\max}}{g}\right)^{m} \tag{5.27}$$

The ratio of pile stiffness to soil stiffness R_k is then given by

$$R_k = \frac{k_p}{k_s} = \frac{\sum E_p I_p / l_c^3}{B\left(\frac{a_{\max}}{g}\right)^{m} \cdot 0.347 c_2 l_c^{0.653} A_{raf} / l_c} \tag{5.28}$$

which may be re-expressed as

$$R_k = \frac{1}{1.388B} \frac{E_p}{c_2 r^{0.653}} \frac{\sum \pi r^2}{A_{raf}} \left(\frac{l_c}{r}\right)^{-2.653} \left(\frac{a_{\max}}{g}\right)^{-m} \tag{5.29}$$

It includes four components, E_p/c_2r^2 the stiffness ratio of the materials, $\sum \pi r^2/A_{raf}$ the area ratio of all the piles in the group to horizontal raft area, l_c/r the critical pile slenderness ratio, and a_{max}/g the normalized peak base acceleration.

Another dimensionless group which may also influence the critical slenderness ratio and maximum pile bending moment is the mass ratio, defined herein as

$$R_m = \frac{m_{str}}{m_{soi}} = \frac{m_{str}}{\rho_{soi} H_{soi} A_{raf}} \tag{5.30}$$

in which m_{str} is the mass of the structure and pile raft, ρ_{soi} is the density of the soil, and H_{soi} is the thickness of the soft soil layer.

5.4.1 Critical pile length, l_c

Combining Eqs(5.29) and (5.30) leads to a dimensionless grouping of the form

$$\frac{l_c}{r} = B_0 \cdot \left(\frac{E_p}{c_2 r^{0.653}} \frac{\sum \pi r^2}{A_{raf}} \left(\frac{l_c}{r} \right)^{-2.653} \right)^{B_1} \left(\frac{a_{\max}}{g} \right)^{B_2} \left(\frac{m_{str}}{\rho_{soi} H_{soi} A_{raf}} \right)^{B_3} \tag{5.31}$$

in which B_0 , B_1 , B_2 , B_3 are fitted quantities.

By combining the stiffness, mass and slenderness ratios of Eq.(5.31) appropriately, the ratio of the natural frequency of the pile raft to that of the soil layer above the critical segment can also be obtained as

$$R_f = \frac{f_{str}}{f_{soi}} = \frac{E_p I_p \rho_{soi}}{m_{str} \tilde{G}_{soi} l_c} \tag{5.32}$$

Hence, the natural frequencies of the pile-raft and soil are implicitly accounted for in Eq(5.31).

By grouping the ℓ_c/r term on the left, Eq(5.31) can also be expressed as

$$\frac{l_c}{r} = \left(B_0\right)^{1/\eta} \cdot \left(\frac{E_p}{c_2 r^{0.653}} \frac{\sum \pi r^2}{A_{raf}} \right)^{B_1/\eta} \left(\frac{a_{\max}}{g} \right)^{B_2/\eta} \left(\frac{m_{str}}{\rho_{soi} H_{soi} A_{raf}} \right)^{B_3/\eta} \tag{5.33}$$

in which $\eta = 1 + 2.653B_1$. Eq (1.32) can be further re-expressed as

$$\frac{l_c}{r} = e^{C_0} \cdot \left(\frac{E_p}{c_2 r^{0.653}} \frac{\sum \pi r^2}{A_{raf}} \right)^{C_1} \left(\frac{a_{\max}}{g} \right)^{C_2} \left(\frac{m_{str}}{\rho_{soi} H_{soi} A_{raf}} \right)^{C3} \tag{5.34}$$

Eq (5.34) contains four exponential coefficients, C_0 , C_1 , C_2 and C_3 , the values of which may be determined via regression analysis using the results from the large-scale finite element simulations. For each finite element analysis, a unique value of the calculated critical depth ℓ_c is obtained corresponding to one set of input parameters E_p, r, m_{str}, A_{raf}, c_1, a_{max}, H_{soi}. Using the calculated results of ℓ_c obtained from an appropriately large number of known parameter sets, a set of coefficients C_0 , C_1 , C_2 and C_3 can be determined which will minimize the difference between the ℓ_c values calculated from Eq(5.34) and that obtained from the large-scale finite element simulation.

For the regression analysis, Eq(5.34) is further re-written as

$$\ln\left(\frac{l_c}{r}\right) = C_0 + C_1 \cdot \ln\left(\frac{E_p}{c_2 r^{0.653}} \frac{\sum \pi r^2}{A_{raf}} \right) + C_2 \cdot \ln\left(\frac{a_{\max}}{g} \right) + C_3 \cdot \ln\left(\frac{m_{str}}{\rho_{soi} H_{soi} A_{raf}} \right) \tag{5.35}$$

from which a benchmark function may be constructed as

$$\aleph = \sum_{i=1,N} \left(C_0 + C_1 \cdot \ln\left(\frac{E_p}{c_2 r^{0.653}} \frac{\sum \pi r^2}{A_{raf}} \right)_i + C_2 \cdot \ln\left(\frac{a_{\max}}{g} \right)_i + C_3 \cdot \ln\left(\frac{m_{str}}{\rho_{soi} H_{soi} A_{raf}} \right)_i - \ln\left(\frac{\hat{l}_c}{r} \right)_i \right)^2 \tag{5.36}$$

where N is the number of finite element analyses with different parameter sets used to obtain the ℓ_c values for the regression exercise.

Through an appropriate optimization process, a set of coefficients C_0 , C_1 , C_2 and C_3 can be obtained which minimizes the resulting benchmark function $\aleph$. Mathematically, this is equivalent to

$$\begin{cases} \dfrac{\partial \aleph}{\partial C_0} = 0 \\ \dfrac{\partial \aleph}{\partial C_1} = 0 \\ \dfrac{\partial \aleph}{\partial C_2} = 0 \\ \dfrac{\partial \aleph}{\partial C_3} = 0 \end{cases} \tag{5.37}$$

or

$$\begin{cases} \displaystyle\sum_{i=1,N} \left(C_0 + C_1 \cdot \ln\left(\frac{E_p}{c_2 r^{0.653}} \frac{\sum \pi r^2}{A_{raf}} \right)_i + C_2 \cdot \ln\left(\frac{a_{\max}}{g} \right)_i + C_3 \cdot \ln\left(\frac{m_{str}}{\rho_{soi} H_{soi} A_{raf}} \right)_i - \ln\left(\frac{\hat{l}_c}{r} \right)_i \right) = 0 \\ \displaystyle\sum_{i=1,N} \left(C_0 + C_1 \cdot \ln\left(\frac{E_p}{c_2 r^{0.653}} \frac{\sum \pi r^2}{A_{raf}} \right)_i + C_2 \cdot \ln\left(\frac{a_{\max}}{g} \right)_i + C_3 \cdot \ln\left(\frac{m_{str}}{\rho_{soi} H_{soi} A_{raf}} \right)_i - \ln\left(\frac{\hat{l}_c}{r} \right)_i \right) \cdot \ln\left(\frac{E_p}{c_2 r^{0.653}} \frac{\sum \pi r^2}{A_{raf}} \right)_i = 0 \\ \displaystyle\sum_{i=1,N} \left(C_0 + C_1 \cdot \ln\left(\frac{E_p}{c_2 r^{0.653}} \frac{\sum \pi r^2}{A_{raf}} \right)_i + C_2 \cdot \ln\left(\frac{a_{\max}}{g} \right)_i + C_3 \cdot \ln\left(\frac{m_{str}}{\rho_{soi} H_{soi} A_{raf}} \right)_i - \ln\left(\frac{\hat{l}_c}{r} \right)_i \right) \ln\left(\frac{a_{\max}}{g} \right)_i = 0 \\ \displaystyle\sum_{i=1,N} \left(C_0 + C_1 \cdot \ln\left(\frac{E_p}{c_2 r^{0.653}} \frac{\sum \pi r^2}{A_{raf}} \right)_i + C_2 \cdot \ln\left(\frac{a_{\max}}{g} \right)_i + C_3 \cdot \ln\left(\frac{m_{str}}{\rho_{soi} H_{soi} A_{raf}} \right)_i - \ln\left(\frac{\hat{l}_c}{r} \right)_i \right) \ln\left(\frac{m_{str}}{\rho_{soi} H_{soi} A_{raf}} \right)_i = 0 \end{cases} \tag{5.38}$$

In this study, the regression analysis is carried out for 46 data sets, as shown on Table 5-1, which cover different combinations of the simulation parameters used in the large-scale finite element analyses. The parameter information for all 46 data sets are entered into a Microsoft Excel spreadsheet, together with the corresponding ℓ_c values obtained from the finite element analyses. The minimization process to obtain the coefficients C_0 , C_1 , C_2 and C_3 was carried out using the Microsoft Excel solver, by solving the system of simultaneous equations shown on Eq.(5.38).

In this study, the solution of Eq.(5.38) yields the following fitting coefficients

$$C_0 = 2.435 \quad C_1 = 0.083 \quad C_2 = 0.069 \quad C_3 = -0.134 \tag{5.39}$$

Accordingly, the critical pile length could be approximately predicted using the relation

$$l_c = 11.42 \cdot r \cdot \left(\frac{E_p}{c_2 r^{0.653}} \frac{\sum \pi r^2}{A_{raf}} \right)^{0.083} \left(\frac{a_{\max}}{g} \right)^{0.069} \left(\frac{m_{str}}{\rho_{soi} H_{soi} A_{raf}} \right)^{-0.134} \tag{5.40}$$

Figure 5-28 plots the critical pile lengths calculated using Eq.(5.40) against those obtained from the large-scale finite element simulations. The agreement is generally favorable, with a R^2 value of 0.9087.

The performance of the fitted formula for the critical pile length ℓ_c is further examined in Figure 5-29 through Figure 5-32, which shows the effect of the pile radius r, the structural mass m_{str} , the equivalent soil stiffness G_{soi} and the peak base acceleration a_{max} on the fitted and finite-element-computed critical lengths.

It is seen that Eq.(5.40) generally provides reasonable predictions of the critical pile length for each parameter, as well as the trend showing how the critical pile length varies with the parameter. Figure 5-29 shows that the critical pile length increases sharply as the pile radius increases, while Figure 5-30 indicates that the critical pile length decreases as the superstructure mass increases. This may be due to the heavier superstructure causing pile bending effects to concentrate more on the upper part of the foundation, thus moving the inflection point upwards. Figure 5-31 illustrates that the critical pile length decrease slightly as the equivalent soil shear modulus increases. The stiffer soil also could restrict the pile bending effects to the upper part of the foundation, thus reducing the critical pile length. Figure 5-32 indicates that the critical pile length increases as the seismic acceleration amplitude increases. The larger ground motion amplitude would cause larger soil deformation, leading to degradation of the soil stiffness.

The trends shown on Figure 5-29 to Figure 5-32 are consistent with the values of the fitted coefficients C_1 , C_2 and C_3 for Eq(5.40). The positive coefficients C_1 and C_2 indicate that the critical pile length ratio would increase with increasing pile-soil stiffness ratio, the pile area replacement ratio, and the dimensionless seismic acceleration. On the other hand, the negative coefficient C_3 indicates that the critical pile length ratio decreases with increasing structure-soil mass ratio.

5.4.2 Maximum bending moment at pile head, M_1

The factors affecting pile behavior have already been expressed in terms of the four dimensionless groups shown in Eq.(5.40). The maximum bending moment at the

pile head M_1 can be expressed in a dimensionless form $\frac{M_1}{E_p I_p/r}$, hereafter known as dimensionless moment, which is a measure of the maximum flexural strain in the pile. This leads to a possible expression for the maximum bending moment of the form

$$\frac{M_1}{E_p I_p/r} = e^{D_0} \cdot \left(\frac{E_p}{c_2 r^{0.653}} \frac{\sum \pi r^2}{A_{raf}} \right)^{D_1} \left(\frac{a_{\max}}{g} \right)^{D_2} \left(\frac{m_{str}}{\rho_{soi} H_{soi} A_{raf}} \right)^{D_3} \left(\frac{l_c}{r} \right)^{D_4} \qquad (5.41)$$

where D_0 , D_1 , D_2 , D_3 and D_4 are the fitting coefficients which can be determined via regression analysis.

Using a similar approach to that described in Section 5.4.1 for the critical pile length, a regression analysis for the maximum bending moment M_1 is performed using the 46 data sets tabulated on Table 5-1. The resulting coefficients are obtained as

$$D_0 = -6.173 \quad D_1 = -0.328 \quad D_2 = 1.071 \quad D_3 = 0.332 \quad D_4 = 1.457 \qquad (5.42)$$

Hence, the maximum pile bending moment at the pile head can be predicted using the fitted relationship

$$M_1 = 0.00209 \times \frac{E_p I_p}{r} \cdot \left(\frac{E_p}{c_2 r^{0.653}} \frac{\sum \pi r^2}{A_{raf}} \right)^{-0.328} \left(\frac{a_{\max}}{g} \right)^{1.071} \left(\frac{m_{str}}{\rho_{soi} H_{soi} A_{raf}} \right)^{0.332} \left(\frac{l_c}{r} \right)^{1.457} \qquad (5.43)$$

Figure 5-33 plots the maximum bending moments M_1 calculated using Eq.(5.43) against those obtained from the large-scale finite element simulations. The overall agreement is favorable, with a R^2 value of 0.9671.

Substituting Eq(5.40) into Eq(5.43) yields

$$M_1 = 0.082 \times \frac{E_p I_p}{r} \cdot \left(\frac{E_p}{c_2 r^{0.653}} \frac{\sum \pi r^2}{A_{raf}} \right)^{-0.207} \left(\frac{a_{\max}}{g} \right)^{1.263} \left(\frac{m_{str}}{\rho_{soi} H_{soi} A_{raf}} \right)^{0.126} \quad (5.44)$$

The performance of the fitted formula for the maximum bending moment M_1 is further examined in Figure 5-34 through Figure 5-37, which shows the effect of the pile radius r, the structural mass m_{str} , the equivalent soil stiffness G_{soi} and the peak base acceleration a_{max} on the predicted and FEM ℓ_c values. Despite some scatter, Eq(5.44) generally provides reasonable predictions of the maximum bending moment M_1 for each parameter, as well as the trend showing how the maximum bending moment varies with the parameter. In contrast to the critical pile length which decreases with the structural mass m_{str}, Figure 5-35 shows that both the predicted and FEM maximum bending moment increases with increasing structural mass. This is consistent with the positive value of D_3 obtained from the regression analysis, as compared with the negative value of C_3 obtained for the critical pile length. Similarly, Figure 5-36 shows that both the predicted and FEM maximum bending moment increases with increasing equivalent soil shear stiffness, which is consistent with the negative value of coefficient D_1 obtained from the regression analysis. Figure 5-37 shows that the effect of the peak base acceleration on both the predicted and FEM maximum bending moment is quite significant, compared with that shown on Figure 5-32 for the critical pile length. This is consistent with the coefficient value of 1.071 obtained for D_2 from the bending moment regression analysis, as compared with the much smaller value of 0.069 obtained for C_2 from the critical pile length regression analysis.

5.4.3 Maximum pile bending moment at clay-stiff soil layer interface M_2

Similarly to Eq.(5.43), an expression for the maximum pile bending moment at the clay-stiff soil layer interface with the following form is proposed

$$\frac{M_2}{E_p I_p / r} = e^{E_0} \cdot \left(\frac{G_{soi}}{G_{stif}}\right)^{E_1} \left(\frac{\sum \pi r^2}{A_{raf}}\right)^{E_4} \left(\frac{a_{\max}}{g}\right)^{E_2} \left(\frac{m_{str}}{\rho_{soi} H_{soi} A_{raf}}\right)^{E_3} \quad (5.45)$$

where E_0 , E_1 , E_2 , E_3 and E_4 are the fitting coefficients which can be determined via regression analysis, and l_a is the pile embedment length (=3 x pile diameter) in the stiff soil layer as shown in Figure 5-7.

Using a similar approach to that described in Sections 5.4.1 and 5.4.2, a regression analysis for the maximum bending moment M_2 is performed using the 46 data sets tabulated on Table 5-1. The resulting coefficients are obtained as

$$E_0 = 0.0028 \quad E_1 = -0.493 \quad E_2 = 1.300 \quad E_3 = 0.234 \quad E_4 = -0.209 \quad (5.46)$$

Hence, the maximum pile bending moment at the clay-stiff soil layer interface may be estimated using the fitted relationship:

$$M_2 = 0.0028 \times \frac{E_p I_p}{r} \cdot \left(\frac{G_{soi}}{G_{stif}}\right)^{-0.493} \left(\frac{\sum \pi r^2}{A_{raf}}\right)^{-0.209} \left(\frac{a_{\max}}{g}\right)^{1.300} \left(\frac{m_{str}}{\rho_{soi} H_{soi} A_{raf}}\right)^{0.234} \quad (5.47)$$

Figure 5-38 plots the maximum bending moments M_2 calculated using Eq.(5.47) against those obtained from the large-scale finite element simulations. The overall agreement is favorable, with a R^2 value of 0.9738.

The performance of the fitted formula for the maximum bending moment M_2 is further examined in Figure 5-39 through Figure 5-41, which shows the effect of the pile radius r, the equivalent soil stiffness G_{soi} and the peak base acceleration a_{max} on the predicted and FEM ℓ_c values. The effect of the structural mass m_{str} is not considered here, as it was previously shown in the parametric studies that the value of M_2 is quite insensitive to changes in structural mass, especially for the 25m and 40m thick soft clay layers. It is seen that Eq.(5.47) provides good predictions of the bending moment M_2 for the three parameters considered. In particular, Figure 5-40 shows that the pile bending moment at the clay-stiff soil interface decreases as the shear modulus of the clay increases, which is consistent with the finding from Nikolaou *et al.* (2001).

5.4.4 An example to illustrate the usage of the simplified bending moment profile

It's assumed that a 14-layer residential building with length 42m and width 18m, supported on a pile-raft foundation. The pile foundation include 189 piles with pile diameter 0.8m, and pile-pile spacing 2m. The soil profile includes two uniform layers, 25m thickness soft clay overlying the hard stiff soil layer. The pile is socketed into the hard layer 3m. The excited earthquake time history is similar with the one in Figure 4-11 except that the maximum acceleration a_{max} is 0.4m/s^2.

The total structural mass $m_{str} = 15{,}876ton$

The pile raft area $A_{raf} = 756m^2$

The pile foundation-soil stiffness ratio $\frac{E_p}{c_2 r^{0.653}} \frac{\sum \pi r^2}{A_{raf}} = 1265$

The dimensionless peak base acceleration $\frac{a_{\max}}{g} = 0.04$

The structure-soil mass ratio $\frac{m_{str}}{\rho_{soi} H_{soi} A_{raf}} = 0.52$

From Eq.(5.40), the critical pile length could be calculated $l_c = 7.22m$

From Eq.(5.44), the maximum pile bending moment at pile head could be calculated $M_1 = 446kN \cdot m$

From Eq.(5.47), the maximum pile bending moment at the soil layer interface could be calculated $M_2 = 170kN \cdot m$.

The Maximum pile bending moment profile could be predicted as shown in Figure 5-42. Comparison with the large-scale finite element simulation indicated that the proposed method could offer an approximate evaluation of pile bending moment profile within large pile foundation.

5.5 Summary

Using the large-scale finite element simulation method, the seismic soil-pile-superstructure analysis is extended to study the influence of different pile radiuses, soft soil depths, soft soil stiffness, superstructure mass and seismic acceleration amplitudes. The influence of each factor on the pile foundation response is discussed. By processing the results using dimensional analysis and data fitting,

three semi-empirical dimensionless expressions for estimating the maximum bending moments and the critical pile length are obtained. Using these estimated moments and the critical pile length, together with the general trends of the computed bending moment profiles obtained from all the analyses, a simplified bending moment envelope is proposed for seismic pile foundation design.

It should be noted that Eqs. 5.40, 5.44 and 5.47 were derived based on ground motions following the characteristic time history and response spectrum shown on Figure 4-11, albeit with different peak values. Such motions are representative of the bedrock ground motions expected in Singapore due to the far-field earthquake events arising from the Great Sumatran Fault. The applicability of these equations to other earthquake motions, such as those associated with near field events, will be examined in Chapter 6.

Table 5-1 Simulation events and main parameters

No	L (m)	r (m)	m_{stru} (ton)	G_0 (kPa)	PGA (m/s²)
1*	25	0.339	13,608	$2060p'^{0.653}$	0.70
2	10	0.339	13,608	$2060p'^{0.653}$	0.70
3	40	0.339	13,608	$2060p'^{0.653}$	0.70
4	25	0.226	13,608	$2060p'^{0.653}$	0.70
5	25	0.452	13,608	$2060p'^{0.653}$	0.70
6	25	0.339	6,804	$2060p'^{0.653}$	0.70
7	25	0.339	20,412	$2060p'^{0.653}$	0.70
8	25	0.339	13,608	$1030p'^{0.653}$	0.70
9	25	0.339	13,608	$3090p'^{0.653}$	0.70
10	25	0.339	13,608	$2060p'^{0.653}$	0.22
11	25	0.339	13,608	$2060p'^{0.653}$	1.00
12	10	0.226	6,804	$1030p'^{0.653}$	0.22
13	10	0.226	6,804	$1030p'^{0.653}$	1.00
14	10	0.226	6,804	$3090p'^{0.653}$	0.22
15	10	0.226	6,804	$3090p'^{0.653}$	1.00
16	10	0.226	20,412	$1030p'^{0.653}$	0.22
17	10	0.226	20,412	$1030p'^{0.653}$	1.00
18	10	0.226	20,412	$3090p'^{0.653}$	0.22
19	10	0.226	20,412	$3090p'^{0.653}$	1.00
20	10	0.452	6,804	$1030p'^{0.653}$	0.22
21	10	0.452	6,804	$1030p'^{0.653}$	1.00
22	10	0.452	6,804	$3090p'^{0.653}$	0.22
23	10	0.452	6,804	$3090p'^{0.653}$	1.00
24	10	0.452	20,412	$1030p'^{0.653}$	0.22
25	10	0.452	20,412	$1030p'^{0.653}$	1.00
26	10	0.452	20,412	$3090p'^{0.653}$	0.22
27	10	0.452	20,412	$3090p'^{0.653}$	1.00

28	40	0.226	6,804	$1030p'^{0.653}$	0.22
29	40	0.226	6,804	$1030p'^{0.653}$	1.00
30	40	0.226	6,804	$3090p'^{0.653}$	0.22
31	40	0.226	6,804	$3090p'^{0.653}$	1.00
32	40	0.226	20,412	$1030p'^{0.653}$	0.22
33	40	0.226	20,412	$1030p'^{0.653}$	1.00
34	40	0.226	20,412	$3090p'^{0.653}$	0.22
35	40	0.226	20,412	$3090p'^{0.653}$	1.00
36	40	0.452	6,804	$1030p'^{0.653}$	0.22
37	40	0.452	6,804	$1030p'^{0.653}$	1.00
38	40	0.452	6,804	$3090p'^{0.653}$	0.22
39	40	0.452	6,804	$3090p'^{0.653}$	1.00
40	40	0.452	20,412	$1030p'^{0.653}$	0.22
41	40	0.452	20,412	$1030p'^{0.653}$	1.00
42	40	0.452	20,412	$3090p'^{0.653}$	0.22
43	40	0.452	20,412	$3090p'^{0.653}$	1.00
44	40	0.452	20,412	$3090p'^{0.653}$	0.70
45	40	0.452	20,412	$3090p'^{0.653}$	0.70

* as baseline case, described and discussed in section 4.5.

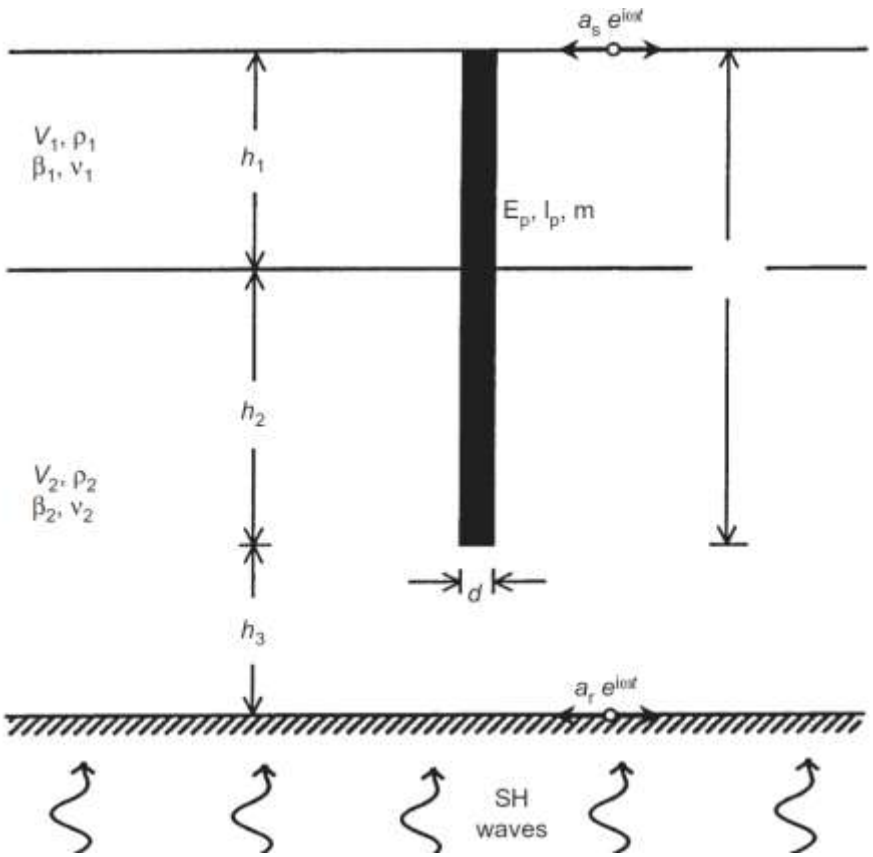

Figure 5-1 Schematic of the model studied by Nikolaou *et al.* (2001) of a single pile embedded in a two-layer profile on rigid bedrock. Nikolaou *et al.* (2001) Nikolaou *et al.* (2001) Nikolaou *et al.* (2001) Nikolaou *et al.* (2001) Nikolaou *et al.* (2001) Nikolaou *et al.* (2001) Nikolaou *et al.* (2001) Nikolaou *et al.* (2001) Nikolaou *et al.* (2001) Nikolaou *et al.* (2001) Nikolaou *et al.* (2001)

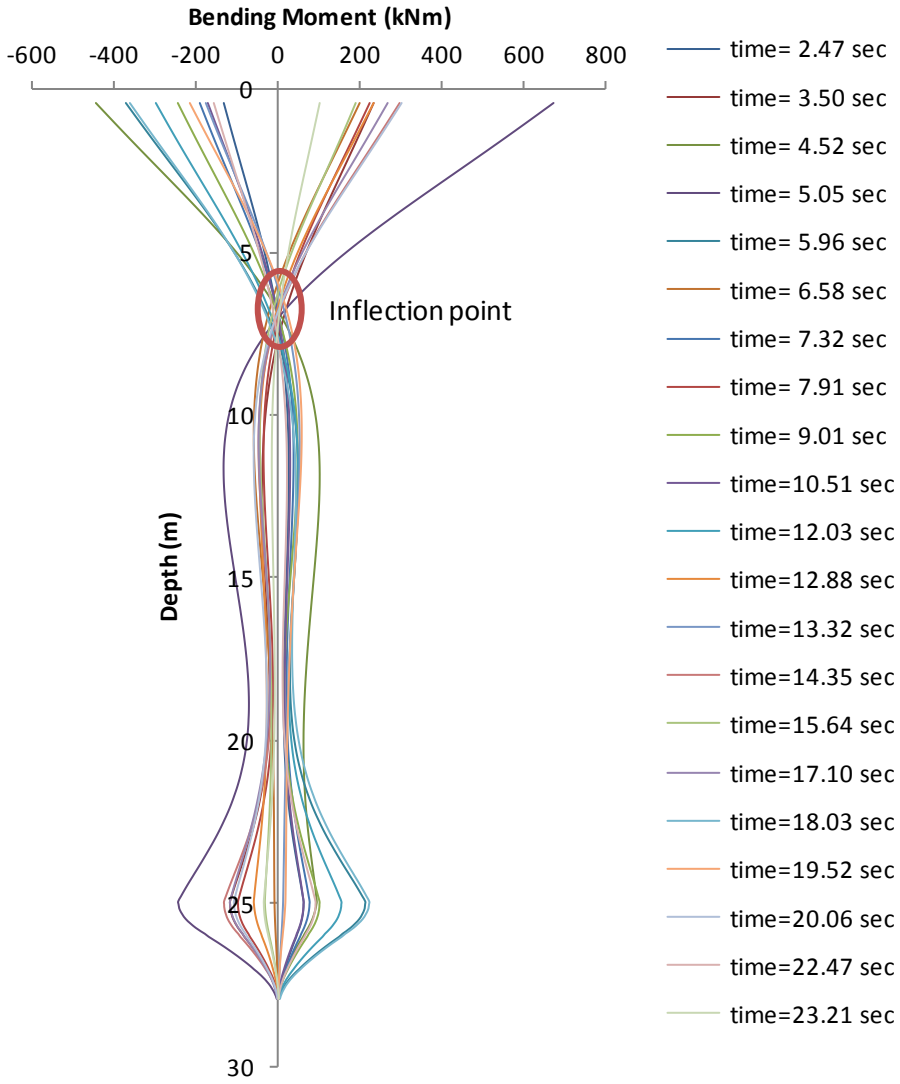

Figure 5-2 Computed bending moment profiles at different times ($H_{soi} = 25m, r = 0.343m, m_{str} = 13{,}608ton, G_0 = 2060p'^{0.653}, a_{max} = 0.70\,m/s^2$)

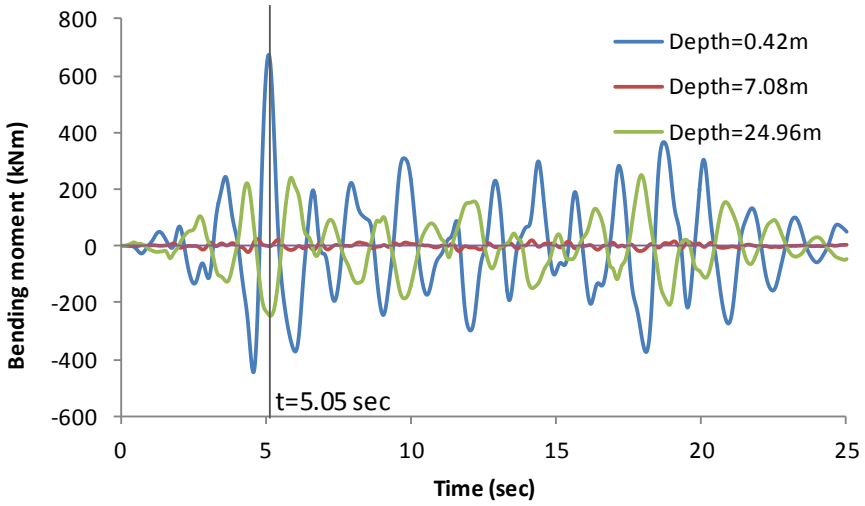

Figure 5-3 Computed bending moment histories at three different depths ($H_{soi} = 25m, r = 0.343m, m_{str} = 13{,}608ton, G_0 = 2060p'^{0.653}, a_{max} = 0.70\,m/s^2$)

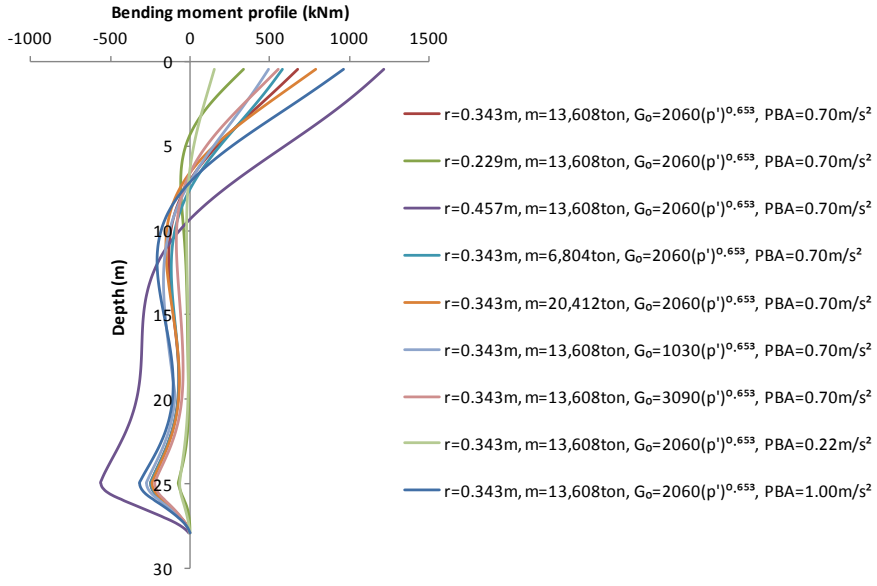

Figure 5-4 Maximum bending moment profiles for different cases ($H_{soi} = 25m$ $H_{soi} = 25m$ soft clay layer)

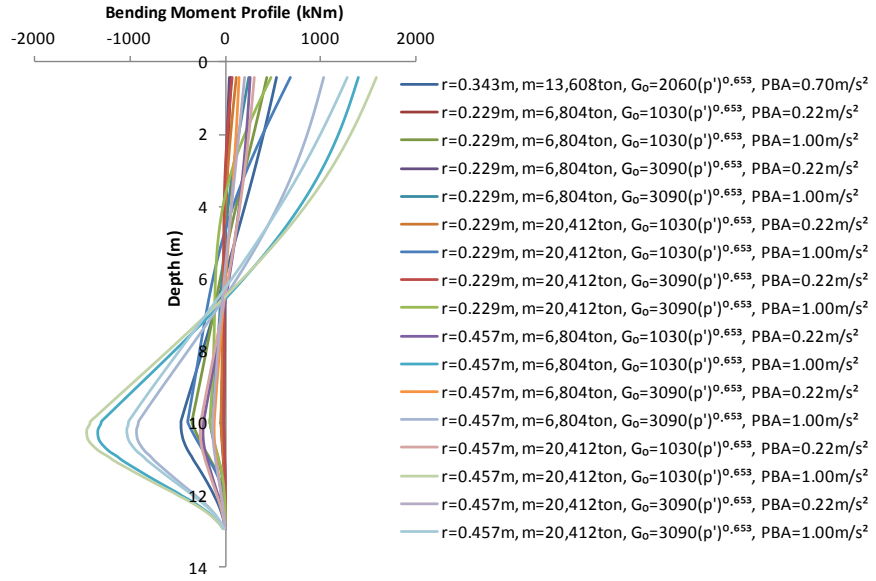

Figure 5-5 Maximum bending moment profiles for different cases ($H_{soi} = 10m$ soft clay layer)

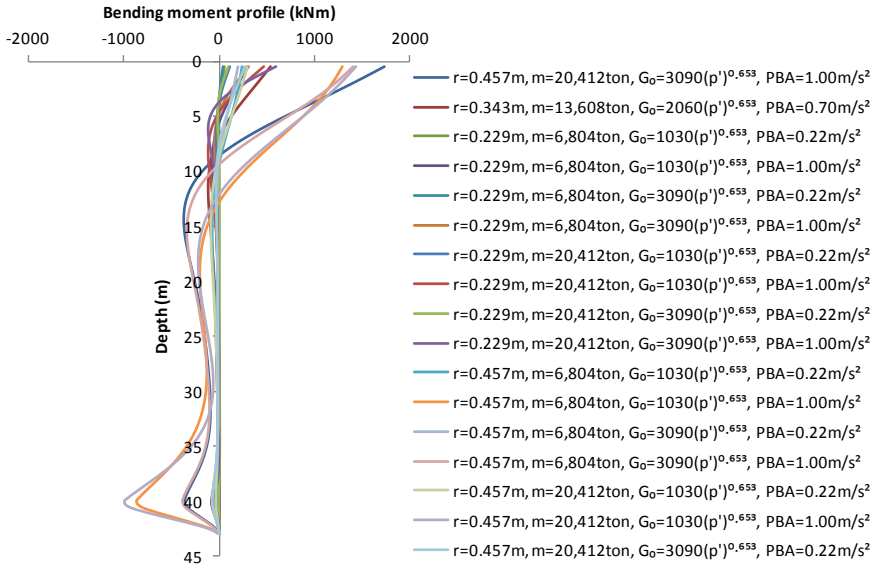

Figure 5-6 Maximum bending moment profiles for different cases ($H_{soi} = 40m$ soft clay layer)

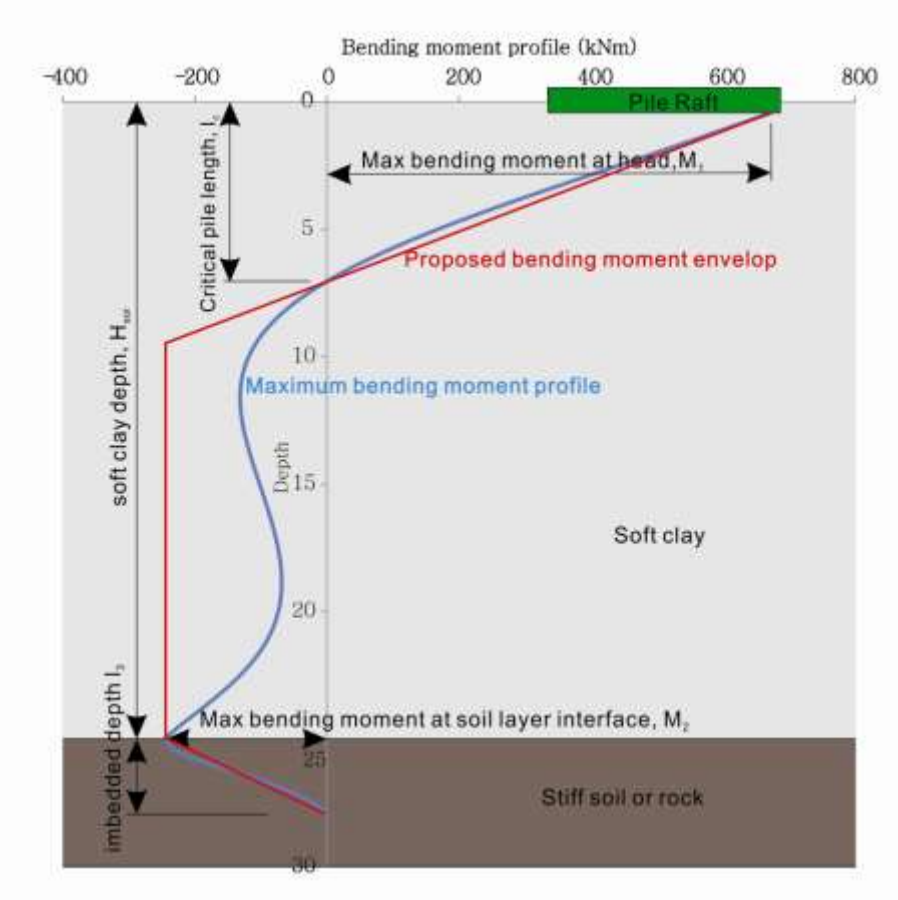

Figure 5-7 Illustration of proposed bending moment envelope for design

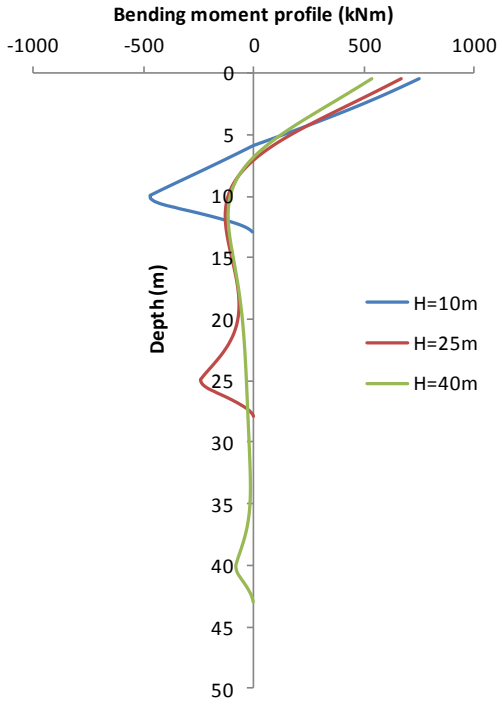

Figure 5-8 Maximum bending moment profiles with different depths of the soft soil layer ($r = 0.343m, m_{str} = 13{,}608ton, G_0 = 2060p'^{0.653}, a_{max} = 0.70\,m/s^2$)

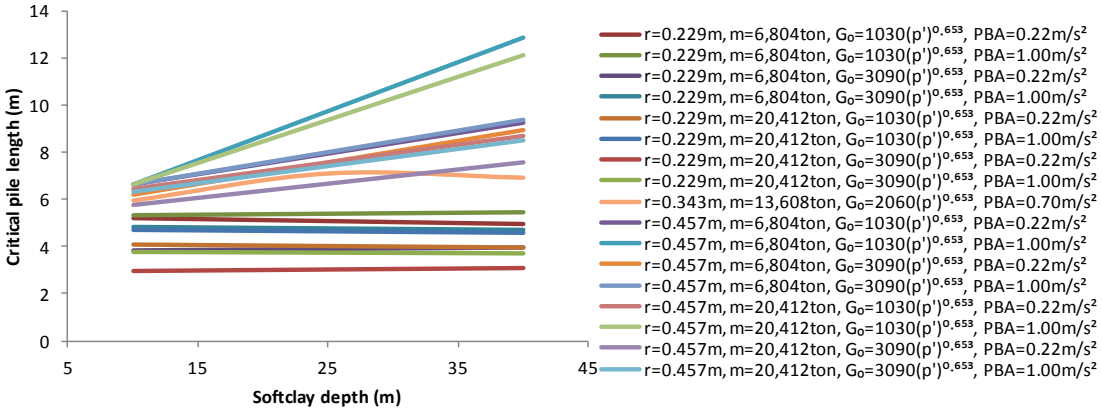

Figure 5-9 Influence of the soft clay thickness on the critical pile length

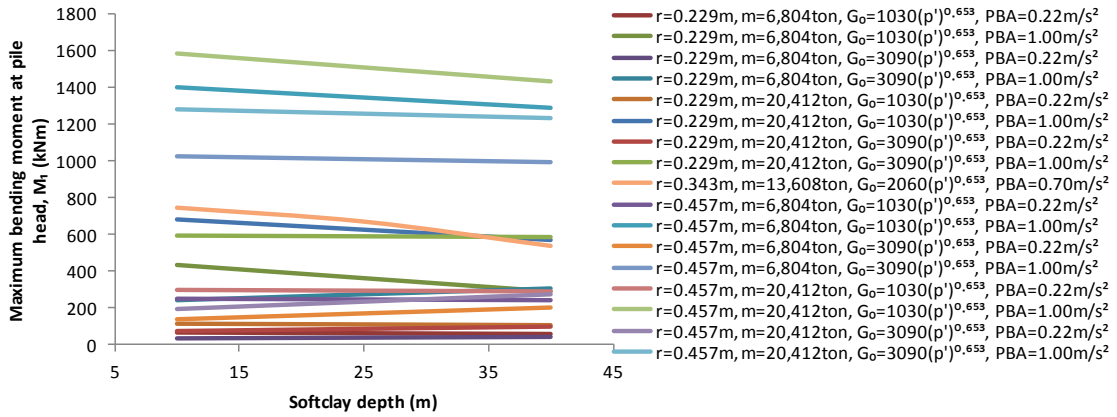

Figure 5-10 Influence of soft clay thickness on the maximum bending moment at the pile head

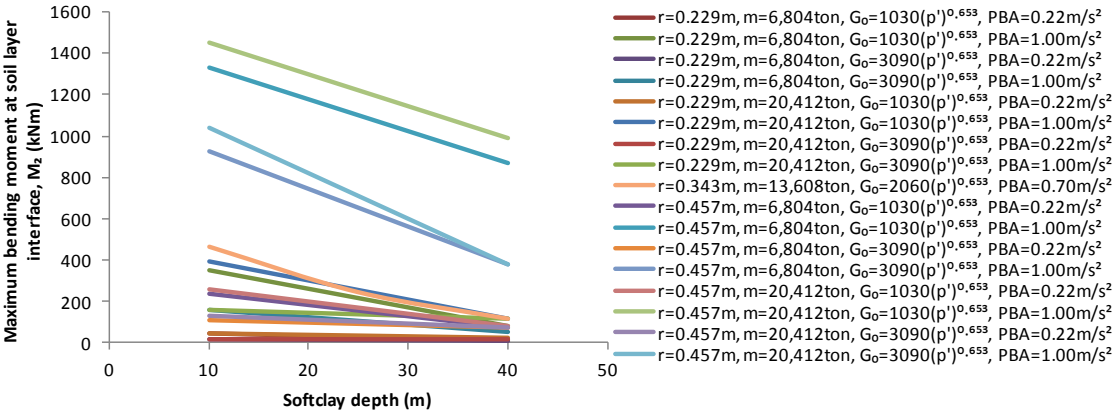

Figure 5-11 Influence of soft clay thickness on maximum bending moment at clay-hard soil interface

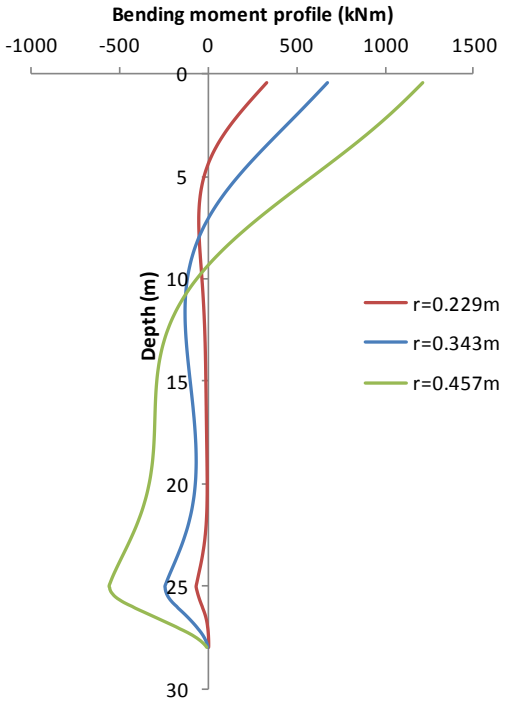

Figure 5-12 Maximum bending moment profiles with different pile radius ($H_{soi} = 25m, m_{str} = 13{,}608ton, G_0 = 20600p'^{0.653}, a_{max} = 0.70\,m/s^2$)

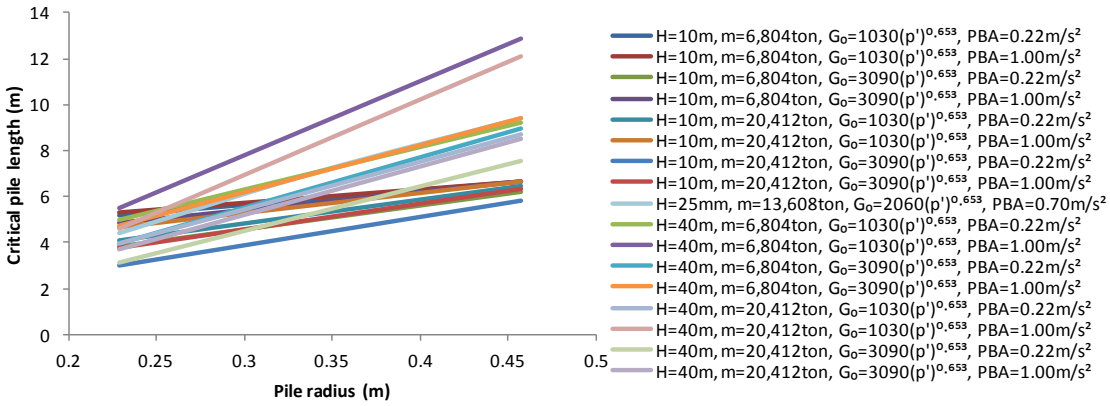

Figure 5-13 Influence of pile radius on critical pile length

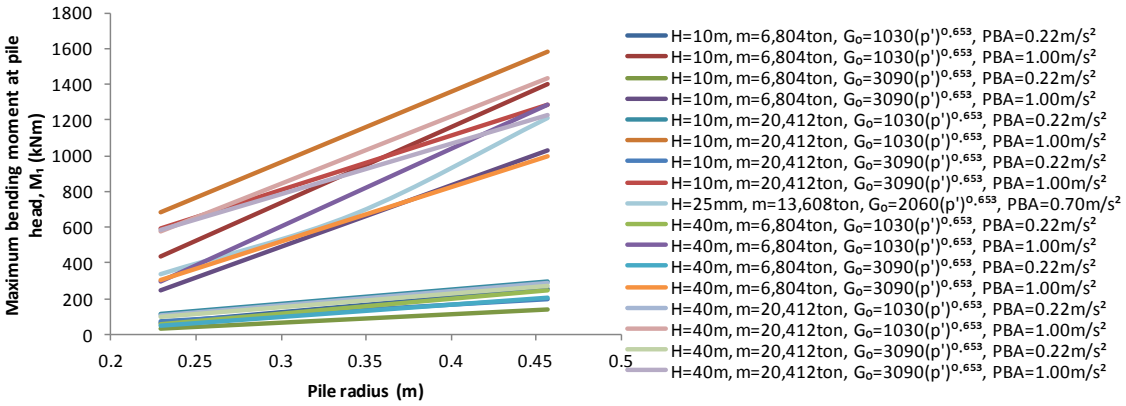

Figure 5-14 Influence of pile radius on maximum bending moment at pile head

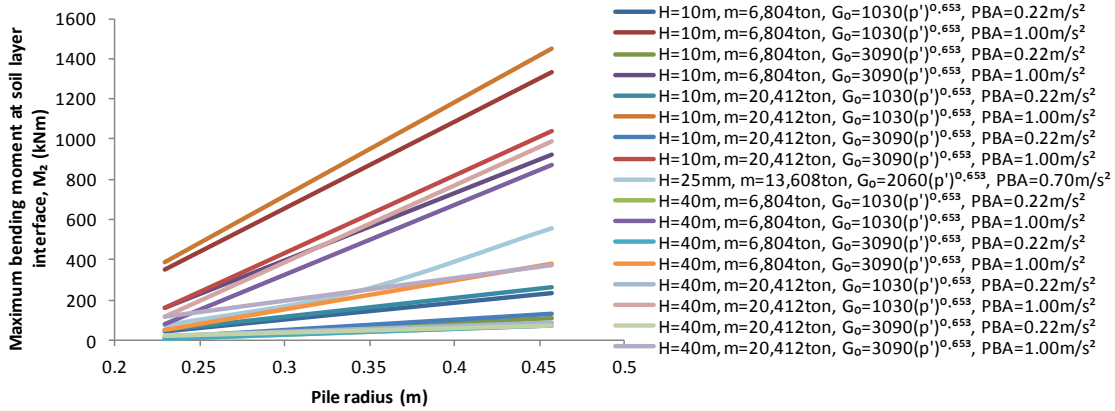

Figure 5-15 Influence of pile radius on maximum bending moment at the clay-hard soil interface

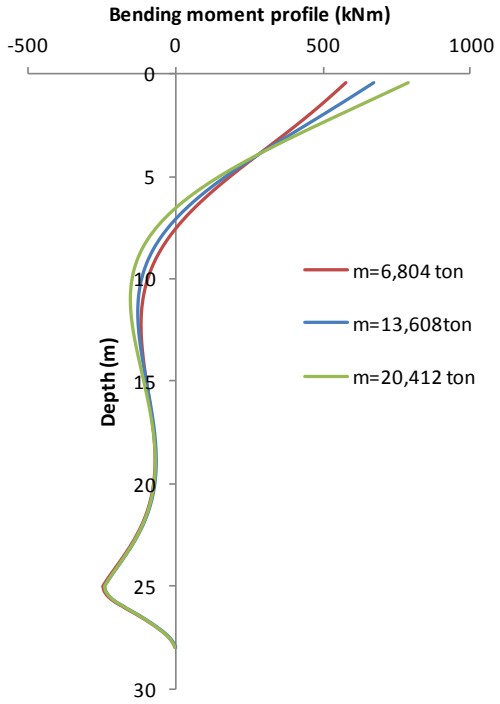

Figure 5-16 Maximum bending moment profiles with different structural mass

$$(H_{soi} = 25m, r = 0.343m,\ G_0 = 2060p'^{0.653}, a_{max} = 0.70\,m/s^2)$$

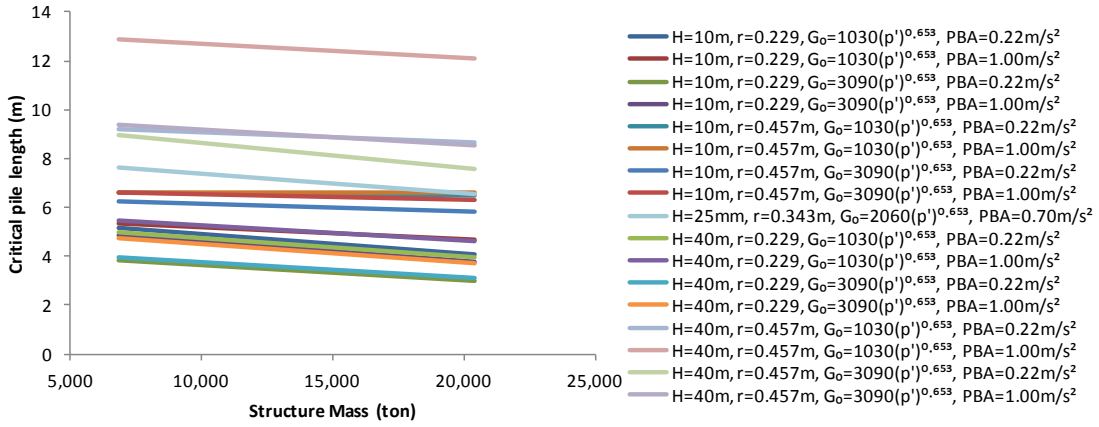

Figure 5-17 Influence of structural mass on critical pile length

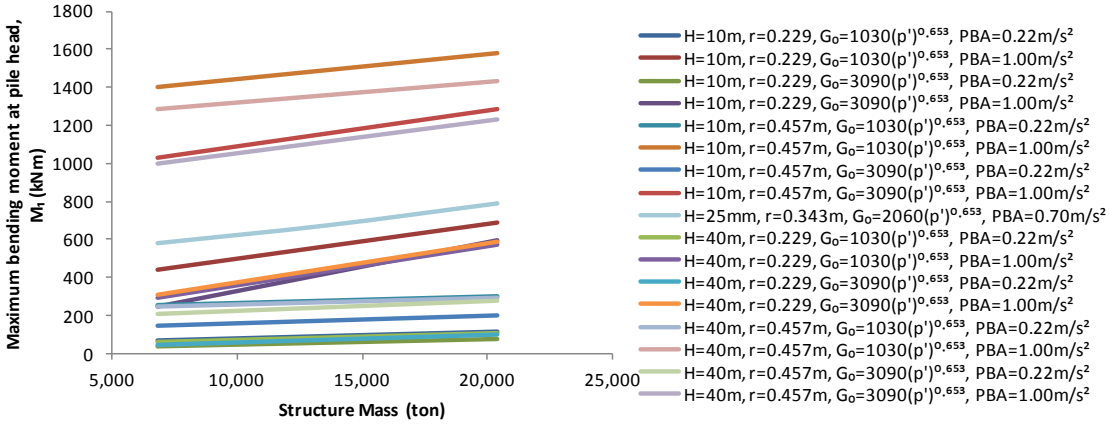

Figure 5-18 Influence of structural mass on maximum bending moment at pile head

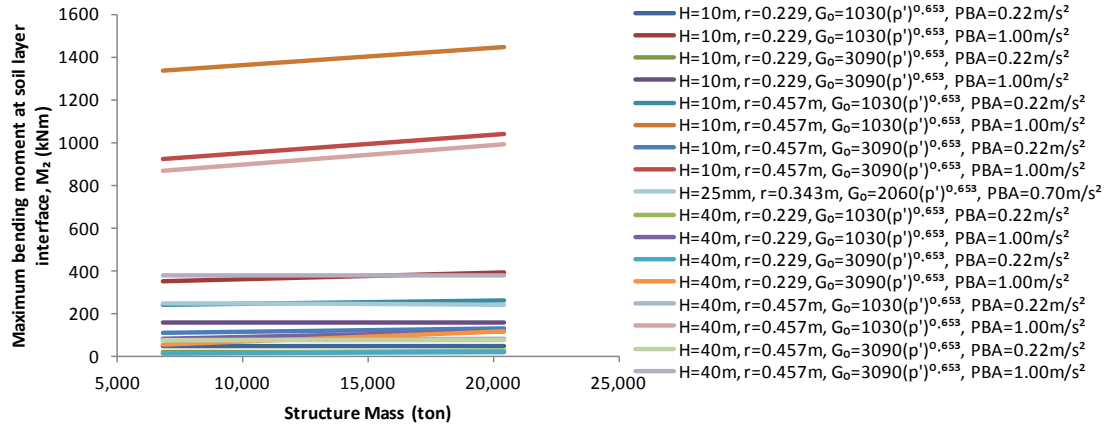

Figure 5-19 Influence of structural mass on maximum bending moment at clay-hard soil interface

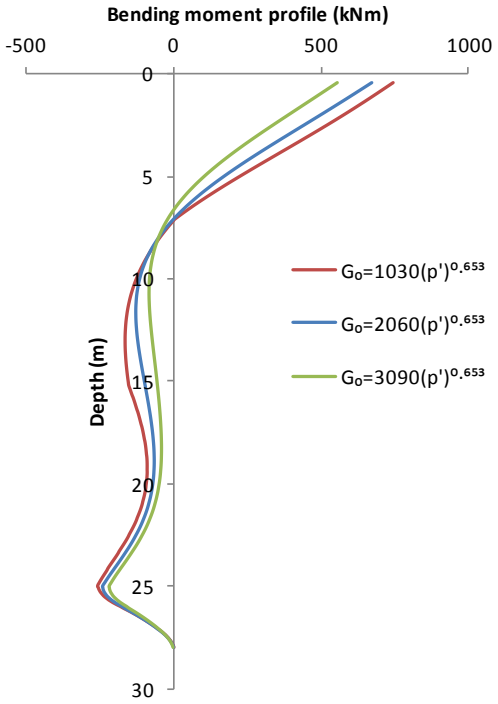

Figure 5-20 Maximum bending moment profiles with different soft soil stiffness

$$(H_{soi} = 25m, r = 0.343m, m_{str} = 13{,}608ton, a_{max} = 0.70\,m/s^2)$$

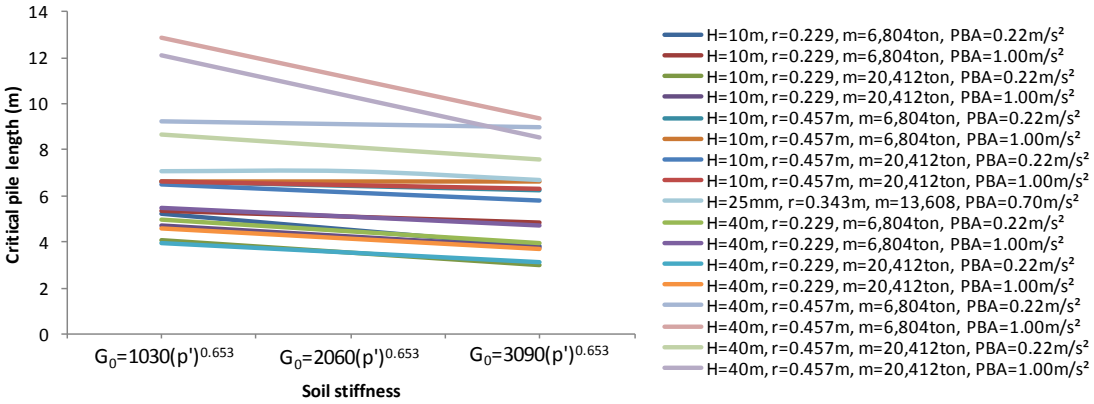

Figure 5-21 Influence of soft soil stiffness on critical pile length

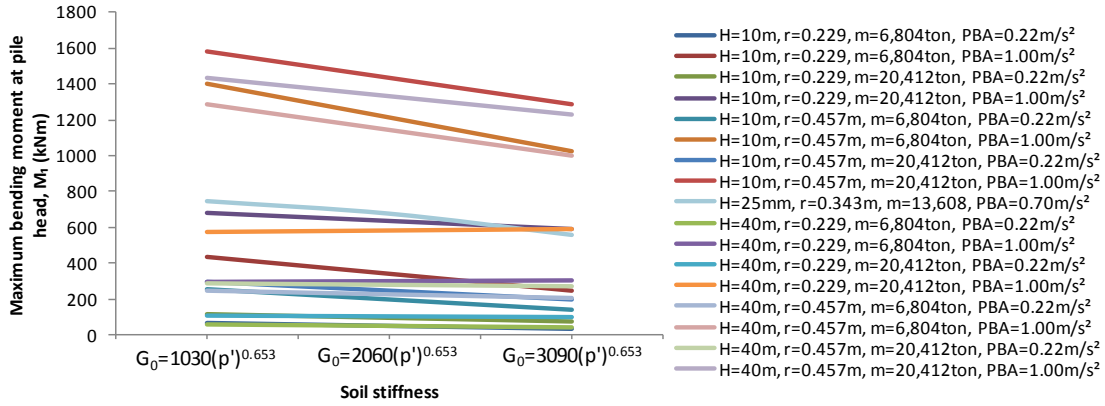

Figure 5-22 Influence of soft soil stiffness on maximum bending moment at pile head

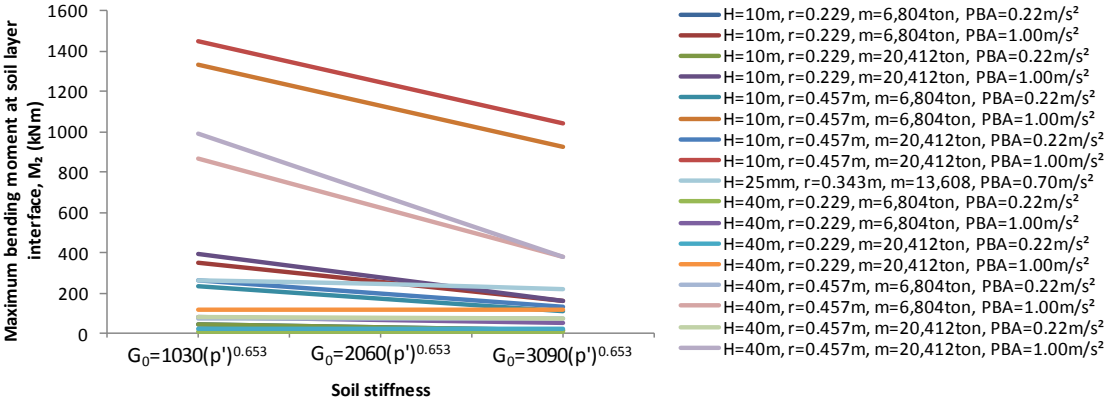

Figure 5-23 Influence of soft soil stiffness on maximum bending moment at clay-hard soil interface

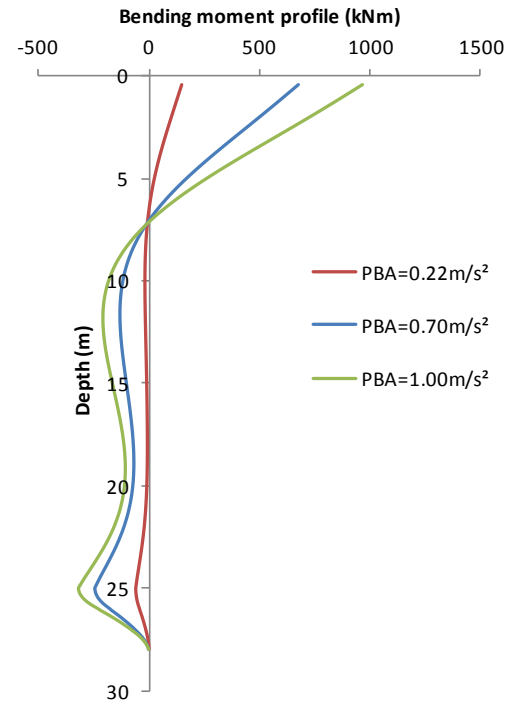

Figure 5-24 Maximum bending moment profiles with different peak base acceleration ($H_{soi} = 25m, r = 0.343m, m_{str} = 13{,}608ton, G_0 = 2060p'^{0.653}$)

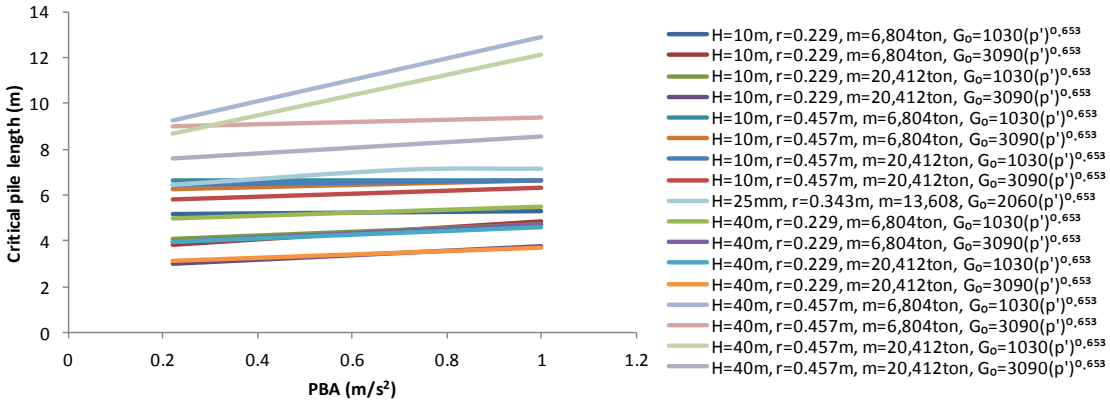

Figure 5-25 Influence of peak base acceleration on critical pile length

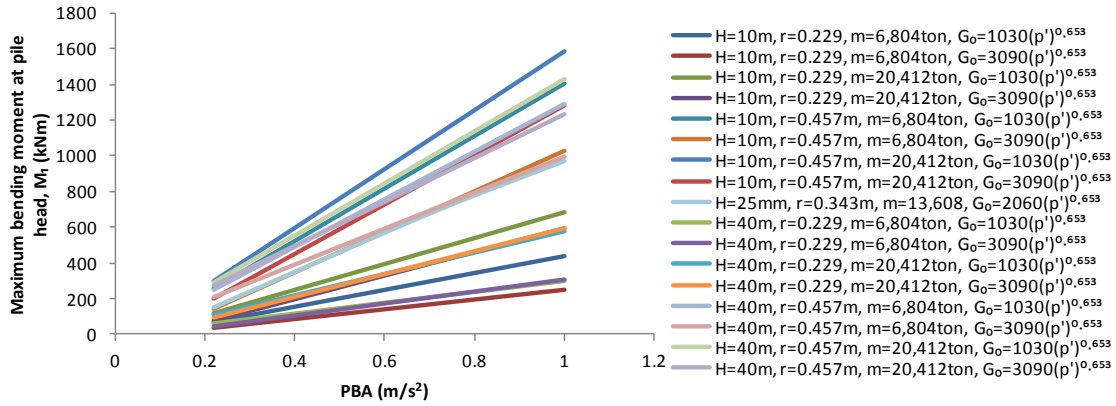

Figure 5-26 Influence of peak base acceleration on maximum bending moment at pile head

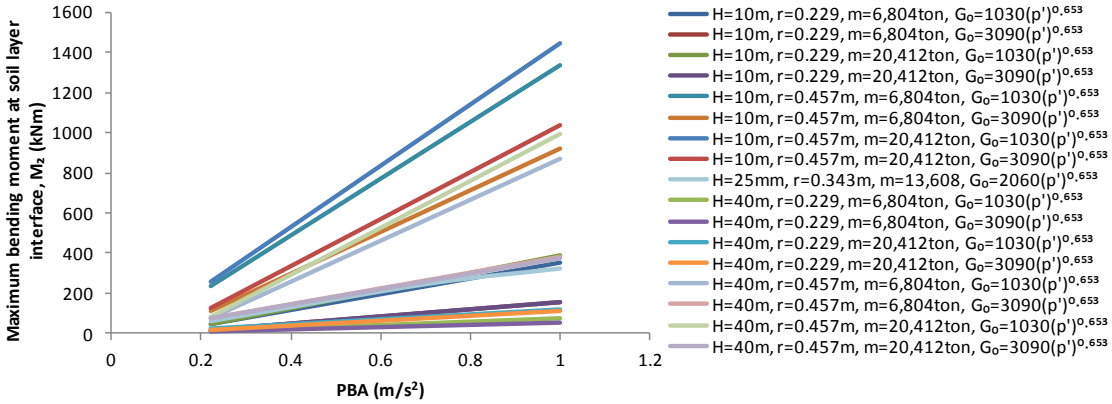

Figure 5-27 Influence of peak base acceleration on maximum bending moment at clay-hard soil interface

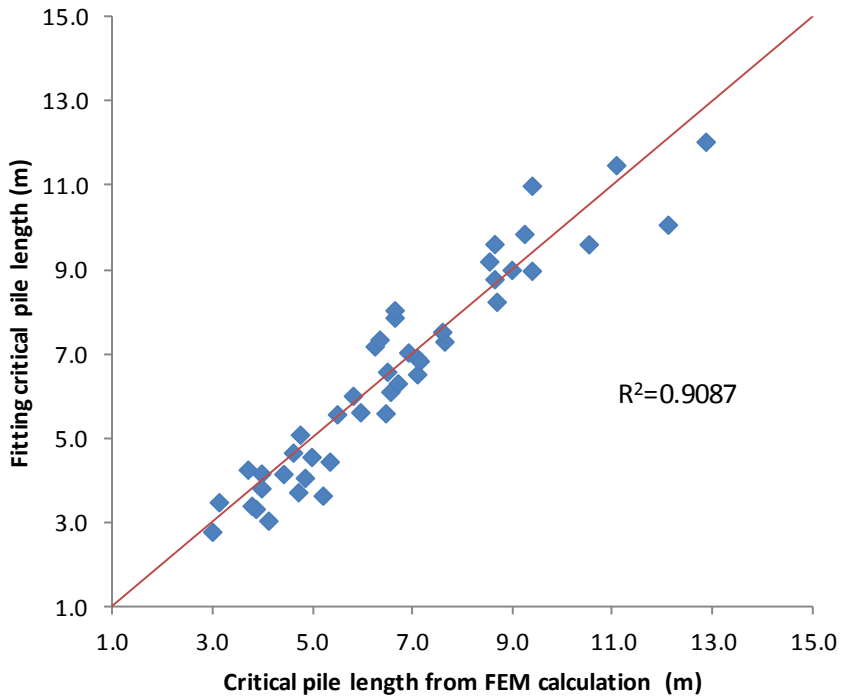

Figure 5-28 Least squares fitting for the critical pile length

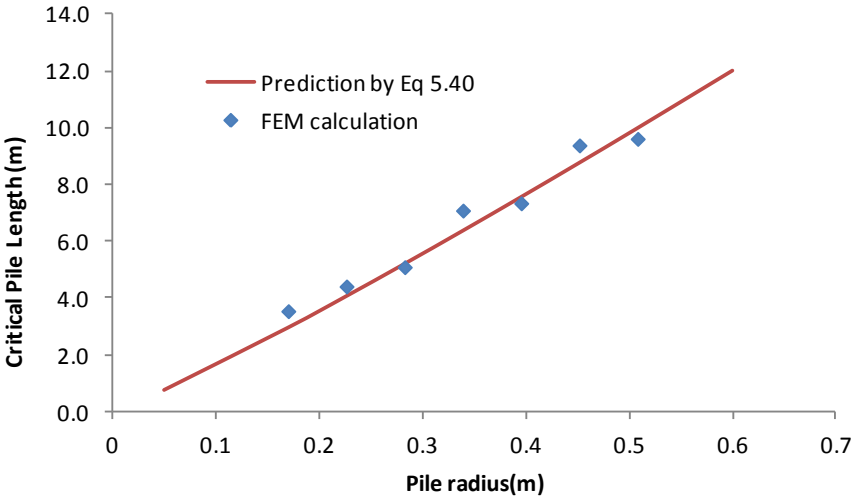

Figure 5-29 Evaluation of critical pile length prediction: effect of pile radius

$$(H_{soi} = 25m, m_{str} = 13{,}608ton, G_0 = 2060p'^{0.653}, a_{max} = 0.70\,m/s^2)$$

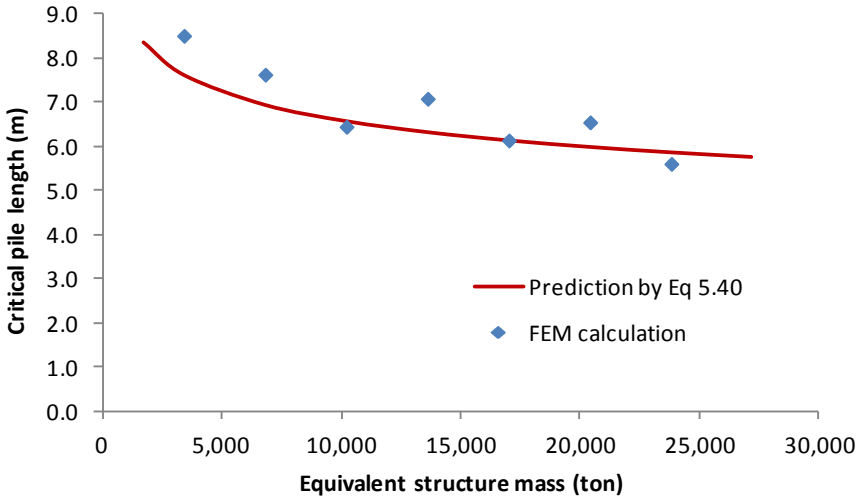

Figure 5-30 Evaluation of critical pile length prediction: effect of equivalent structure mass

$(H_{soi} = 25m, r = 0.343m, G_0 = 2060{p'}^{0.653}, a_{max} = 0.70\, m/s^2)$

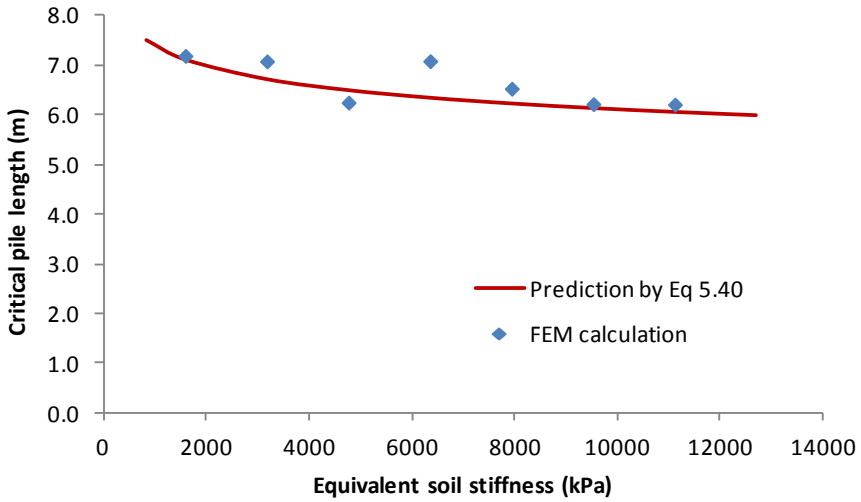

Figure 5-31 Evaluation of critical pile length prediction: effect of soil stiffness

$(H_{soi} = 25m, r = 0.343m, m_{str} = 13{,}608ton, a_{max} = 0.70\, m/s^2)$

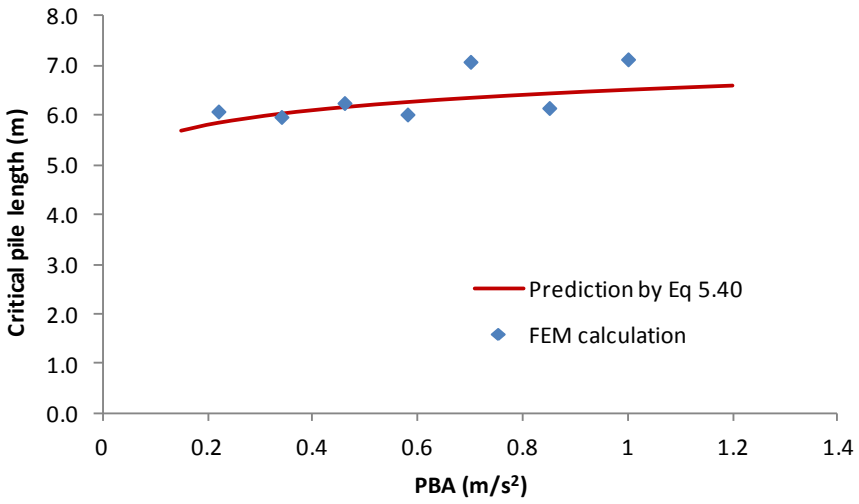

Figure 5-32 Evaluation of critical pile length prediction: effect of peak base acceleration, $\left(H_{soi}=25m, r=0.343m, m_{str}=13,608ton, G_0=2060\,p'^{0.653}\right)$

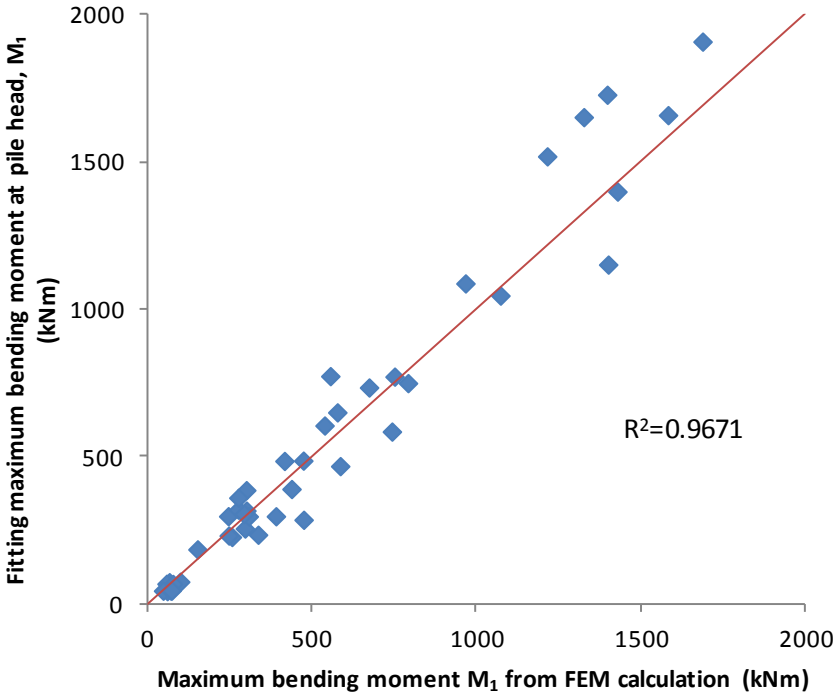

Figure 5-33 Least squares fitting for maximum pile bending moment at pile head

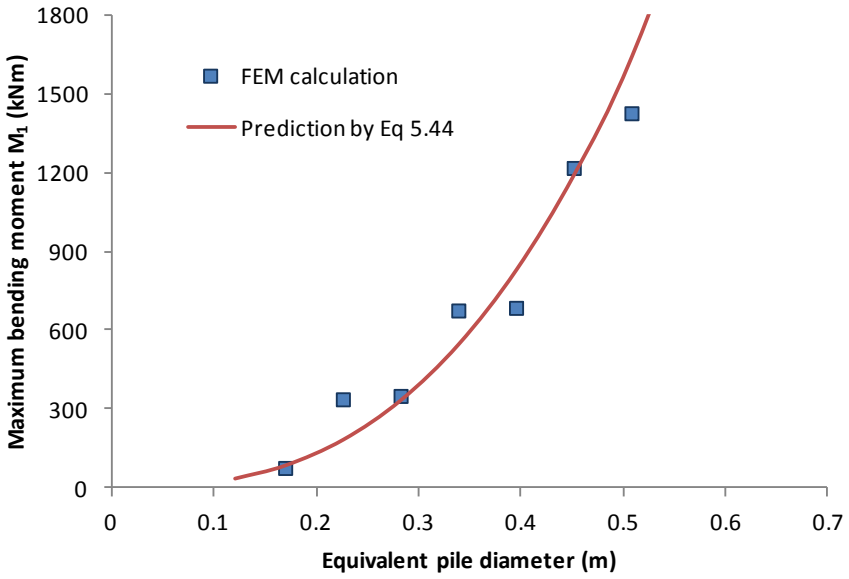

Figure 5-34 Evaluation of maximum pile bending moment at pile head: effect of pile radius $\left(H_{soi}=25m, m_{str}=13,608ton, G_0=2060p'^{0.653}, a_{\max}=0.70\,m/s^2\right)$

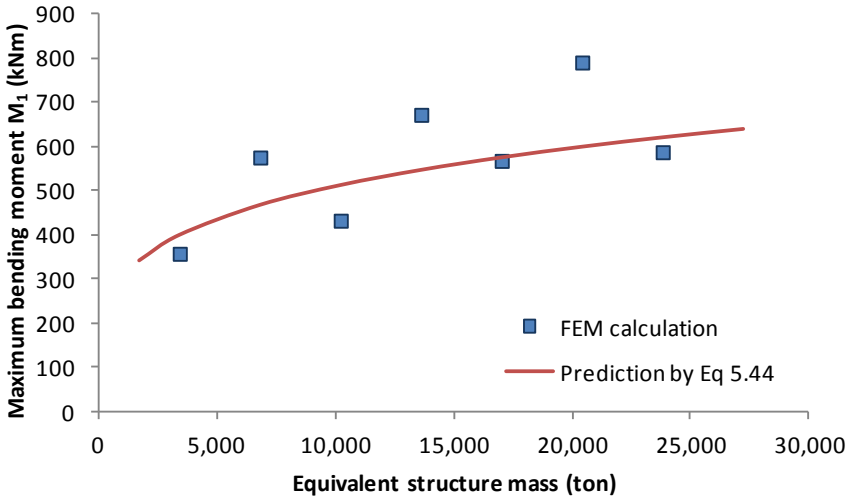

Figure 5-35 Evaluation of maximum pile bending moment at pile head: effect of structure mass

$(H_{soi}=25m, r=0.343m, G_0=2060p'^{0.653}, a_{max}=0.70\,m/s^2)$

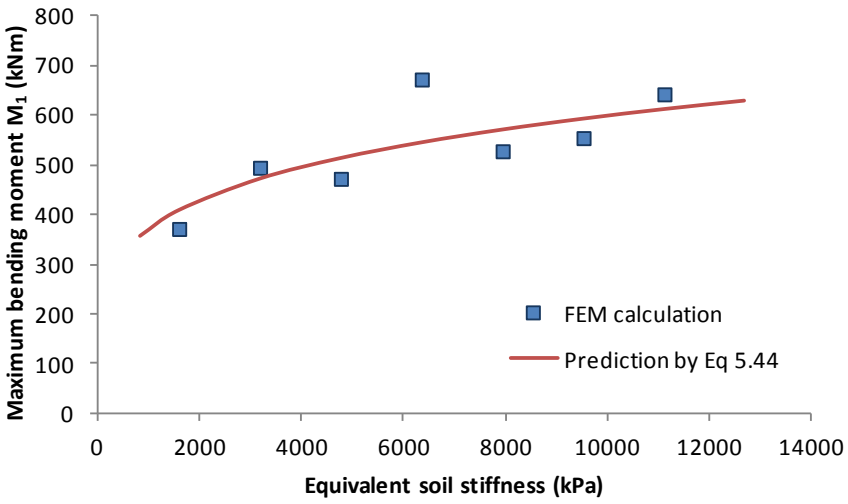

Figure 5-36 Evaluation of maximum pile bending moment at pile head: effect of soil stiffness

$(H_{soi} = 25m, r = 0.343m, m_{str} = 13{,}608ton, a_{max} = 0.70\,m/s^2)$

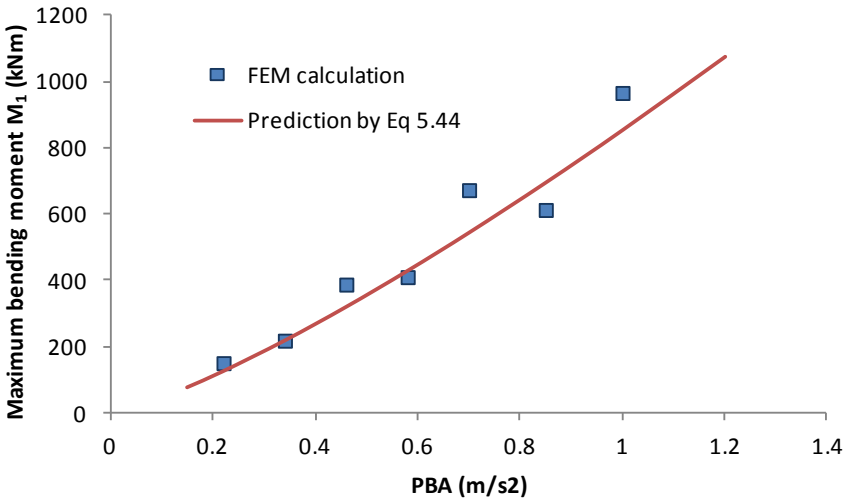

Figure 5-37 Evaluation of maximum pile bending moment at pile head: effect of peak base acceleration

$\left(H_{soi} = 25m, r = 0.343m, m_{str} = 13,608ton, G_0 = 2060\,p'^{0.653}\right)$

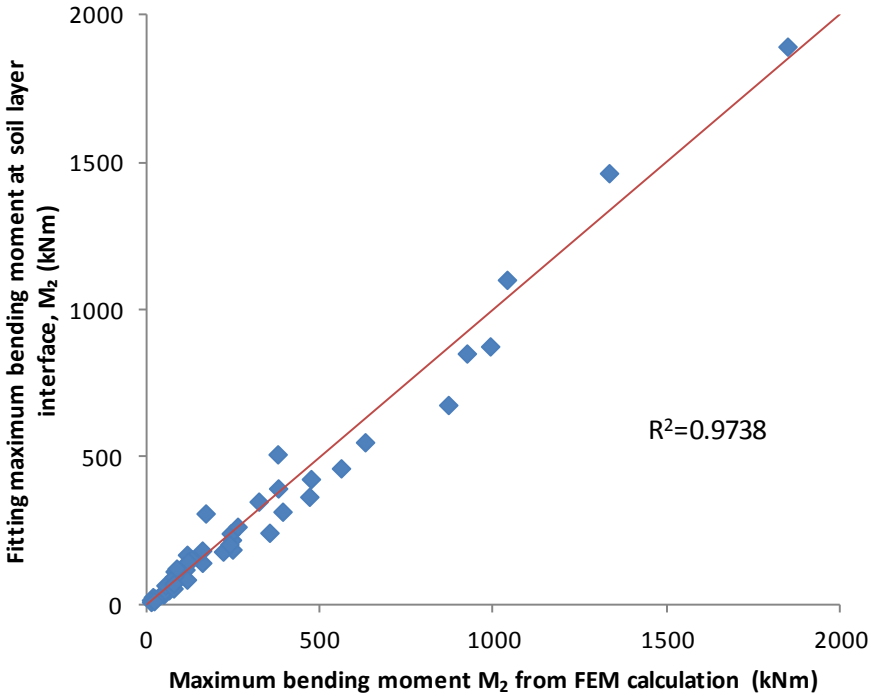

Figure 5-38 Least squares fitting for maximum pile bending moment at clay-hard soil interface

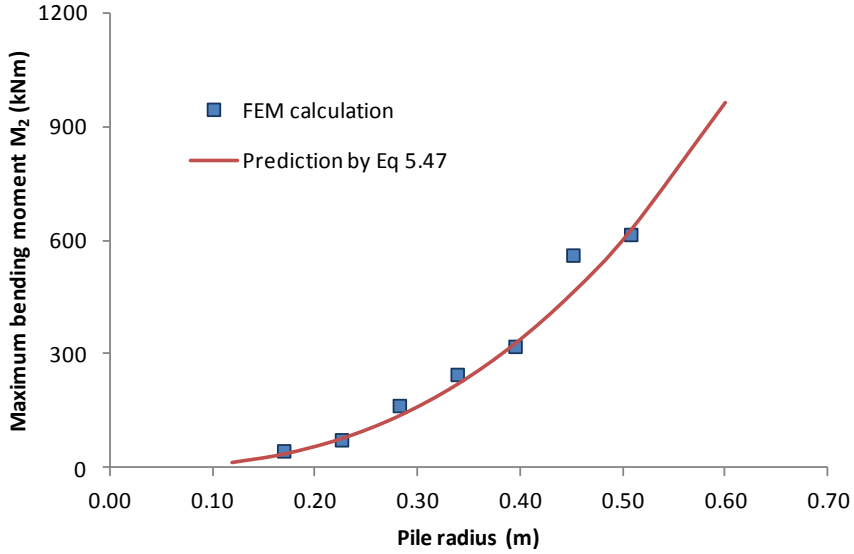

Figure 5-39 Evaluation of maximum pile bending moment at clay-hard soil interface: effect of pile radius

$(H_{soi} = 25m, m_{str} = 13{,}608ton, G_0 = 2060p'^{0.653}, a_{max} = 0.70\,m/s^2)$

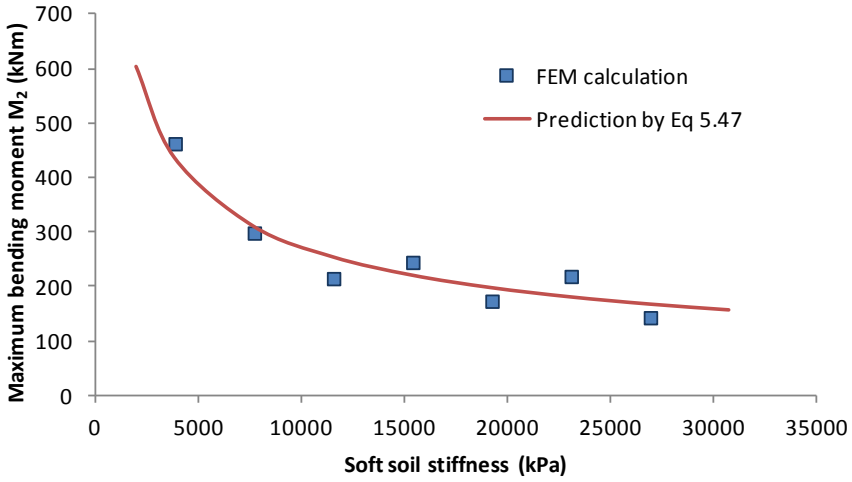

Figure 5-40 Evaluation of maximum pile bending moment at clay-hard soil interface: effect of soft soil stiffness

$(H_{soi} = 25m, r = 0.343m, m_{str} = 13{,}608ton, a_{max} = 0.70\,m/s^2)$

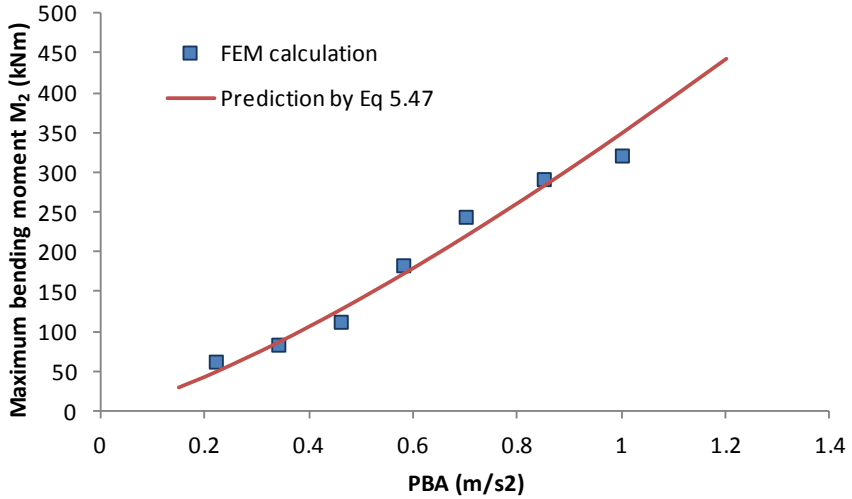

Figure 5-41 Evaluation of maximum pile bending moment at clay-hard soil interface: effect of peak base acceleration

$\left(H_{soi} = 25m, r = 0.343m, m_{str} = 13,608ton, G_0 = 2060\,p'^{0.653}\right)$

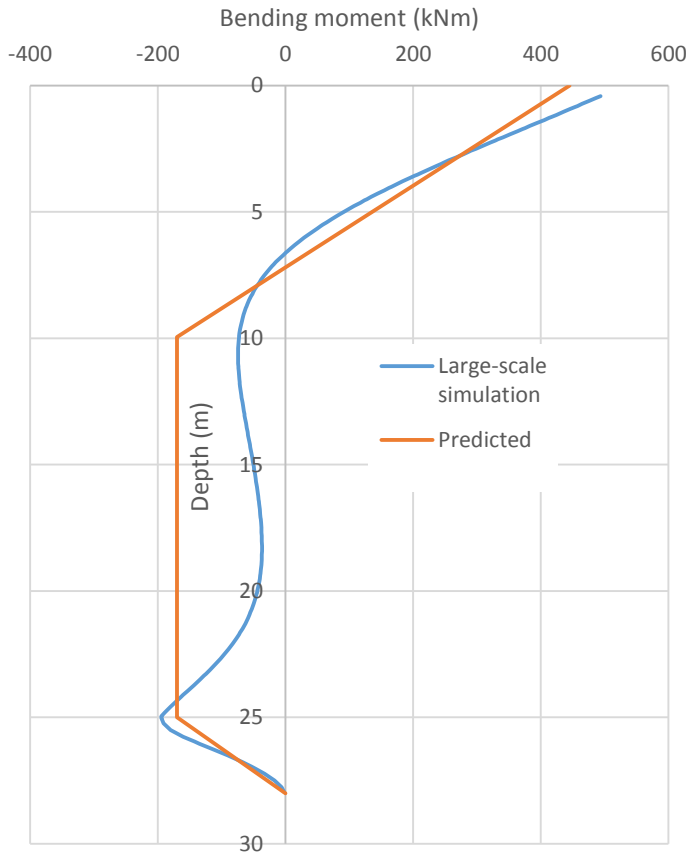

Figure 5-42 Comparison of predicted bending moment profile with the large-scale simulated result

Chapter 6 Influence of Some Other Factors on Seismic Soil-Pile foundation-Structure Interaction

6.1 Introduction

In Chapter 4, the implementation and validation of a numerical code for carrying out 3-D finite element analysis of a soil-pile-raft system was presented and discussed. Using a locally connected network of high performance personal computers, the feasibility of performing such 3-D analyses for a realistic, large-scale soil-pile-raft system involving approximately 200 piles was demonstrated. In Chapter 5, a comprehensive series of parametric studies was carried out to examine the influence of the key geometrical and material parameters, as well as the earthquake motion characteristics, on the pile response and the maximum bending moment profile and magnitude. The results were processed using dimensional analysis to derive a semi-empirical relationship to obtain the critical pile length and the maximum pile bending moment.

The baseline analysis for the parametric studies of Chapter 5 invokes several simplifications involving the modelling of the building superstructure, the soil stratigraphy and the earthquake motion. These simplifications were made in order not to complicate the analyses unnecessarily, so that they can be carried out within reasonable run-times while still allowing the results to be interpreted in a meaningful way.

In this chapter, the effects of these simplifications are examined by carrying out further analyses in which more detailed models are set up which incorporate the full building superstructure, non-horizontal soil layering and different earthquake motions. The results of these analyses will provide additional insight into the response of large soil-pile-superstructure systems, and how they are affected by simplifications invoked during the earlier analyses.

6.2 Effect of Dynamic Characteristics of Superstructure

The response of the superstructure to earthquake excitation can be characterized within an elastic framework using its structural mass and natural period (e.g. Bolton Seed and Lysmer, 1978; Hosni, 1993; Yu, 1995; Tabesh and Poulos, 2001; Elahi *et al.*, 2010). In Chapters 4 and 5, the superstructure was not modelled explicitly, but was simplified into an equivalent lumped mass whose weight was incorporated into that of the pile raft. The magnitude of the equivalent lumped mass was determined based using the relationship between the dominant period of free field and the natural period of superstructure. Hence, the influence of the superstructure stiffness and its natural period on the soil-pile foundation system was not explicitly examined in Chapter 4.

Figure 6-1(a) shows the finite element model of the soil-pile-building system which incorporates the discretized superstructure. The properties of the soil and pile foundation are the same as those adopted for the earlier model shown in Figure 4-40 and are previously summarized in Table 4-3. The piled raft system is made up

of a 9x21 pile foundation, with an equivalent pile diameter of 1m and a uniform pile length of 28m, embedded in a 25m thick layer of soft clay with 3m socketing near its base. The superstructure considered in the analysis was a twelve-storey, moment-frame building with shear-walls, which is representative of a typical residential apartment building constructed by the Housing and Development Board (HDB) for public housing in Singapore. Figure 6-1b shows the close-up view of the discretized superstructure. The floors and shear walls were modelled using thin 20-node hexahedral elements, while the columns were modelled with 3-node beam elements. The infill walls and other non-structural fixtures were not modelled explicitly, but were treated as lumped masses whose weights were added to those of the adjacent floors; in other words, their stiffnesses were not considered. The superstructure has a total mass of 13,608 tons and a fundamental period of 1.07 second, which is consistent with the equivalent mass used in Chapter 4. The soil-pile-superstructure model of Figure 6-1 was subjected to the earthquake motion shown on Figure 4-12.

6.2.1 Response of the Pile-Raft System

Figure 6-2 shows the computed acceleration history at point D on the pile raft (denoted as 'coupled'), obtained from the analysis using the fully coupled soil-pile-superstructure model. Also shown on the same figure is the raft response obtained from the earlier analysis performed in Section 4.5.1 and presented previously in Figure 4-46, wherein the superstructure was represented by a lumped-mass whose weight was added to that of the raft, hereafter termed "lumped-mass" analysis. The

two histories are almost identical, with very good agreement observed between the magnitudes of the peak responses as well as their time of occurrences.

The corresponding response spectra are plotted in Figure 6-3. Again, there is generally very good agreement between the response spectrum obtained from the coupled soil-pile-superstructure model and the lumped mass model. Some slight discrepancy between the response spectra is observed near vibration periods of about 1 sec. This is not unexpected, given that the superstructure, which has a fundamental period of 1.07s, was not explicitly modelled in the lumped mass analysis. Overall, the comparisons of Figures 6-2 and 6-3 indicate that the lumped mass analysis can reasonably capture the effect of the superstructure on the raft acceleration response.

Figure 6-4 plots the maximum corner pile bending moment profile obtained from the coupled soil-pile-superstructure simulation, together with the corresponding profile obtained from the lumped-mass simulation previously carried out in Section 4.5.2. Except for a slight difference of about 7% in the computed bending moments near the pile head, the bending moment distributions obtained from the two simulations are almost identical at depths of below 4 m. This suggests that the lumped-mass approximation of the building superstructure does not significantly affect the bending moment response of the piles.

6.2.2 Response of the Superstructure

The preceding results suggest that the lumped-mass approach for modelling the superstructure provides a reasonable means of simplifying the model without significantly affecting the computed response of the pile-raft foundation. However, the lumped-mass approach does not yield the response of the superstructure itself. In cases where the superstructural response is required, a more detailed finite element model such as that shown on Figure 6-1 should be considered. However, the current state-of-the-practice is such that a fully-coupled approach which accounts for the interaction between the soil, pile, raft and superstructure is still not readily available to the practicing engineers due to the computational resources required. Hence, some form of simplification and approximation is usually adopted when analysing the response of a building structure to earthquake shaking. Some commonly used simplified approaches are considered in this section.

For comparison purpose, the fully-coupled approach involving the soil, piles, raft and superstructure shall be denoted as Method A. In Methods B, C and D, the soil-pile-raft system is not explicitly modelled, and only the building structure shown on Figure 6-1b is analysed. In Method B, the seismic response of the building is computed by subjecting the finite element model of Figure 6-1b to an input base motion defined by the bedrock acceleration history of Figure 4-12. In this way, the effect of the overlying soft clay layer and the pile-raft system is not considered. Method C is similar to Method B, except that the input base motion for the building structure uses the free-field ground surface acceleration generated by the upward propagation of the bedrock acceleration of Figure 4-12. For horizontally layered

soils, the free-field ground surface acceleration can be quite easily calculated using commercially available 1-D softwares such as SHAKE-91 or DEEP. Method D uses the computed raft acceleration history shown on Figure 4-46 as input base motion of the structure, which was obtained using the lumped-mass approach of Section 4.5.1. Hence, Method D can be considered as a decoupled approach, in which the pile-raft acceleration response is first calculated using the soil-pile-raft model of Section 4.5.1 with the lumped-mass approximation for the building, and then applied to a separate model for the building structure to obtain the structural response.

Among the four methods, the most rigorous or complete approach is that of Method A, which incorporates all four components: soil, piles, raft and building. Hence, the finite element analysis using Method A may be expected to provide the best approximation to the field situation. Accordingly, in the following discussion, the results obtained from Method A shall be taken as the reference against which the other methods are compared.

Figure 6-5 presents the computed acceleration time histories at the top of the building (point H in Figure 6-1) obtained using the four different methods. It is observed that among Methods B, C and D, the acceleration history at point H obtained using Method D comes closest to that of the fully-coupled response associated with Method A. This agreement is also reflected in the corresponding response spectra plotted in Figure 6-6. As can be seen, the response spectrum at Point H obtained using Method D is almost identical to that of Method A for the

most part, except for a narrow band of vibration periods near the building's fundamental period of 1s.

Methods B and C are widely used in practice by structural earthquake engineers. However, as shown on Figure 6-5 and Figure 6-6, the use of Method B results in a much smaller response at point H, which may result in an unconservative design. Method C, on the other hand, yields a larger response in the high frequency or short period range and a smaller response in the long period range, which may also lead to errors during design.

The results from the preceding analyses indicate that the use of Methods B and C may lead to erroneous results in the computed structural response of the building. In other words, the foundation system plays an important role in the structural response of the building and cannot be ignored in the analysis. As shown by Method D, an approximate simplification can be made in which the building is decoupled from the underlying soil-pile-raft system. This involves a two-stage analysis in which an analysis is first carried out for the soil-pile-raft system using the lumped mass approach to approximate the building effects, from which the computed pile-raft acceleration history is used as the base input motion for a separate analysis to compute the structural response. While still somewhat cumbersome, it does provide a means of decoupling the complete soil-pile-superstructure system so that the geotechnical and the superstructural aspects of the analysis can be treated separately by different teams of engineers.

6.3 The Influence of Uneven Soil Geometries

Actual subterranean soil profiles are usually uneven and complicated. To date, there has been little or no study on the influence of uneven or non-horizontal soil profiles on the seismic response of foundations and structures. Most published studies in the literature simplify the soil profile into uniform layers (e.g. Trochanis *et al.*, 1988; Wu, 1994; Guin and Banerjee, 1998; Lok *et al.*, 1998; Zhang *et al.*, 2000; Lu *et al.*, 2005; Lu *et al.*, 2008; Banerjee, 2009; Chau *et al.*, 2009). Lu (2006) and Ilankatharan *et al.* (2006) analyzed pile foundations in uneven soil profiles, but they did not study the influence of the uneven soil layers on the pile foundations. In this section, unevenness in subterranean soil profile is examined by analyzing the effect of subterranean slope and valley on the motion of the raft and the bending moment response of the piles.

6.3.1 Pile-Raft System founded on a Soft Clay Layer overlying a Sloping Bedrock, with Earthquake Excitation applied along the Slope

In this study, the seismic response of a pile-raft system founded on a soft clay layer of varying thickness overlying sloping bedrock is examined. The bedrock is assumed to be planar, with a gradient of 1:3. The properties of the soil and pile foundation are the same as those adopted for the earlier model shown in Figure 4-40 and are previously summarized in Table 4-3. The same 9x21 pile foundation is considered, with an equivalent pile diameter D of 1m and the pile-to-pile spacing of 3D. Adopting a socketing criterion of 3D, the pile lengths increase from one end

of the raft to the other, as the bedrock depth varies from 6.7 m to 20.6 m over this distance.

Figure 6-7(a) shows the discretized finite element half-model for this soil-pile-raft system founded on the sloping bedrock. For comparison purposes, three other analyses with the pile-raft system founded on different uniform thicknesses of the soft clay layer were also carried out. Figure 6-7(b) shows the uniform half-model with the bedrock at a depth of H_A = 6.7 m, which corresponds to the condition at the shallow end of the sloping model shown on Figure 6-7(a). In Figure 6-7(c), the uniform bedrock depth is H_B = 20.6 m, which corresponds to the condition at the deepest end of the sloping. The uniform bedrock depth in Figure 6-7(d) is H_C = 13.65 m, which model corresponds to the condition at the middle of the raft.

The different models of Figure 6-7 were subjected to the earthquake motion shown on Figure 4-12. The motion was applied horizontally in the direction along the sloping bedrock.

Figure 6-8 compares the computed raft acceleration histories at the points A, B and C of the pile-raft system for the sloping bedrock (Figure 6-7(a)) with the corresponding acceleration histories at A', B' and C' for the respective uniform clay models of Figure 6-7(b-d). The acceleration histories at points A, B and C of the pile in the sloping bedrock model plot as a single line due to the rigid response of the pile-raft system arising from its large stiffness compared to the surrounding soil. The corresponding response spectra are plotted in Figure 6-9. Both the computed time histories and the response spectra show that the raft accelerations

for piled foundations founded on sloping bedrock are quite different from those founded on a uniform soil layer. This is due to the highly complex interaction arising from the different soil thicknesses and different pile lengths in the different models. Even though the dominant period and amplitude at point C' of the pile raft in the uniform soil layer with thickness H_C = 13.65 m are close to the corresponding values at point C of the raft in the sloping bedrock model, there are still significant difference in the overall response spectrum.

Figure 6-10 plots the maximum bending moment profiles for piles A and B at the two ends of the pile-raft system founded on a sloping bedrock, as well as the corresponding profiles of piles A' and B' for the respective uniform clay thicknesses of 6.7 m and 20.6 m. It is noted that piles A and A', both of which are associated with a shallow bedrock depth, develop much larger bending moments at the pile heads compared to piles B and B' founded on deeper bedrock. These results suggest that, under the same earthquake excitation, the shorter piles founded on shallower bedrock are generally subjected to larger seismic loadings compared to those founded on deeper bedrock.

Even though piles A and A' are both founded at the same shallow bedrock depth, the maximum positive and negative bending moments that develop in the two piles are quite different. The bending moments in pile A, which is part of the pile-raft system founded on the sloping bedrock, are larger than those that developed in pile A' located in the uniform clay layer. On the other hand, the trend is reversed at the deeper bedrock depth, where the bending moments in pile B' located in the

uniform clay layer are larger than those that develop in pile B in the sloping bedrock.

From the comparisons of raft accelerations and pile bending moments shown on Figure 6-8 to Figure 6-10, it can be seen that response of a pile-raft system founded on a uniform soil layer may not be representative of a similar system founded on sloping bedrock. Hence, for problems involving such sloping bedrock conditions, the assumption of an equivalent uniform horizontal layering may not be valid, and it may be necessary to conduct large-scale simulations that account for the uneven or non-horizontal bedrock.

6.3.2 Pile-Raft System founded on a Soft Clay Layer overlying a Sloping Bedrock, with Earthquake Excitation Perpendicular to the Slope

In this section, the case of the bedrock excitation being perpendicular to the slope, as shown in Figure 6-11, is examined. Under such loading conditions, the half-model is no longer applicable, and a full model is necessary in order to analyzed the response of the pile-raft system founded on a soft clay layer overlying a sloping bedrock. To minimize the influence from the lateral boundary conditions, the finite element soil domain is extended in the direction of the shaking.

Apart from the direction of earthquake shaking, all other geometrical and material parameters associated with the pile and raft are identical to those applied previously in section 6.3.1. The earthquake excitation is based on the ground motion shown on Figure 4-12.

Due to the earthquake excitation, the computed response acceleration at the two ends of the pile raft corresponding to the deep and shallow bedrock is compared in Figure 6-12 and Figure 6-13. It is clearly seen that the pile raft shows a larger acceleration response at the deeper bedrock end than the shallower bedrock end. The response spectrum of Figure 6-13 also shows that the computed raft motion has a higher dominant period at the deeper bedrock end. The difference in raft accelerations between the deeper and shallower bedrock end suggests that the raft does not undergo a pure translational motion, as was the case in section 6.3.1 when the earthquake excitation was applied horizontally along the sloping bedrock direction. Figure 6-14 plots the computed displacement histories at the two ends of the raft. It is clear that the two ends of the raft undergo different displacements with different magnitudes and frequency content. The motion at the shallower bedrock end has a smaller peak displacement but is relatively richer in the higher frequency components compared to the response at the deeper bedrock end.

Figure 6-15 plots the deformed shape of the raft (at a magnified scale) at two different instances corresponding to t = 5.125s and 5.81s. As can be seen from the figure, the raft undergoes a twisting motion which will subject the piles to induced torsion. However, such effects are often not considered in earthquake design.

The maximum pile bending moment profiles at the two ends of the raft are compared in Figure 6-16. As can be seen, the shorter pile at the shallower bedrock end experiences larger bending moments compared to the longer pile at the deeper

bedrock end. This is similar to the trend previously observed in section 6.3.1, when the earthquake excitation is applied along the sloping bedrock direction.

6.3.3 Structure Overlying a Subterranean Valley

Figure 6-17 shows the half-model of a pile-raft system in the middle of a subterranean valley formed by a protruding rockhead. The properties of the soil and pile foundation are the same as those adopted for the earlier model shown in Figure 4-40 and previously summarized in Table 4-3. The same 9x21 pile foundation is considered, with an equivalent pile diameter D of 1m and the pile-to-pile spacing of 3D. The pile-raft system is founded on the deepest portion of the valley, where the soft clay layer has a uniform thickness of 25m.

The computed results for this subterranean valley analyses are compared with those obtained earlier for a pile-raft system founded on a 25m thick uniform soft soil layer, the thickness of which corresponds to that at the bottom of the valley underlying the entire raft. As Figure 6-18 shows, even though the sides of the valley are relatively far away from the foundation, the raft founded in the valley is subjected to a much larger peak acceleration than that in the uniform soil. This is also reflected in the acceleration response spectrum of Figure 6-19. The pile foundation in the valley also experiences larger pile bending moments, as shown in Figure 6-20.

Based on the above comparisons of the raft accelerations and the pile bending moments, it is observed that computed the responses of the pile-raft system in the subterranean valley are larger than those in the uniform clay layer. This may be

attributed to wave reflections and soil amplification effects within the valley. The soil amplification effect arising from the trapping of waves in a subterranean basin under green field conditions, i.e. without structures, is quite well-known and has previously been reported (e.g. Wood, 1955; Nuttli, 1973). The present study shows that subterranean valleys may exhibit similar wave trapping effects which affect the soil-pile-raft system response, even when the valley walls are located quite far away from the pile-raft structure.

6.4 Different earthquake motions

The numerical simulations up to this point are based on three scaled artificial earthquake acceleration time histories, as discussed and shown in Section 4.2.5. These synthetic earthquakes have different peak accelerations (0.022g, 0.07g and 0.1g) but identical frequency contents. In actual earthquakes, both the frequency contents and the peak accelerations may vary quite significantly from one event to another. In this section, the influence of the ground motion frequency distribution on the response of the soil-pile-raft system is examined, while keeping the peak acceleration value the same. Figure 6-21(a) shows the reference ground motion adopted for this section, based on the synthetic earthquake with a peak acceleration of 0.07g previously used in the analyses of Chapters 4 and 5. This is the same earthquake previously shown on Figure 4-12, in which the strong shaking occurs over a relatively short duration of about 25 s.

The measured ground motion records from two historical earthquakes are adopted as alternative base motion inputs in the following analyses. The first set of records

is derived from the bedrock motion measured at the Bukit Timah Dairy Farm (BTDF) station in Singapore arising from the Kepulauan Mentawai earthquake on April 4th, 2005, as shown on Figure 6-21(b). Note that the strong shaking for this earthquake occurs over a duration of about 200 s. The second set of records derives from the widely used ground motion from the 1940 El Centro earthquake, as shown on Figure 6-21(c). The strong shaking for this earthquake occurs over duration of about 30 s, similar to that of the synthetic earthquake. To eliminate the influence of seismic amplitude, the two sets of earthquake records are scaled to a peak ground acceleration of 0.7m/s^2 or 0.07g, as previously discussed.

The response spectra corresponding to the three earthquakes are shown on Figure 6-22. It is noted that the response spectrum for the 2005 Kepulauan Mentawai earthquake is broadly similar to the synthetic earthquake considered in this study, with both showing a significant contribution from long period components typical of ground motions measured from far-field earthquakes. On the other hand, the 1940 El Centro earthquake ground motion is much richer in the short period components, which is consistent with the measurements from near-source earthquakes. The three ground motions were applied to the finite element model shown in Figure 4-40. The properties of the soil and pile foundation are summarized in Table 4-3.

The computed raft acceleration time histories are plotted in Figure 6-23. Even though the peak input accelerations are the same, the resulting raft motions are quite different. This illustrates the influence of different frequency components on the raft response. Furthermore, as Figure 6-24 shows, the computed raft response

spectrum from the 2005 Kepulauan Mentawai earthquake is similar to that from the synthetic earthquake, whereas the raft response for the 1940 El Centro earthquake consists mainly of short period components and smaller amplitude. The influence of the ground motion frequency content on the foundation response has also been noted by other researchers (e.g. Kaynia, 1982; Gohl, 1991; Meymand, 1998; Nikolaou *et al.*, 2001).

Figure 6-25 shows the computed maximum pile bending moment profiles arising from the different earthquakes. It is noted that the maximum bending moment profile from the 2005 Kepulauan Mentawai earthquake is very close to that computed using the synthetic earthquake. This may be attributed to the broadly similar response spectrum of the two input ground motions, even though the duration of shaking for these two earthquakes is quite different. On the other hand, the pile bending moments arising from the 1940 El Centro earthquake are generally smaller than those obtained using the other two earthquakes. Again, it appears that the frequency contents of the input motion plays an important role, given that the El Centro earthquake motion is much richer in short period components due to its near-source characteristics. Hence, the results strongly suggest that, for the same peak ground acceleration, the frequency contents of the earthquake ground motion can significantly affect the pile response.

This finding has significant implications for the results presented and discussed in Chapters 4, 5 and 6. As the trends and the generalizations made on the pile foundation response, including the dimensionless equations for the maximum

bending moments, are based on expected earthquake ground motions in Singapore representative of those arising from far-field earthquakes occurring along the Great Sumatran Fault, care should be taken when using these equations to predict pile foundation performance at other sites subjected to near-field earthquake excitation. More study is needed to shed light on the influence of near-field earthquakes on complex soil-pile-superstructure systems.

6.5 Summary

The influence of super-structural characteristics, uneven geometries and earthquake loading types on seismic soil-pile foundation -structure interaction was examined in this chapter. The approach of replacing the superstructure by an equivalent lumped mass whose weight was incorporated into that of the raft was validated. It was also shown that the raft accelerations obtained using this lumped mass approach can be used as the input base motion for a separate structural analysis to obtain reasonable predictions of the building's seismic response. On the other hand, the simplified approaches of carrying out such structural seismic analysis, which do not consider the influence of the soil-pile raft interaction, may lead to erroneous results.

The influence of uneven soil geometries was examined for several cases. For pile-raft systems founded on sloping bedrock, the piles at the shallower bedrock end generally develops larger bending moments than those located at the deeper bedrock end. In some cases, such as when the earthquake motion occurs perpendicular to the sloping bedrock, the pile raft may be subjected to torsion. The wave trapping effect associated with the propagation of earthquake motion in

subterranean valleys was also simulated. It is shown that, even in a relatively wide valley whose sides are quite far from the pile-raft system, the foundation response is generally larger than that obtained for a uniform soil layer. This is a highly complex problem involving the interaction of many factors, and should be studied systematically as part of the future work.

Finally, the influence of the earthquake ground motion is examined with regard to its frequency contents. It is noted that the frequency contents may affect not only the raft motion response, but also the maximum bending moments developed in the piles. The difference in foundation response may be quite significant for frequency contents arising from near-field vs. far-field earthquakes, as the former tends to be richer in short period components.

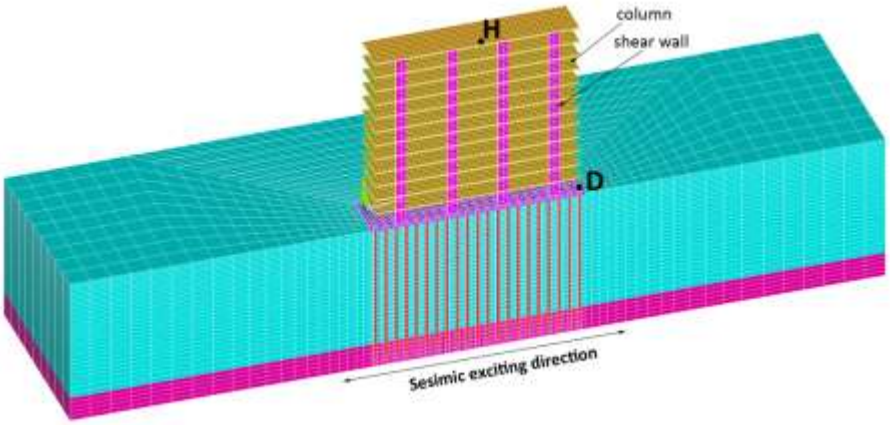

(a) Complete Soil-Pile-Superstructure Model

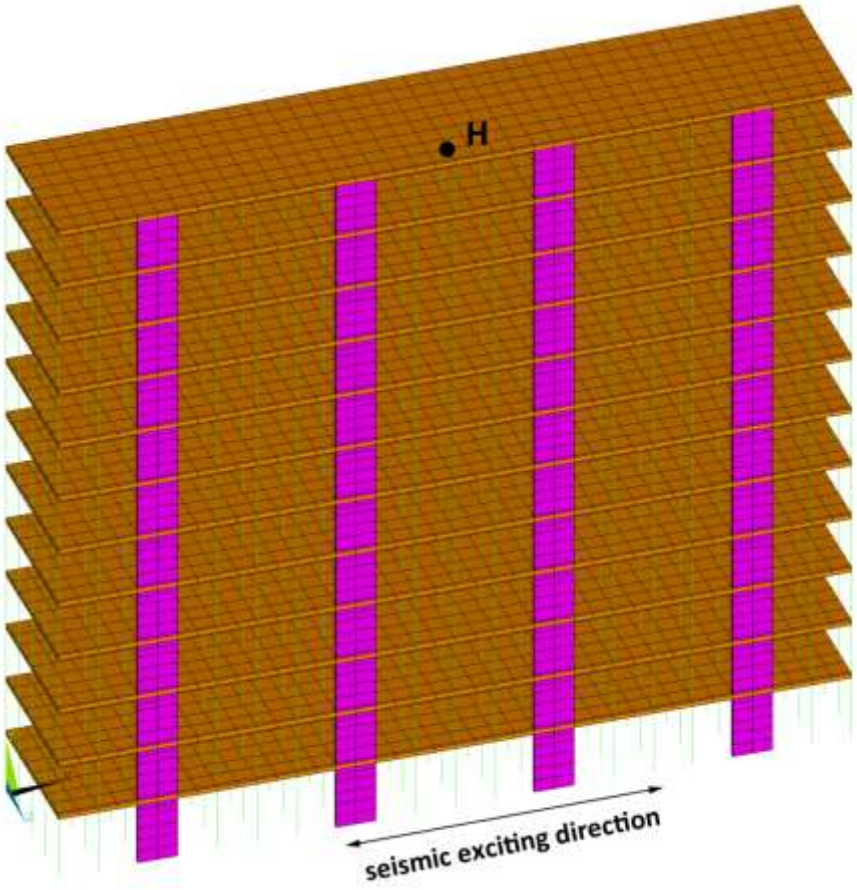

(b) Close-up of the Superstructure Model

Figure 6-1 Finite element model for the fully coupled soil-pile-superstructure simulation

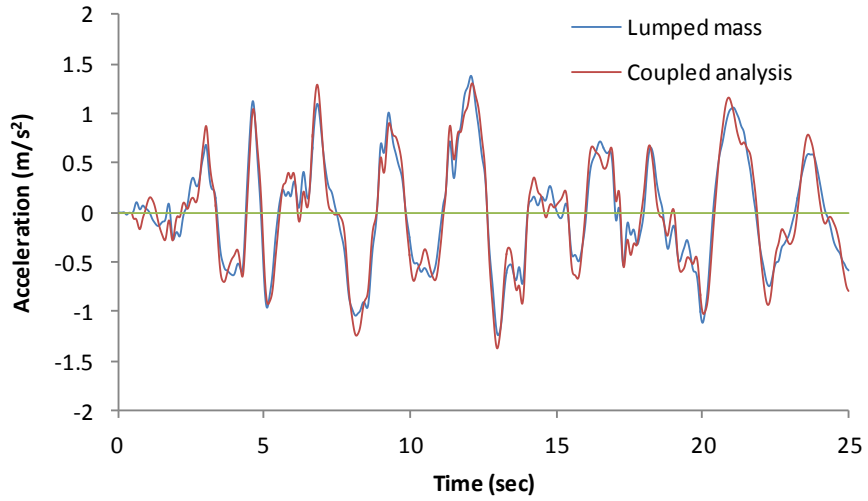

Figure 6-2 Comparison of acceleration time histories at pile raft from coupled and lumped analysis

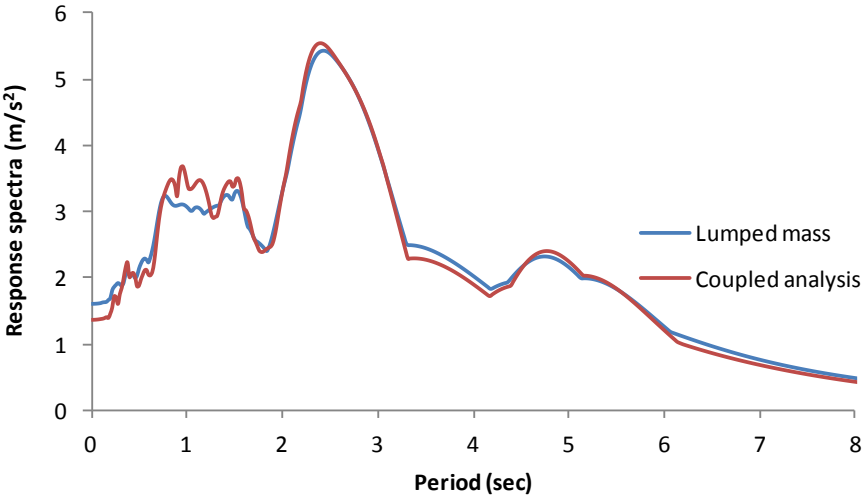

Figure 6-3 Comparison of acceleration response spectrum at pile raft from coupled and lumped analysis

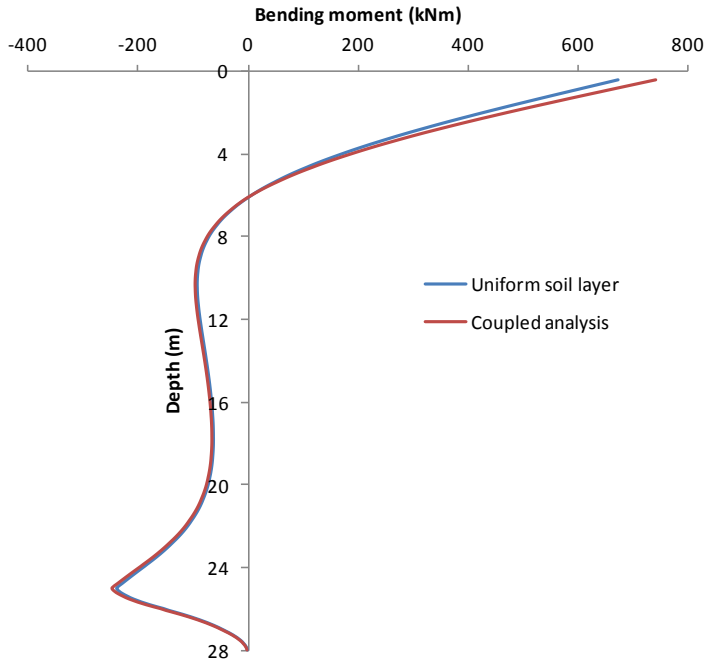

Figure 6-4 Comparison of bending moment profiles from coupled and lumped analysis

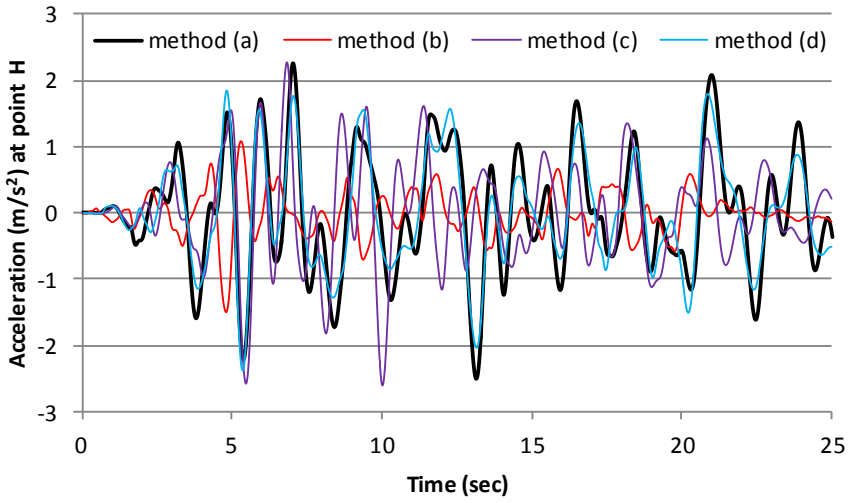

Figure 6-5 Comparison of structural response acceleration histories from four different methods:

Method (a) -- directly from fully-coupled analysis,

Method (b) -- from a dynamic structural analysis using the bedrock acceleration as base input,

Method (c) -- from a dynamic structural analysis using the ground surface acceleration as base input, and

Method (d) -- from a dynamic structural analysis using the raft acceleration as base input.

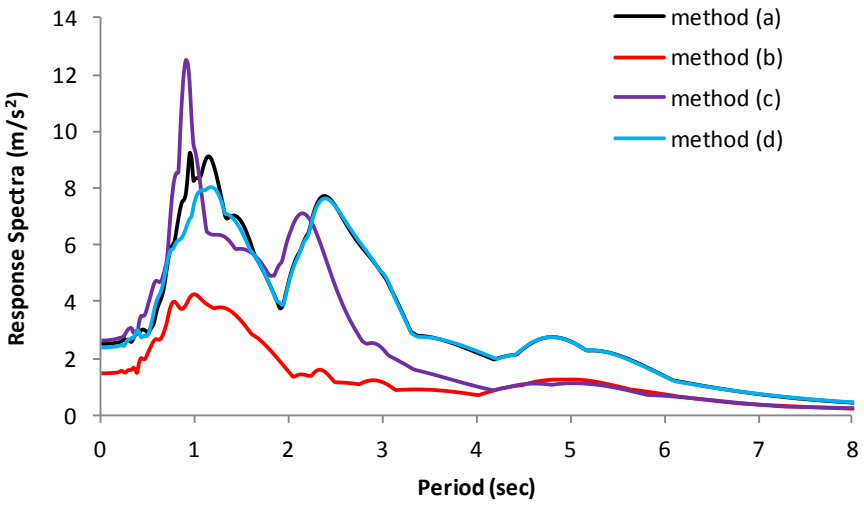

Figure 6-6 Structural response spectra comparison with different simulation methods

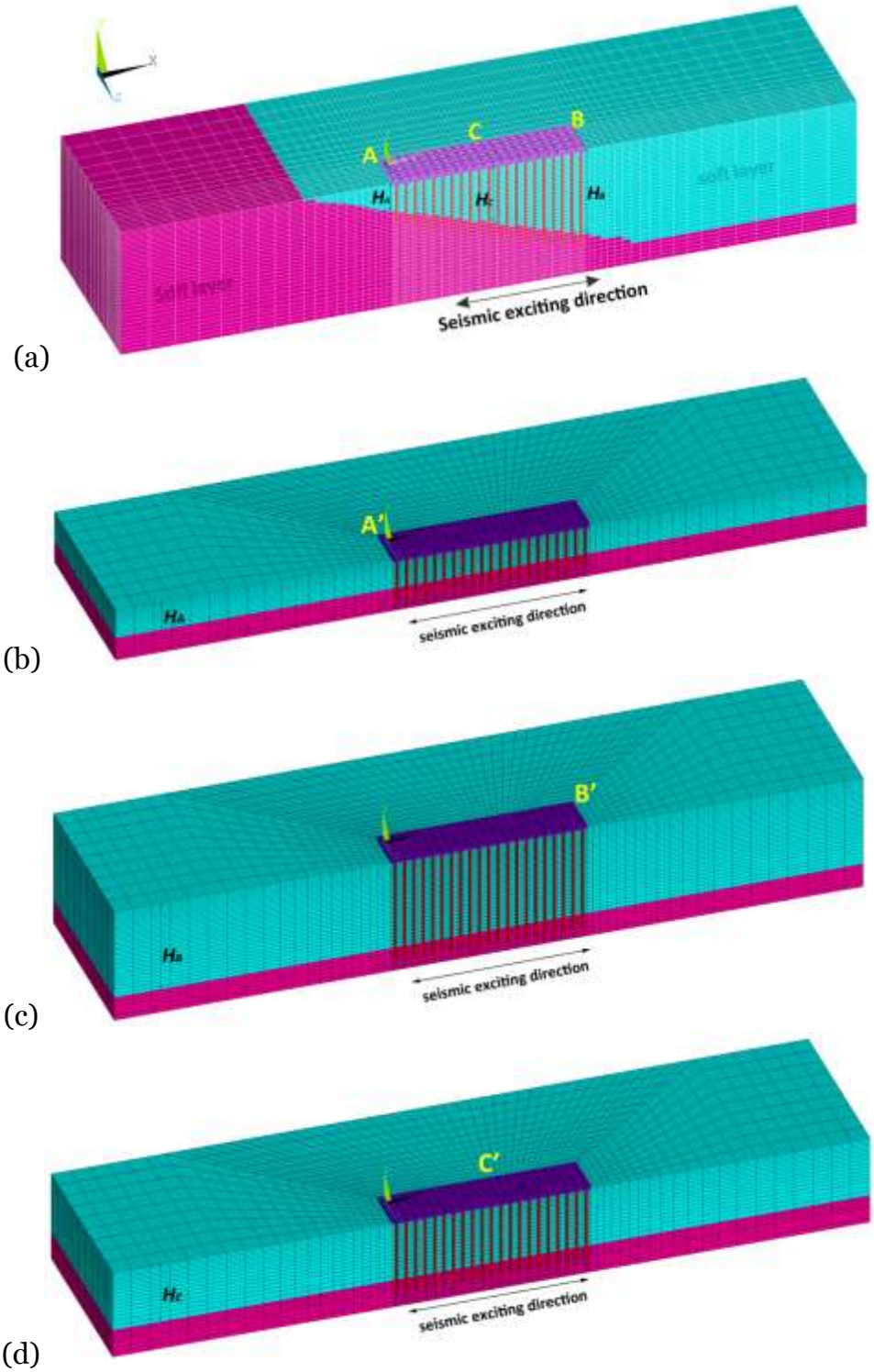

Figure 6-7 Soil-pile-structure model to study the effect of uneven soil profiles: (a) Clay layer overlying sloping bedrock, (b) Uniform clay layer with thickness H_A =6.7m (c) Uniform clay layer with thickness H_B,= 20.6m (d) Uniform clay layer with thickness H_C, =13.65m

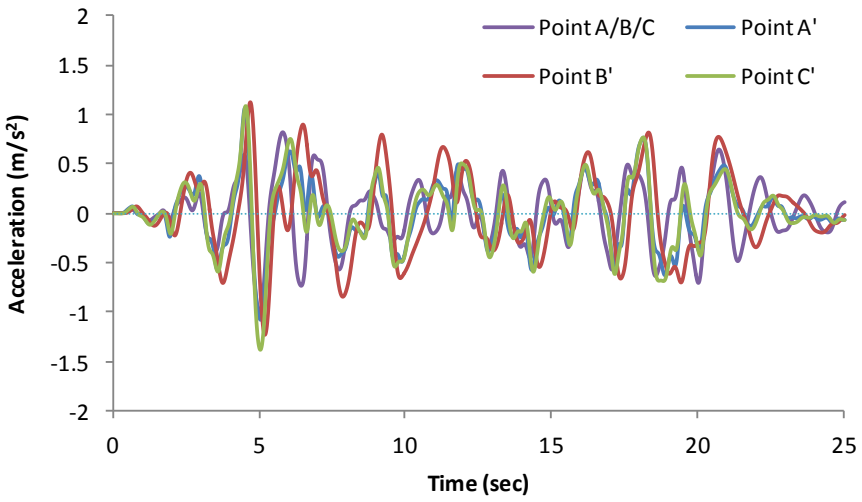

Figure 6-8 Comparison of acceleration histories at pile raft for the sloping clay layer and uniform clay layers with different thickness

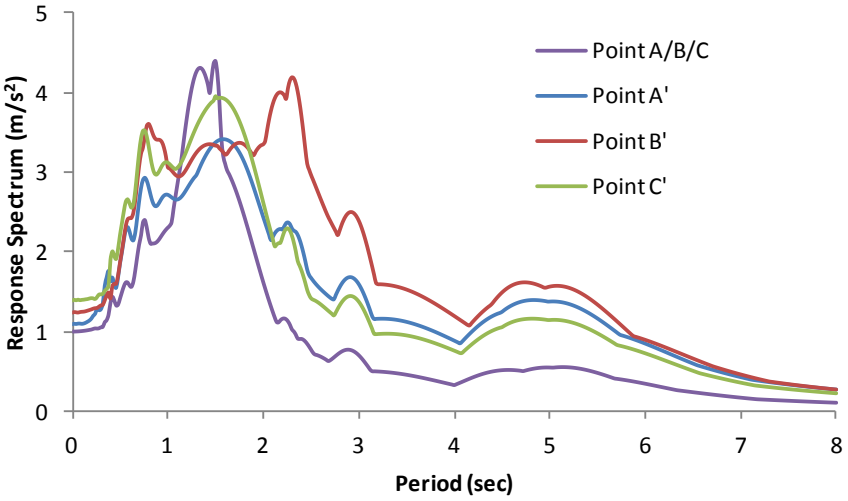

Figure 6-9 Comparison of response spectra at pile raft for the sloping clay layer and uniform clay layers with different thickness

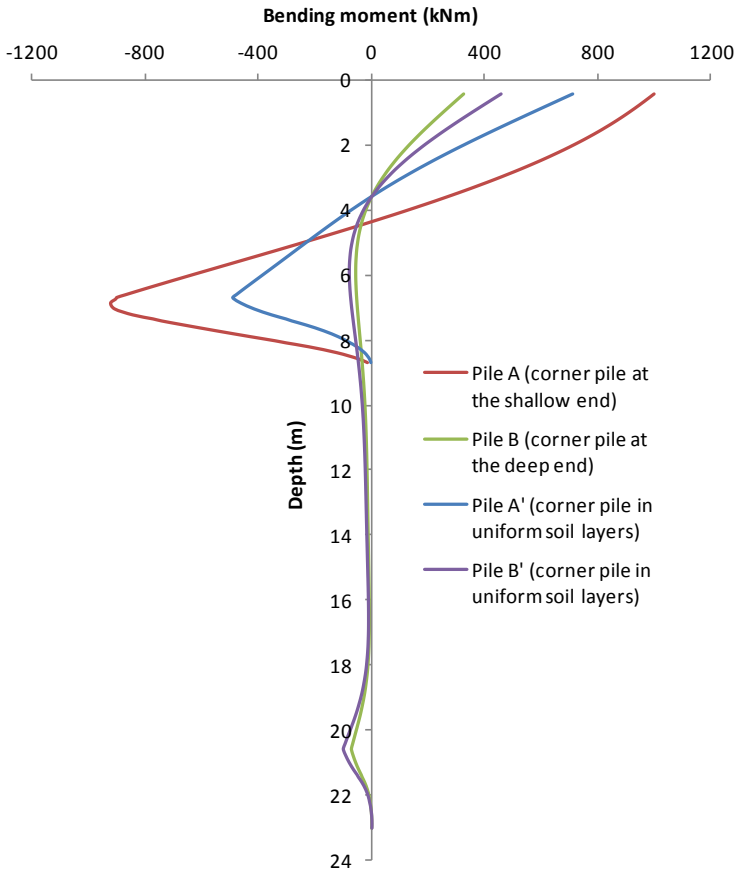

Figure 6-10 Comparison of pile bending moment profile for the sloping clay layer and uniform clay layers with different thickness

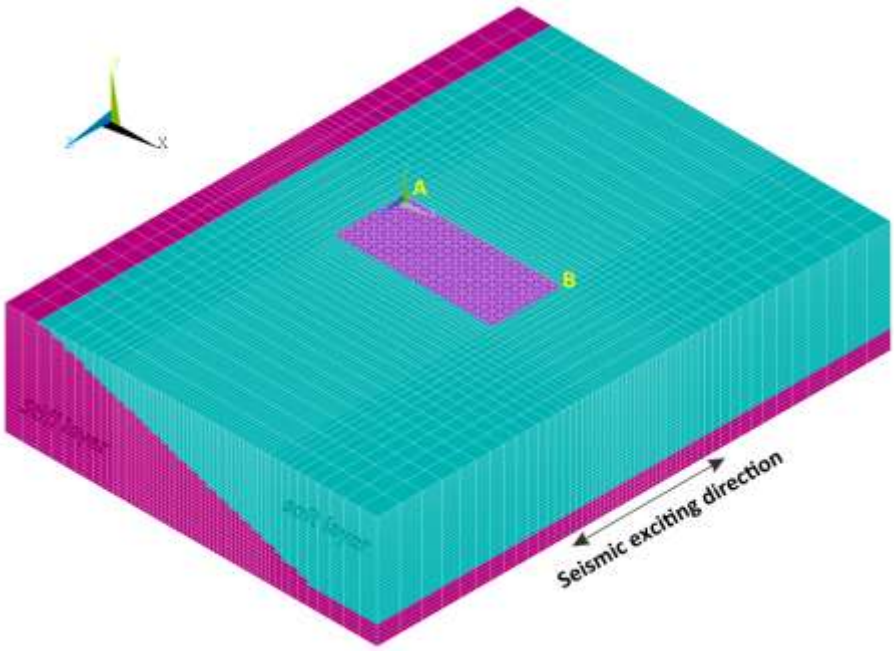

Figure 6-11 Pile foundation on sloping bedrock (perpendicular to seismic excitation direction)

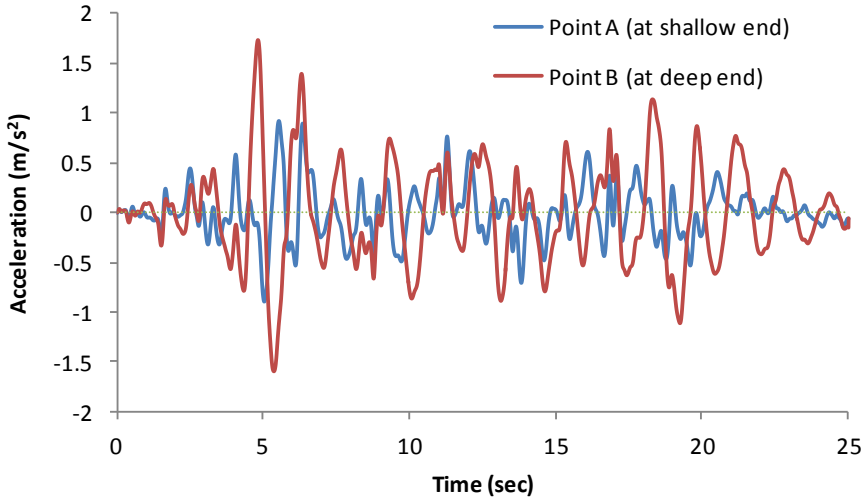

Figure 6-12 Comparison of pile raft acceleration histories at different locations when the earthquake excitation is perpendicular to the sloping bedrock

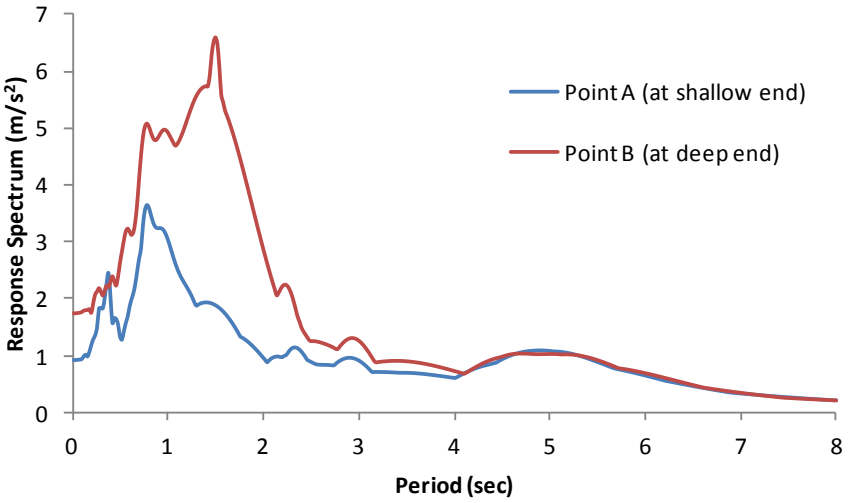

Figure 6-13 Comparison of pile raft response spectrum at different locations when the earthquake excitation is perpendicular to the sloping bedrock

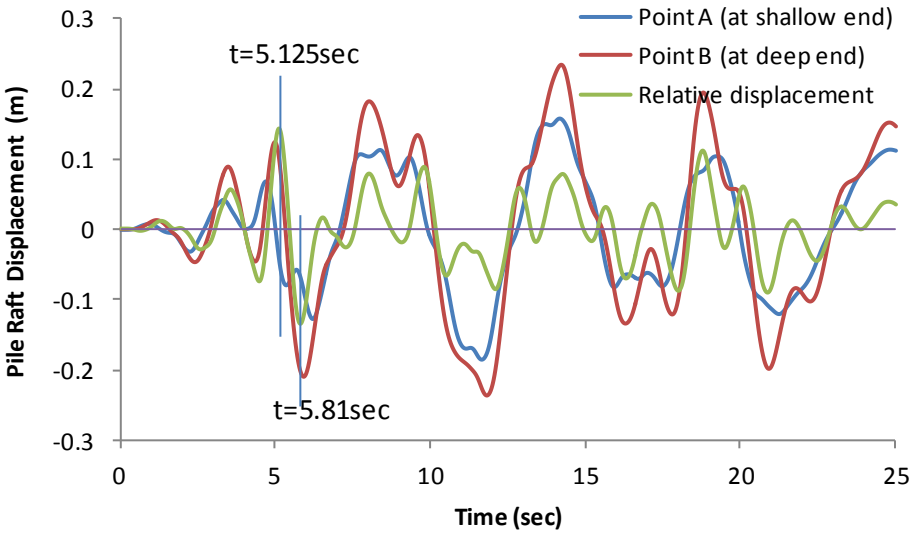

Figure 6-14 Comparison of pile raft displacement histories at different locations when the earthquake excitation is perpendicular to the sloping bedrock

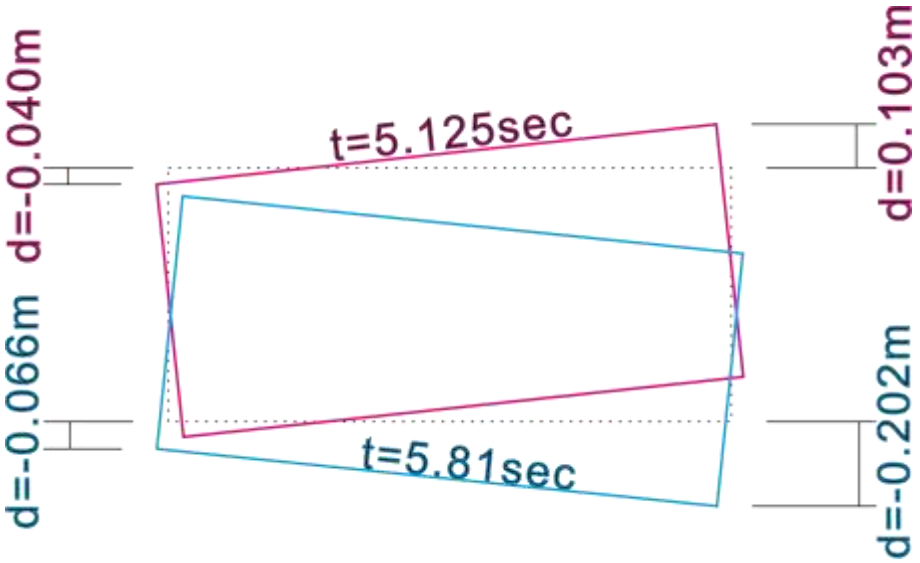

Figure 6-15 Torsion of pile foundation (magnified 30 times)

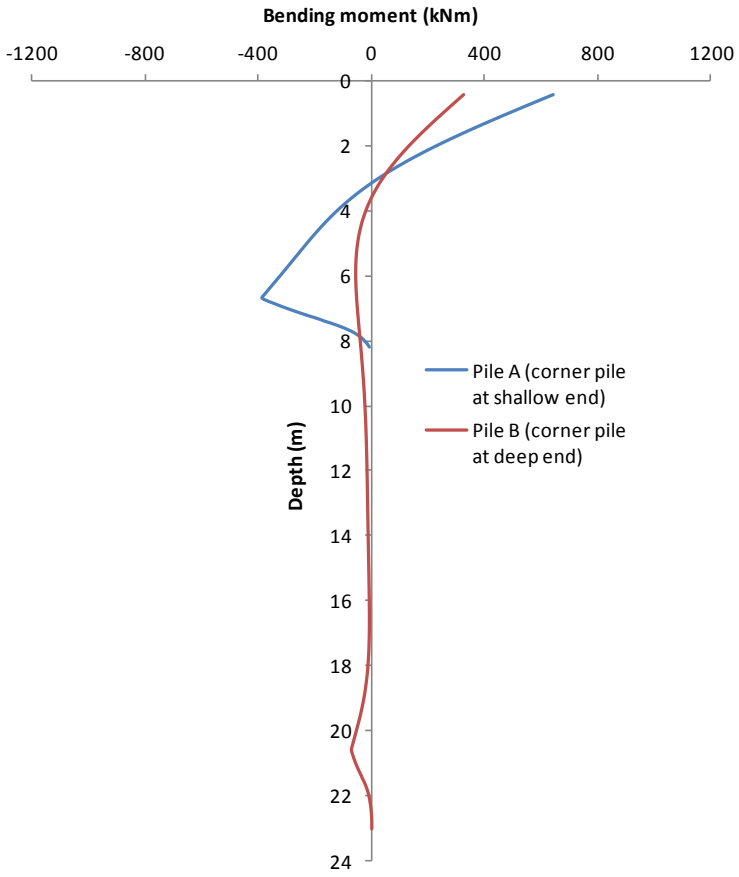

Figure 6-16 Comparison of pile bending moment profiles at two locations when the earthquake excitation is perpendicular to the sloping bedrock

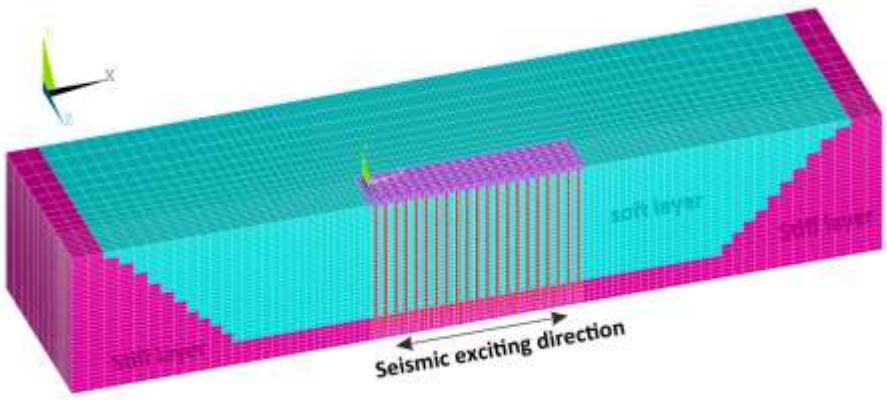

Figure 6-17 Pile foundation overlying a subterranean valley

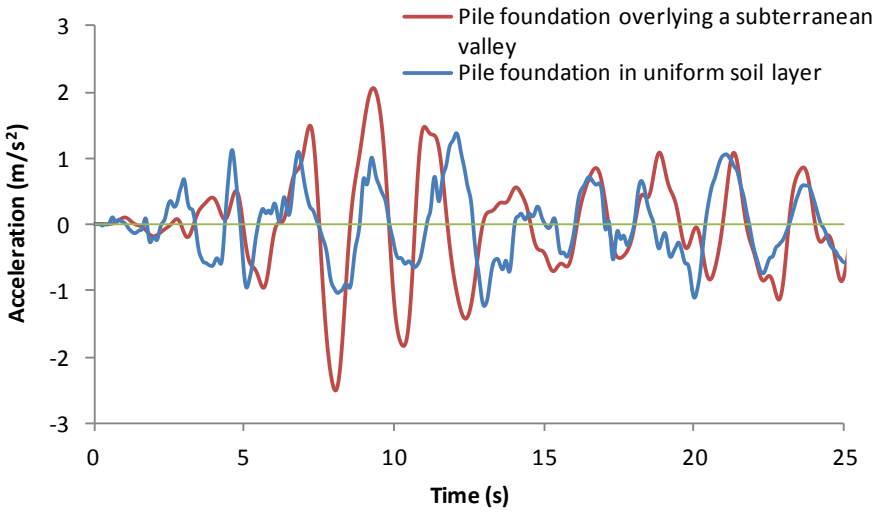

Figure 6-18Comparison of computed acceleration histories at pile raft for a foundation located in the subterranean valley vs uniform soil layer

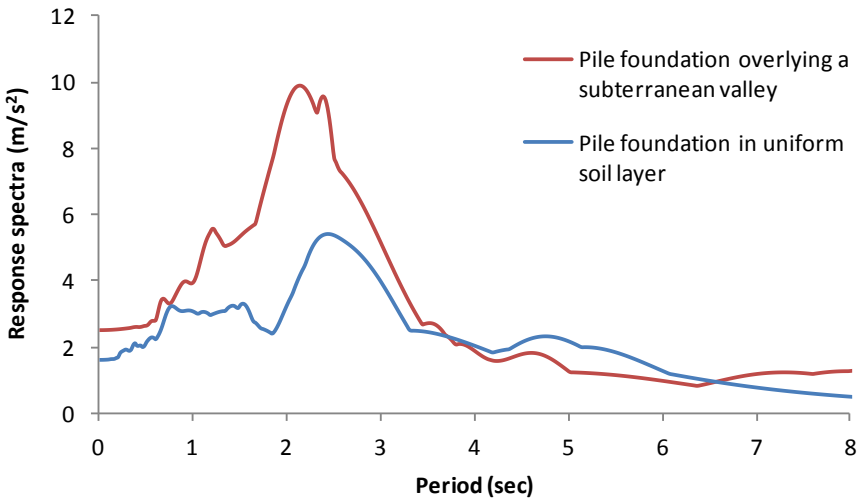

Figure 6-19 Comparison of response spectra at pile raft for a foundation located in the subterranean valley vs uniform soil layer

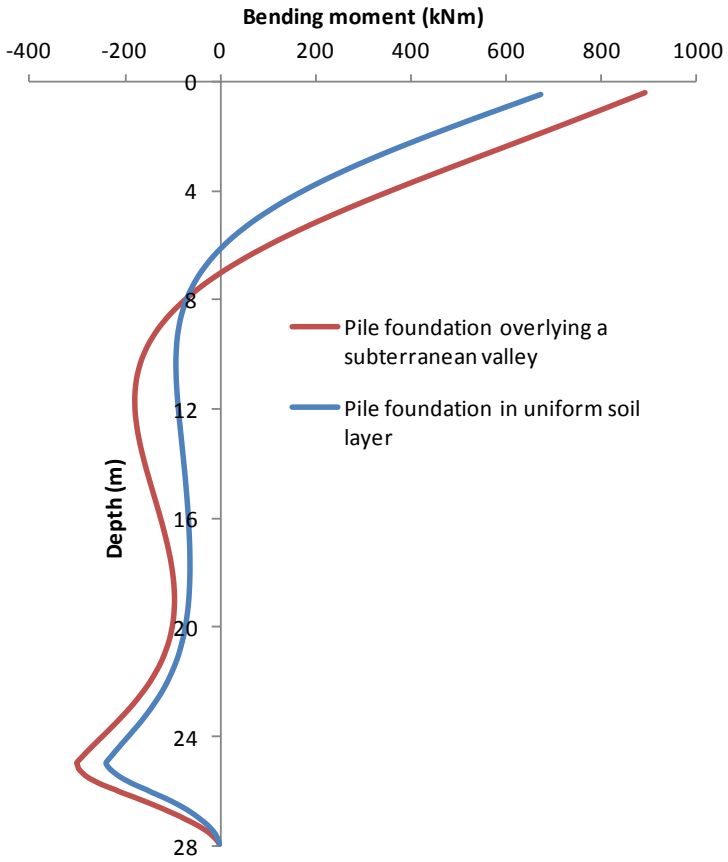

Figure 6-20 Comparison of pile bending moment profiles for a foundation located in the subterranean valley vs uniform soil layer

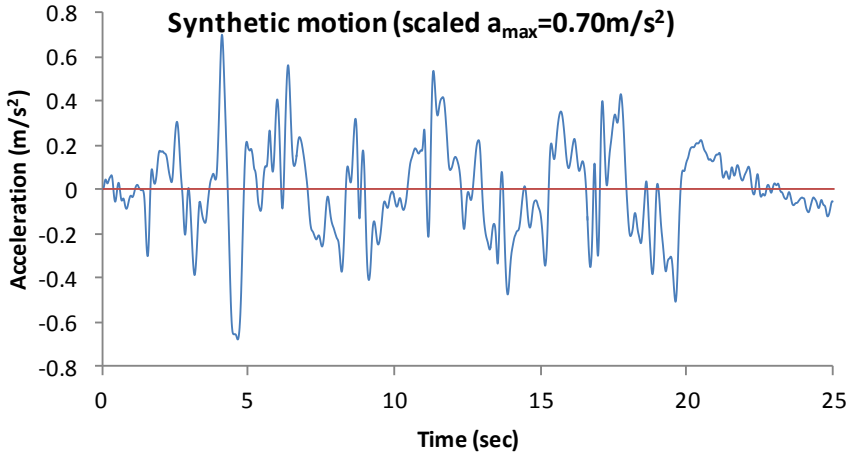

(a)

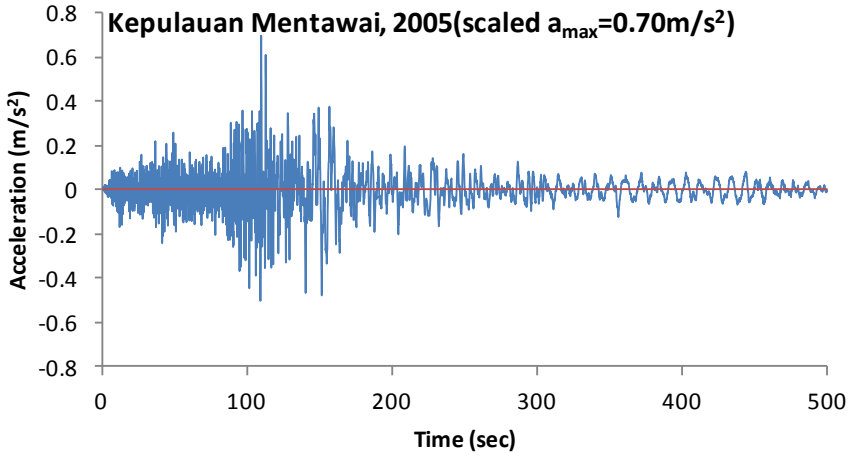

(b)

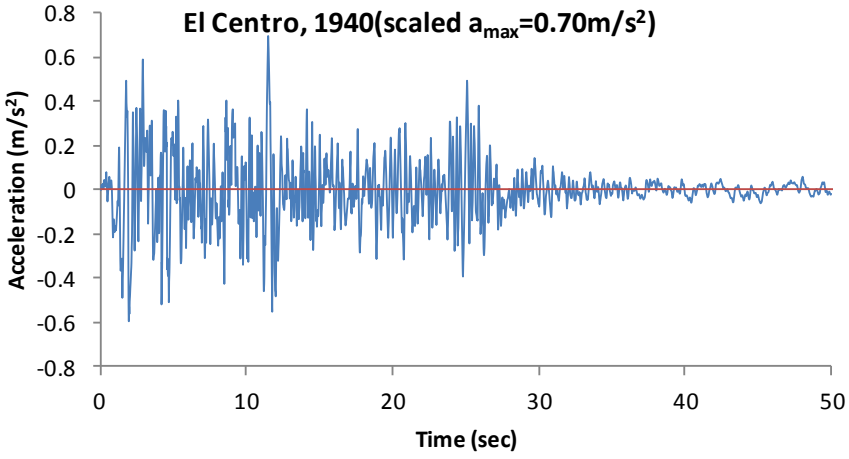

(c)

Figure 6-21 Three earthquake input base motions: (a) synthetic motion generated by Yu and Lee (2002); (b) measured records from Kepulauan Mentawai 2005 earthquake ; (c) measured records from El Centro 1940 earthquake (Chopra, 2007).

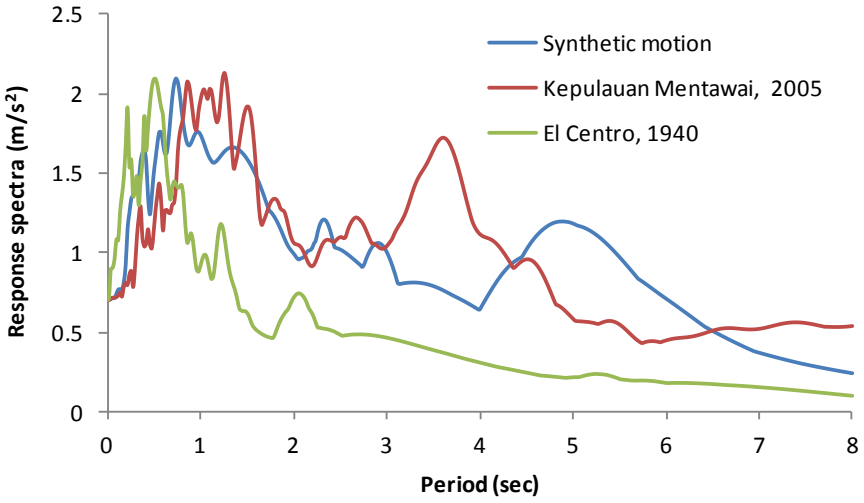

Figure 6-22 Response spectra of the three earthquake records

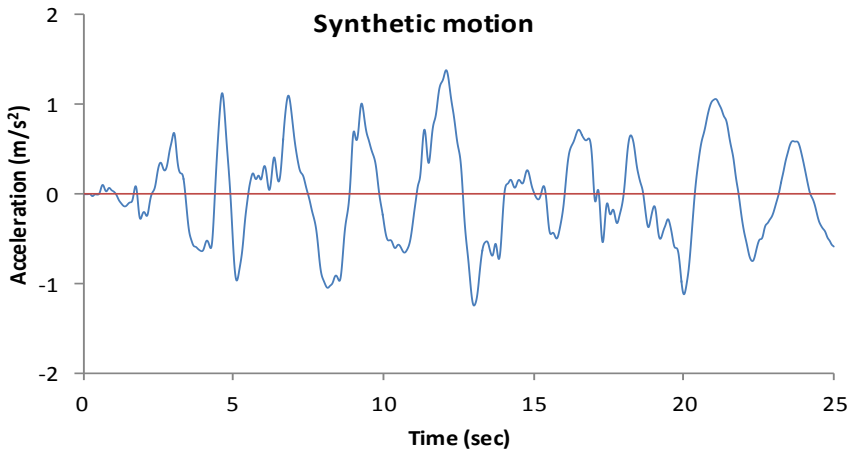

(a)

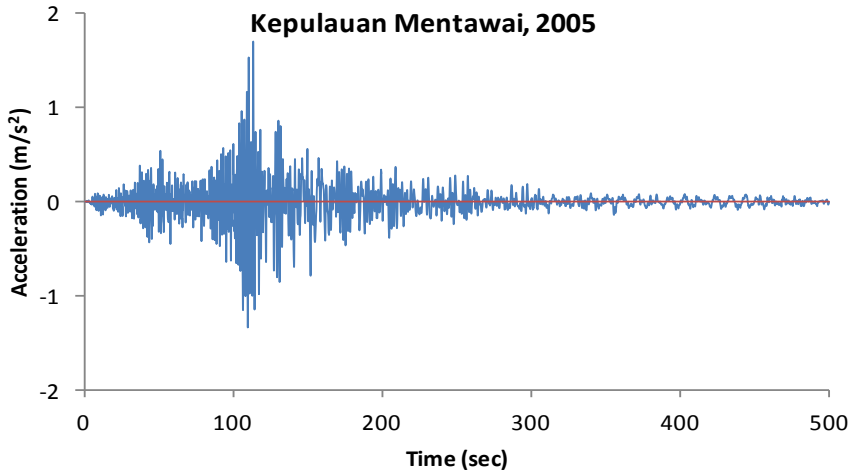

(b)

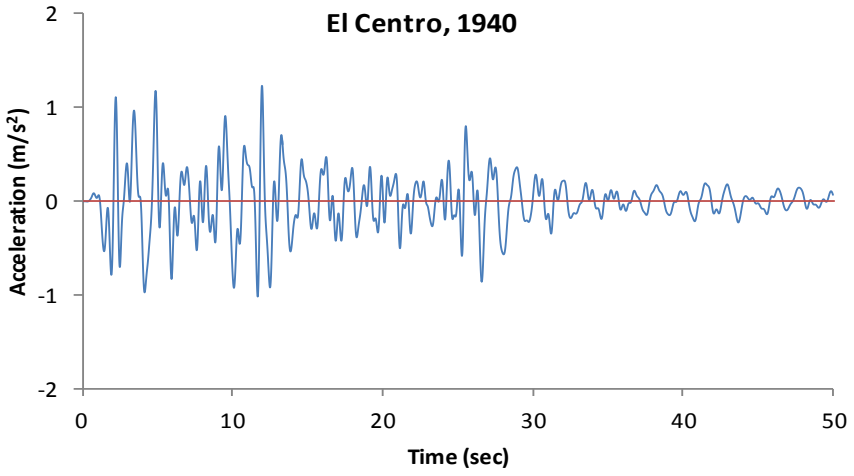

(c)

Figure 6-23 Computed raft acceleration histories: (a) with synthetic motion; (b) with 2005 Kepulauan Mentawai motion (c) with 1940 El Centro bedrock motion

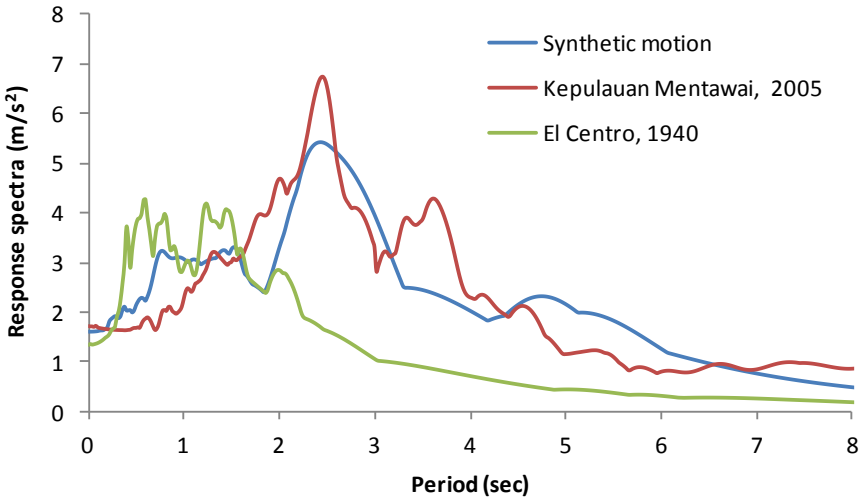

Figure 6-24 Comparison of pile raft response spectra subjected to different earthquake loadings

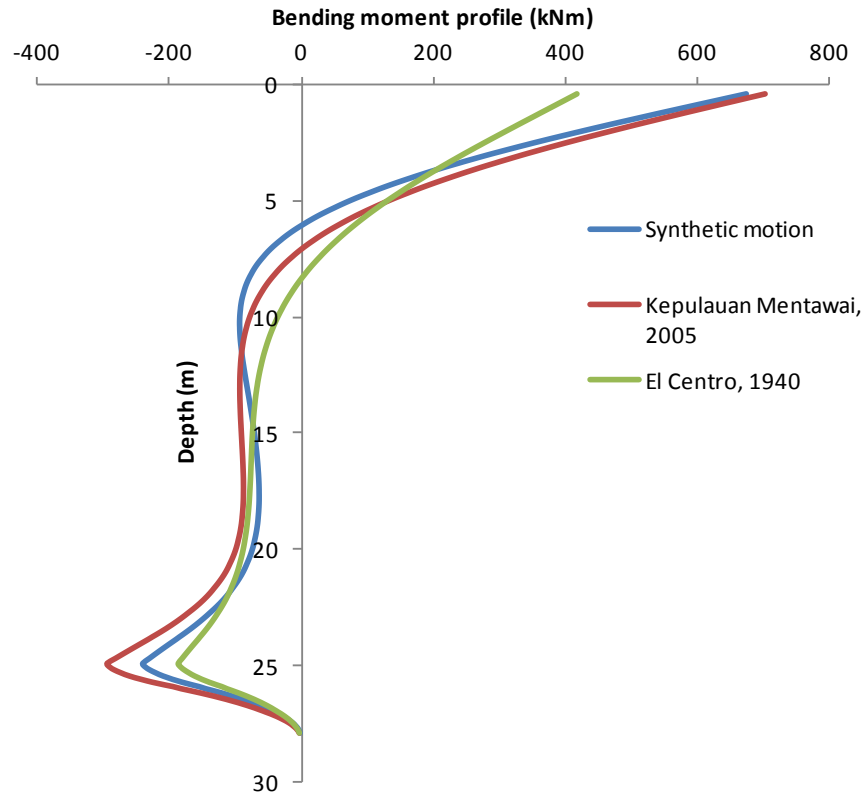

Figure 6-25 Comparison of maximum pile bending moment profiles subjected to different earthquake loadings

Chapter 7 Conclusions

7.1 Introduction

The interaction among soft soil, pile foundation and superstructure under earthquake loading is highly nonlinear and complex, and has not been studied systematically up till now. As stated in Chapter 2, most of the previous studies focused on either single piles or small pile groups, whose response may not be representative of larger pile foundation with dozens or more piles. Such large pile foundation are commonly used in the foundation systems for tall, heavy structures. However, the difference in performance between large pile foundation foundations and single pile or small pile foundation is still not clear, especially with regard to the seismic bending moments induced in the piles. As discussed in Chapter 2, this is largely due to the difficulties and challenges of carrying out realistic physical and numerical studies of such foundations under seismic shaking.

This research seeks to improve our understanding of the behaviour of realistic soil-pile-structure systems under seismic loading conditions, by performing large-scale parallel finite element analysis on a local network PC cluster. Details of the hardware specifications and the network configuration are presented in Chapter 3. This chapter also addresses and discusses the parallelization aspects related to the software development. In Chapter 4, the key features of the parallel dynamic finite element code GeoFEA for carrying out seismic soil-pile-structure analyses are highlighted and discussed. Validation analyses are then carried out using the measurements from centrifuge experiments involving small pile-groups. These

are followed by additional analyses using a much larger soil-pile-structure model that is representative of a typical block of residential flats in Singapore and its foundation system. In Chapter 5, parametric studies are carried out for the large soil-pile-structure model to examine the influence of the clay layer thickness, the clay shear modulus, the superstructural mass and the peak base acceleration. The results are processed and interpreted using dimensional analysis to obtain dimensionless expressions for the maximum pile bending moments at the pile-head and the clay-hard soil interface. In Chapter 6, additional analyses are carried out to examine the influence of other factors such as the superstructure's characteristics, uneven soil geometry and earthquakes with different frequency contents.

7.2 Summaries of research finding

7.2.1 Parallel finite element program

The dynamic undrained finite element formulation was derived using Galerkin's method and Newmark's integration scheme, and implemented in an existing geotechnical static finite element code GeoFEA. For efficient large-scale parallel computations, the EBE-MJPCG and EBE-GJSQMR iterative solvers were tested and implemented. The derivation of the Newton-Raphson method for dynamic time-stepping analysis was also presented, and incorporated into the code to handle the errors arising from non-linearity in the problem.

The hardware and software implementations for parallel processing in this study were presented. The high-speed networked computer resources in the NUS EIT laboratory were described, including some of the hardware limitations and how they were overcome. The finite element code features two levels of parallel architecture: message passing interface (MPI) approach and hyper-threading technology (OpenMP), which are both implemented in GeoFEA.

It was shown that the combination of (i) element-by-element approach, (ii) iterative solver and (iii) network PC cluster results in a highly efficient and cost-effective computational tool for large-scale finite element analyses.

7.2.2 Large-scale simulation

The finite element analysis of seismic soil-pile-structure interaction involves several special considerations, such as an appropriate constitutive soil model for soft clay under repeated loading, proper modelling of the piles to obtain accurate bending moment profiles, realistic pile-soil interface behaviour, and lateral boundary conditions that can minimize wave reflections and allow free-field ground response at an appropriate distance from the foundation. These specifications were discussed and implemented in the program, and validated with measurements from centrifuge experiments.

The results from the current finite element analyses show that, compared to a single pile, the individual piles in a pile foundation have larger displacements and larger maximum bending moments due to pile-soil-pile interaction. However, the pile-to-pile influence would reduce as the pile spacing increases, and could be

negligible when the pile spacing is larger than a certain critical value. The critical pile spacing is usually about five to nine pile diameters, and will reduce as the peak ground acceleration or the structural mass increase. Furthermore, with the same pile spacing, e.g. three pile diameters, both the pile raft displacement and maximum pile bending moment would increase as the pile foundation size increases. Hence, the present results indicate that the response of a large-scale pile foundation is greater than that of a single pile or small-scale pile group. Hence, for design and analysis of seismic pile response, it may not be conservative to treat the single pile or small-scale pile group as representative of a much larger pile foundation that supports a tall, heavy structure.

A large soil-pile-structure system that is representative of a typical block of residential flats in Singapore was analyzed with the 9x21 pile raft foundation subjected to seismic shaking. By comparing the results from different models, it was shown that, in order to reduce the influence of lateral boundary conditions, the horizontal extent of the soil domain should be larger than the sum of three times the foundation length and model depth. The results also show that the computed response of the pile raft is different from that at the bed rock or the far-field ground surface, both in terms of the maximum displacement and the response spectrum. Hence, in analyzing the seismic response of the building structure, it is not appropriate to ignore the interaction effects and simply apply the bedrock accelerations to the base of the structure.

The combination of a linear elastic soil model with Rayleigh damping may provide an approximate prediction of the pile foundation response subjected to earthquake loading, but it is difficult to determine the shear modulus of the soft soil which is dependant not only on the mean effective stress but also the seismic amplitude. The pseudo-static approach could also provide an approximate prediction of the maximum pile bending moment, but the distribution of the pile bending moments in the group may not be right.

7.2.3 Parametric studies

Using the large-scale finite element simulation method, the seismic soil-pile-superstructure analysis is extended to study the influence of different pile radiuses, soft soil depths, soft soil stiffness, superstructure mass and seismic acceleration amplitudes. The influence of each factor on the pile foundation response is discussed. By processing the results using dimensional analysis and data fitting, three semi-empirical dimensionless expressions for estimating the maximum bending moments and the critical pile length are obtained. Using these estimated moments and the critical pile length, together with the general trends of the computed bending moment profiles obtained from all the analyses, a simplified bending moment envelope is proposed for seismic pile foundation design.

7.2.4 Influence of Some Other Factors

The influence of the superstructure's characteristics, uneven soil geometries and earthquake motion characteristics on seismic soil-pile-structure interaction was discussed and examined. The approach using the raft acceleration from the lumped

mass analysis for structural computation was validated. For pile foundations located on a sloping bedrock, the pile at the shallower end experiences larger bending moments than the pile at the deeper end. When the earthquake excitation is perpendicular to the sloping bedrock, the phenomenon of pile raft torsion was illustrated. The wave trapping effects in subterranean valleys were also simulated. The factors are complicated and were neglected before, and should be studied systematically in future.

7.3 Suggestions for further research

Based on the work and findings in this study, the following suggestions for further research are proposed:

1. In this study, the superstructure was simplified as an equivalent lumped mass on the pile raft, which was shown to approximately capture the influence of the structural mass and the first natural period. However, such an approach may not capture the higher modes of response. In future studies, more detailed modeling of the superstructure should be performed to examine the influence of the structure type, the distribution of mass and the vibration modes, among others.
2. During seismic excitation, excess pore water pressure may be generated in soft clay. Even though the excess pore water pressure does not cause liquefaction in soft clay, it can sharply reduce the soil strength and stiffness. Furthermore, the dissipation of excess pore water pressure after the earthquake may produce additional settlement in the soil and increase the bearing pressure exerted by the pile foundation. Hence, the influence of plasticity effects associated with soft clay behaviour should be further discussed.

3. In this study, a two-layered soil stratigraphy was adopted, consisting of an upper soft clay layer overlying a harder soil layer or bedrock. Actual soil profiles may be more complicated, involving more soil layers with irregular thicknesses. Large bending moments may be generated in the piles at the interfaces between layers with significant stiffness contrast. Hence, the influence of more complex soil profiles on the pile response should be examined.
4. In section 6.3, it was shown that uneven soil layerings can significantly affect the pile foundation response. This situation is quite common in Singapore and should be studied systematically in more detail, especially with regard to the interface gradients and soil stiffness contrast.
5. In this study, the input earthquake accelerations are obtained by scaling an artificial earthquake time series. While this is acceptable for studying the influence of the peak ground acceleration on the pile response, it cannot account for different ground motion frequency distributions arising from different earthquake sources. The results presented in this study are valid for predominantly long-period ground motions caused by far-field earthquakes. Future studies should examine the pile responses due to predominantly short-period ground motions arising from near-field earthquakes.

The preceding suggestions for future research would contribute significantly to the understanding of seismic soil-pile-structure interaction, which will potentially lead to improvements in the state-of-the-practice for pile foundation analysis and design under earthquake conditions.

References

Abghari A. and Chai J.(1995) Modeling of Soil-Pile-Superstructure Interaction for Bridge Foundations, Performance of Deep Foundations Under Seismic Loading. pp. 45-59.

Adeli H. and Kamal O.(1992) Concurrent analysis of large structures—I. Algorithms. Computers & Structures 42:413-424. DOI: 10.1016/0045-7949(92)90037-z.

Agarwal P., Wood S., Kurtulus A., Menq F.-Y., Rathje E.M. and Stokoe K.(2010) Dynamic Field Tests of Small-scale Bridge Bents Supported on Drilled Shafts, NESS hub

Ahn K. and Gould P.L.(1989) Soil-pile-structure interaction effects on the seismic response of a cooling tower. Earthquake Engineering & Structural Dynamics 18:593-609

Akhter S. and Roberts J. (2007) Use OpenMP for programming parallel threads in multicore applications, http://www.eetimes.com/design/embedded/4007154/Use-OpenMP-for-programming-parallel-threads-in-multicore-applications-Part-1.

Amdahl G.M.(1968) The Validity of the Single-Processor Approach to Achieving Large-scale Computing Capabilities, in: A. City (Ed.), The American Federation of Information Processing Society

Badoni D. and Makris N.(1996) Nonlinear response of single piles under lateral inertial and seismic loads. Soil Dynamics and Earthquake Engineering 15:29-43. DOI: 10.1016/0267-7261(95)00027-5.

Banerjee S. (2009) Centrifuge and Numerical Modeling of Soft Clay-Pile-Raft Foundations Subjected to Seismic Shaking, Ph.D. thesis, in National University of Singapore.

Barrett R., Berry M., Chan T., Demmel J., Donato J., Dongarra J., Eijkhout V., Pozo R., Romine C. and van der Vorst H.(1994) Templates for the Solution of Linear Systems: Building Blocks for Iterative Methods, SIAM Press, Philadelphia.

Basile F.(2010) Kinematic Bending Moments in Pile Groups, 14th European Conference on Earthquake Engineering

Blaney G.W. and O'Neill M.W.(1989) Dynamic lateral response of a pile group in clay. Geotechnical Testing Journal 12:22-29

Bolton Seed H. and Lysmer J.(1978) Soil-structure interaction analyses by finite elements - State of the art. Nuclear Engineering and Design 46:349-365. DOI: 10.1016/0029-5493(78)90020-1.

Bosello C.A., Lazzari B. and Nibbi R.(2007) A viscous boundary condition with memory in linear elasticity. International Journal of Engineering Science 45:94-110. DOI: 10.1016/j.ijengsci.2006.07.013.

Boulanger R.W., Curras C.J., Kutter B.L., Wilson D.W. and Abghari A.(1999) Seismic soil-pile-structure interaction experiments and analyses. Journal of Geotechnical and Geoenvironmental Engineering 125:750-759. DOI: 10.1061/(asce)1090-0241(1999)125:9(750).

British Standards Institution.(2006) Eurocode 8 : design of structures for earthquake resistance. Part 4, Silos, tanks and pipelines, British Standards Institution, London.

Britto A.M. and Gunn M.J.(1987) Critical State Soil Mechanics via Finite Elements, Halsted Press, New York.

Brown D., Reese L. and O'Neill M.(1987) Cyclic Lateral Loading of a Large-Scale Pile Group. Journal of Geotechnical Engineering 113:1326-1343. DOI: doi:10.1061/(ASCE)0733-9410(1987)113:11(1326).

Brown D., Morrison C. and Reese L.(1988) Lateral Load Behavior of Pile Group in Sand. Journal of Geotechnical Engineering 114:1261-1276. DOI: doi:10.1061/(ASCE)0733-9410(1988)114:11(1261).

Brown D.A., O'Neill M.W., Hoit M., McVay M., El Naggar M.H. and Chakraborty S.(2001) Static and Dynamic Lateral Loading of Pile Groups, NCHRP Report, Transportation Research Board Business Office

Byrne P.M., Anderson D.L. and Janzen W.(1984) RESPONSE OF PILES AND CASINGS TO HORIZONTAL FREE-FIELD SOIL DISPLACEMENTS. Canadian Geotechnical Journal 21:720-725. DOI: 10.1139/t84-079.

Cai Y.X. (1995) Three-dimensional nonlinear analysis of seismic soil-pile-structure interaction and its application, D.Sc. thesis, in Washington University.

Castelli F. and Maugeri M.(2009) Simplified Approach for the Seismic Response of a Pile Foundation. Journal of Geotechnical and Geoenvironmental Engineering 135:1440-1451. DOI: 10.1061/(asce)gt.1943-5606.0000107.

Chacko M.J. (1995) Analysis of Dynamic Soil-pile-structure Interaction, Master thesis, in University of California, Davis.

Chan S.H., Phoon K.K. and Lee F.H.(2001) A modified Jacobi preconditioner for solving ill-conditioned Biot's consolidation equations using symmetric quasi-minimal residual method. International Journal for Numerical and Analytical Methods in Geomechanics 25:1001-1025

Chang D. (2007) Inertial and lateral spreading demands on soil-pile-structure systems in liquefied and laterally spreading ground during earthquakes, Ph.D. thesis, in University of California, Davis.

Chau K.T., Shen C.Y. and Guo X.(2009) Nonlinear seismic soil-pile-structure interactions: Shaking table tests and FEM analyses. Soil Dynamics and Earthquake Engineering 29:300-310. DOI: 10.1016/j.soildyn.2008.02.004.

Chen X. (2006) Preconditioners for iterative solutions of large-scale linear systems arising from Biot's consolidation equations, Ph.D. thesis, in National University of Singapore.

Chen X. and Phoon K.K.(2009) Some numerical experiences on convergence criteria for iterative finite element solvers. Computers and Geotechnics 36:1272-1284. DOI: 10.1016/j.compgeo.2009.05.012.

Chopra A.K.(2007) Dynamics of Structures: Theory and Applications to Earthquake Engineering, Prentice Hall

Chu D. (2006) Three-dimensional nonlinear dynamic analysis of soil-pile-structure interaction, D.Sc. thesis, in Washington University.

Crouse C. and Cheang L.N.(1987) Dynamic Testing and Analysis of Pile-Group Foundation, in: T. Nogami (Ed.), Dynamic response of pile foundations--experiment, analysis, and observation, New York. pp. 79-98.

Curras C.J., Boulanger R.W., Kutter B.L. and Wilson D.W.(2001) Dynamic experiments and analyses of a pile-group-supported structure. Journal of Geotechnical and Geoenvironmental Engineering 127:585-596. DOI: 10.1061/(asce)1090-0241(2001)127:7(585).

Dasari G.R. (1996) Modelling the Variation of Soil Stiffness During Sequential Construction, Ph.D. thesis, in Cambridge University.

Day R.A. and Potts D.M.(1994) Zero thickness interface elements—numerical stability and application. International Journal for Numerical and Analytical Methods in Geomechanics 18:689-708. DOI: 10.1002/nag.1610181003.

Deng Q.(2003) An optimal parallel nonoverlapping domain decomposition iterative procedure. SIAM Journal on Numerical Analysis 41:964-982. DOI: 10.1137/s0036142902401281.

Desai C.S., Zaman M.M., Lightner J.G. and Siriwardane H.J.(1984) Thin-layer element for interfaces and joints. International Journal for Numerical and Analytical Methods in Geomechanics 8:19-43. DOI: 10.1002/nag.1610080103.

Dezi F., Carbonari S. and Leoni G.(2009) A model for the 3D kinematic interaction analysis of pile groups in layered soils. Earthquake Engineering & Structural Dynamics 38:1281-1305. DOI: 10.1002/eqe.892.

Dezi F., Carbonari S. and Leoni G.(2010) Kinematic bending moments in pile foundations. Soil Dynamics and Earthquake Engineering 30:119-132. DOI: 10.1016/j.soildyn.2009.10.001.

Dobry R. and O'Rourke M.(1983) Discussion of “Seismic Response Of End-bearing Piles” by Raul Flores Berrones and Robert V. Whitman (April, 1982).

Journal of Geotechnical Engineering 109:778-781. DOI: doi:10.1061/(ASCE)0733-9410(1983)109:5(778).

Duff I.S., Erisman A.M. and Reid J.K.(1989) Direct Methods for Sparse Matrices, Oxford University Press, USA

Duncan J.M. and Chang C.-Y.(1970) Nonlinear Analysis of Stress and Strain in Soils. Journal of the Soil Mechanics and Foundations Division (ASCE) 96:1629-1653

Duncan J.M. and Buchignani A.L.(1987) An engineering manual for settlement studies

Dungca J.R., Kuwano J., Takahashi A., Saruwatari T., Izawa J., Suzuki H. and Tokimatsu K.(2006) Shaking table tests on the lateral response of a pile buried in liquefied sand. Soil Dynamics and Earthquake Engineering 26:287-295. DOI: 10.1016/j.soildyn.2005.02.021.

Dupros F., De Martin F., Foerster E., Komatitsch D. and Roman J.(2010) High-performance finite-element simulations of seismic wave propagation in three-dimensional nonlinear inelastic geological media. Parallel Computing 36:308-325. DOI: 10.1016/j.parco.2009.12.011.

Elahi H., Moradi M., Poulos H.G. and Ghalandarzadeh A.(2010) Pseudostatic approach for seismic analysis of pile group. Computers and Geotechnics 37:25-39. DOI: 10.1016/j.compgeo.2009.07.001.

Elgamal A., Lu J. and Yan L.(2008) Large Scale Computational Simulation in Geotechnical Earthquake Engineering, The 12th International Conference of International Association for Computer Methods and Advances in Geomechanics (IACMAG), Goa, India

Erhel J., Traynard A. and Vidrascu M.(1991) An element-by-element preconditioned conjugate gradient method implemented on a vector computer. Parallel Computing 17:1051-1065

Estorff O.v. and Firuziaan M.(2000) Coupled BEM/FEM approach for nonlinear soil/structure interaction. Engineering Analysis with Boundary Elements 24:715-725. DOI: 10.1016/s0955-7997(00)00054-0.

Fan K., Gazetas G., Kaynia A., Kausel E. and Ahmad S.(1991) Kinematic seismic response of single piles and pile groups. Journal of Geotechnical Engineering 117:1860-1879

Finlayson.(1972) The Method of Weighted Residuals and Variational Principles, with Application in Fluid Mechanics, Heat and Mass Transfer, Elsevier Science

Finn W.D.L.(2005) A study of piles during earthquakes: Issues of design and analysis. Bulletin of Earthquake Engineering 3:141-234. DOI: 10.1007/s10518-005-1241-3.

Fox R.L. and Stanton E.L.(1968) DEVELOPMENTS IN STRUCTURAL ANALYSIS BY DIRECT ENERGY MINIMIZATION. Aiaa Journal 6:1036-&. DOI: 10.2514/3.4670.

Fried I.(1969) MORE ON GRADIENT ITERATIVE METHODS IN FINITE-ELEMENT ANALYSIS. Aiaa Journal 7:565-&. DOI: 10.2514/3.5166.

Fukouka M.(1966) Damage to Civil Engineering Structures. Soils and Foundation 6:45-52

Fukuoka M.(1966) Damage to Civil Engineering Structures. Soils and Foundations 1:45-52

Gazetas G., Fan K., Kaynia A. and Kausel E.(1991) DYNAMIC INTERACTION FACTORS FOR FLOATING PILE GROUPS. Journal of Geotechnical Engineering-Asce 117:1531-1548. DOI: 10.1061/(asce)0733-9410(1991)117:10(1531).

George A., Heath M.T., Liu J. and Ng E.(1986) Solution of sparse positive definite systems on a shared-memory multiprocessor. International Journal of Parallel Programming 15:309-325. DOI: 10.1007/bf01407878.

Girault P.(1986) Analysis of Foundation Failures, The Mexico Earthquake, 1985 -- Factors Involved and Lessons Learned, ASCE

Goh S.H. and O'Rourke T.D.(2008) Soil-pile interaction during liquefaction-induced lateral spread. Journal of Earthquake and Tsunami 2:53-85. DOI: 10.1142/s1793431108000232.

Gohl W.B. (1991) Response of pile foundations to simulated earthquake loading: Experimental and analytical results, Ph.D. thesis, in The University of British Columbia (Canada).

Gu Q. (2008) Finite element response sensitivity and reliability analysis of Soil-Foundation-Structure-Interaction (SFSI) systems, Ph.D. thesis, in University of California, San Diego.

Guin J. and Banerjee P.K.(1998) Coupled soil-pile-structure interaction analysis under seismic excitation. Journal of Structural Engineering 124:434-444

Gullerud A.S. and Dodds R.H.(2001) MPI-based implementation of a PCG solver using an EBE architecture and preconditioner for implicit, 3-D finite element analysis. Computers & Structures 79:553-575. DOI: 10.1016/s0045-7949(00)00153-x.

Gummadi L.N.B. and Palazotto A.N.(1997) Nonlinear finite element analysis of beams and arches using parallel processors. Computers & Structures 63:413-428. DOI: 10.1016/s0045-7949(96)00343-4.

Hadjian A.H., Fallgren R.B. and Tufenkjian M.R.(1992) Dynamic Soil-Pile-Structure Interaction—The State-of-Practice. Geotechnical Special Publication, ASCE 34:1-26

Hamada M.(1991) Damage to Piles by Liquefaction-Induced Ground Displacements, 3rd US Conference Lifeline Earthquake Engineering, Los Angeles. pp. 1172-1181.

Hardin B.O. and Drnevich V.P.(1972) SHEAR MODULUS AND DAMPING IN SOILS: MEASUREMENT AND PARAMETER EFFECTS. ASCE J Soil Mech Found Div 98:603-624

Hashash Y.M.A., Hook J.J., Schmidt B. and I-Chiang Yao J.(2001) Seismic design and analysis of underground structures. Tunnelling and Underground Space Technology 16:247-293. DOI: 10.1016/s0886-7798(01)00051-7.

Hearn E.J.(1997) Mechanics of materials volume 1 an introduction to the mechanics of elastic and plastic deformation of solids and structural materials, Butterworth-Heinemann,, Oxford England. pp. 2 v. ill. 25 cm.

Hibbitt K.S., I.N.C.(1997) Abaqus/Standard User's Manual

Hilber H.M., Hughes, T.J.R. and Taylor, R.L.(1977) Improved Numerical Dissipation for Time Algorithms in Structural Dynamics. Earthquake Engineering & Structural Dynamics 5:283-292

Hipp M. and Rosenstiel W.(2004) Parallel Hybrid Particle Simulations Using MPI and OpenMP

Euro-Par 2004 Parallel Processing, in: M. Danelutto, et al. (Eds.), Springer Berlin / Heidelberg. pp. 189-197.

Horikoshi K., Tateishi A. and Ohtsu H.(2000) Detailed investigation of piles damaged by Hyogoken Nambu earthquake, in: N. Z. Silverstream (Ed.), 12th world congress on earthquake engineering, Auckland, New Zealand

Hosni S. (1993) A study of the implications of soil-structure interaction effects on the seismic response of high-rise reinforced concrete buildings, Ph.D. thesis, in McMaster University (Canada).

Houbolt J.C.(1950) A Recurrence Matrix Solution for the Dynamic Response of Elastic Aircraft. Journal of the Aeronautical Sciences 17:540-550

Hsieh Y.-M. (2004) Parallel Computation in Effecient Non-Linear Finite Element Analysis with Applications to Soft-Ground Tunneling Project, Ph.D. thesis, in Massachusetts Institute of Technology.

Huang Y., Zhang F., Yashima A. and Ye W.(2008) Numerical simulation of mitigation for liquefaction-induced soil deformations in a sandy ground improved by cement grouting. Environmental Geology 55:1247-1252. DOI: 10.1007/s00254-007-1069-z.

Huang Y., Zhang F., Yashima A., Sawada K., Ye G.-L. and Kubota N.(2004) Three-dimensional numerical simulation of pile-soil seismic interaction in saturated deposits with liquefiable sand and soft clay., in: M. Yuan and W. Zhong (Eds.), the Sixth World Congress on Computational Mechanics in

Conjunction with the Second Asian-Pacific Congress on Computational Mechanics, Beijing, China

Hughes T.J.R.(1990) The Finite Element Method, Prentice-Hall

Hughes T.J.R., Levit I. and Winget J.(1983a) An element-by-element solution algorithm for problems of structural and solid mechanics. Computer Methods in Applied Mechanics and Engineering 36:241-254

Hughes T.J.R., Ferencz R.M. and Hallquist J.O.(1987) Large-scale vectorized implicit calculations in solid mechanics on Cray X-MP/48 utilizing EBE preconditioned conjugate gradients. Computer Methods in Applied Mechanics and Engineering 61:215-248

Hughes T.J.R., Winget J., Levit I. and Tezduyar T.E.(1983b) New alternating direction procedures in finite element analysis based upon EBE approximate factorizations. Computer Methods for nonlinear solids and structural mechanics 54:75-109

Hyodo M., Tanimizu H., Yasufuku N. and Murata H.(1994) Undrained cyclic and monotonic triaxial behaviour of saturated loose sand. Soils and Foundations 34:19-32

Idriss I.M. and Sun J.I.(1992) User's manual for SHAKE91: a computer program for conducting equivalent linear seismic response analyses of horizontally layered soil deposits, University of California, Davis

Idriss I.M., Dobry R. and Singh R.D.(1978) NONLINEAR BEHAVIOR OF SOFT CLAYS DURING CYCLIC LOADING. ASCE J Geotech Eng Div 104:1427-1447

Ilankatharan M. (2008) Centrifuge modeling for soil-pile-bridge systems with numerical simulations accounting for soil-container-shaker interaction, Ph.D. thesis, in University of California, Davis.

Ilankatharan M., Kutter B.L., Shin H., Arduino P., Kramer S.L., Johnson N. and Sasaki T.(2006) Comparison of centrifuge and 1 g shake table models of a pile supported bridge structure, Hong Kong. pp. 1313-1318.

Institute A.P.(1993) Recommended Practice for Planning, Designing and Constructing Fixed Offshore Platforms

Institute A.P.(2006) Recommended Practice for Planning, Designing and Constructing Fixed Offshore Platforms—Working Stress Design, API RECOMMENDED PRACTICE 2A-WSD

International Code Council., Building Officials and Code Administrators International., International Conference of Building Officials. and Southern Building Code Congress International.(2009) International building code 2009, International Code Council, Country Club Hills, Ill.

Irons B.M.(1970) A frontal solution program for finite element analysis. International Journal for Numerical Methods in Engineering 12:5-32

Ishibashi I. and Zhang X.(1993) Unified dynamic shear moduli and damping ratios of sand and clay. Soils and Foundations 33:182-191

Iwasaki T.(1972a) Earthquake-resistant design of bridges in Japan, Public Works Research Institute, Ministry of Construction

Iwasaki T.(1972b) Earthquake-resistant design of bridges in Japan, Ministry of Construction, Tokyo.

Jakrapiyanun W. (2002) Physical modeling of dynamics soil-foundation-structure-interaction using a laminar container, Ph.D. thesis, in University of California, San Diego.

Jardine R.J., Potts D.M., Fourie A.B. and Burland J.B.(1986) STUDIES OF THE INFLUENCE OF NONLINEAR STRESS-STRAIN CHARACTERISTICS IN SOIL STRUCTURE INTERACTION. Geotechnique 36:377-396

Javan M.R.M., Noorzad A. and Namin M.L.(2008) Three-dimensional nonlinear finite element analysis of pile groups in saturated porous media using a new transmitting boundary. International Journal for Numerical and Analytical Methods in Geomechanics 32:681-699. DOI: 10.1002/nag.642.

Johnson N. (2006) Large-scale experimental and analytical seismic studies of a two-span reinforced concrete bridge system, Ph.D. thesis, in University of Nevada, Reno.

Kagawa T.(1980) SRANG: User's Manual, Houston, Texas

Kagawa T.(1981) Seismic soil-pile-structure interaction: pile groups, McClelland Engineers, Inc.

Kagawa T.(1983a) DYNAMIC LATERAL PILE-GROUP EFFECTS. Journal of Geotechnical Engineering 109:1267-1285

Kagawa T.(1983b) NONSPS (Nonlinear Response Analysis of Soil-Pile-Structure Systems): User's Manual, Houston, Texas

Kagawa T.(1983c) LATERAL PILE-GROUP RESPONSE UNDER SEISMIC LOADING. Soils and Foundations 23:75-86

Kagawa T.(1992) Moduli and damping factors of soft marine clays. Journal of Geotechnical Engineering 118:1360-1375

Kagawa T., Minowa C., Mizuno H., Abe A. and Earthquake Engn Res I.(1994) SHAKING-TABLE TESTS ON PILES IN LIQUEFYING SAND, Fifth U.S National Conference on Earthquake Engineering - Earthquake Awareness and Mitigation across the Nation, Proceedings, Vol Iv. pp. 107-116.

Kagawa T., Sato M., Minowa C., Abe A. and Tazoh T.(2004) Centrifuge simulations of large-scale shaking table tests: Case studies. Journal of Geotechnical and Geoenvironmental Engineering 130:663-672. DOI: 10.1061/(asce)1090-0241(2004)130:7(663).

Kashiyama K., Tanaka S. and Sakuraba M.(2002) PC cluster parallel finite element analysis of sloshing problem by earthquake using different network environments. Communications in Numerical Methods in Engineering 18:681-690. DOI: 10.1002/cnm.527.

Kavvadas M. and Gazetas G.(1993) Kinematic seismic response and bending of free-head piles in layered soil. Geotechnique 43:207-222

Kawakami F. and Asada A.(1966a) Damage to the Ground and Earth Structures by the Niigata Earthquake of June 16, 1964. Soils and Foundation 6:14-30

Kawakami F. and Asada A.(1966b) Damage to the ground and earth structures by the Niigata earthquake of June 16, 1964. Soils and Foundations 6:14-30

Kaynia A.M. (1982) Dynamic Stiffness and Seismic Response of Pile Groups, thesis, in Massachusetts Institute of Technology.

Kim J.K., Koh H.M., Kwon K.J. and Yi J.S.(2000) A three-dimensional transmitting boundary formulated in Cartesian co-ordinate system for the dynamics of non-axisymmetric foundations. Earthquake Engineering & Structural Dynamics 29:1527-1546. DOI: 10.1002/1096-9845(200010)29:10<1527::aid-eqe978>3.0.co;2-s.

Kobori T., Nakazawa M., Hijikata K., Kobayashi Y., Miura K., Miyamoto Y. and Moroi T.(1991) STUDY ON DYNAMIC CHARACTERISTICS OF A PILE GROUP FOUNDATION. Second International Conference on Recent Advances in Geotechnical Earthquake Engineering and Soil Dynamics, Vols 1 and 2:853-860

Kokusho T., Yoshida Y. and Esashi Y.(1982) DYNAMIC PROPERTIES OF SOFT CLAY FOR WIDE STRAIN RANGE. Soils and Foundations 22:1-18

Komatitsch D. and Tromp J. (2001) Modeling Seismic Wave Propagation on a 156GB PC Cluster, http://www.linuxjournal.com/article/4671.

Komatitsch D. and Tromp J.(2003) A perfectly matched layer absorbing boundary condition for the second-order seismic wave equation. Geophysical Journal International 154:146-153. DOI: 10.1046/j.1365-246X.2003.01950.x.

Komatitsch D., Tsuboi S., Chen J. and Tromp J.(2003) A 14.6 billion degrees of freedom, 5 teraflops, 2.5 terabyte earthquake simulation on the Earth Simulator, Supercomputing, 2003 ACM/IEEE Conference. pp. 4-4.

Kong D.S., Li C.J., Ling X.Z. and Men Y.Q.(2011) Shaking table tests on pile group-soil-structure interaction to seismic loading on liquefied ground. Yantu Gongcheng Xuebao/Chinese Journal of Geotechnical Engineering 33:143-149

Kuhlemeyer R.L.(1979) Static and Dynamic Laterally Loaded Floating Piles. Journal of the Geotechnical Engineering Division-Asce 105:289-304

Kumar S. and Adeli H.(1995) Distributed Finite-Element Analysis on Network of Workstations---Implementation and Applications. Journal of Structural Engineering 121:1456-1462

Laemmer L., Meissner U.F. and Ruben J.(2003) Finite element modelling of soil-structure systems in workstation clusters, in: K. J. Bathe (Ed.), Computational Fluid and Solid Mechanics 2003, Elsevier Science Ltd, Oxford. pp. 2312-2316.

Lam I.P. and Cheang L.(1995) Dynamic soil-pile interaction behavior in submerged sands, ASCE, San Diego, CA, USA. pp. 110-135.

Law K.H. and Mackay D.R.(1993) A parallel row-oriented sparse solution method for finite element structural analysis. International Journal for Numerical Methods in Engineering 36:2895-2919. DOI: 10.1002/nme.1620361704.

Lee F.H., Phoon K.K., Lim K.C. and Chan S.H.(2002) Performance of Jacobi preconditioning in Krylov subspace solution of finite element equations. International Journal for Numerical and Analytical Methods in Geomechanics 26:341-372. DOI: 10.1002/nag.204.

Leong E.C., Anand S., Cheong H.K. and Pan T.C.(2003) In-situ measurement of shear wave velocities at two soft soil sites in Singapore, Third Pacific Conference on Earthquake Engineering, Melbourne, Australia

Li P., Ren H., Lu X., Song H. and Chen Y.(2007) Shaking table testing of hard layered soil-pile-structure interaction system. Frontiers of Architecture and Civil Engineering in China 1:346-352. DOI: 10.1007/s11709-007-0046-7.

Lim K.C. (2003) Three-dimensional finite element analysis of earth pressure balance tunneling, Ph. D. thesis, in National University of Singapore.

Liu Y., Zhou W. and Yang Q.(2007) A distributed memory parallel element-by-element scheme based on Jacobi-conditioned conjugate gradient for 3D finite element analysis. Finite elements in analysis and design 43:494-503. DOI: 10.1016/j.finel.2006.12.007.

Liyanapathirana D.S. and Poulos H.G.(2005) Pseudostatic approach for seismic analysis of piles in liquefying soil. Journal of Geotechnical and Geoenvironmental Engineering 131:1480-1487. DOI: 10.1061/(asce)1090-0241(2005)131:12(1480).

Lok M.H. (1999) Numerical modeling of seismic soil-pile-superstructure interaction in soft clay, Ph.D. thesis, in University of California, Berkeley.

Lok T.M., Pestana J.M. and Seed R.B.(1998) Numerical modeling and simulation of coupled seismic soil-pile-structure interaction. Geotechnical Special Publication:1211-1222

Lu C.W., Oka F. and Zhang F.(2008) Analysis of soil-pile-structure interaction in a two-layer ground during earthquakes considering liquefaction. International Journal for Numerical and Analytical Methods in Geomechanics 32:863-895. DOI: 10.1002/nag.646.

Lu J. (2006) Parallel finite element modeling of earthquake ground response and liquefaction, Ph.D. thesis, in University of California, San Diego.

Lu X., Li P., Chen B. and Chen Y.(2005) Computer simulation of the dynamic layered soil-pile-structure interaction system. Canadian Geotechnical Journal 42:742-751. DOI: 10.1139/t05-016.

Lysmer J. and Kuhlemeyer R.L.(1969) Finite Dynamic Model For Infinite Media. Journal of the Engineering Mechanics Division, ASCE 95:859-878

Ma K. (2010) Dynamic pile-raft-soil interaction in soft clay condition during earthquakes, Ph.D. thesis, in SiChuan University.

Mahboubi A. and Panaghi K.(2010) Analysis of the effect of pile length in a pile group on the transfer and impedance functions in soil-pile interaction models, Trondheim. pp. 429-433.

Maheshwari B.K. and Sarkar R.(2011) Seismic behavior of soil-pile-structure interaction in liquefiable soils: Parametric study. International Journal of Geomechanics 11:335-347. DOI: 10.1061/(asce)gm.1943-5622.0000087.

Maheshwari B.K., Truman K.Z., El Naggar M.H. and Gould P.L.(2004a) Three-dimensional nonlinear analysis for seismic soil-pile-structure interaction. Soil Dynamics and Earthquake Engineering 24:343-356. DOI: 10.1016/j.soildyn.2004.01.001.

Maheshwari B.K., Truman K.Z., El Naggar M.H. and Gould P.L.(2004b) Three-dimensional nonlinear analysis for seismic soil–pile-structure interaction. Soil Dynamics and Earthquake Engineering 24:343-356. DOI: 10.1016/j.soildyn.2004.01.001.

Maheshwari B.K., Truman K.Z., El Naggar M.H. and Gould P.L.(2004c) Three-dimensional finite element nonlinear dynamic analysis of pile groups for lateral transient and seismic excitations. Canadian Geotechnical Journal 41:118-133. DOI: 10.1139/t03-073.

Maiorano R.M.S., de Sanctis L., Aversa S. and Mandolini A.(2009) Kinematic response analysis of piled foundations under seismic excitation. Canadian Geotechnical Journal 46:571-584. DOI: 10.1139/t09-004.

Makris N., Tazoh T., Yun X. and Fill A.C.(1997) Prediction of the measured response of a scaled soil-pile-superstructure system. Soil Dynamics and Earthquake Engineering 16:113-124. DOI: 10.1016/s0267-7261(96)00037-1.

Margason E.(1975) Pile bending during earthquakes, ASCE-UC/Berkeley Seminar on Design Construction and Per-formance of Deep Foundations

Masin D.(2012) Hypoplastic Cam-clay model. Geotechnique 62:549-553. DOI: 10.1680/geot.11.T.019.

Matasovic N. and Vucetic M.(1995) Generalized cyclic-degradation-pore-pressure generation model for clays. Journal of Geotechnical Engineering - ASCE 121:33-42

Matlock H., Foo S.H.C. and Bryant L.M.(1978) SIMULATION OF LATERAL PILE BEHAVIOR UNDER EARTHQUAKE MOTION v:600-619

McClelland B. and Focht J.(1956) Soil Modulus for Laterally Loaded Piles. Journal of the Soil Mechanics and Foundations Division (ASCE) 82:1-22

McCullouch D. and Bonilla M.(1967) Railroad Damage in the Alaska Earthquake. Journal of Soil Mechanics and Foundation Division (ASCE) 93:89-100

Meem J.C., Thomson T.K., Niederhoff A.E., White L., Chang Y.L. and Krynine D.P.(1937) Discussion of "Lateral Pile-Loading Tests". Transactions of the American Society of Civil Engineers 102:255-282

Meymand P.J. (1998) Shaking table scale model tests of nonlinear soil-pile-superstructure interaction in soft clay, Ph.D. thesis, in University of California, Berkeley.

Miao L.F., Goh A.T.C., Wong K.S. and Teh C.I.(2006) Three-dimensional finite element analyses of passive pile behaviour. International Journal for Numerical and Analytical Methods in Geomechanics 30:599-613

Mitrofanov A. (2008) Intel X58 and ASUS P6T Deluxe, http://www.digital-daily.com/motherboard/intel_x58_and_asus_p6t_deluxe/print.

Miwa S., Ikeda T. and Sato T.(2006) Damage process of pile foundation in liquefied ground during strong ground motion. Soil Dynamics and Earthquake Engineering 26:325-336. DOI: 10.1016/j.soildyn.2005.05.001.

Mizuno H.(1987) Pile Damage During Earthquake in Japan (1923-1983), Dynamic Response of Pile Foundations—Experiment, Analysis and Observation. pp. 53-78.

Mizuno H., Liba M. and Kitagawa Y.(1984) Shaking Table Testing of Seismic Building-Pile-Two Layered-Soil Interaction, EIGHTH WORLD CONFERENCE ON EARTHQUAKE ENGINEERING, SAN FRANCISCO, CALIFORNIA. pp. 649-656.

Motamed R. and Towhata I.(2010) Shaking table model tests on pile groups behind quay walls subjected to lateral spreading. Journal of Geotechnical and Geoenvironmental Engineering 136:477-489. DOI: 10.1061/(asce)gt.1943-5606.0000115.

Mylonakis G.(2001) Simplified model for seismic pile bending at soil layer interfaces. Soils and Foundations 41:47-58

Newmark N.M.(1959) A Method of Computation for Structural Dynamics. Journal of Engineering Mechanics Division, ASCE:67-94

Nikolaou S., Mylonakis G., Gazetas G. and Tazoh T.(2001) Kinematic pile bending during earthquakes: Analysis and field measurements. Geotechnique 51:425-440. DOI: 10.1680/geot.51.5.425.39973.

Nishimura S., Minh N.A. and Jardine R.J.(2007) Shear strength anisotropy of natural London Clay. Geotechnique 57:49-62. DOI: 10.1680/geot.2007.57.1.49.

Niu J. (1997) Centrifuge modelling of earthquake effects on sand and soft clay strata, Master thesis, in National University of Singapore.

Nogami T., Otani J., Konagai K. and Chen H.L.(1992) NONLINEAR SOIL-PILE INTERACTION-MODEL FOR DYNAMIC LATERAL MOTION. Journal of Geotechnical Engineering-Asce 118:89-106. DOI: 10.1061/(asce)0733-9410(1992)118:1(89).

Nuttli O.W.(1973) The Mississippi Valley earthquakes of 1811 and 1812: Intesities, ground motion and magnitudes. Bulletin of the Seismological Society of America 63:227-248

Papadrakakis M. and Dracopoulos M.C.(1991) Improving the efficiency of incomplete Choleski preconditionings. Communications in Applied Numerical Methods 7:603-612. DOI: 10.1002/cnm.1630070806.

Parra E., Adalier K., Elgamal A.W., Zeghal M. and Ragheb A.(1996) Analyses and modeling of site liquefaction using centrifuge tests, 11th World Conference on Earthquake Engineering, Acapulco, Mexico

Pastor M., Zienkiewicz O.C. and Chan A.H.C.(1990) Generalized plasticity and the modelling of soil behaviour. International Journal for Numerical and Analytical Methods in Geomechanics 14:151-190. DOI: 10.1002/nag.1610140302.

Peng J., Lu J., Law K.H. and Elgamal A.(2004) ParCYCLIC: Finite element modelling of earthquake liquefaction response on parallel computers. International Journal for Numerical and Analytical Methods in Geomechanics 28:1207-1232. DOI: 10.1002/nag.384.

Petropoulos G. (2008) Soil-structure interaction analysis using high-performance parallel computation, Ph.D. thesis, in University of California, Berkeley.

Phoon K.-K.(2004) Iterative Solution of Large-Scale Consolidation and Constrained Finite Element Equations for 3D Problems, International e-Conference on Modern Trends in Foundation Engineering: Geotechnical Challenges and Solutions, IIT Madras, India

Phoon K.-K., Chan S.-H., Toh K.-C. and Lee F.-H.(2003) Fast iterative solution of large undrained soil-structure interaction problems. International Journal for Numerical and Analytical Methods in Geomechanics 27:159-181. DOI: 10.1002/nag.268.

Phoon K.K., Toh K.C., Chan S.H. and Lee F.H.(2002) An efficient diagonal preconditioner for finite element solution of Biot's consolidation equations. International Journal for Numerical Methods in Engineering 55:377-400. DOI: 10.1002/nme.500.

Potts D.M. and Ganendra D.(1991) Discussion on Finite Element Analysis of the Collapse of Reinforced Embankments on Soft Ground. Geotechnique 41:627-630

Puri V.K. and Prakash S.(2008) Pile design in liquefycing soil, 24th world conference on earthquake engineering, Beijing, China

Pyke R.M.(1979) Nonlinear soil models for irregular cyclic loadings. Journal Geotechnical Engineering Division, ASCE 105:715-726

Randolph M.F.(1981) THE RESPONSE OF FLEXIBLE PILES TO LATERAL LOADING. Geotechnique 31:247-259

Rizos D.C. and Wang Z.(2002) Coupled BEM-FEM solutions for direct time domain soil-structure interaction analysis. Engineering Analysis with Boundary Elements 26:877-888. DOI: 10.1016/s0955-7997(02)00057-7.

Rollins, Peterson K. and Weaver.(1998) Lateral Load Behavior of Full-Scale Pile Group in Clay. Journal of Geotechnical and Geoenvironmental Engineering 124:468-478. DOI: doi:10.1061/(ASCE)1090-0241(1998)124:6(468).

Rollins K., Gerber T., Lane J. and Ashford S.(2005) Lateral Resistance of a Full-Scale Pile Group in Liquefied Sand. Journal of Geotechnical and Geoenvironmental Engineering 131:115-125. DOI: doi:10.1061/(ASCE)1090-0241(2005)131:1(115).

Rollins K.M., Johnson S.R., Petersen K.T. and Weaver T.J.(2003) Static and dynamic lateral load behavior of pile groups based on full-scale testing, in: J. S. Chung and T. Matsui (Eds.), Proceedings of the Thirteenth. pp. 506-513.

Ross G., Seed H. and Migliacio R.(1973) Performance of highway bridge foundations, The Great Alaska Earthquake of 1964 -- Engineering, Comm. on the Alaskan Earthquake of the Division of Earth Sciences, Washton, D.C.

Rovithis E., Kirtas E. and Pitilakis K.(2009) Experimental p-y loops for estimating seismic soil-pile interaction. Bulletin of Earthquake Engineering 7:719-736. DOI: 10.1007/s10518-009-9116-7.

Saad Y.(1996) Iterative method for sparse linear systems, PWS Publishing Company, Boston.

Saitoh M.(2005) Fixed-head pile bending by kinematic interaction and criteria for its minimization at optimal pile radius. Journal of Geotechnical and Geoenvironmental Engineering 131:1243-1251. DOI: 10.1061/(asce)1090-0241(2005)131:10(1243).

Sakajo S., Chai J.C., Nakajima K. and Maeda M.(1995) Effect of group pile on liquefaction resistance of sandy ground, in: K. Ishihara (Ed.), 1st International Conference on Earthquake Geotechnical Engineering, TOKYO, JAPAN. pp. 755-760.

Sanctis L.d., Maiorano R.M.S. and Aversa S.(2010) A method for assessing kinematic bending moments at the pile head. Earthquake Engineering & Structural Dynamics 39:1133-1154. DOI: 10.1002/eqe.996.

Sato M., Harada H., Hasegawa A. and Ishikawa Y.(2001) Cluster-enabled OpenMP: An OpenMP compiler for the SCASH software distributed shared memory system. Scientific Programming 9:123-130

Scoot R., Tsai C., Steussy D. and Ting J.(1982) Full-Scale Dynamic Lateral Pile Tests, 12th Offshore Technology Conference, Houston. pp. 435-450.

Scott R.F., Ting J.M., Tsai C.F. and Steussy D.(1982) Full-scale dynamic lateral pile tests. IN: PROC. FOURTEENTH ANNUAL OFFSHORE TECHNOL. CONF., (HOUSTON, U.S.A.: MAY 3-6, 1982) 1 , Dallas, U.S.A., Offshore Technol. Conf., 1982, Paper OTC 4203:435-450

Seed H.B. and Lysmer J.(1975) Soil Structure Interaction Analyses for Seismic Response. Journal of the Geotechnical Engineering Division ,ASCE 101:439-457

Seed H.B., Lysmer J. and Hwang R.(1975) SOIL-STRUCTURE INTERACTION ANALYSES FOR SEISMIC RESPONSE. ASCE J Geotech Eng Div 101:439-457

Seed R., Dickenson S., Riemer M., Bray J., Sitar N., Mitchell J., Idriss I., Kayen R., Kropp A., Harder L.J. and Power M.(1990) Preliminary Report on the Principal Geotechnical Aspects of the October 17, 1989 Loma Prieta Earthquake, Earthquake Engineering Research Center, University of California

Seo C.-G., Yun C.-B. and Kim J.-M.(2007) Three-dimensional frequency-dependent infinite elements for soil–structure interaction. Engineering Structures 29:3106-3120. DOI: 10.1016/j.engstruct.2007.02.006.

Shamsabadi A. (2007) Three-dimensional nonlinear seismic soil-abutment-foundation-structure interaction analysis of skewed bridges, Ph.D. thesis, in University of Southern California.

Shirato M., Nonomura Y., Fukui J. and Nakatani S.(2008) Large-scale shake table experiment and numerical simulation on the nonlinear behavior of pile-groups subjected to large-scale earthquakes. Soils and Foundations 48:375-396. DOI: 10.3208/sandf.48.375.

Sihota A.K. (2004) Conjugate gradient methods using MPI for distributed systems, M.Eng. thesis, in McGill University (Canada).

Sitar N., Akai K., Bray J.D., Boulanger R.W., Christian J.T., Finn W.D.L., Leslie F. Harder J., Idriss I.M., Ishihara K., Iwasaki Y.T., Mitchell J.K., Moriwaki Y., Nakagawa K., O'Rourke T.D., Seed R.B., Soga K., Somerville P., Towhata I. and Youd T.L.(1995) Geotechnical reconnaissance of the effects of the January 17, 1995, Hyogoken-Nanbu earthquake, Japan, Earthquake Engineering Research Center, University of California. pp. 151.

Smith I.M.(2000) A general-purpose system for finite element analyses in parallel. Engineering Computations 17:75-91

Snir M. and Gropp W.(1998) MPI: The Complete Reference, MIT Press

Snyder J.L. (2004) Full-Scale Lateral-Load Tests of a 3x5 Pile Group in Soft Clays and Silts, Msc thesis, in Brigham Young University.

Stanton J.F., Banerjee S. and Hasayen I.(1988) Shaking Table Tests on Piles, National Technical Information Service

Stavroulakis G.M. and Papadrakakis M.(2009) Advances on the domain decomposition solution of large scale porous media problems. Computer Methods in Applied Mechanics and Engineering 198:1935-1945. DOI: 10.1016/j.cma.2009.01.003.

Sugimura Y.(1981) Earthquake Damage and Design Method of Piles, 10th International Conference for Soil Mechanics and Geotechnical Engineering, stockholm, Sweden. pp. 865-868.

Systems G.E.E.(1994) San Francisco - Oakland Bay Bridge East Crossing Earthquake Assessment, California Department of Transportation

Tabesh A. and Poulos H.G.(2001) Pseudostatic approach for seismic analysis of single piles. Journal of Geotechnical and Geoenvironmental Engineering 127:757-765. DOI: 10.1061/(asce)1090-0241(2001)127:9(757).

Tabesh A. and Poulos H.G.(2007) Design charts for seismic analysis of single piles in clay. Proceedings of the ICE - Geotechnical Engineering 160:85 –96

Tafreshi S.N.M.(2008) Uncouple Nonlinear Modeling of Seismic Soil-Pile-Superstructure Interaction in Soft Clay. International Journal of Civil Engineering 6:275-283

Takahashi A. (2002) Soil-pile interaction in liquefaction-induced lateral spreading of soils, Dr.Eng. thesis, in Tokyo Institute of Technology.

Tang L., Ling X., Xu P., Gao X. and Wang D.(2009) Shake table test of soil-pile groups-bridge structure interaction in liquefiable ground. Earthquake Engineering and Engineering Vibration:1-12. DOI: 10.1007/s11803-009-8131-7.

Tao X., Kagawa T., Minowa C. and Abe A.(1998) Verification of dynamic soil-pile interaction, in: P. Y. M. H. B. Dakoulas (Ed.), Geotechnical Earthquake Engineering and Soil Dynamics. pp. 1199-1210.

Teachavorasinskun S., Thongchim P. and Lukkunaprasit P.(2002) Stress rate effect on the stiffness of a soft clay from cyclic, compression and extension triaxial tests. Geotechnique 52:51-54. DOI: 10.1680/geot.52.1.51.40831.

Tezduyar T.E., Behr, M., Aliabadi, S.K., Mittal, S. and Ray, S.E.(1992) A new mixed preconditioning method for finite element computations. Computer Methods in Applied Mechanics and Engineering 99:27-42

Toki K., Sato T., Kiyono J., Garmroudi N.K., Emi S. and Yoshikawa M.(1991) Seismic behaviour of pile groups by hybrid experiments. Earthquake Engineering & Structural Dynamics 20:895-909. DOI: 10.1002/eqe.4290201002.

TOKIMATSU K., MIZUNO H. and KAKURAI M.(1996) Building damage associated with geotechnical problems, Japanese Geotechnical Society, Tokyo, JAPON.

Tokimatsu K., Suzuki H. and Sato M.(2005) Effects of inertial and kinematic interaction on seismic behavior of pile with embedded foundation. Soil Dynamics and Earthquake Engineering 25:753-762. DOI: 10.1016/j.soildyn.2004.11.018.

Trochanis A.M., Bielak J. and Christiano P.(1988) A Three-dimensional Nonlinear Study of Piles Leading to the Development of a Simplified Model, Carnegie Institute of Technology

Tzong T.-j. and Penzien J.(1983) Hybrid modelling of soil-structure interaction in layered media Earthquake Engineering Research Center, University of California, Berkeley

Ueng T.S.(2010) Shaking table tests for studies of soil liquefaction and soil-pile interaction. Geotechnical Engineering 41

Unjoh S. and Terayama T.(1998) Design Specifications of Highway Bridges, Public Works Research Institute, Earthquake Disaster Prevention Research Center.

Uzdensky D.A. and Kulsrud R.M.(1998) On the viscous boundary layer near the center of the resistive reconnection region. Physics of Plasmas 5:3249-3256. DOI: 10.1063/1.872992.

Uzuoka R., Sento N., Kazama M., Zhang F., Yashima A. and Oka F.(2007) Three-dimensional numerical simulation of earthquake damage to group-piles in a liquefied ground. Soil Dynamics and Earthquake Engineering 27:395-413. DOI: 10.1016/j.solidyn.2006.10.003.

Varun, Assimaki D. and Shafieezadeh A.(2012) Soil-pile-structure interaction simulations in liquefiable soils via dynamic macroelements: Formulation and validation. Soil Dynamics and Earthquake Engineering. DOI: 10.1016/j.soildyn.2012.03.008.

Viggiani G. and Atkinson J.H.(1995) Stiffness of fine-grained soil at very small strains. Geotechnique 45:249-265

Vucetic M.(1990) Normalized behavior of clay under irregular cyclic loading. Canadian Geotechnical Journal 27:29-46

Vucetic M. and Dobry R.(1991) EFFECT OF SOIL PLASTICITY ON CYCLIC RESPONSE. Journal of Geotechnical Engineering-Asce 117:89-107. DOI: 10.1061/(asce)0733-9410(1991)117:1(89).

Wada A., Yamada S., Kobayashi K. and Inagaki H.(2002) Shaking Table Tests for Damage Controlled Pile Foundation, 4th Forum on Implications of Recent Earthquake on Seismic Risk, Tokyo, Japan

Wang A. (1996) Three Dimensional Finite Element Analysis of Pile Groups and Piled-rafts, Ph.D. thesis, in University of Manchester.

Wang B., Shu J., Zheng W., Wang J. and Chen M.(2005) Hybrid Decomposition Method in Parallel Molecular Dynamics Simulation Based on SMP Cluster Architecture. Tsinghua Science & Technology 10:183-188. DOI: 10.1016/s1007-0214(05)70052-3.

Wang Z., Zhao C. and Dong L.(2009) An approximate spring–dashpot artificial boundary for transient wave analysis of fluid-saturated porous media. Computers and Geotechnics 36:199-210. DOI: 10.1016/j.compgeo.2008.01.008.

Wei X., Fan L. and Wu X.(2001) Shaking table tests of seismic pile–soil–pier–structure interaction, the fourth international conference on recent advances in geotechnical earthquake engineering and soil dynamics

Wijaya P.K.(2009) Boundary element model coupled with finite element model for dynamic soil-pile interaction, Bandung, Bali. pp. 491-496.

Wikipedia (2007) Motherboard, http://en.wikipedia.org/wiki/Motherboard.

Wilson D.W. (1998) Soil-Pile-Superstructure Interaction in Liquefying Sand and Soft Clay, Ph.D. thesis, in UNIVERSITY OF CALIFORNIA AT DAVIS.

Wilson E.L.(1968) A Computer Program for the Dynamic Stress Analysis of Underground Structures

Wood H.O.(1908) Distribution of apparent intensity in San Francisco, The California Earthquake of April 18, 1906, Carnegie Institution of Washington, Washington, D.C. pp. 220-245.

Wood H.O.(1955) The 1857 earthquake in California. Bulletin of the Seismological Society of America 45:47-67

Wu G. (1994) Dynamic soil-structure interaction: Pile foundations and retaining structures, Ph.D. thesis, in The University of British Columbia (Canada).

Wu G. and Finn W.D.L.(1997a) Dynamic elastic analysis of pile foundations using finite element method in the frequency domain. Canadian Geotechnical Journal 34:34-43. DOI: 10.1139/t96-87.

Wu G.X. and Finn W.D.L.(1997b) Dynamic nonlinear analysis of pile foundations using finite element method in the time domain. Canadian Geotechnical Journal 34:44-52. DOI: 10.1139/cgj-34-1-44.

Yagawa G., Soneda N. and Yoshimura S.(1991) A Large scale finite element analysis using domain decomposition method on a parallel computer. Computers and Structures 38:615-625

Yang D. (1992) Dynamic Properties of Beaufort Sea Soils, MEng thesis, in Memeorial University of Newfoundland.

Yao S., Kobayashi K., Yoshida N. and Matsuo H.(2004) Interactive behavior of soil-pile-superstructure system in transient state to liquefaction by means of

large shake table tests. Soil Dynamics and Earthquake Engineering 24:397-409. DOI: 10.1016/j.soildyn.2003.12.003.

Yerli H.R., Kacin S. and Kocak S.(2003) A parallel finite–infinite element model for two-dimensional soil–structure interaction problems. Soil Dynamics and Earthquake Engineering 23:249-253. DOI: 10.1016/s0267-7261(03)00022-8.

Yoshida N. and Hamada M.(1991) Damage to foundation piles and deformation pattern of ground due to liquefaction-induced permanent ground deformations, in: O. R. T.D. and M. Hamada (Eds.), 3rd Japan-US Workshop on Earthquake Resistant Design of Lifeline Facilities and Countermeasures for Soil Liquefaction. pp. 147-161.

Yu H.-S., Khong C. and Wang J.(2007) A unified plasticity model for cyclic behaviour of clay and sand. Mechanics Research Communications 34:97-114. DOI: 10.1016/j.mechrescom.2006.06.010.

Yu J. (1995) Response analysis of structures including effects of soil-structure interaction, Ph.D. thesis, in Florida Atlantic University.

Yu Y. and Lee F.H.(2002) Seismic response of soft ground, in: R. Phillips, et al. (Eds.), Physical Modelling in Geotechnics-ICPMG '02, St. Jhon's, Canada. pp. 519-524.

Zanvoral D.Z. and Campanella R.G.(1994) Frequency effects on damping/modulus of cohesive soil, in: R. J. Ebelhar, et al. (Eds.), Dynamic Geotechnical Testing II. pp. 191-201.

Zhang C., White D. and Randolph M.(2011) Centrifuge Modeling of the Cyclic Lateral Response of a Rigid Pile in Soft Clay. Journal of Geotechnical and Geoenvironmental Engineering 137:717-729. DOI: doi:10.1061/(ASCE)GT.1943-5606.0000482.

Zhang F., Kimura M., Nakai T. and Hoshikawa T.(2000) Mechanical behavior of pile foundations subjected to cyclic lateral loading up to the ultimate state. Soils and Foundations 40:1-17

Zhao B., Goh S.H. and Lee F.H.(2010) Implicit Domain Decomposition Scheme for Parallel Dynamic Finite Element Geotechnical Analysis, in: L. A. Zadeh, et al. (Eds.), 9th WSEAS International Conference on Software Engineering, Parallel and Distributed Systems, WSEAS Press, Cambridge, UK. pp. 127-132.

Zhao P. (1999) Centrifuge modelling of seismic amplification in some Singapore soil conditions, Master thesis, in National University of Singapore.

Zhou J. and Gong X.N.(2001) Strain degradation of saturated clay under cyclic loading. Canadian Geotechnical Journal 38:208-212. DOI: 10.1139/cgj-38-1-208.

Zienkiewicz O.C. and Taylor R.L.(1989) The Finite Element Method: Basic formulation and linear problems, McGraw-Hill

Zienkiewicz O.C. and Taylor R.L. (Ed.) (1999) The Finite Element Method, McGraw-Hill, London,